

Program and Abstracts for the

2019 BES/Separation Science Research PI Meeting



U.S. DEPARTMENT OF
ENERGY

Office of
Science

Gaithersburg Marriott Washingtonian Center
9751 Washingtonian Boulevard
Gaithersburg, Maryland, 20878

September 9 – 11, 2019

The research grants and contracts described in this document are supported by the U.S. Department of Energy, Office of Science/Basic Energy Sciences, as part of the Separation Science Program within the Chemical Sciences, Geosciences and Biosciences Division.

FOREWORD

This abstract booklet provides a record of the 2019 U.S. Department of Energy (DOE) contractors' meeting in Separation Science. This meeting, held at the Marriott Washingtonian Hotel in Gaithersburg, Maryland on September 9 – 11, 2019, was sponsored by the Chemical Sciences, Geosciences and Biosciences Division of the Office of Basic Energy Sciences (BES). The purpose of the meeting was to accelerate research progress through collegial interaction. The objectives of the meeting were to develop a common understanding of researchers' activities at the time of the meeting; to maximize potential for collaborative exchange among research groups; to identify the scientific needs of the research community; and to discuss areas for future research directions.

The agenda has oral presentations delivered by a number of the Principle Investigators (PIs), as well as an evening poster session. In this way, all PIs within the BES Separation Science Program presented their most recent work that was supported by the program. With ample time for discussion and interactions, this meeting was focused on the exchange of information and building of collaborations; rather than a formal review of researchers' achievements or a forum to deliberate and choose future directions for the program.

I thank all of the PIs whose dedication and innovation have advanced separation science research, and made this meeting possible and productive. I also hope that all of the PIs will build on their successes that we can then discuss when we assemble for our next PI meeting. Finally, I thank Teresa Crockett of DOE BES and Connie Lansdon of the Oak Ridge Institute for Science and Education for their technical and logistical support of this meeting.

Daniel Matuszak, Program Manager
Separation Science Program - Office of Basic Energy Sciences
U.S. Department of Energy

2019 Separation Science PI Meeting

U.S. Department of Energy
Office of Science, Office of Basic Energy Sciences

Gaithersburg Marriott Washingtonian Center
9751 Washingtonian Boulevard
Gaithersburg, Maryland, 20878

September 9 – 11, 2019

Monday Morning, September 9

- 7:30am Breakfast
- 8:30am Welcome, News from DOE-BES Chemical Sciences, Geosciences, and Biosciences Division
Dan Matuszak and Bruce Garrett, DOE Office of Basic Energy Sciences

SESSION I

ION RECOGNITION

Santa Jansone-Popova, Chair

- 9:00am Expanding Chemical Methods for Separating Mixtures of Rare Earth Metals with Coordination Chemistry under Thermodynamic and Kinetic Controls
Eric J. Schelter, Bren E. Cole, Joshua Nelson, Thibault Cheisson, Robert Higgins
University of Pennsylvania
- 9:30am Multi-tasking Anion Hosts with Primary and Secondary Assignments
Kristin Bowman-James, University of Kansas
- 10:00am Break
- 10:30am Binding Anions Selectively with Modular Triazolophanes and Releasing Them with Light
Amar H. Flood and Krishnan Raghavachari, Indiana University
- 11:00am Macrocyclic-based Ion Pair Receptors Controlling Recognition, Extraction, Function, and Structure
Jonathan L. Sessler, The University of Texas at Austin
- 11:30am Principles of Chemical Recognition and Transport in Extractive Separations: The Iminoguanidinium Group as Versatile Oxoanion Recognition Unit
Bruce A. Moyer, Vyacheslav Bryantsev, **Radu Custelcean**, and Santa Jansone-Popova
Oak Ridge National Laboratory
- 12:00pm Working Lunch

Monday Afternoon, September 9

**SESSION II
INTERFACES**

Ahmet Uysal, Chair

- 1:30pm X-ray studies of molecular ordering at the liquid/liquid interface in solvent extraction
Mark L. Schlossman^a and Ilan Benjamin^b
^a University of Chicago; ^b University of California Santa Cruz
- 2:00pm Solvent Extraction - Interfacial Chemistry and Phase Separation
Aurora E. Clark, Michael J. Servis, Zhu Liu, Nitesh Kumar
Washington State University
- 2:30pm Linking Self-Assembly and Organization at Liquid/Liquid Interfaces to Selective Chemical Separations using Nonlinear Spectroscopy
Benjamin Doughty, Oak Ridge National Laboratory
- 3:00pm Interfacial Structure and Dynamics in Separations
Grant E. Johnson, Venky Prabhakaran, and Vanda Glezakou
Pacific Northwest National Laboratory
- 3:30pm Break

**SESSION III
LIGHTNING ROUND A**

- 4:00pm *Introductory presentations for Poster Group A, conveying (a) the scientific need being addressed by the research, and (b) the research approach. Duration: 3-4 minutes each.*
1. Combinatorial Membrane Synthesis: Fundamentals of Hybrid Metal-Organic Brush (MOB) Membranes for Organic Solvent Nanofiltration
Georges Belfort *et al.*, Rensselaer Polytechnic Institute
 2. Exploiting Insertion Processes for Continuous Membrane-free Ion Separations
Richard M. Crooks *et al.*, The University of Texas at Austin
 3. CO₂ Separation via Guanidines Crystallization
Radu Custelcean *et al.*, Oak Ridge National Laboratory
 4. Efforts Towards the Selective Volatilization of f-Element Complexes using Mechanochemistry and Chelating Borohydrides
Gregory S. Girolami *et al.*, University of Illinois at Urbana-Champaign
Scott Daly, University of Iowa
 5. Interfacial Structure and Dynamics in Separations: When Molecular Simulations Meet Machine Learning
Vasiliki-Alexandra Glezakou *et al.*, Pacific Northwest National Laboratory
 6. Microscopy Methods for Investigating Separation Processes within Porous Particles
Joel M. Harris *et al.*, University of Utah

7. Molecular Diffusion in Self-Assembled Organic Nanotubes Studied Using Imaging Fluorescence Correlation Spectroscopy
Takashi Ito, Daniel A. Higgins *et al.*, Kansas State University
8. Tuning Oxoanion Selectivity in Ionic COFs
Santa Jansone-Popova *et al.*, Oak Ridge National Laboratory
9. Advanced Membranes for Gas Separation: Design, Simulation, and Guided Synthesis
De-en Jiang *et al.*, University of California, Riverside
10. Tailoring High Performance Carbon Molecular Sieve Membranes for Energy Intensive Separations
William J. Koros *et al.*, Georgia Institute of Technology
11. Differences in the extent of counterion condensation of ordered block copolymer electrolytes (BCEs) versus random copolymer electrolytes (RCEs)
Revati Kumar and Christopher G. Arges *et al.*, Louisiana State University
12. Tunable, Nanoporous, Two-dimensional Covalent Organic Frameworks for Size and Charge Separations
Katie D. Li-Oakey *et al.*, University of Wyoming

5:00pm Afternoon ends

Monday Evening, September 9

5:30pm Dinner, Networking
Offsite, laissez-faire, depart lobby

7:30pm Poster Session (Group A)

Tuesday Morning, September 10

7:30am Breakfast

SESSION IV MEMBRANES

William J. Koros, Chair

8:30am Fundamental Studies of Novel Separations
Sheng Dai *et al.*, Oak Ridge National Laboratory

9:00am Gas Transport Properties in Poly(benzimidazoles) Physical aging and humidified permeation
Melanie M. Merrick, Joshua D. Moon, and **Benny D. Freeman**
The University of Texas at Austin

9:30am Highly Permeable and Selective Model Network Membranes for Gas Separations
Ruilan Guo, University of Notre Dame

10:00am	Break
10:30am	Transport and Stability Characterization for Free-Volume-Generating Bottlebrush Polymers Zachary P. Smith <i>et al.</i> , Massachusetts Institute of Technology
11:00am	Understanding and controlling water-organic co-transport in amorphous microporous materials Ryan P. Lively , Daniel O’Nolan, Young Hee Yoon; Georgia Institute of Technology
11:30am	Design and Study of Hybrid Polyimide-Ionene Architectures for Membrane Separations Jason E. Bara , C. Heath Turner, Irshad Kammakakam, Kathryn E. O’Harra University of Alabama
12:00pm	Working Lunch

Tuesday Afternoon, September 10

SESSION V
THEORY & DATA SCIENCE
Vanda Glezakou, Chair

1:30pm	Design of OSDAs to Direct the Synthesis of Zeolites for CO ₂ /CH ₄ Membrane Separations Michael W. Deem , Rice University
2:00pm	Coordination-Chemistry-Derived Compounds Featuring Nanoscale Porosity and Selective Chemical Separation Capabilities Joseph T. Hupp , Randall Q. Snurr, and Omar K. Farha; Northwestern University
2:30pm	A Machine Learning Approach to Understanding Chemical Separations Lynne Soderholm <i>et al.</i> , Argonne National Laboratory
3:00pm	Computer Simulation of Complex Systems at the Extremes of pH Gregory A. Voth , The University of Chicago
3:30pm	Break

SESSION VI
LIGHTNING ROUND B

4:00pm	<i>Introductory presentations for Poster Group B, conveying (a) the scientific need being addressed by the research, and (b) the research approach. Duration: 3-4 minutes each.</i>
	<ol style="list-style-type: none"> 1. Alkoxysilane-Substituted Polynorbornenes: High Tg Glassy Membranes that behave like Rubbers Brian K. Long <i>et al.</i>, University of Tennessee, Knoxville 2. Probing the Structure of Ionic Liquids for Separations Shannon Mahurin <i>et al.</i>, Oak Ridge National Laboratory 3. Identifying the Presence of Nanoscale Spatial Heterogeneities in Deep Eutectic Solvent (DES) Films by Fluorescence Correlation Spectroscopy Jacob W. Petrich <i>et al.</i>, The Ames Laboratory

4. Potential-Driven Ion Separations at Solvated Electrified Interfaces
Venky Prabhakaran *et al.*, Pacific Northwest National Laboratory
5. Binding Anions Selectively with Modular Triazolophanes and Releasing Them with Light
Amar H. Flood and **Krishnan Raghavachari**, Indiana University
6. Energy Transfer in Lanthanide Luminescent Complexes
Kenneth N. Raymond and Michael W. Mara, University of California, Berkeley
7. Layer-by-Layer Assembly of a Polymer of Intrinsic Microporosity: Targeting the CO₂/N₂ Separation Problem
Steven L. Regen and Nabendu B. Pramanik, Lehigh University
8. Single-molecule Dynamics in Interface-rich Separations Environments
Daniel K. Schwartz, University of Colorado, Boulder
9. Separation Science at Argonne National Laboratory
Ahmet Uysal *et al.*, ANL
10. Enhanced Cation Selectivity and Transport by Electroosmotic Flow in the Hysteresis Charge Transport through Single Conical Nanopores
Gangli Wang *et al.*, Georgia State University
11. Understanding the Molecular-Level Interactions Between Ionic Liquids and Molecular Species: Applications in Separations
Kevin N. West *et al.* University of South Alabama
12. SEPARATIONML: A Data-Driven Separation Agent/Solvent Design Model
Ping Yang *et al.*, Los Alamos National Laboratory

5:00pm Afternoon ends

Tuesday Evening, September 10

5:30pm Dinner, Networking
Offsite, laissez-faire, depart lobby

7:30pm Poster Session (Group B)

Wednesday Morning, September 11

7:30am Breakfast

SESSION VII

FIELDS & FILMS

Katie D. Li-Oakey, Chair

8:30am Electrically Driven Ion Separations in Permeable Membranes
Merlin L. Bruening *et al.*, University of Notre Dame

- 8:55am Molecular Aspects of Transport in Thin Films of Controlled Architecture
Paul W. Bohn, University of Notre Dame
- 9:20am Differences in the extent of counterion condensation of ordered block copolymer electrolytes (BCEs) versus random copolymer electrolytes (RCEs)
Qi Lei, Ke Li, **Christopher G. Arges**, and Revati Kumar; Louisiana State University

**SESSION VIII
KEYNOTE**

- 9:45am *Invited presentation summarizing the recently released report from the National Academies*

A Research Agenda for Transforming Separation Science
David Sholl et al., Georgia Institute of Technology

- 10:25am Break

**SESSION IX
REACTIVE SEPARATION**
Radu Custelcean, Chair

- 10:40am Efforts Towards the Selective Volatilization of f-Element Complexes using Mechanochemistry and Chelating Borohydrides
Scott R. Daly et al., The University of Iowa
Gregory S. Girolami *et al.*, The University of Illinois at Urbana-Champaign
- 11:05am Assessing Reactive Separations of CO₂
David J. Heldebrant et al., Pacific Northwest National Laboratory

**SESSION X
MEETING CLOSURE**

- 11:30am Closing Discussion
Chairs summarize key points for each session. Session participants add/clarify. Observations from audience as time allows. (5-minutes per session chair)
- 12:00pm Adjourn

Table of Contents

TITLE PAGE	i
FOREWORD	ii
AGENDA	iii
Table of Contents.....	ix
ABSTRACTS.....	1
PI ABSTRACTS SESSION I: ION RECOGNITION	2
<i>Expanding Chemical Methods for Separating Mixtures of Rare Earth Metals with Coordination Chemistry under Thermodynamic and Kinetic Controls</i>	
Eric J. Schelter , University of Pennsylvania	3
<i>Multi-tasking Anion Hosts with Primary and Secondary Assignments</i>	
Kristin Bowman-James , University of Kansas	7
<i>Binding Anions Selectively with Modular Triazolophanes and Releasing Them with Light</i>	
Amar H. Flood and Krishnan Raghavachari, Indiana University	11
<i>Macrocyclic-based Ion Pair Receptors Controlling Recognition, Extraction, Function, and Structure</i>	
Jonathan L. Sessler , The University of Texas at Austin	15
<i>Principles of Chemical Recognition and Transport in Extractive Separations: The Iminoguanidinium Group as Versatile Oxoanion Recognition Unit</i>	
Bruce A. Moyer, Vyacheslav Bryantsev, Radu Custelcean , and Santa Jansone-Popova, Oak Ridge National Laboratory	19
PI ABSTRACTS SESSION II: INTERFACES	24
<i>X-ray studies of molecular ordering at the liquid/liquid interface in solvent extraction</i>	
Mark L. Schlossman University of Chicago; and Ilan Benjamin, University of California Santa Cruz.....	25
<i>Solvent Extraction - Interfacial Chemistry and Phase Separation</i>	
Aurora E. Clark , Michael J. Servis, Zhu Liu, Nitesh Kumar, Washington State University.....	29
<i>Linking Self-Assembly and Organization at Liquid/Liquid Interfaces to Selective Chemical Separations using Nonlinear Spectroscopy</i>	
Benjamin Doughty , Oak Ridge National Laboratory	33
<i>Interfacial Structure and Dynamics in Separations</i>	
Grant E. Johnson , Venky Prabhakaran, and Vanda Glezakou, Pacific Northwest National Laboratory.	34
PI ABSTRACTS SESSION III: POSTER SESSION	36
<i>Combinatorial Membrane Synthesis: Fundamentals of Hybrid Metal-Organic Brush (MOB) Membranes for Organic Solvent Nanofiltration</i>	
Georges Belfort et al. , Rensselaer Polytechnic Institute	37

<i>Exploiting Insertion Processes for Continuous Membrane-free Ion Separations</i>	
Richard M. Crooks et al. , The University of Texas at Austin	41
<i>CO₂ Separation via Guanidines Crystallization</i>	
Radu Custelcean et al. , Oak Ridge National Laboratory.....	45
<i>Interfacial Structure and Dynamics in Separations: When Molecular Simulations Meet Machine Learning</i>	
Vassiliki-Alexandra Glezakou et al. , Pacific Northwest National Laboratory	48
<i>Microscopy Methods for Investigating Separation Processes within Porous Particles</i>	
Joel M. Harris et al. , University of Utah	49
<i>Molecular Diffusion in Self-Assembled Organic Nanotubes Studied Using Imaging Fluorescence Correlation Spectroscopy</i>	
Takashi Ito, Daniel A. Higgins et al. , Kansas State University.....	54
<i>Tuning Oxoanion Selectivity in Ionic COFs</i>	
Santa Jansone-Popova et al. , Oak Ridge National Laboratory.....	60
<i>Advanced Membranes for Gas Separation: Design, Simulation, and Guided Synthesis</i>	
De-en Jiang et al. , University of California, Riverside.....	62
<i>Tailoring High Performance Carbon Molecular Sieve Membranes for Energy Intensive Separations</i>	
William J. Koros et al. , Georgia Institute of Technology	64
<i>Tunable, Nanoporous, Two-dimensional Covalent Organic Frameworks for Size and Charge Separations</i>	
Katie D. Li-Oakey et al. , University of Wyoming	72
PI ABSTRACTS SESSION IV: MEMBRANES	73
<i>Fundamental Studies of Novel Separations</i>	
Sheng Dai et al. , Oak Ridge National Laboratory.....	74
<i>Gas Transport Properties in Poly(benzimidazoles) Physical aging and humidified permeation</i>	
Melanie M. Merrick, Joshua D. Moon, and Benny D. Freeman , The University of Texas at Austin	76
<i>Highly Permeable and Selective Model Network Membranes for Gas Separations</i>	
Ruilan Guo , University of Notre Dame	81
<i>Transport and Stability Characterization for Free-Volume-Generating Bottlebrush Polymers</i>	
Zachary P. Smith et al. , Massachusetts Institute of Technology.....	86
<i>Understanding and controlling water-organic co-transport in amorphous microporous materials</i>	
Ryan P. Lively , Daniel O’Nolan, Young Hee Yoon; Georgia Institute of Technology	89
<i>Design and Study of Hybrid Polyimide-Ionene Architectures for Membrane Separations</i>	
Jason E. Bara , C. Heath Turner, Irshad Kammakakam, Kathryn E. O’Harra, University of Alabama	92

PI ABSTRACTS SESSION V: THEORY & DATA SCIENCE	97
<i>Design of OSDAs to Direct the Synthesis of Zeolites for CO₂/CH₄ Membrane Separations</i>	
Michael W. Deem , Rice University	98
<i>Coordination-Chemistry-Derived Compounds Featuring Nanoscale Porosity and Selective Chemical Separation Capabilities</i>	
Joseph T. Hupp , Randall Q. Snurr, and Omar K. Farha; Northwestern University	101
<i>A Machine Learning Approach to Understanding Chemical Separations</i>	
Lynne Soderholm et al. , Argonne National Laboratory.....	108
<i>Computer Simulation of Complex Systems at the Extremes of pH</i>	
Gregory A. Voth , The University of Chicago	111
PI ABSTRACTS SESSION VI: POSTER SESSION	115
<i>Alkoxysilane-Substituted Polynorbornenes: High T_g Glassy Membranes that behave like Rubbers</i>	
Brian K. Long et al. , University of Tennessee, Knoxville.....	116
<i>Probing the Structure of Ionic Liquids for Separations</i>	
Shannon Mahurin et al. , Oak Ridge National Laboratory	122
<i>Identifying the Presence of Nanoscale Spatial Heterogeneities in Deep Eutectic Solvent (DES) Films by Fluorescence Correlation Spectroscopy</i>	
Jacob W. Petrich et al. , The Ames Laboratory.....	123
<i>Potential-Driven Ion Separations at Solvated Electrified Interfaces</i>	
Venky Prabhakaran et al. , Pacific Northwest National Laboratory	125
<i>Energy Transfer in Lanthanide Luminescent Complexes</i>	
Kenneth N. Raymond and Michael W. Mara, University of California, Berkeley.....	127
<i>Layer-by-Layer Assembly of a Polymer of Intrinsic Microporosity: Targeting the CO₂/N₂ Separation Problem</i>	
Steven L. Regen and Nabendu B. Pramanik, Lehigh University.....	130
<i>Single-molecule Dynamics in Interface-rich Separations Environments</i>	
Daniel K. Schwartz , University of Colorado, Boulder	134
<i>Separation Science at Argonne National Laboratory</i>	
Ahmet Uysal et al. , ANL.....	139
<i>Enhanced Cation Selectivity and Transport by Electroosmotic Flow in the Hysteresis Charge Transport through Single Conical Nanopores</i>	
Gangli Wang et al. , Georgia State University	140
<i>Understanding the Molecular-Level Interactions Between Ionic Liquids and Molecular Species: Applications in Separations</i>	

Kevin N. West et al. , University of South Alabama	142
<i>SEPARATIONML: A Data-Driven Separation Agent/Solvent Design Model</i>	
Ping Yang et al. , Los Alamos National Laboratory	143
PI ABSTRACTS SESSION VII: FIELDS & FILMS	144
<i>Electrically Driven Ion Separations in Permeable Membranes</i>	
Merlin L. Bruening et al. , University of Notre Dame.....	145
<i>Molecular Aspects of Transport in Thin Films of Controlled Architecture</i>	
Paul W. Bohn , University of Notre Dame	151
<i>Differences in the extent of counterion condensation of ordered block copolymer electrolytes (BCEs) versus random copolymer electrolytes (RCEs)</i>	
Qi Lei, Ke Li, Christopher G. Arges , and Revati Kumar; Louisiana State University.....	157
PI ABSTRACTS SESSION IX: REACTIVE SEPARATION	161
<i>Efforts Towards the Selective Volatilization of f-Element Complexes using Mechanochemistry and Chelating Borohydrides</i>	
Scott R. Daly et al. , The University of Iowa; Gregory S. Girolami et al., The University of Illinois at Urbana-Champaign	162
<i>Assessing Reactive Separations of CO₂</i>	
David J. Heldebrant et al. , Pacific Northwest National Laboratory	166
LIST OF PARTICIPANTS	170

ABSTRACTS

PI ABSTRACTS SESSION I: ION RECOGNITION

Expanding Chemical Methods for Separating Mixtures of Rare Earth Metals with Coordination Chemistry Under Thermodynamic and Kinetic Controls

Eric J. Schelter, Bren E. Cole, Joshua Nelson, Thibault Cheisson, Robert Higgins
Chemistry Department, University of Pennsylvania

Presentation Abstract

Solvent extraction has been the most important technology for purifying rare earth metals. However, stepwise extraction and stripping steps have low selectivity. And the large investment and expertise required for running multi-stage countercurrent extraction presents barriers for metals recovery from spent technologies or for setting up new capabilities for separating rare earth concentrates from mineral sources. During the past project period, we have developed new chemistry that targets separating rare earth metals from specific, high value mixtures. For example, we have developed a new ligand system, H₃tren-1,2,3-HOPO. This ligand chelates RE³⁺ ions, even under aqueous, acidic conditions. We also developed a high throughput experimentation protocol that enabled identification of conditions for separation of Dy/Nd mixtures. Using a redox driven chelation reaction of a tris(nitroxide) species we have also demonstrated that kinetic aspects, rather than thermodynamic control, can be used to separate rare earth cations. Finally, we have demonstrated that magnetic fields applied to reaction mixtures can amplify separations factors in selective crystallization. These results provide new directions for separating rare earths from anthropogenic- and natural sources, methods that are complementary to solvent extraction.

DE-SC0017259: Advancing Separations of Rare Earth Elements through Coordination and (Photo)Redox Chemistry

PI: Eric J. Schelter

Postdoc(s): (Since 2015) Thibault Cheisson, Robert Higgins, Huayi Fang

Student(s): (Since 2015) Joshua Nelson, Bren Cole, Yusen, Qiao, Justin Bogart, Jee Eon Kim, Jessica Levin, Walter Dorfner, Haolin Yin

RECENT PROGRESS

High Throughput Separations Methods

We have developed the synthesis and characterization of the new ligand tris[(1-hydroxy-2-oxo-1,2-dihydropyridine-3-

carboxamido)ethyl]amine, H₃1•TFA, and complexes 1•RE (RE = La, Nd, Dy, Figure 1, top). A high-throughput experimentation (HTE) screen was developed to quantitatively

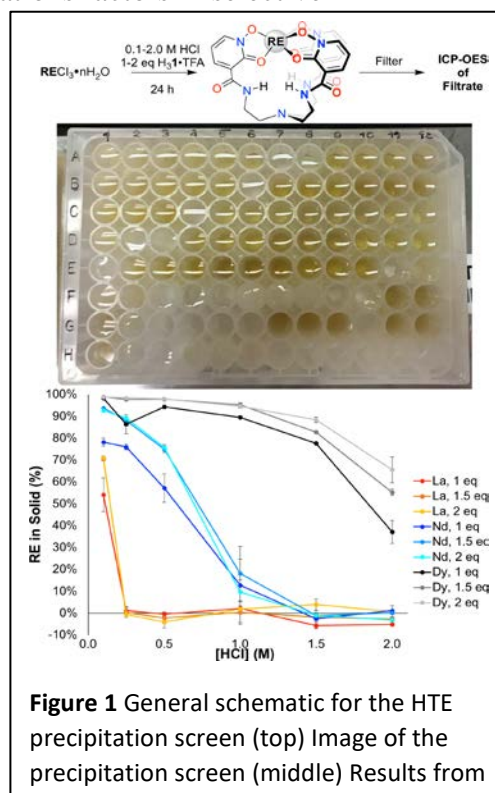


Figure 1 General schematic for the HTE precipitation screen (top) Image of the precipitation screen (middle) Results from

determine precipitation of $1 \bullet \text{RE}$ as a function of pH and equivalents of $\text{H}_31 \bullet \text{TFA}$. This method allowed us to determine optimal conditions for the separation of RE mixtures rapidly, while minimizing materials consumption. The HTE-predicted conditions were used to achieve the separation of Nd/Dy ($S_{\text{Nd/Dy}} = 213 \pm 34$) and La/Nd ($S_{\text{La/Nd}} = 16.2 \pm 0.2$) mixtures in acidic aqueous media. We expect the development of the HTE screen will enable discovery of new separations systems that contribute to new chemistry for recycling rare earth metals from spent technology.

Magnetic Enhancement in Separations

Nearly all rare-earth separations rely upon small changes in ionic radii to direct speciation or reactivity. We have shown that the intrinsic magnetic properties of the rare-earth ions impact the separations of light/heavy and selected heavy/heavy binary mixtures. Using TriNOx^{3-} ($\{(2\text{-}^t\text{BuNO})\text{C}_6\text{H}_4\text{CH}_2\}_3\text{N}\}^{3-}$), a ligand that we developed previously in this project, we efficiently and selectively crystallized TriNOx complexes of heavy rare earths (Tb–Yb) in mixture with light rare earths (La and Nd) in the presence of an external $\text{Fe}_{14}\text{Nd}_2\text{B}$ magnet, concomitant with the

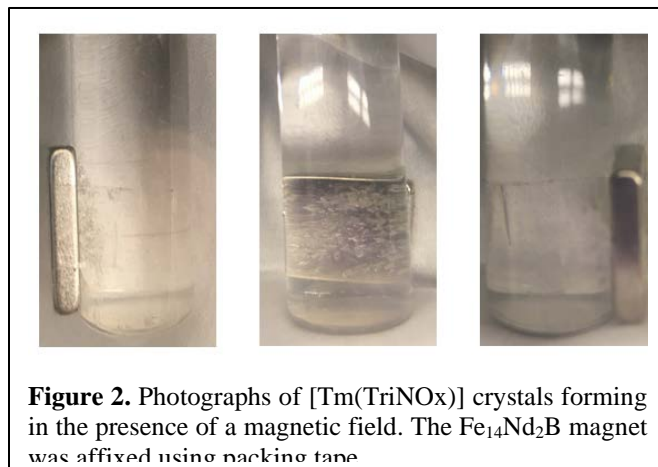


Figure 2. Photographs of $[\text{Tm}(\text{TriNOx})]$ crystals forming in the presence of a magnetic field. The $\text{Fe}_{14}\text{Nd}_2\text{B}$ magnet was affixed using packing tape.

introduction of a concentration gradient (decrease in temperature, Figure 2). The optimal separation was observed for an equimolar mixture of La:Dy, which gave an enrichment factor of $D_{\text{La:Dy}} = 297 \pm 31$ for the solid fraction, achieving a 99.7% pure Dy sample in one step. These results indicate that the individual paramagnetism of the rare-earth ions provides an added effect to amplify separations by selective crystallization.

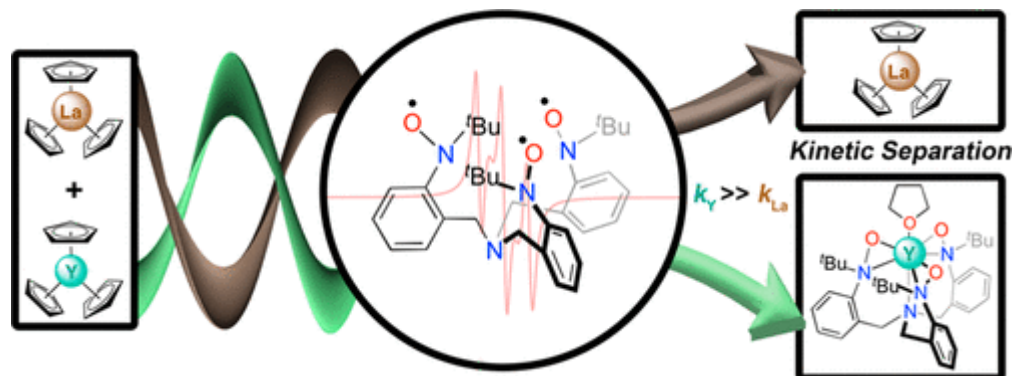


Figure 3. Proligand TriNOx^{3-} (center) that shows variable rates of reaction with $\text{RE}(\text{Cp})_3$ RE = La, Y that underpins a kinetic separations process for those ions.

Kinetic Separations

The development of separation processes driven by kinetic factors represents a new area for this field. Previously, we described the first separations method for rare earth elements using a kinetic basis through variable oxidation rates of $\text{RE}(\text{TriNOx})$ complexes. Recently, we disclosed a novel method of separating select rare earths by reacting RE cyclopentadienides with the triradical species tris(2-*tert*-butylnitroxyl)-benzylamine,

TriNOx^{•••} (Figure 3.) The key proligand TriNOx^{•••} was characterized using a variety of techniques including X-ray crystallography, magnetometry, and EPR spectroscopy. When applied to an equimolar mixture of La:Y cyclopentadienide complexes, RECP₃, different rates of chelation of these organometallic precursors by TriNOx^{•••} were observed, affording a separation factor La/Y of 26 under the reported conditions. These results indicate that simple reaction chemistry can afford good selectivity in RE separations from variable reaction rates.

Publications Acknowledging this Grant (and Immediate Previous Grant) in 2015 – present

1. (I) Cole, B. E.; Cheisson, T.; Higgins, R. F.; Nakamaru-Ogiso, E.; Manor, B. C.; Carroll, P. J.; Schelter, E. J. *Inorg. Chem.* **2019**, <https://doi.org/10.1021/acs.inorgchem.9b00975>.
2. (III) Galley, S. S.; Pattenaude, S. A.; Higgins, R. F.; Tatebe, C. J.; Stanley, D. A.; Fanwick, P. E.; Zeller, M.; Schelter, E. J.; Bart, S. C. *Dalton Trans.* **2019**, *48*, 8021-8025.
3. (I) Qiao, Y.; Cheisson, T.; Manor, B. C.; Carroll, P. J.; Schelter, E. J. *Chem. Comm.* **2019**, *55*, 4067-4070.
4. (III) Galley, S. S.; Pattenaude, S. A.; Gaggioli, C. A.; Qiao, Y.; Sperling, J. M.; Zeller, M.; Pakhira, S.; Mendoza-Cortes, J. L.; Schelter, E. J.; Albrecht-Schmitt, T. E.; Gagliardi, L.; Bart, S. C. *J. Am. Chem. Soc.* **2019**, *141*, 2356-2366.
5. (I) Cheisson, T.; Schelter, E. J. *Science* **2019**, *363*, 489-493.
6. (I) Cheisson, T.; Cole, B. E.; Manor, B. C.; Carroll, P. J.; Schelter, E. J. *ACS Sustainable Chem. Eng.* **2019**, *7*, 4993-5001.
7. (I) Nelson, J. M.; Schelter, E. J. *Inorg. Chem.* **2019**, *58*, 979-990.
8. (III) Coughlin, E. J.; Qiao, Y.; Lapsheva, E.; Zeller, M.; Schelter, E. J.; Bart, S. C. *J. Am. Chem. Soc.* **2019**, *141*, 1016-1026.
9. (II) Qiao, Y.; Schelter, E. J. *Acc. Chem. Res.* **2018**, *51*, 2926-2936.
10. (I) Cole, B. E.; Falcones, I. B.; Cheisson, T.; Manor, B. C.; Carroll, P. J.; Schelter, E. J. *Chem. Comm.* **2018**, *54*, 10276-10279.
11. (II) Friedrich, J.; Qiao, Y.; Maichle-moessmer, C.; Schelter, E. J.; Anwander, R. *Dalton Trans.* **2018**, *47*, 10113-10123.
12. (III) Vanagas, N. A.; Wacker, J. N.; Rom, C. L.; Glass, E. N.; Colliard, I.; Qiao, Y.; Bertke, J. A.; Van Keuren, E.; Schelter, E. J.; Nyman, M.; Knope, K. E. *Inorg. Chem.* **2018**, *57*, 7259-7269.
13. (III) Pattenaude, S. A.; Mullane, K. C.; Schelter, E. J.; Ferrier, M. G.; Stein, B. W.; Bone, S. E.; Lezama Pacheco, J. S.; Kozimor, S. A.; Fanwick, P. E.; Zeller, M.; Bart, S. C. *Inorg. Chem.* **2018**, *57*, 6530-6539.
14. (I) Qiao, Y.; Sargentu, D.-C.; Yin, H.; Zabula, A. V.; Cheisson, T.; McSkimming, A.; Carroll, P. J.; Anna, J. M.; Autschbach, J.; Schelter, E. J. *J. Am. Chem. Soc.* **2018**, *140*, 4588-4595.
15. (I) Fang, H.; Cole, B. E.; Qiao, Y.; Bogart, J. A.; Cheisson, T.; Manor, B. C.; Carroll, P. J.; Schelter, E. J. *Angew. Chem. Int. Ed.* **2017**, *56*, 13450-13454.
16. (I) Bogart, J. A.; Cole, B. E.; Boreen, M. A.; Lippincott, C. A.; Manor, B. C.; Carroll, P. J. Schelter, E. J. *Proc. Natl. Acad. Sci. U. S. A.* **2016**, *113*, 14887-14892.
17. (I) Levin, J. R.; Cheisson, T.; Carroll, P. J.; Schelter, E. J. *Dalton Trans.* **2016**, *45*, 15249-15258.

18. (I) Yin, H.; Carroll, P. J.; Schelter, E. J. *Chem. Comm.* **2016**, 52, 9813-9816.
19. (I) Yin, H.; Carroll, P. J.; Schelter, E. J. *Inorg. Chem.* **2016**, 55, 5684-5692.
20. (I) Yin, H.; Zabula, A. V.; Schelter, E. J. *Dalton Trans.* **2016**, 45, 6313-6323.
21. (I) Kim, J. E.; Bogart, J. A.; Carroll, P. J.; Schelter, E. J. *Inorg. Chem.* **2016**, 55, 775-784.
22. (III) Herb, T. M.; Poitras, A. M.; Richardson, K. G.; Cole, B. E.; Bogart, J. A.; Carroll, P. J.; Schelter, E. J.; Graves, C. R. *Polyhedron* **2016**, 114, 194-199.
23. (III) Cary, S. K.; Silver, M. A.; Liu, G.; Wang, J. C.; Bogart, J. A.; Stritzinger, J. T.; Arico, A. A.; Hanson, K.; Schelter, E. J.; Albrecht-Schmitt, T. E. *Inorg. Chem.* **2015**, 54, 11399-11404.
24. (III) Poitras, A.; Bogart, J. A.; Cole, B.; Carroll, P. J.; Schelter, E. J.; Graves, C. R. *Inorg. Chem.* **2015**, 54, 10901-10908.
25. (I) Bogart, J. A.; Lippincott, C. A.; Carroll, P. J.; Booth, C. H.; Schelter, E. J. *Chem. Eur. J.* **2015**, 21, 17850-17859.
26. (I) Boreen, M. A.; Bogart, J. A.; Carroll, P. J.; Schelter, E. J. *Inorg. Chem.* **2015**, 54, 9588-9593.
27. (I) Kim, J. E.; Carroll, P. J.; Schelter, E. J. *Chem. Comm.* **2015**, 51, 15047-15050.
28. (I) Levin, J. R.; Dorfner, W. L.; Carroll, P. J.; Schelter, E. J. *Chem. Sci.* **2015**, 6, 6925-6934.
29. (III) Anderson, N. H.; Yin, H.; Kiernicki, J. J.; Fanwick, P. E.; Schelter, E. J.; Bart, S. C. *Angew. Chem. Int. Ed.* **2015**, 54, 9386-9389.
30. (III) Pattenaude, S. A.; Kuehner, C. S.; Dorfner, W. L.; Schelter, E. J.; Fanwick, P. E.; Bart, S. C. *Inorg. Chem.* **2015**, 54, 6520-6527.
31. (I) Bogart, J. A.; Lippincott, C. A.; Carroll, P. J.; Schelter, E. J. *Angew. Chem. Int. Ed.* **2015**, 54, 8222-8225.
32. (I) Kim, J. E.; Carroll, P. J.; Schelter, E. J. *New J. Chem.* **2015**, 39, 6076-6084.
33. (III) Silver, M. A.; Dorfner, W. L.; Cary, S. K.; Cross, J. N.; Lin, J.; Schelter, E. J.; Albrecht-Schmitt, T. E. *Inorg. Chem.* **2015**, 54, 5280-5284.
34. (III) Anderson, N. A.; Odoh, S. O.; Williams, U. J.; Lewis, A. J.; Wagner, G. L.; Pacheco, J. L.; Kozimor, S. A.; Gagliardi, L.; Schelter, E. J.; Bart, S. C. *J. Am. Chem. Soc.* **2015**, 137, 4690-4700.
35. (I) Bogart, J. A.; Lewis, A. J.; Boreen, M. A.; Lee, H. B.; Medling, S. A.; Carroll, P. J.; Booth, C. H.; Schelter, E. J. *Inorg. Chem.* **2015**, 54, 2830-2837.

Multi-tasking Anion Hosts with Primary and Secondary Assignments

Kristin Bowman-James

Department of Chemistry, University of Kansas

Presentation Abstract

Multi-tasking hosts have been designed to accomplish enhanced functions above primary binding of anions through secondary binding assignments, e.g., ion-pair cooperative binding, catch and release binding, and cooperatively manipulating gel properties. *Task #1* targets ion pair hosts for higher valent anions. A comparative study between a urea-based chelate and macrocycle was followed by examining ion-pair binding of the two hosts fitted with two crown ethers. *Task #2* targets Lewis acid binding and release of anions using tetracarboxamide-appended bimetallic pyrazine pincers as hosts for two anions. The nature of two short hydrogen bonds between the adjacent pyrazine carbonyl groups responsible for the switching capability has been probed using Electron Localization Function calculations. Anion binding studies of pyrazines with hydrophilic and hydrophobic pyrazine chains have allowed for addressing a secondary assignment: modifying solvent dependencies of binding. *Task #3* targets a secondary assignment of added cooperative gelling effects in extended frameworks. Tetrahexyl pyrazine-2,3,5,6-tetracarboxamide forms a fluorescent gel, which undergoes quenching and regeneration of fluorescence in an anion-dependent gel-sol-gel sequence.

Molecular to Mesoscale Targeting of Oxoanions with Multi-Tasking Hosts

DE-SC0018629

Postdocs: Sandeep Kaur and Subhamay Pramanik

Student: Jessica Lohrman

RECENT PROGRESS

Task 1: Ion pair hosts for higher valent ions

A urea-based macrocycle was synthesized. Design principles used built on a structurally related urea chelate synthesized in a previously funded DOE project (DE-SC0010555). The tetraurea acyclic chelate and macrocycle were found to bind SO_4^{2-} ion selectively (Chart 1, **1** and **2**). A corollary urea chelate with two attached crown ethers, one on each of the phenylene groups, was also synthesized (Chart 1, **3**). Synthesis of the corollary crown-attached macrocycle is in progress. The macrocycle **2** was found to be selective for SO_4^{2-} , as seen for the urea precursor, **1** (Table 1). The crystal structure of the SO_4^{2-} complex of the macrocycle (**2**) showed similarities with the previous urea chelate (**1**) structure with SO_4^{2-} (Figure 1, (A) and (B)). Crystal structures of the macrocycle were also obtained with chloride ion and biphenyl dicarboxylate [$\text{BP}(\text{CO}_2)_2$] (Figure 1, (C) and (D)).

Chart 1. Urea hosts synthesized for Task #1.

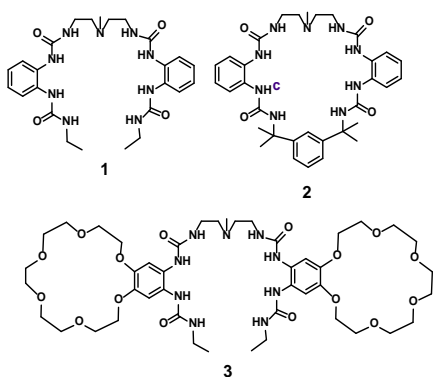
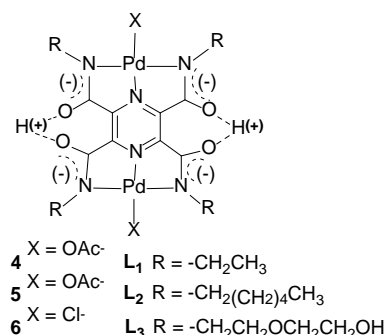


Table 1. Anion binding of **2** with different anions in $\text{DMSO}-d_6 \cdot \text{H}_2\text{O}$.

Anions	$K_{as} \times 10^4 \text{ (M}^{-1}\text{)}$
$[\text{TBA}^+]_2[\text{SO}_4^{2-}]$	9.05
$[\text{TBA}^+][\text{HSO}_4^-]$	6.86
$[\text{TBA}^+][\text{H}_2\text{PO}_4^-]$	4.98
$[\text{TBA}^+][\text{CH}_3\text{COO}^-]$	5.16
$[\text{TBA}^+][\text{Cl}^-]$	0.343
$[\text{TBA}^+]_2[\text{BP}(\text{COO})_2^{2-}]$	0.696 (K_1) 328 (K_2)

Chart 2. ChemDraw diagram of Pd(II) complexes **4 - 6**.



Task 2. Hosts capable of binding and release of anions.

Pyrazine tetracarboxamide pincers were synthesized as precursors to extended frameworks, and were found to bind Pd(II) quite effectively (**4 - 6**). Additionally the fourth, relatively labile Pd(II) coordination site was found to hold an anion (so far acetate or chloride), with charge neutralized by two very short hydrogen bonds between adjacent carbonyl groups on the pyrazine (Figure 2). These proton counterions can be released on the addition of

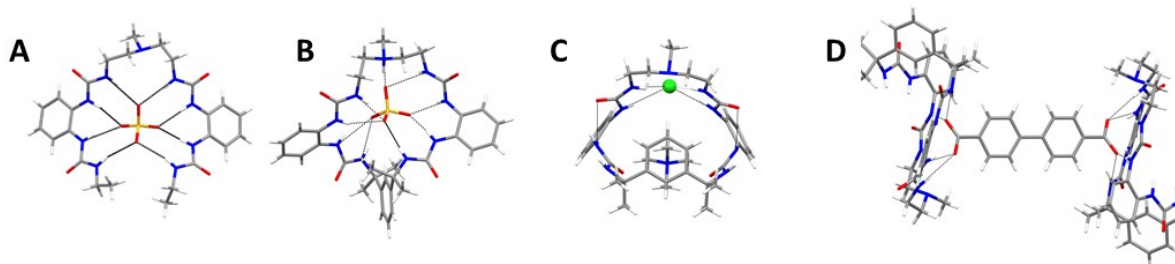


Figure 1. Crystal structure perspective view of **1** with (A) SO_4^{2-} , and views of **2** with (B) SO_4^{2-} , (C) Cl^- , and (D) with $\text{BP}(\text{CO}_2)_2^{2-}$.

base, also releasing the bound anion. The proton counterions were found to be consistent for several Pd(II) complexes, including those with different carboxamide chains.

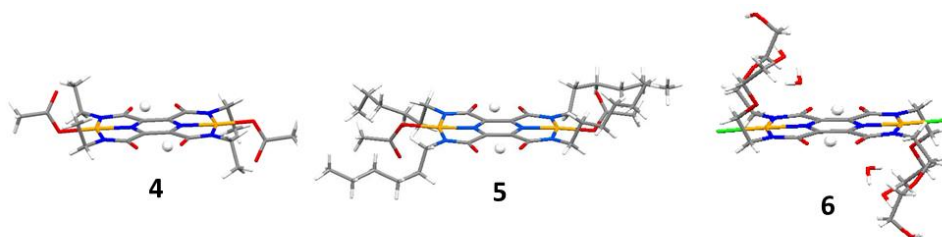


Figure 2. Crystallographic perspective views of **4**, **5**, and **6** showing the very short hydrogen bonds.

Electron Localization Function (ELF) calculations carried out in collaboration with Prof. Andrés Cisneros at the University of North Texas indicated that the strength of the hydrogen bond was dependent on electronic factors and factors such as the identity of the anion, the amide appendages, and the coordination capabilities of the solvent. Additional solution studies and attempts to remove the protons indicated that they are bound quite tightly.

Task 3. Cooperativity in Extended Frameworks.

The tetracarboxamide ligands (and complexes) form gels under certain conditions. This is especially true for the extended carboxamide appendages, such as the tetrahexyl-pyrazine-tetracarboxamide (Chart 2 - free base of **5**). In the crystal structure the host forms extended arrays, with intermolecular hydrogen bonds between the stacked molecules (Figure 3).

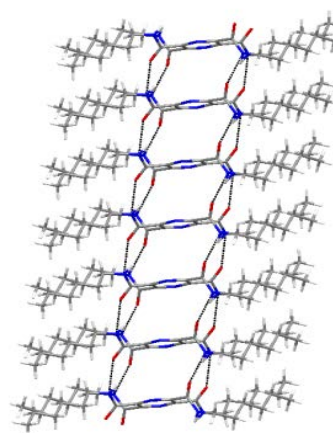
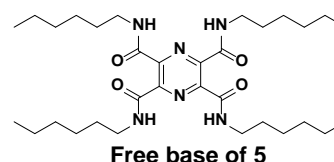


Figure 3. ChemDraw diagram of the free base of **5** and perspective view of hydrogen bond promoted stacking in the crystal structure.

In addition to gel formation, emission enhancement is observed during the transformation of the free base of **5**

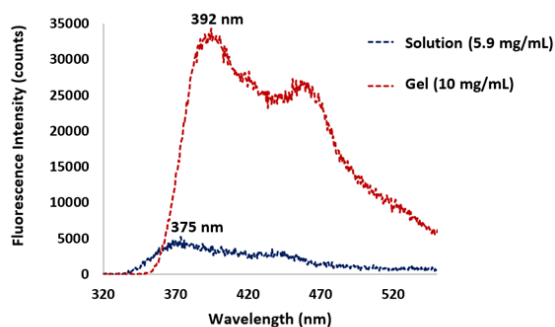


Figure 4. Fluorescence spectra of solution (5.9 mg/mL) and gel (10 mg/mL) free base of **5** from sol to gel. At low concentrations (e.g., 5.9 mg/mL) in ethanol ($\lambda_{ex}=285$ nm) only a broad emission

band with emission maxima at 375 nm on excitation at 285 nm is observed. Upon increasing concentration to 10 mg/mL, a gel forms and emission increases 10-fold with a shifted maximum of 392 nm and shoulder band at 468 nm (Figure 4). This high emission along with bathochromic shift ($\Delta\lambda=17$ nm) is attributed to strong intermolecular hydrogen bonding and π - π stacking upon gelation.

The gels are disrupted by the presence of different anions, an example of which is shown in Figure 5. A gel to sol transition occurs at different rates for different anions, with acetate ion promoting the fastest transition. The gel-sol transformations can be reversed by the addition of phytic acid (hexaphosphorylated inositol), which also regenerates the fluorescence emission.

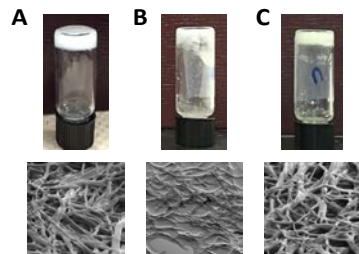


Figure 5. Reversible gel-sol transitions showing gels from the free base of **5** (top) and SEM images (bottom): (A) initial gel; (B) after addition of acetate; and (C) after addition of phytic acid, *myo*-inositol-hexakisphosphate.

Publications Acknowledging this Grant in 2015 – present

(I) *Exclusively funded by this grant:*

None yet.

(II) *Jointly funded by this grant and other grants with leading intellectual contribution from this grant;*

Lohrman, J.; Vázquez-Montelongo, E.A.; Pramanik, S.; Day, V. W.; Hix, M. A.; Bowman-James, K.; Cisneros, G. A. Characterizing Hydrogen-Bond Interactions in Pyrazinetetracarboxamide Complexes: Insights from Experimental and Quantum Topological Analyses. *Inorg. Chem.* **2018**, *57*, 9775-9778.

(III) *Jointly funded by this grant and other grants with relatively minor intellectual contribution from this grant;*

None.

Binding Anions Selectively with Modular Triazolophanes and Releasing Them with Light

Amar H Flood and Krishnan Raghavachari
Department of Chemistry, Indiana University, Bloomington, IN

Presentation Abstract

Anion recognition with shape-persistent and shape-dynamic receptors offers a platform to transfer concepts from biology to synthetic systems for functional, smart, and responsive recognition. This effort includes adding function to receptors, expressed as binding affinity, trans-membrane communication, self-assembled tubes, and catalysis. Here we seek to control and understand deeply the binding affinity and selectivity of macrocycles and cryptand-like cages. We complement our understanding of these rigid systems with the shape-dynamic ones based on foldamers. Specifically, we present results from controlling the extent of photodriven switching of those properties. We have recently explored allosteric regulation of the photoactivity of foldamers, anion selective binding profiles, and the role of sequences on single-double foldamer preferences. Ongoing work focuses on solvent-driven changes in binding affinity as well as solvent-independent binding using capsules, and use of different photoswitches to enhance affinity switching. Future studies will involve small and simple targets for separation science, detailed understanding to underpin computer-aided design, and strategies to remove bottlenecks in synthesis and characterization.

DE-SC0002728: Binding Anions Selectively with Modular Triazolophanes and Releasing Them with Light

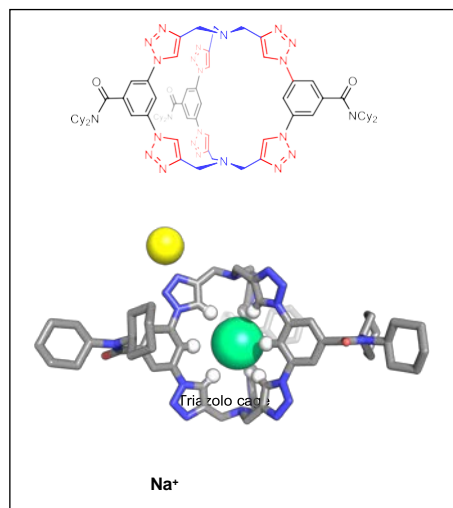
Postdoc(s): Zhao, W.

Student(s): Liu, Y.; Parks, F. C.; Stutsman, S. R.; Debnath, S.; Sengupta, A.; Qiao, B.; McDonald, K. P.; Anderson, J.

RECENT PROGRESS

Chloride capture using a C–H hydrogen-bonding cage

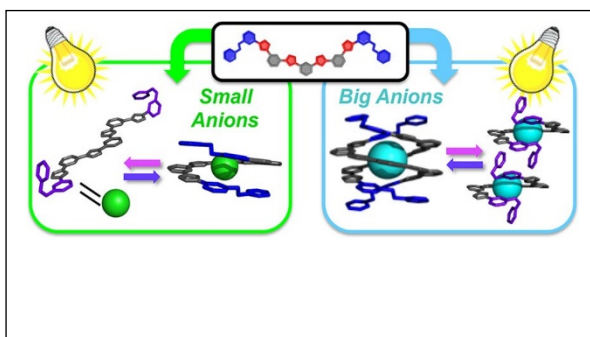
Tight binding and high selectivity are hallmarks of biomolecular recognition. Achieving these behaviors with synthetic receptors has usually been associated with OH and NH hydrogen bonding. Contrary to this conventional wisdom, we designed a chloride-selective receptor in the form of a cryptand-like cage (**Figure 1**) using only CH hydrogen bonding. Crystallography showed chloride stabilized by six short 2.7-angstrom



hydrogen bonds originating from the cage's six 1,2,3-triazoles. Attomolar affinity (10^{17} M^{-1}) was determined using liquid-liquid extractions of chloride from water into nonpolar dichloromethane solvents. Controls verified the additional role of triazoles in rigidifying the three-dimensional structure to effect recognition affinity and selectivity: $\text{Cl}^- > \text{Br}^- > \text{NO}_3^- > \text{I}^-$. This cage shows anti-Hofmeister salt extraction and corrosion inhibition.

Allosteric Control of Photofoldamers for Selecting between Anion Regulation and Double-to-Single Helix Switching

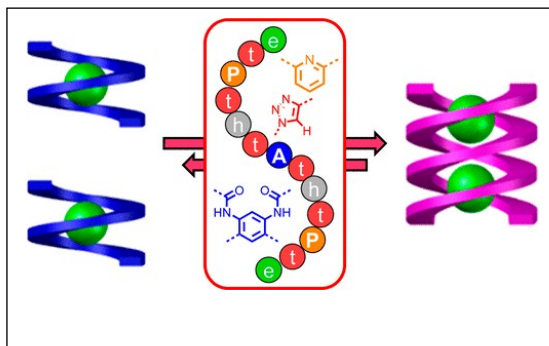
Allosteric regulation of protein structure and function is a hallmark of biology. The structures of protein-like abiological foldamers have been subject to allosteric control, however, regulation of their function is rare. We report this behavior (**Figure 2**) using a photoactive foldamer following the discovery that small and large anions select between single and double helical structures, respectively.



These anions activate different functions in the photo-foldamer; small anions turn on photoregulation of anion concentrations while large anions turn on chiroptical switching of quaternary structure. For this demonstration, we used an aryl-triazole based photofoldamer in which the light-driven *trans*-*cis* isomerization of azobenzenes alters intrastrand π - π contacts while the triazoles define the allosteric anion-binding site. Binding to 11 anions of increasing size was quantified (Cl^- , Br^- , NO_2^- , I^- , NO_3^- , SCN^- , BF_4^- , ClO_4^- , ReO_4^- , PF_6^- , SbF_6^-). Contrary to expectations that single helices will expand to accommodate larger and larger guests, this behavior only occurs for smaller anions (Cl^- to NO_3^- ; $<45 \text{ \AA}^3$) beyond which the larger anions form double helices (SCN^- to SbF_6^- ; $>45 \text{ \AA}^3$). With small anions, the single helix regulates anion concentrations when the azobenzenes are photoswitched. The binding of large anions favors a chiral double helix and activates light-driven switching into racemic single helices thereby modulating the quaternary structure and chiroptical activity. This work shows how complex multifunctional outcomes emerge when allosteric changes in structure are expressed in intrinsically functional foldamers.

Sequence-controlled Stimuli-responsive Single-Double Helix Conversion between 1:1 and 2:2 Chloride-Foldamer Complexes

The primary sequence in biopolymers carries the information to direct folded secondary structures, to modulate their stabilities, and to control the resultant functions. Our ability to encode such information into nonbiological oligomers



and polymers, however, is still limited. Here, we describe a C_2 -symmetric aryl-triazole foldamer that assembles into a chloride-templated 2:2 double helix, and the discovery that

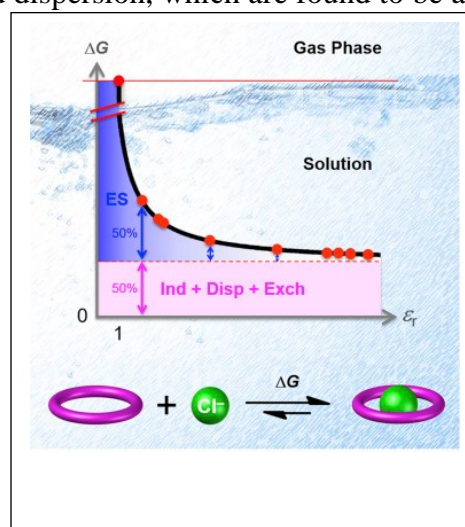
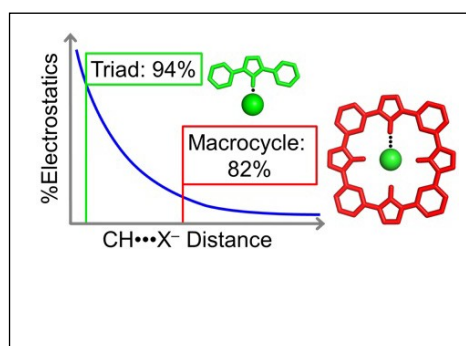
its interconversion with the simpler 1:1 single helix can be driven by solvent properties, temperature, and concentration (**Figure 3**). We use single-site substitutions in the 13-residue sequence (two terminal sites and one central site) to reveal that the stability of the double helix is largely dictated by the differences in the anion binding power between single and double helices as well as the location of the modified residues. Specifically, placement of stabilizing $\text{CH}\cdots\text{Cl}^-$ hydrogen-bonding interactions at the chain ends in the form of bisamide phenylene residues is found to highly favor the double helix. While the burial of π surfaces and the solvophobic effect also help to stabilize the double helix, their role was found to be less sensitive to the modifications considered. This understanding of how chemical information is programmed into the primary sequence provides a powerful tool for controlling structure and properties of abiological foldamers.

Anion-Binding Macrocycles Operate Beyond the Electrostatic Regime: Interaction Distances Matter

Anion recognition impacts many areas of chemistry and often relies on receptors with multiple hydrogen-bond donors. Previous studies of these donors in small molecules have long promoted the idea that electrostatic interactions alone correlate with association strength, yet this correlation has not been critically evaluated in the framework of larger, macrocyclic receptors. Here, we provide that assessment by evaluating how much electrostatics contributes to the gas-phase binding energy of macrocyclic receptors with various anions (**Figure 4**). Whereas small-molecule complexes behave as expected, we find that electrostatic interactions fail to accurately describe total binding energies of many common macrocyclic receptors: calix[4]pyrroles, dipyrrolyldiketones, indolocarbazoles, amido-pyrroles, triazolophanes, and cyanostars. This deviation arises from the fact that most macrocycles have multiple points of contact with the anion. Whereas the hydrogen-bond donors collectively stabilize the anion, the interaction distances are typically larger than equilibrium values seen with small molecules. This leads to increases in the relative contributions of the attractive components such as induction (e.g., induced dipoles) and dispersion, which are found to be as high as 32% for CH-donor based tricarbazole triazolophane complex with large polarizable ClO_4^- . This study augments previous observations of the importance of dispersion and induction towards anion binding of macrocyclic receptors in solution.

Anion Binding in Solution: Beyond the Electrostatic Regime

A fundamental understanding of anion binding by receptors is essential for managing salts during energy, water, and food production. However, the limited understanding of solvent effects in ion recognition leads to a persistent blind spot that prevents effective receptor design. We



experimentally discovered an underlying $1/\epsilon_r$ dependence of anion affinity on solvent dielectric constant (ϵ_r); see **Figure 5**. We found this relationship by measuring how chloride binds to macrocyclic triazolophane receptors across a wide range of solvents: $\epsilon_r = 4.7$ – 56.2 . Solvent weakens affinity by screening electrostatics; electrostatics dominates when $\epsilon_r < 4.7$ (chloroform) and then transits a cross-over region ($4.7 < \epsilon_r < 20.5$; acetone), after which it no longer governs affinity (acetonitrile and DMSO). Density functional theory helped us understand this dependence. Our theory-backed model accurately predicts Cl^- affinity in solvents used in liquid-liquid extractions in the nuclear fuel cycle. This model offers a general foundation for anion recognition and electrostatically driven complexation.

Publications Acknowledging this Grant in 2015 – 2019 are all exclusively funded by this grant

Publications supported by this project 2017-2019

- 7 Liu, Y.; Zhao, W.; Chen, C.-H.; Flood, A. H., Chloride capture using a C–H hydrogen-bonding cage, *Science* **2019**, *365*, 159-161. <http://doi.org/10.1126/science.aaw5145>
- 6 Parks, F. C.; Liu, Y.; Stutsman, S. R.; Debnath, S.; Raghavachari, K.; Flood, A. H., “Allosteric Control of Photofoldamers for Selecting between Anion Regulation and Double-to-Single Helix Switching, *J. Am. Chem. Soc.* **2018**, *140*, 17711-17723. <http://doi.org/10.1021/jacs.8b10538>
- 5 Liu, Y.; Parks, F. C.; Zhao, W.; Flood, A. H., “Sequence-controlled Stimuli-responsive Single-Double Helix Conversion between 1:1 and 2:2 Chloride-Foldamer Complexes” *J. Am. Chem. Soc.*, **2018**, *140*, 15477-15486. <http://doi.org/10.1021/jacs.8b09899>
- 4 Sengupta, A.; Liu, Y.; Flood, A. H., Raghavachari, Anion-binding Macrocycles Operate Beyond the Electrostatic Regime: Interaction Distances Matter, *Chem. Eur. J.* **2018**, *24*, 14409-14417. <https://doi.org/10.1002/chem.201802657>
- 3 Liu, Y.; Sengupta, A.; Raghavachari, K.; Flood, A. H., Anion binding in solution: Beyond the electrostatic regime, *Chem* **2017**, *3*, 411-427. **Cover Art.** <http://dx.doi.org/10.1016/j.chempr.2017.08.003>

Publications supported by this project 2015-2017

2. Flood, A. H., Creating molecular macrocycles for anion recognition, *Beilstein J. Org. Chem.* **2016**, *12*, 611-627. <http://dx.doi.org/10.3762/bjoc.12.60>
1. Qiao, B.; Sengupta, A.; Liu, Y.; McDonald, K. P.; Pink, M.; Anderson, J.; Raghavachari, K.; Flood, A. H., Electrostatic and Allosteric Cooperativity in Ion-pair Binding: A Quantitative and Coupled Experiment-Theory Study with Aryl-Triazole-Ether Macrocycles, *J. Am. Chem. Soc.* **2015**, *137*, 9746. <http://dx.doi.org/10.1021/jacs.5b05839>

Macrocycle-based Ion Pair Receptors Controlling Recognition, Extraction, Function, and Structure

Jonathan L. Sessler

Department of Chemistry, The University of Texas at Austin

Presentation Abstract

This BES has traditionally been used to support efforts to develop new ligands for the early actinide cations (Th, U, and Np) and receptors for ion pairs. The latter theme relates more closely to the area of separations and will be the primary focus of this presentation. Within the latter context, emphasis since the time of competitive renewal in 2016 has been placed on the development of pyrrolic and other macrocyclic systems that permit the specific recognition and competitive extraction of hard ions of interest to the DOE mission, including the lithium cation and the hydroxide and carbonate anions. Within the context of ion pair recognition, an effort has been made to control structure beyond the first coordination sphere. This has been done by creating systems whose polarity and hence morphology changes as a function of ion recognition, allowing for control over, e.g., micelle formation. Within this context, responsive polymeric systems that permit the capture of dianions and hydroxide anion have also been the subject of attention. Separately, several responsive recognition systems have been prepared with the view to being able to bind and release complex anions that have traditionally proved difficult to capture using synthetic receptors. These three broad themes are illustrated below.

Grant Number: DE-FG02-01ER15186 **Grant Title:** Functional Ion Pair Receptors-Targeting Cesium, Lithium, Sulfate, and Uranyl

Postdoc(s): Xiaodong Chi, Gretchen Marie Peters

Student(s): Inhong Hwang, James T. Brewster II, Harrison Root, Daniel Mangel

RECENT PROGRESS

Recognition and Extraction of Hard Ions

For many years our group has sought to develop so-called strapped calix[4]pyrroles as ion pair receptors. This approach has allowed for the creation of systems containing at least one anion recognition subunit (the calix[4]pyrrole NH protons) and one or more cation recognition sites (the straps and in certain instances the calixpyrrole aromatic "walls"). Since the time of the 2016 renewal, this generalized approach has been refined to target lithium salts and to extract the hard anions, hydroxide and carbonate, from simulated solid waste forms and from aqueous media. Again, this work will be reviewed in detail in this presentation. However, a brief overview is provided in Figure 1.

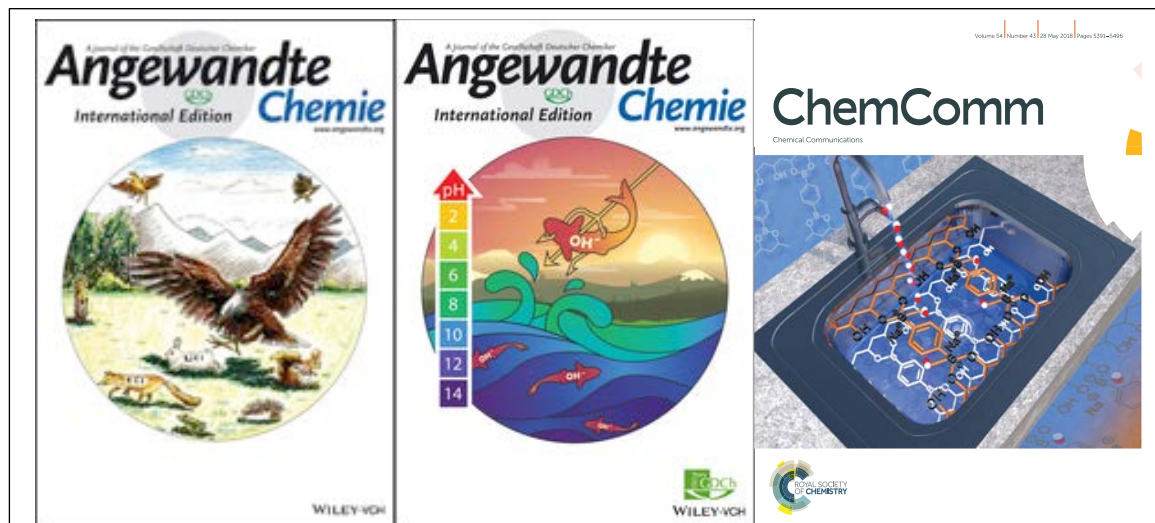


Figure 1. Cover images (inside front, inside back, and front, respectively) showing approaches that are being pursued to target hard ions, such as lithium, hydroxide, and carbonate. Images taken from *Angew. Chem. Int. Ed. Engl.* **2018**, *57*, 11924, *Angew. Chem. Int. Ed.* **2017**, *56*,

Controlling Structure Through Polymers and Micelles

Several approaches have been taken. These involve the creation of responsive polymers and receptor-functionalized molecules whose polarity and structure beyond the first coordination sphere is controlled through ion pair recognition. This will be detailed in the presentation with the schematics in Figure 2 highlighting several of the approaches taken.

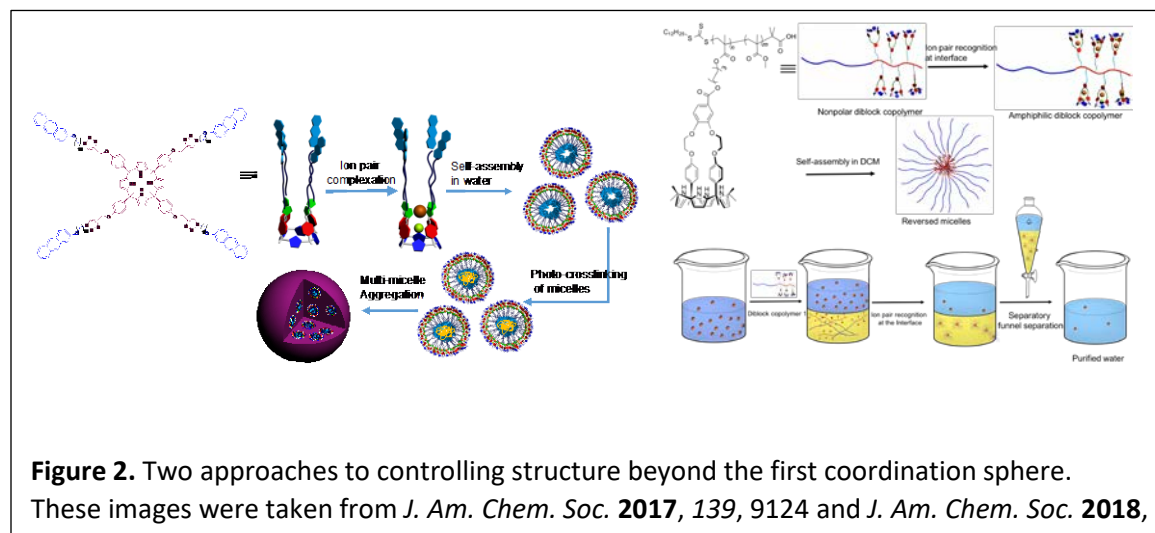
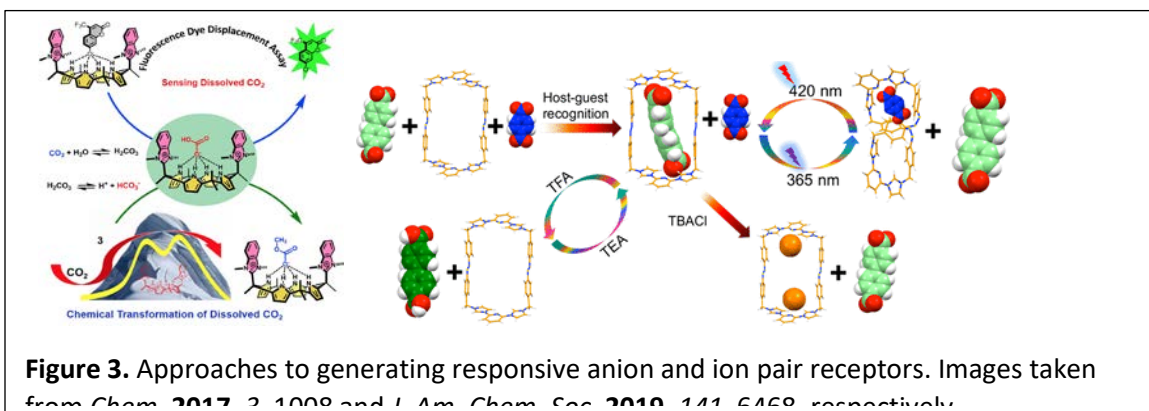


Figure 2. Two approaches to controlling structure beyond the first coordination sphere. These images were taken from *J. Am. Chem. Soc.* **2017**, *139*, 9124 and *J. Am. Chem. Soc.* **2018**,

Responsive Receptors

Recent progress has been made in creating receptors that respond to different stimuli, including chemical and energetic inputs, and using them to target potentially important anionic analytes. This progress is summarized in schematic fashion in Figure 3.



Publications Acknowledging this Grant in 2016 – present

Note: In 2017, the PI was promoted to the Doherty-Welch Chair at The University of Texas at Austin. The R.A. Welch Foundation now pays for 20% of the PI's academic year salary and is to be acknowledged on papers emerging from the PI's group. The papers in Category 2 below reflect this reality.

(IV) Exclusively funded by this grant:

Deliomeroğlu, M. K.; Lynch, V. M.; Sessler, J. L. "Non-cyclic formylated dipyrromethanes as phosphate anion receptors," *Chem. Sci.* **2016**, *7*, 3843–3850 DOI: 10.1039/c6sc00015k

Lee, J.; Waggoner, N. W.; Polanco, L.; You, G. R.; Lynch, V. M.; Kim, S. K.; Humphrey, S. M.; Sessler, J. L. "Ship in a breakable bottle: fluoride-induced release of an organic molecule from a Pr(III)-linked molecular cage," *Chem. Commun.* **2016**, *52*, 8514 – 8517 (cover). DOI: 10.1039/c6cc03471c

Sessler, J.; Vargas-Zúñiga, G. I.; Bähring, S. "Functionalized Calixpyrroles: Building Blocks for Self-Assembly," in Neri, P.; Wang, M.-X.; Sessler, J. L., Eds. *Calixarenes and Beyond*, Springer, 2016.

He, Q.; Zhang, Z.; Brewster, J. T.; Lynch, V. M.; Kim, S. K.; Sessler, J. L. "Hemispherand-strapped Calix[4]pyrrole: An Ion-pair Receptor for the Recognition and Extraction of Lithium Nitrite," *J. Am. Chem. Soc.* **2016**, *138*, 9779–9782. DOI: 10.1021/jacs.6b05713. Highlighted in "Extracting inorganic ions organically," Jyllian Kemsley, *C & E News*, **2016**, *94*(24), 18-19.

Yeon, Y.; Leem, S. J.; Wagen, C.; Lynch, V. M.; Kim, S. K.; Sessler, J. L. "A 3-(Dicyanomethylidene)indan-1-one Functionalized Calix[4]arene-Calix[4]pyrrole Hybrid: An Ion-Pair Sensor for Cesium Salts," *Org. Lett.* **2016**, *18*, 4396–4399. DOI: 10.1021/acs.orglett.6b02155

Brewster, J. T. II; He, Q.; Anguera, G.; Moore, M. D.; Ke, X.-S.; Lynch, V. M.; Sessler, J. L. "Synthesis and characterization of a dipyrriamethyrin-uranyl complex," *Chem. Commun.*, **2017**, *53*, 4981-4984. DOI: 10.1039/C7CC01674C

Kim, S. K.; Lee, H. G.; Vargas-Zúñiga, G. I.; Ju Hyun Oh, J. H.; Lynch, V. M.; Lee, M. H.; Sessler, J. L. "A fluorogenic calix[4]pyrrole with a small rigid strap showing different fluorescent responses to anions," *Supramol. Chem.* **2017**, *29*, 651-657. DOI: oi.org/10.1080/10610278.2017.1324624

Peters, G. M.; Chi, X.; Brockman, C.; Sessler, J. L. "Polyvinyl alcohol–boronate gel for sodium hydroxide extraction," *Chem. Commun.* **2018**, *54*, 5407-5409 (cover). DOI: 10.1039/c8cc02610f.

Deliomeroğlu, M. K.; Lynch, V. M.; Sessler, J. L. "Schiff-base appended polymers for phosphate removal," *Supramol. Chem.* **2018**, *30*, 807-821. DOI: 10.1080/10610278.2017.1372581.

Lee, J.; Brewster, J. T. II; Song, B.; Lynch, V. M.; Hwang, I.; Li, X.; Sessler, J. L. "Uranyl dication mediated photoswitching of a calix[4]pyrrole-based metal coordination cage," *Chem. Commun.* **2018**, *54*, 9422-9425 DOI: 10.1039/C8CC05160G

Chi, X.; Peters, G. M.; Brockman, C.; Lynch, V. M.; Sessler, J. L. "Controlling Structure Beyond the Initial Coordination Sphere: Complexation-Induced Reversed Micelle Formation in Calix[4]pyrrole-containing Diblock Copolymers," *J. Am. Chem. Soc.* **2018**, *140*, 13219–13222. DOI: 10.1021/jacs.8b09620

Brewster, J. T. II; Zafar, H.; Root, H. D.; Thiabaud, G. D.; Sessler, J. L. "Porphyrinoid f-Element Complexes," *Inorg. Chem.*, on line. DOI: 10.1021/acs.inorgchem.9b00884

(V) *Jointly funded by this grant and other grants with leading intellectual contribution from this grant:*

Vargas-Zuniga, G.; Sessler, J. L. "Pyrrole N-H Anion Complexes," *Coord. Chem. Rev.* **2017**, 345, 281–296. DOI: 10.1016/j.ccr.2017.04.004

Chi, X.; Peters, G. M.; Hammel, F.; Brockman, C.; Sessler, J. L. "Molecular Recognition Under Interfacial Conditions: Calix[4]pyrrole-based Cross-linkable Micelles for Ion Pair Extraction," *J. Am. Chem. Soc.* **2017**, 139, 9124–9127. DOI: 10.1021/jacs.7b04529.

Anguera, G.; Brewster, J. T. II; Moore, M.D.; Lee, J.; Vargas-Zúñiga, G. I.; Zafar, H.; Lynch, V. M.; Sessler, J. L. "Naphthylbipyrrole-Containing Amethyrin Analogue: A New Ligand for the Uranyl (UO₂²⁺) Cation," *Inorg. Chem.* **2017**, 56, 9409–9412. DOI: 10.1021/acs.inorgchem.7b01668.

He, Q.; Peters, G. M.; Lynch, V. M.; Sessler, J. L. "Recognition and Extraction of Cesium Hydroxide and Carbonate by using a Neutral Multitopic Ion-Pair Receptor," *Angew. Chem. Int. Ed.* **2017**, 56, 13396–13400 (inside back cover). DOI: 10.1002/anie.201705788

Mulugeta, E.; He, Q.; Saren, D.; Hong, S. J.; Oh, J. H.; Lynch, V. M.; Sessler, J. L.; Kim, S. K.; Lee, C. H. "Recognition, Sensing, and Trapping of the Bicarbonate Anion using a Dicationic *meso*-bis(Benzimidazolium) Calix[4]pyrrole," *Chem*, **2017**, 3, 1008–1020. DOI: <http://dx.doi.org/10.1016/j.chempr.2017.10.007>

Thiabaud, G.; Radchenko, V.; Wilson, J. J.; John, K. D.; Birnbaum, E. R.; Sessler, J. L. "Rapid insertion of bismuth radioactive isotopes into texaphyrin in aqueous media," *J. Porphyr. Phthalocyn.* **2017**, 21, 882–886. DOI: 10.1142/S1088424617500870.

Brewster, J. T., III.; Aguilar, A.; Anguera, G.; Zafar, H.; Moore, M. D.; Sessler, J. L. "Synthesis and Characterization of an Amethyrin-Uranyl Complex Displaying Aromatic Character," *J. Coord. Chem.* **2018**, 71, 1808–1813 (Dan Meyerstein Special Issue). DOI: 10.1080/00958972.2018.1458230.

He, Q.; Williams, N. J.; Oh, J. H.; Lynch, V. M. Kim, S. K.; Moyer, B. A.; Sessler, J. L. "Selective Solid–liquid Extraction and Liquid–liquid Extraction of Lithium Chloride using Strapped Calix[4]pyrroles," *Angew. Chem. Int. Ed. Engl.* **2018**, 57, 11924–11928 (inside cover). DOI: 10.1002/anie.201805127.

Chi, X.; Cen, W.; Queenan, J. A.; Long, L.; Lynch, V. M.; Khashab, N. M.; Sessler, J. L. "Azobenzene-Bridged Expanded "Texas-sized" Box: A Dual-Responsive Receptor for Aryl Dianion Encapsulation," *J. Am. Chem. Soc.* **2019**, 141, 6468–6472. DOI: 10.1021/jacs.9b01241.

Brewster, J. T. II; Root, H. D.; Mangel, D.; Samia, A.; Zafar, H.; Sedgwick, A. C.; Lynch, V. M.; Sessler, J. L. "UO₂²⁺-Mediated ring contraction of pyrihexaphyrin: Synthesis of a contracted expanded porphyrin-uranyl complex," *Chem. Sci.* **2019**, 10, 5596–5602. DOI: 10.1039/C9SC01593K

Oh, J. H.; Kim, J. H.; Kim, D. S.; Han, H. J.; Lynch, V. M.; Sessler, J. L.; Kim, S. K. "Synthesis and Anion Recognition Features of a Molecular Cage Containing Both Hydrogen Bond Donors and Acceptors," *Org. Lett.* **2019** 21, 4336–4339. DOI: 10.1021/acs.orglett.9b01515.

(VI) *Jointly funded by this grant and other grants with relatively minor intellectual contribution from this grant:*

He, Q.; Vargas-Zúñiga, Kim, S. H.; Kim, S. K.; Sessler, J. L. "Macrocycles as Ion Pair Receptors," *Chem. Rev.*, online. DOI: 10.1021/acs.chemrev.8b00734

Ji, X.; Chi, X.; Ahmed, M.; Long, L.; Sessler, J. L. "Soft Materials Constructed Using Calix[4]pyrrole- and "Texas-Sized" Box-based Anion Receptors," *Acc. Chem. Res.*, online. DOI: 10.1021/acs.accounts.9b00187.

Principles of Chemical Recognition and Transport in Extractive Separations: The Iminoguanidinium Group as Versatile Oxoanion Recognition Unit

Bruce A. Moyer, Vyacheslav Bryantsev, Radu Custelcean, and Santa Jansone-Popova
Chemical Sciences Division, Oak Ridge National Laboratory

Presentation Abstract

This research integrates experimental and computational science to understand the principles of molecular recognition primarily in the context of anion separations in crystallization, ion exchange, and liquid-liquid systems. Targeting oxoanions as representative model anions, receptor structures delivering parallel dual H-bonding motifs have been under investigation, evolving from ureas to guanidiniums and, most recently, to iminoguanidiniums. The latter offer synthetic versatility as well as remarkable preorganization and selectivity, whether used in the context of liquid-liquid or solid-liquid systems. Case studies will be presented for selective sulfate extraction, uptake of various oxoanions by ionic covalent organic frameworks, and carbon dioxide capture from air.

ERKCC08: Principles of Chemical Recognition and Transport in Extractive Separations

Postdoc(s): Neil J. Williams, Alexander Ivanov, Santanu Roy

Student(s): Pierrick Agullo, Flavien Brethome, Kathleen A. Garrabrant, Antoine Konter, Charles A. Seipp

RECENT PROGRESS

Guanidinium Groups as Anion-Recognition Motifs

Although a variety of H-bonding groups can in principle be utilized for anion binding and separation, most of them are too weak to compete in competitive aqueous environments. The guanidinium group stands out among them, as it offers a distinct edge-binding motif based on parallel organization of H-bonds that is particularly conducive to recognition of oxoanions (1). It was realized early achieving directional and cooperative anion binding with simple guanidinium-based receptors lies in the ability to control their intrinsic conformational flexibility. While this elegantly accomplished by locking the guanidinium subunit within a rigid bicyclic framework, poor synthetic accessibility hindered progress. Stabilization of pseudocyclic species through intramolecular H-bonds offers an alternative strategy via design of a persistent pseudo-bicyclic

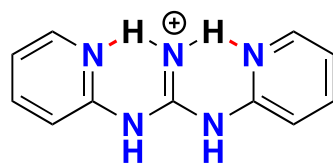
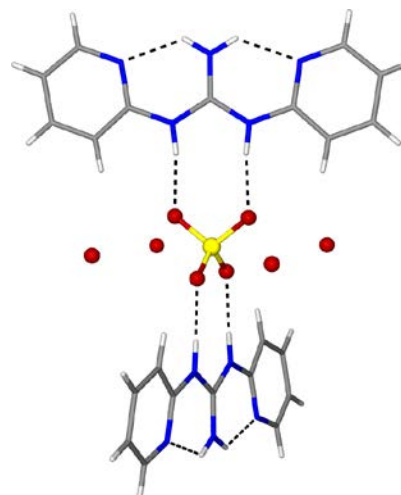


Figure 1. Bispyridyl-guanidinium featuring pseudocyclic motif (above) and its binding to sulfate in a crystalline tetrahydrate structure, O-atoms shown in red (right) (Seipp, 2015, 7017)



two
(Fig.
on by
that

was

framework based on the *N,N'*-bis(2-pyridyl)guanidinium system (Seipp, 2015, 2017). This internal buttressing resulted in the desired parallel H-bonds along a sulfate O–S–O edge and corresponding strong preference for sulfate both in homogeneous solution and liquid-liquid extraction (Seipp, 2017). More recently, a simple iminoguanidinium motif for aqueous oxoanion recognition and separation incorporating a similar pseudocyclic framework has been developed in our group (Custelcean, 2015; Williams 2018). Besides its synthetic accessibility, this novel anion-binding motif presents a number of advantages, including its propensity for a rigid and planar conformation ideally suited for π -stacking, which promotes crystallization and increased H-bond donor strength.

Anion Separation with Diiminoguanidinium (DIG) Extractants

Lipophilic diiminoguanidinium (DIG) anion exchangers have proven to be remarkably selective for sulfate anion in liquid-liquid extraction. This finding was all the more remarkable because the DIG extractants are simple monofunctional H-bond donors (Fig. 2). Since it proved synthetically difficult to incorporate our bis(pyridyl)guanidinium (Fig. 1) into more elaborate multitopic anion receptors, we shifted our attention to the more tractable iminoguanidinium chemistry that was growing out of the crystallization research in our program (Custelcean, 2015, 2016). Reacting diaminoguanidine with two equivalents of a lipophilic aldehyde led directly to the DIG compound in high yield, as shown in Figure 2 (Williams, 2018). Its extraction selectivity for sulfate over chloride was over five orders of magnitude greater than for a simple quaternary ammonium anion exchanger not capable of H-bonding. A crystal structure of a truncated DIG analog showed multiple H-bond interactions with sulfate. Reverse-micelle behavior of DIG chloride was indicated by small-angle X-ray scattering and a high-water content of the organic phase.

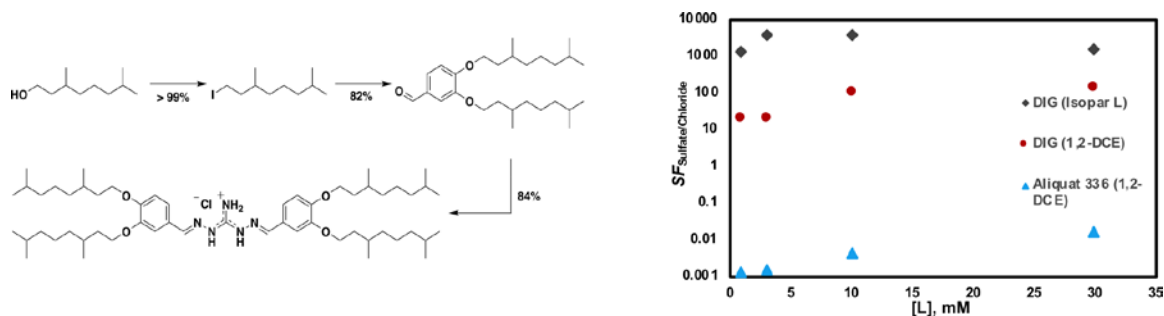


Figure 2. Synthesis of DIG and its separation factor for sulfate over chloride in liquid-liquid extraction as compared with the quaternary ammonium anion exchanger Aliquat 336.

Anion Separation with Ionic Covalent Organic Frameworks (iCOFs)

Given the remarkable selectivity imparted to liquid-liquid extraction by the iminoguanidinium group, it was of interest to examine whether similar selectivity could be captured in solid ion-exchange materials bearing the iminoguanidinium group in fixed positions. In pursuing this idea, we discovered a novel class of materials, ionic COFs (BT-DGCl, Fig. 3), with unparalleled affinity for chromium(VI) oxoanions (Jansone-Popova, 2018). The recognition is predominantly driven by electrostatic forces and strong H-bonding interactions between the tetrahedral oxoanion and positively charged DIG moiety incorporated in the COF. Although, the framework can bind a variety of tetrahedral oxoanions (MoO_4^{2-} , SO_4^{2-} , SeO_4^{2-} , HAsO_4^{2-}), these are displaced by Cr(VI) oxoanions when present in solution, even at very low concentrations (<100 ppb). The new material rapidly lowers the Cr(VI) concentration in water from 1 ppm to 10 ppb level, an order of magnitude below the US Environmental Protection Agency maximum contaminant level. Additionally, the material releases the sequestered oxoanion with adjustment of the solution pH. We foresee the acidity of guanidinium unit as well as its structural role in the framework (2D vs 3D, distance

among the binding sites, etc.) will have a profound effect on the performance of iCOFs in selective sequestration of oxoanions.

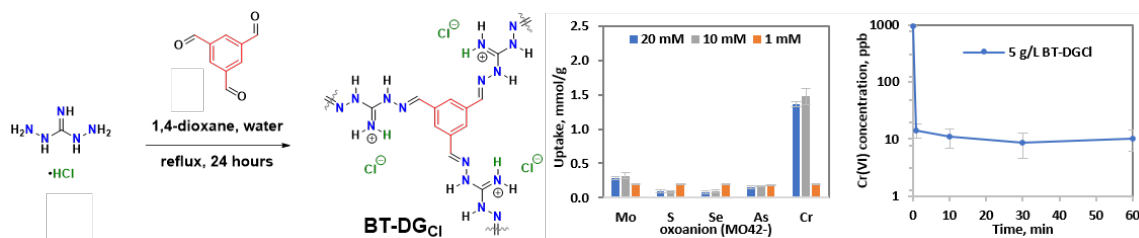


Figure 3. Selective recognition of Cr(VI) oxoanions using an ionic COF, **BT-DGCl**.

CO₂ Separation by Bis-Iminoguanidinium (BIG) Carbonate Crystallization

Given the selective affinity of the iminoguanidinium group for sulfate, the possibility of binding carbonate was a leading question with ramifications for climate change. This line of inquiry led to a new approach to CO₂ capture from flue gas or air based on crystallization of bis-iminoguanidinium (bi)carbonate salts (Seipp 2017; Brethome, 2018; Garrabrant, 2019). The chemical cycle consists of three steps: 1) CO₂ absorption with aqueous amino acids, such as glycine or sarcosine, yielding the corresponding (bi)carbonate salts; 2) crystallization of the carbonate anions with a bis(iminoguanidine) (BIG) solid, which regenerates the amino acid; and 3) solid-state CO₂ release from the carbonate crystals and regeneration of the BIG (Fig. 4). This crystallization-based approach to CO₂ capture combines the benefits of aqueous sorbents, such as relatively fast CO₂ absorption rates with the advantages of solid-state sorbents, such as lower energy and temperature

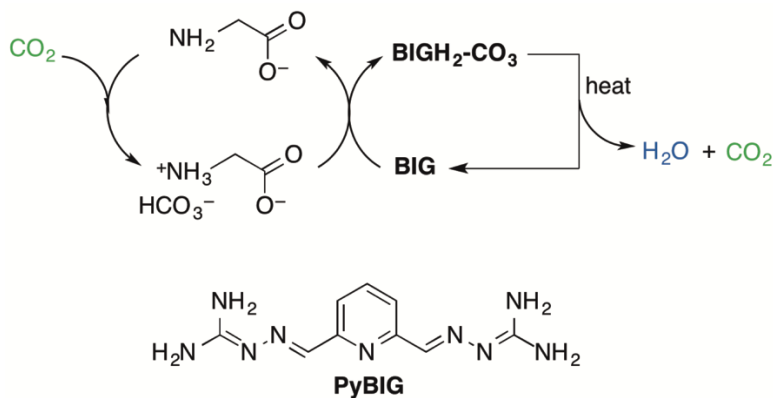


Figure 4. CO₂ capture by absorption with aqueous amino acids and carbonate crystallization with BIGs.

requirements and minimal sorbent loss through evaporation. In the prototype system, we employed 2,6-pyridine-bis(iminoguanidine) (PyBIG), which crystallized with CO₂ as a hydrated carbonate salt (PyBIGH₂(CO₃)(H₂O)₄) of very low aqueous solubility (on a par with CaCO₃), attributed in part to the strong H-bonds involving the carbonate, guanidinium, and water in the crystals (Gianopoulos, 2019). The CO₂ release from PyBIG-CO₃ can be done at much lower temperatures (80–120 °C) vs inorganic carbonates (e.g., CaCO₃ requires 900 °C), which we surmise is a consequence of completely different reaction mechanism of CO₂ release involving proton transfer along the guanidinium-carbonate hydrogen bonds, with the formation of carbonic acid intermediate (Williams, 2019).

Publications Acknowledging this FWP in 2015–present

(I) Exclusively funded by this grant

1. Custelcean, R.; Williams, N. J.; Seipp, C. A. Aqueous Sulfate Separation by Crystallization. *Angew. Chem. Int. Ed.* **2015**, *54*, 10525- 10529. [Journal Cover]
2. Seipp, C. A.; Williams, N. J.; Bryantsev, V. S.; Custelcean, R.; Moyer, B. A. A Conformationally Persistent Pseudo-Bicyclic Guanidinium for Anion Coordination, as Stabilized by Dual Intramolecular Hydrogen Bonds. *RSC Advances* **2015**, *5*, 107266-107269.
3. Custelcean, R.; Williams, N. J.; Seipp, C. A.; Ivanov, A. S.; Bryantsev, V. S. Aqueous Sulfate Separation by Sequestration of $[(\text{SO}_4)_2(\text{H}_2\text{O})_4]^{4-}$ Clusters within Highly Insoluble Imine-Linked Bis-Guanidinium Crystals. *Chem. Eur. J.* **2016**, *22*, 1997-2003. [Journal Cover]
4. Williams, N. J.; Bryantsev, V.; Custelcean, R.; Seipp, C. A.; Moyer, B. A. $\alpha, \alpha', \alpha'', \alpha'''$ Meso-Tetrahexyltetramethyl-Calix[4]Pyrrole: An Easy-to-Prepare, Isomerically Pure Anion Extractant with Enhanced Solubility in Organic Solvents. *Supramol. Chem.* **2016**, *28*, 176-187.
5. Seipp, C. A.; Williams, N. J.; Custelcean, R. Sulfate Separation by Selective Crystallization with a Bis-Iminoguanidinium Ligand. *Journal of Visualized Experiments* **2016**, *115*, e54411.
6. Seipp, C. A.; Williams, N. J.; Kidder, M. K.; Custelcean, R. CO₂ Capture from Ambient Air by Crystallization with a Guanidine Sorbent. *Angew. Chem. Int. Ed.* **2017**, *56*, 1042-1045.
7. Brethome, F. M.; Williams, N. J.; Seipp, C. A.; Kidder, M. K.; Custelcean, R. Direct Air Capture of CO₂ via Aqueous-Phase Absorption and Crystalline-Phase Release Using Concentrated Solar Power. *Nature Energy* **2018**, *3*, 553-559.
8. Williams, N. J.; Seipp, C. A.; Garrabrant, K. A.; Custelcean, R.; Holguin, E.; Keum, J. K.; Ellis, R. J.; Moyer, B. A. Surprisingly Selective Sulfate Extraction by a Simple Monofunctional Di(imino)guanidinium Micelle-Forming Anion Receptor. *Chem. Commun.* **2018**, *54*, 10048-10051.
9. Jansone-Popova, S.; Moinel, A.; Schott, J. A.; Mahurin, S. M.; Popovs, I.; Veith G. M.; Moyer, B. A. Guanidinium-Based Ionic Covalent Organic Framework (iCOF) for Rapid and Selective Removal of Toxic Cr(VI) Oxoanions from Water. *Environ. Sci. Technol.*, **2018**, *53* (2), 878-883. [Journal Cover]
10. Williams, N. J.; Seipp, C. A.; Brethome, F. M.; Ma, Y.-Z.; Ivanov, A. S.; Bryantsev, V. S.; Kidder, M. K.; Martin, H. J.; Holguin, E.; Garrabrant, K. A.; Custelcean, R. CO₂ Capture via Crystalline Hydrogen-Bonded Bicarbonate Dimers. *Chem* **2019**, *5*, 719-730.
11. Williams, N. J.; Custelcean, R. CO₂ Capture Going BIG. *Carbon Capture Journal* **2019**, *68*, Mar/Apr, 4-6.
12. Williams, N. J.; Roy, S.; Reynolds, C. O.; Custelcean, R. Bryantsev, V. S.; Moyer, B. A. Enhancing Selectivity of Cation Exchange with Anion Receptors. *Chem. Commun.* **2019**, *55*, 3590-3593.

(II) Jointly funded by this grant and other grants with leading intellectual contribution from this grant

1. Jia, C.; Zuo, W.; Yang, D.; Chen, Y.; Cao, L.; Custelcean, R.; Hostas, J.; Hobza, P.; Glaser, R.; Wang, Y.-Y.; Yang, X.-J.; Wu, B. Selective Binding of Choline by a Phosphate-

Coordination-Based Triple Helicate Featuring an Aromatic Box. *Nature Commun.* **2017**, 938.

2. Gianopoulos, C. G.; Chua, Z.; Zhurov, V. V.; Seipp, C. A.; Wang, X.; Custelcean, R.; Pinkerton, A. A. Direct Air Capture of CO₂ – Topological Analysis of the Experimental Electron Density (QTAIM) of the Highly Insoluble Carbonate Salt of 2,6-Pyridine-bis(iminoguanidine), (PyBIGH₂)(CO₃)(H₂O)₄. *IUCrJ* **2019**, 6, 56-65.
3. Huang, Z.; Jia, C.; Wu, B. Jansone-Popova, S.; Seipp, C. A.; Custelcean, R. Selective Binding of (Thio)sulfate and Phosphate in water by Quaternary Ammonium Functionalized Oligo-Ureas. *Chem. Commun.* **2019**, 55, 1714-1717.
4. Garrabrant, K. A.; Williams, N. J.; Holguin, E.; Brethome, F. M.; Tsouris, C.; Custelcean, R. Energy-Efficient CO₂ Capture from Flue Gas by Absorption with Amino Acids and Crystallization with a Bis-Iminoguanidine. *Ind. Eng. Chem. Res.* **2019**, 58, 10510-10515. **[Journal Cover]**

(III) *Jointly funded by this grant and other grants with relatively minor intellectual contribution from this grant*

1. Wang, J. C.; Aswartham, S.; Ye, F.; Terzic, J.; Zheng, H.; Haskel, D.; Chikara, S.; Choi, Y.; Schlottmann, P.; Custelcean, R.; Yuan, S. J.; Cao, G. Decoupling of the Antiferromagnetic and Insulating States in Tb-doped Sr₂IrO₄. *Phys. Rev. B*, **2015**, 92, 214411.
2. Sefat, A. S.; Li, L.; Cao, H. B.; McGuire, M. A.; Sales, B.; Custelcean, R.; Parker, D. S. Anomalous Magneto-Elastic and Charge Doping Effects in Thallium-Doped BaFe₂As₂. *Scientific Reports* **2016**, 6:21660.
3. Stack, A. G.; Stubbs, J. E.; Srinivasan, S. G.; Roy, S.; Bryantsev, V. S.; Eng, P. J.; Custelcean, R.; Gordon, A. D.; Hexel, C. R. Mineral-Water Interface Structure of Xenotime (YPO₄) {100}. *J. Phys. Chem. C* **2018**, 122, 20232.
4. Hachtel, J. A.; Huang, J.; Popovs, I.; Jansone-Popova, S.; Keum, J.; Jakowski, J.; Lovejoy, T. C.; Dellby, N.; Krivanek, O. L.; Idrobo, J. C. Identification of Site-Specific Isotopic Labeling in Amino Acids by Vibrational Spectroscopy in the Electron. *Science*, **2019**, 363, 525-528.
5. Ivanov, A. S.; Parker, B. F.; Zhang, Z.; Aguila, B.; Ma, S.; Jansone-Popova, S.; Arnold, J.; Mayes, R. T.; Dai, S.; Bryantsev, V. S.; Rao, L.; Popovs, I. Siderophore-inspired chelator hijacks uranium from aqueous medium. *Nature Comm.*, **2019**, 10, 819.

PI ABSTRACTS SESSION II: INTERFACES

X-ray studies of molecular ordering at the liquid/liquid interface in solvent extraction

Mark L. Schlossman¹ and Ilan Benjamin²

¹ Department of Physics, University of Illinois at Chicago, Chicago, IL 60607, USA

² Department of Chemistry and Biochemistry, University of California at Santa Cruz, Santa Cruz 95064, USA

Presentation Abstract

During solvent extraction, amphiphilic extractants assist the transport of metal ions across the liquid-liquid interface between an aqueous solution and an organic solvent. Complexation of metal ions and extractants is believed to take place at or near the organic-aqueous interface, though different authors have suggested that the extractant binds metal ions either in the aqueous phase near the interface, or in the organic phase near the interface, or at the interface itself. Largely missing from earlier investigations of this interfacial complexation has been the application of experimental techniques that can locate and characterize metal ions, extractants, and ion-extractant complexes in the liquid-liquid interfacial region, though recent X-ray studies have begun to do just that. These studies apply X-ray scattering techniques that characterize the spatial arrangement of ions and molecules at the interface with a resolution that can be as low as several angstroms depending upon the technique and the sample. X-ray fluorescence methods can identify elements at the interface and determine their interfacial density. This presentation will describe recent X-ray studies of model systems relevant to lanthanide extraction. These results suggest a connection between the observed interfacial structures and the extraction mechanism, which ultimately affects the extraction kinetics.

DE-SC0018200: The Role of Molecular Ordering at the Liquid/Liquid Interface in Solvent Extraction

PI: Mark Schlossman (PI), Ilan Benjamin (co-PI)

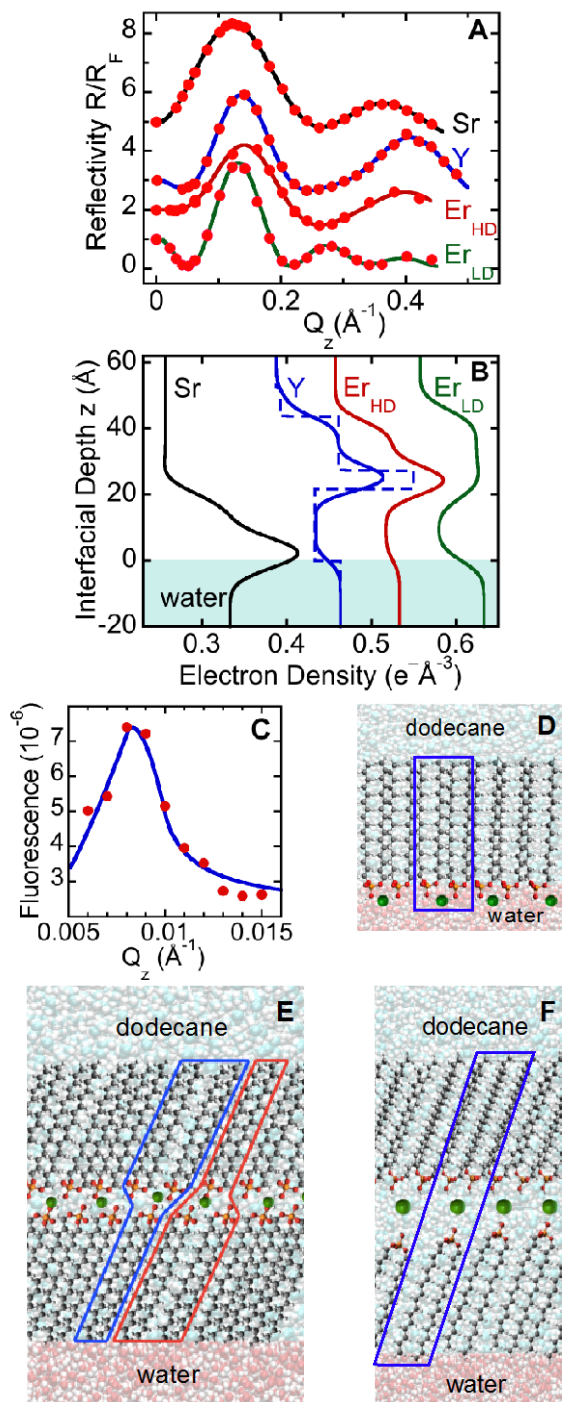
Student(s): Zhu Liang

RECENT PROGRESS

A nanoscale view of assisted ion transport across the liquid-liquid interface

Interface-sensitive X-ray scattering and fluorescence techniques were used to locate and identify interfacial species in model extraction systems. Our experimental system consisted of a macroscopically flat liquid-liquid interface between a dilute, acidic aqueous solution of metal chlorides (where the metal ion is Y(III), Er(III), or Sr(II)), and a dilute organic solution of the extractant DHDP ($[\text{CH}_3(\text{CH}_2)_{15}\text{O}]_2\text{POOH}$, bis(hexadecyl) phosphoric acid, 10^{-4} M) in *n*-dodecane ($\text{CH}_3(\text{CH}_2)_{10}\text{CH}_3$). Figure 1 illustrates data and intermediate states in the extraction process of Er(III), Y(III) and Sr(II).

Figure 1. (A) The variation of X-ray reflectivity $R(Q_z)$ with wave vector transfer Q_z normalized to the Fresnel reflectivity $R_F(Q_z)$, as measured from the interface between metal (Y, Er, or Sr) chlorides in water (pH 2.5 for Y and Er, pH 5.3 for Sr) and 10^{-4} M DHDP in dodecane (upper three curves shifted for clarity). Curves labeled Er_{HD} and Er_{LD} refer to two different interfacial structures: the high-density and low-density Er interfaces described below. Lines are the best fits to the model electron density profiles shown in panel (B) (right three curves shifted for clarity). The profiles are rounded as the result of capillary wave roughness of the interface; the dashed line for Y shows an example of the underlying zero-roughness profile. (C) X-ray fluorescence near total internal reflection (XFNTR) data (dots) and analysis (line) for the YCl_3 sample. (D-F) Cartoon representations of the interfacial structures with zero interfacial roughness. (D) Monolayer with Sr(II). (E) Hypothetical (not observed) maximum density inverted bilayer. (F) Low density (LD) inverted bilayer of DHDP with Er(III). High density (HD) inverted bilayers containing Y(III) or Er(III) consist of a configuration intermediate to those shown in (E) and (F). Red and blue boxes identify the ion-extractant complexes.



One such intermediate state in the extraction process consisted of supramolecular yttrium-extractant or erbium-extractant complexes condensed at the interface into an inverted bilayer structure in the form of a 2-dimensional layer of Y or Er ions sandwiched between two layers of extractant (Fig. 1F). The detailed analysis of the data and justification for the structures shown in Fig. 1 are presented in Ref. (1). Similar experiments with strontium ions revealed, instead, a conventional monolayer of extractants with bound Sr ions located on the aqueous-side of the interface, with no obvious route to transfer ions into the organic phase (Fig. 1D). Nevertheless, extraction was observed for Y, Er, and Sr, though a larger fraction of the lanthanides was extracted.

Classical molecular dynamics (MD) simulations were used to investigate the stability of the inverted bilayer structure. Figure 2A shows the last frame of this simulation and Fig. 2B shows the time-averaged electron density profile. Both illustrate the qualitative features of the measured electron density profiles of the high-density inverted bilayers containing Y and Er (Fig. 1B), namely, a high-density peak from the headgroups and metal ions, with shoulders from the DHDP tailgroups in the upper and lower leaflets of the bilayer. The experimental electron density profiles

appear more disordered because they are roughened by capillary waves at the interface, which have a much smaller effect on profiles calculated from small simulation boxes.

These simulations were designed to test the stability, but not the formation, of the low-density Er inverted bilayer. They demonstrated that the structure of the inverted bilayer is stable at the interface for the 100 ns span of the simulation, with occasional motion of dodecane molecules between the two leaflets.

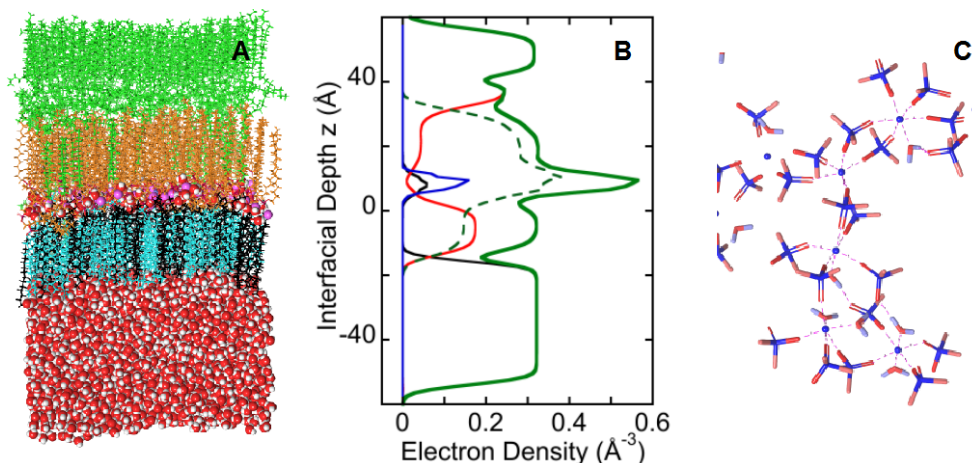


Figure 2 MD simulation results. (A) Snapshot of inverted bilayer from the last frame of the simulation – water (bottom, red and white), dodecane (top, green), inverted bilayer: ions in blue, dodecane that started in the top leaflet is shown in green, dodecane that started in the bottom leaflet is colored cyan, DHDP molecules that started in the top leaflet are colored gold, and DHDP that started in the bottom leaflet are colored black. Topmost layer of dodecane is ordered at the vapor interface, which is not relevant for comparison to the results of X-ray measurements. A smaller, disordered layer of dodecane exists immediately adjacent to the inverted bilayer. (B) MD electron density profile averaged over the final 100 ns of the simulation: total density profile in solid green, water in black, dodecane in red, Er ions in blue, DHDP in dashed green. (C) Er coordination showing only DHDP headgroups and water molecules.

Our results demonstrate that Y(III) and Er(III) are more effective at coordinating with DHDP than Sr(II). For instance, the formation of inverted bilayers containing Y(III) and Er(III), as well as their extraction at temperatures above the adsorption transition T_0 , were observed with pH 2.5 water for which 94% of the phosphoric acid headgroups would have been protonated and uncharged in the absence of metal ions. However, Sr(II) binding to the charge neutral DHDP monolayer under similar low pH conditions was not observed. Instead, Sr(II) binding was observed only at higher pH, with one Sr(II) for every two DHDP measured at pH 5.3 and higher pH values. Even under these conditions of Sr saturation of the interface, combined X-ray reflectivity and XFNR results show that approximately one third of the interfacial Sr(II) ions are not closely bound to the DHDP headgroups, but exist only in a diffuse electrical double layer near the interface.²

Y(III) and Er(III) are also more efficiently extracted from the aqueous phase than Sr(II). Analysis of the metal content in the aqueous phase before and after extraction by inductively coupled plasma atomic emission spectroscopy (ICP-AES) and ICP mass spectroscopy showed that 87(3)% of the Y(III) was extracted at 50 °C, more than 80% of the Er(III) was extracted at 55 °C, but only 45% of Sr(II) was extracted at 50 °C (pH 5.3).

The interfacial state of Y(III) and Er(III) sandwiched between layers of DHDP extractants suggests the prompt transfer of these cations from the aqueous side of the liquid-liquid interface to a coordinated ion-extractant environment on the organic side. These ion-extractant complexes represent an intermediate state in which ions have been transported across the aqueous-organic interface, but have not yet been dispersed in the organic phase. In contrast to this, the observation of a conventional monolayer of DHDP extractants with Sr(II) bound to DHDP headgroups, but remaining in contact with the water phase, suggests a slower kinetics of transfer of Sr(II) from water to dodecane, whose mechanism involves at least one additional step to transport the ion across the aqueous-organic interface. Although further studies are required to identify this additional step in the transport of Sr(II), it appears plausible to hypothesize that the monolayer configuration observed for Sr(II) acts to retard the process.

(1) Liang, Z.; ... Benjamin, I.; Schlossman, M. L. A Nanoscale View of Assisted Ion Transport across the Liquid-Liquid Interface. *Proceedings of the National Academy of Sciences (USA)* **2018**, published online; DOI: 10.1073/pnas.1701389115.

(2) Bu, W.; ... Schlossman, M. L. X-Ray Studies of Interfacial Strontium-Extractant Complexes in a Model Solvent Extraction System. *J. Phys. Chem. B* **2014**, *118*, 12486-12500.

Publications Acknowledging this Grant in 2015 – present

- (II) Liang, Z.; Bu, W.; Schweighofer, K. J.; Jr., D. J. W.; Harvey, J. S.; Hanlon, G. R.; Amoanu, D.; Erol, C.; Benjamin, I.; Schlossman, M. L. A Nanoscale View of Assisted Ion Transport across the Liquid-Liquid Interface. *Proceedings of the National Academy of Sciences (USA)* **2018**, published online; DOI: 10.1073/pnas.1701389115.
- (II) Bu, W.; Schlossman, M. L. X-ray Studies of Liquid Interfaces in Model Solvent Extraction Systems. In *Ion Exchange and Solvent Extraction*; Moyer, B. A., Ed.; CRC Press: New York, **2019**; Vol. 23; pp 115-146.

Solvent Extraction - Interfacial Chemistry and Phase Separation

Aurora E. Clark, Michael J. Servis, Zhu Liu, Nitesh Kumar
Department of Chemistry, Washington State University
Pacific Northwest National Laboratory

Presentation Abstract

Hierarchical structural organization and collective motions are an essential element of solvent extraction process chemistry. The focus of our work is to understand and rigorously quantify such multiscale correlations to provide a predictive understanding of solution conditions that favor specific process attributes. Using both molecular simulation as well as new analysis algorithms, this work will discuss how mechanisms of solute transport are modulated by solution conditions. Surfactants have the ability to accentuate or dampen interfacial roughness and in turn alter speciation and chemical reaction pathways. The unique chemical composition at the interface can further lend itself to phase instabilities – so called 3rd phase formation. New graph theoretical algorithms have been developed that distinguish between aggregation phenomena of 3rd phase formation that best align with microemulsion vs. molecular solution chemistry.

Grant or FWP Number: The interfacial chemistry of solvent extraction: Predictive insight into mechanisms and kinetic regimes for actinide separations

PI: Aurora E. Clark

Postdoc(s): Michael Servis, Zhu Liu

Student(s): Nitesh Kumar

Affiliations(s): Department of Chemistry, Washington State University

RECENT PROGRESS

Phase separation and phase transitions of aqueous:organic binary solutions. Liquid/liquid phase transitions are inherent to multicomponent solutions, which often contain a diversity of intermolecular interactions between their molecular constituents. In one such example, a phase transition is observed in liquid/liquid extraction where the nonpolar organic phase separates into two phases under sufficiently high metal and acid extraction by the amphiphilic extractant molecule. This deleterious phenomenon, known as third phase formation, complicates processing and limits efficiency. While empirically well documented, the molecular origin of this phenomenon is not understood. The prevailing conceptualization of organic phase solutions treats them as a microemulsion where extractant molecules form reverse micelles that contain the extracted aqueous solutes in their polar cores. Yet recent studies indicate that a microemulsion paradigm is insufficient to describe molecular aggregation in some solvent extraction systems, implying that an alternative description of aggregation and explanation for third phase formation

is needed. We have recently demonstrated that the formation of a third phase is consistent with crossing the liquid-liquid miscibility gap for a molecular solution rather than a Winsor II to Winsor III transition as presumed in the microemulsion paradigm. This insight is provided by using a graph theoretic methodology, generalizable to other complex multicomponent molecular solutions, to identify the onset of phase splitting. This approach uses connectivity obtained from molecular dynamics simulation to correlate the molecular-scale association to their phase behavior using percolation theory. The method is applied

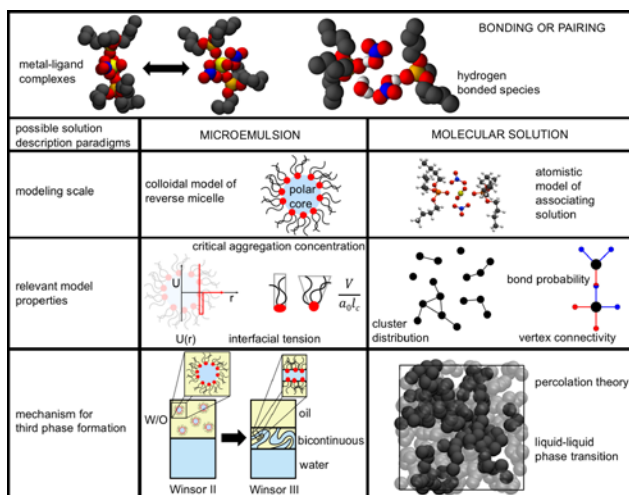


Figure 2. Two different models for third phase formation.

to investigate a solvent extraction system relevant to ore purification and used nuclear fuel recycling: tri-n-butyl phosphate/uranyl nitrate/water/nitric acid/n-dodecane. In analogy to a molecular solution, immediately preceding the liquid-liquid coexistence curve from the single phase region, the metal-ligand complexes percolate. This demonstrates that describing this solution with microemulsion chemistry is neither applicable here nor broadly required to explain third phase formation. This study provides a method for predicting third phase formation phase boundaries from simulation for this and potentially other solvent extraction systems.

Interfacial Structure and Transport Reactivity.

A) Water/Octanol Interfaces. In ongoing work, we are exploring how different solvent combinations influence interfacial properties. Of particular interest is the water and aqueous electrolyte interface with octanol and octanol/non-polar solvent mixtures. Octanol has the unique ability act as both a surfactant and have bulk solvent effects that influence interfacial characteristics. We have recently demonstrated that the water/octanol interface is less heterogeneous than the interface of water with non-polar solvents like hexane. The instantaneous interface of water/octanol exhibits significant interdigitation of water and octanol molecules – in turn this dampens capillary wave characteristics and the differences in environments of capillary crests vs. troughs.

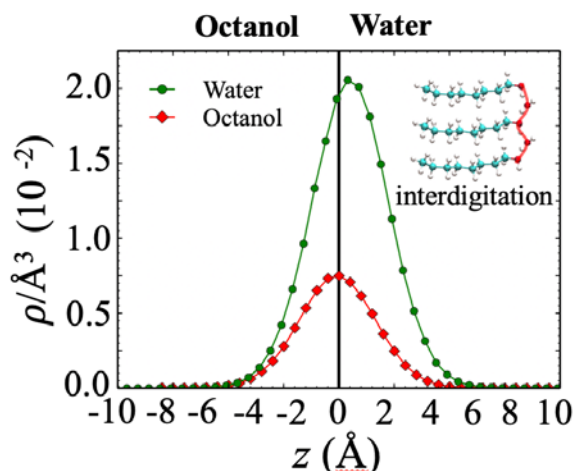


Figure 3. Density profile of truly interfacial water and octanol molecules, illustrating overlap and interdigitation.

Octanol also has the ability to form a bilayer-like structure at the interfaces that significantly alters water uptake. Unlike protrusion-based mechanisms for water transport into non-polar solvents, bilayer formation presents an alternative mechanism for water transport into octanol solutions. We observe distinct correlations in water uptake in regions of the interface that exhibit bilayer “islands” in the interface.

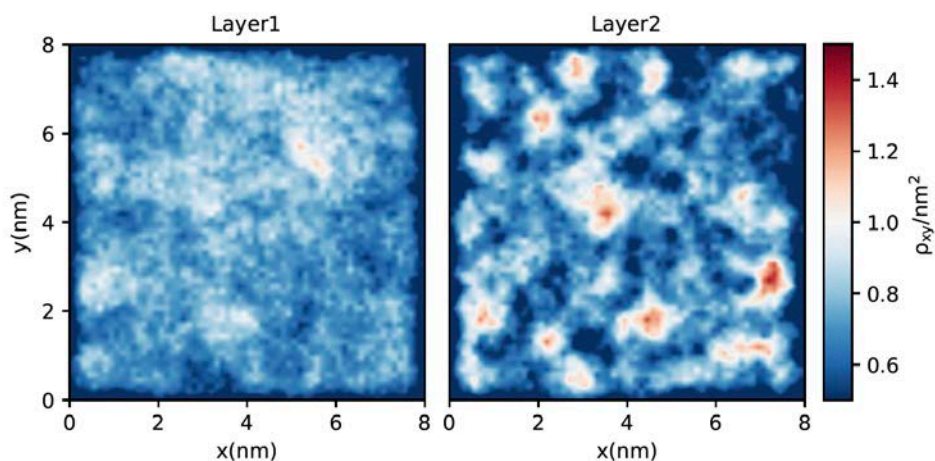


Figure 4. Octanol density maps of the truly interfacial layer (layer 1) and the 2nd interfacial layer that forms islands of “bilayer” like structure.

B) Electrolyte/Octanol Interfaces. The impact of interfacial heterogeneity upon ion adsorption and metal-ligand complexation is currently under study. In preliminary work we demonstrate that ions preferentially adsorb to trough regions of a rough interface, and further, that the solvation environments of ions are distinctly different in trough vs. crest regions. Interfaces that exhibit little variation in crest vs. trough regions (i.e. water/octanol) do not exhibit such preferential behavior nor changes to the interfacial solvation environment.

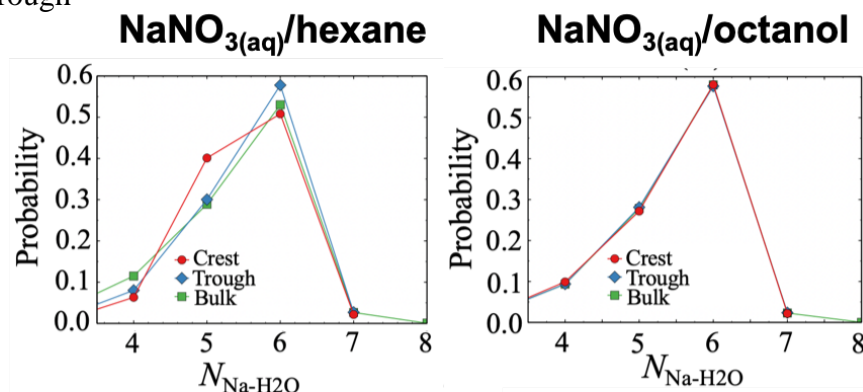


Figure 5. Na cation solvation in different interfacial conditions.

**Publications
Acknowledging this
Grant in 2015 – present**

(I) Exclusively funded
by this grant;

Ghadar, Y.; Christiansen, S. L.; Clark, A. E. Influence of Aqueous Ionic Strength Upon Liquid:Liquid Interfacial Structure and Dynamics, *Fluid Phase Equilibria*, **2016**, *407*, 126-134. *Invited article – special issue Aqueous Solutions: Bulk Fluids and Interfaces.*

Clark, A. E.; Samuels, A.; Wisuri, K.; Landstrom, S.; Saul, T. Sensitivity of Solvation Environment to Oxidation State and Position in the Early Actinide Period, *Inorganic Chemistry*, **2015**, *54*, 6216-6225.

Ghadar, Y.; Parmar, P.; Samuels, A.; Clark, A. E. Solutes at the Liquid:Liquid Phase Boundary – Solubility and Solvent Conformational Response Alter Interfacial Microsolvation Reactions, *Journal of Chemical Physics*, **2015**, *142*, 104707.

Clark, A. E. Intermolecular Network Theory: A General Approach for Understanding the Structural and Dynamic Properties of Liquids and Solutions. In *Annual Reports in Computational Chemistry*; Dixon, D. A., Ed.; **2015**; pp 313–359

(II) *Jointly funded by this grant and other grants with leading intellectual contribution from this grant;*

Servis, M. J.; Wu, D. T.; Shafer, J. C.; Clark, A. E. Reimagining third phase formation as the miscibility gap of a molecular solution. *Chemical Science*. **2019**, *submitted*.

Kelley, M. P.; Yang, P.; Clark, S. B.; Clark, A. E. Competitive Interactions Within Cm(III) Solvation in Binary Water/Methanol Solutions, *Inorganic Chemistry*, **2018**, *57*, 10050-10058.

Servis, M.; Wu, D.; Shafer, J.; Clark, A. E. Square supramolecular assemblies of uranyl complexes in organic solvents, *Chemical Communications*, **2018**, *54*, 10064 – 10067.

Zhou, T.; McCue, A.; Ghadar, Y.; Bako, I.; Clark, A. E. On the Behavior of Capillary Wave Fronts and Their Role in Defining Interfacial Regions of Water, *Journal of Physical Chemistry B*, **2017**, *121*, 9052 – 9062.

Freiderich, J.; Burn, A.; Leigh, M.; Nash, K.; Clark, A. E. A Combined Density Functional Theory and Spectrophotometry Study of the Bonding Interactions of $[\text{NpO}_2\text{M}]^{4+}$ Cation-Cation Complexes, *Inorganic Chemistry*, **2017**, *56*, 4788–4795

Kelley, M. P., Yang, P.; Clark, S. B.; Clark, A. E. Structural and Thermodynamics Properties of the Curium(III) Ion Solvated by Water and Methanol. *Inorganic Chemistry*, **2016**, *55*, 4992-4999.

Kelley, M.; Donley, A.; Clark, S.; Clark, A. E. Structure and Dynamics of NaCl Ion Pairing in Solutions of Water and Methanol *Journal of Physical Chemistry B* **2015**, *119*, 15652-15661.

(III) *Jointly funded by this grant and other grants with relatively minor intellectual contribution from this grant;*

Servis, M.; Liu, Z.⁺; Martinez-Baez, E.; Su, J.; Stetina, T.; Wildman, A.; Newcomb, K.⁺; Autshbach, J.; Dixon, D. A.; Maginn, E. J.; Batista, E. R.; Yang, P.; Li, X.; Clark, A. E. Solvent Extraction Through the Lens of Advanced Modeling and Simulation, in Ion Exchange and Solvent Extraction, **2018**, *In Press*, Ed. Bruce Moyer, *CRC Press*.

Clark, A. E.; Braley, J.; Yang, P. Coordination of Actinides and the Chemistry Behind Solvent Extraction, *Experimental and Theoretical Approaches to Actinide Chemistry*, Wiley, **2018**, DOI: 10.1002/9781119115557.ch5 ISBN: 978-1-119-11552-6.

Rock, W.; Qiao, B.; Zhou, T.; Clark, A. E.; Uysal, A. Heavy Anion Complex Creates a Unique Water Structure at a Soft Charged Interface, *J. Phys. Chem. C*, **2018**, *122*, 29228-29236.

Kelley, M. P.; Davis, A.; Clowers, B.; Clark, A. E.; Clark, S. B. Acceleration of Metal-Ligand Complexation Kinetics by Electrospray Ionization. *The Analyst*, **2017**, *142*, 4468-4475. DOI: 10.1039/C7AN01142C

Linking Self-Assembly and Organization at Liquid/Liquid Interfaces to Selective Chemical Separations using Nonlinear Spectroscopy

Benjamin Doughty

Chemical Sciences Division, Oak Ridge National Laboratory, Oak Ridge, TN, 37831,
USA

Abstract:

The interface between two liquids is a hotspot for self-assembly and anomalous chemical processes that ultimately dictate how species adsorb, order, and react. These key mechanistic steps ultimately dictate how molecules are transported from one phase to another and how chemical specificity is manifested on the molecular level, which differs greatly from the bulk. Despite the widespread interest in understanding these interfacial phenomena, particularly for applications in chemical separations, the fundamental events governing selectivity and efficiency are not well understood. A key barrier to obtaining this insight is the current inability to directly probe the structure and dynamics of the molecularly thin interface using conventional methods without being overwhelmed by signals originating from the neighboring bulk phases. In this talk I will detail new results using surface specific vibrational sum frequency generation spectroscopy that link molecular self-assembly, interfacial hydrogen bonding, molecular ordering, and orientation to selective chemical separations at an interface *during* extraction. Taking advantage of intrinsic optical polarization control and high time-resolution we are able to obtain equilibrium structural insight into ligand ordering at the interface as a function of bulk pH, but also watch in real time as that interface transforms during the extraction of a model divalent cation. These results highlight the importance of ligand preorganization as moderated by unique interfacial hydrogen bonding structures assumed in the aqueous phase. Our findings reveal new insight into the chemical and physical phenomena taking place at these complex interfaces that govern selectivity in chemical separations and molecular transport.

Interfacial Structure and Dynamics in Separations

Grant E. Johnson, Venky Prabhakaran, and Vanda Glezakou
Pacific Northwest National Laboratory, Richland, Washington 99352

Abstract

Underlying performance metrics that are used to evaluate the efficiency of different separation media are molecular-level phenomena such as ion coordination, solvent confinement, double layer formation at interfaces, hydrophobicity, and electric field-driven solvent structuring and ion transport. For example, in graphene oxide laminates, the influence of what is thought to be the main factor determining ion selectivity, the size of the interlayer transport channels, is actually the result of complex interactions including differences in ion coordination, solvation, changes in the coordination environment, and changes in free energies due to nanoconfinement. Our research makes use of unique capabilities that enable precise control over matter, to prepare extremely well-defined model systems with which to investigate the molecular-level interactions underlying the selectivity and efficiency of potentially transformative materials for separating ions from liquids. Specifically, we are studying interlayer transport through channels in graphene oxide laminates and electric potential-driven separations at solvated interfaces containing ionic liquid domains. Ion soft landing, a versatile surface modification approach, provides unprecedented control over the composition of model separation systems and avoids the solvent, counterions, and contaminants that often complicate experiments on less-defined samples prepared using conventional bulk methods. A combination of characterization techniques including *in-situ* infrared reflection-absorption (IRRAS), Raman spectroscopy, and electrochemistry are employed to study the local structural changes of solvation shells and double layers in nanoconfinement, under applied electric fields, and in structured hydrophobic domains. High-level molecular simulations are also used as a powerful cross-cutting tool to describe key physical properties and how they change over time with temperature, pressure, and environment.

Grant or FWP Number: Interfacial Structure and Dynamics in Ion Separations, FWP 47327

PI: Grant E. Johnson, Vanda Glezakou, Venky Prabhakaran

Postdoc(s): Eric Baxter, Jun Zhang

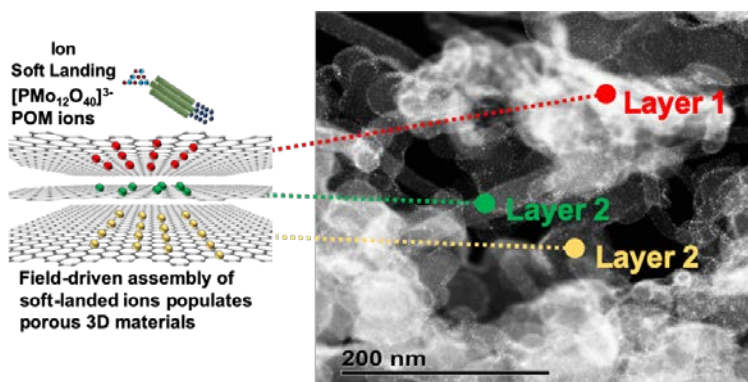
Student(s): N/A

Affiliations(s): Same as above

RECENT PROGRESS

Separation of Solvated Species in Nanoconfined Environments

We achieved electric field-driven assembly of soft landed ions in porous 3D carbon hosts opening up new exciting opportunities for precise control of the spacing of the interlayer transport channels in graphene oxide laminates that are used for separation of ions from liquids. Precise control over these transport channels will enable us to explore how nanoconfinement influences selective separation of ions from liquids.



Publications Acknowledging this Grant in 2018 – present

(I) *Exclusively funded by this grant;*

P. Su, V. Prabhakaran, **G.E. Johnson**, J. Laskin, *In situ* Infrared Spectroelectrochemistry for Understanding Structural Transformations of Precisely-Defined Ions at Electrochemical Interfaces, *Anal. Chem.* **2018**, 90, 10935.

(II) *Jointly funded by this grant and other grants with leading intellectual contribution from this grant;*

V. Prabhakaran, Z. Lang, A. Clotet, J. M. Poblet, **G.E. Johnson**, J. Laskin, Controlling the Activity and Stability of Electrochemical Interfaces Using Atom-by-Atom Metal Substitution of Redox Species, *ACS Nano* **2019**, 13, 458.

J. Laskin, **G.E. Johnson**, J. Warneke, V. Prabhakaran, From Isolated Ions to Multilayer Functional Materials Using Ion Soft - Landing, *Angew. Chem. Int. Ed.* **2018**, 57, 16270.

G. E. Johnson, V. Prabhakaran, N. D. Browning, B. L. Mehdi, J. Laskin, P. A. Kottke, and A. G. Fedorov, DRILL Interface Makes Ion Soft Landing Broadly Accessible for Energy Science and Applications, *Batteries & Supercaps* **2018**, 1, 97.

(III) *Jointly funded by this grant and other grants with relatively minor intellectual contribution from this grant;*

None

PI ABSTRACTS SESSION III: POSTER SESSION

Combinatorial Membrane Synthesis: Fundamentals of Hybrid Metal-Organic Brush (MOB) Membranes for Organic Solvent Nanofiltration (Renewal)

Weiwei Xu and Pranav Ramesh and Georges Belfort,

Howard P. Isermann Department of Chemical and Biological Engineering,
Rensselaer Polytechnic Institute, Troy, NY 12180; P: 518.276.6948; E: belfog@rpi.edu

Presentation Abstract

The goals of our current 2-year research project is to produce, characterize and simulate dense hydrophobic brushes onto a non-selective membrane supports. So far, we report three seminal discoveries: (a) Formed a stable non-swelling, non-selective support layer through crosslinking, and modelled and optimized the activators regenerated by electron transfer (ARGET)-atom transfer radical polymerization (ATRP) reaction cascade with combinatorial methods to graft a series of polymer brushes (AIM 1). (b) Initiated, modeled and tested an alternative, faster, “greener” and simpler grafting method called single-electron transfer (SET)-living radical polymerization (LRP) (AIM 1 extended). (c) Formed *in situ* metal organic frameworks (MOFs, e.g. HKUST-1) into the void spaces of a brush layer and measured filtration performance. Rose Bengal rejection of > 90% in ethanol was obtained with a SET-LRP- grafted polymer brush on crosslinked polyimide membrane with and without MOFs. However, the permeability was two times higher with MOFs than without them (AIM 2). Our **Preliminary Results** demonstrate that we can produce a solvent stabilized P84 polyimide support membrane, graft alkyl methacrylate branched brushes thereon, form *in situ* HKUST-1 MOFs within the brush structure, replace ARGET-ATRP with SET-LRP, and obtain encouraging filtration results. The next step is to correlate the structural properties of these brush membranes with OSN performance.

Grant Number: DE-FG02-09ER16005

Grant Title: Combinatorial Membrane Synthesis: Fundamentals of Hybrid Metal-Organic Brush (MOB) Membranes for Organic Solvent Nanofiltration (Renewal)

PI: Georges Belfort (PI)

Postdoc(s): Dr Mirco Sorci and Dr Weiwei Xu

Student(s): Graduate Students: John J. Keating IV, Pranav Ramesh, Undergraduate students: Alex Lee

Affiliations(s): Howard P. Isermann Department of Chemical and Biological Engineering, RPI, Troy, NY 12180.

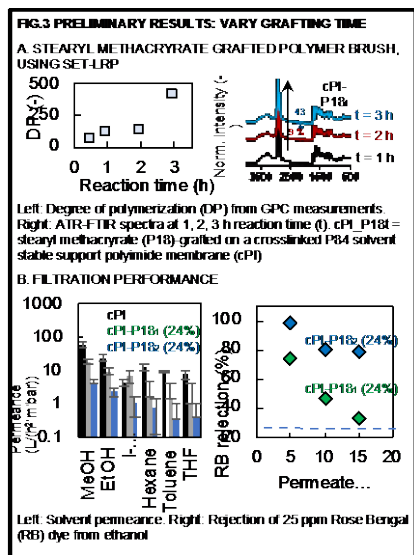
RECENT PROGRESS

A. Summary:

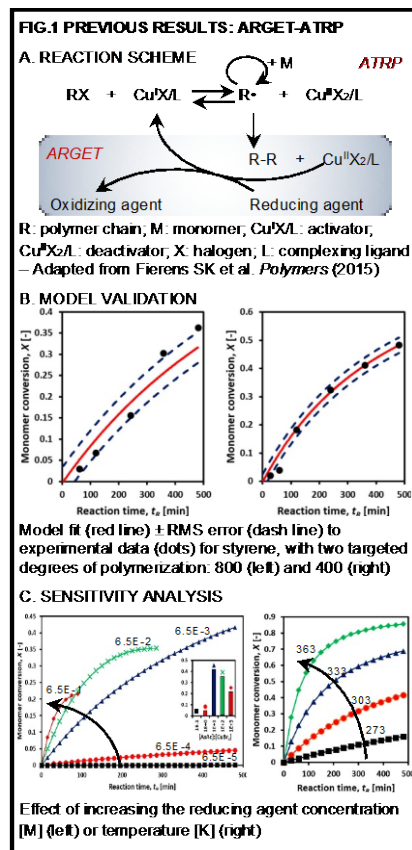
(a) Goals: The goals of our current 2-year research project were to produce, characterize and simulate dense hydrophobic brushes onto a non-selective membrane supports (e.g. poly(ether sulfone) (PES)).

(b) Approach: The aspects of the research were to: (i) graft hydrophobic monomers to PES using two methods: the activators regenerated by electron transfer (ARGET) - atom transfer radical polymerization (ATRP) reaction cascade, (ii) use a multitude of analytical techniques to characterize the brush microstructure and dynamic behavior; and (iii) to embed or form MOFs within the void spaces of brush membranes.

(c) Findings: Selected findings from the past year are summarized below (papers resulting from this work are listed below).



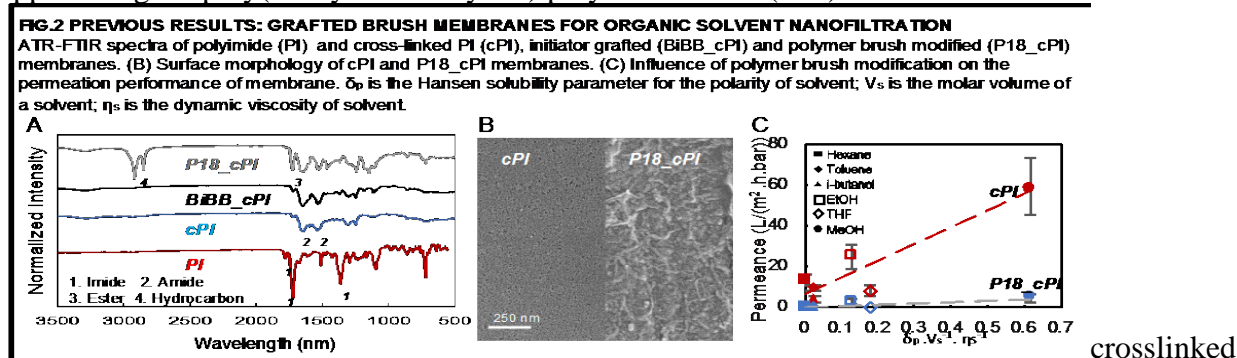
(i) *Mathematical modeling (ARGET-ATRP)*: We developed a simplified model to follow the temporal conversion of monomer to polymer using the *ARGET-ATRP* reaction cascade[1] (**Fig. 1A**). The main assumptions were that termination reactions occur through radical coupling only and the propagation and termination reaction rates are chain length



independent. The model was first verified against published experimental data for methacrylate, styrene (**Fig. 2B**) and glycidyl methadrylate monomers: Conversion trajectories were accurately described within the fit \pm RMSE, especially up to 0.4. This simplified model can be utilized by researchers to design experiments to target a given conversion for a specific monomer at a specified temperature. A sensitivity analysis was also conducted (**Fig. 3C**). Based on these results, the [catalyst]:[initiator] and [reducing agent]:[catalyst] ratios were shown to be critical parameters in the *ARGET-ATRP* mechanism, with optimal values on the order of 0.1:1 and 10:1, respectively. Moreover, adding sacrificial initiator in order to increase the concentration of dormant species when grafting from surfaces was necessary to prevent loss of control and premature halting of the polymerization. Finally, increasing the *ARGET-ATRP* reaction temperature was the most viable way to increase polymerization rate while maintaining high attainable conversions.

(ii) *Mathematical modeling (SET-LRP)*: Analogous to the method described above, we have implemented a MATLAB reaction scheme for SET-LRP[2] based on the reaction model. The model is compared with data from the literature[3] and a manuscript is in preparation[4].

(iii) *Grafting brush membranes for organic solvent nanofiltration*: SET-LRP method was applied to graft poly(stearyl methacrylate) polymer brushes (P18) on



polyimide (cPI) membranes. **Fig. 2A** shows the ATR-FTIR spectra of a cPI membrane before (blue curve) and after (grey curve) polymer brush modification, the ester and hydrocarbon stretch peaks observed at 1726 and 2918 cm^{-1} , respectively, indicate successful grafting of polymer

brushes on membrane surface. The SEM image (**Fig. 2B**) shows that, after polymerization, cPI membrane was covered with a layer of brush like structures, which further confirmed the existence of P18 brushes on membrane surface. The performance of polymer brush grafted cPI membranes (P18_cPI) was evaluated by measuring the permeance of 6 organic solvents (**Fig. 2C**) and followed with dye rejection tests, although the permeance of membrane dropped significantly after polymer brush modification, P18_cPI membrane still possessed MeOH permeance of $\sim 5 \text{ L}\cdot\text{m}^{-2}\cdot\text{h}^{-1}\cdot\text{bar}^{-1}$, and Rose Bengal rejection that increased from 30% to 61%.

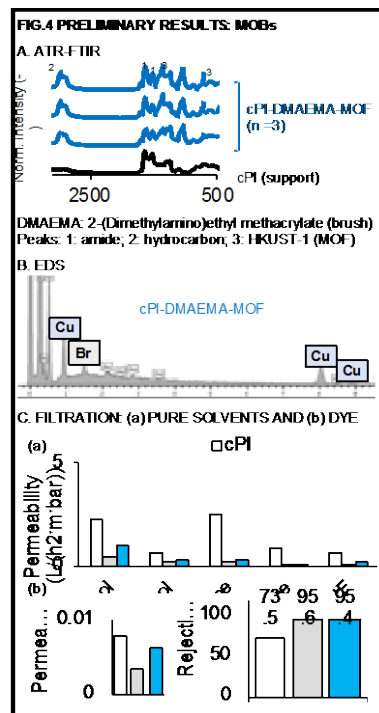
(iv) *In situ formation of MOF (HKUST-1):*

Most of our previous work involved forming brush branched membranes with ARGET-ATRP (**Fig. 1**), while initial research with SET-LRP is presented (**Fig. 2**). Although the 2 methods involve similar chemistry, SET-LRP starts with solid copper Cu(0) instead of dissolved Cu(I) and is thus faster, “greener” and a simpler grafting method than ARGET-ATRP. The preliminary experimental results are also shown in **Figs. 2** and **3**[5]. Hence, SET-LRP was used to graft brushes of stearyl methacrylate onto a crosslinked solvent-stable polyimide porous non-rejecting support membrane. Grafting was confirmed with ATR-FTIR, XPS and FESEM, and the degree of grafting ($DP = Mn/MW_{\text{unit}}$, where Mn is the number average molecular weight of homopolymer, MW_{unit} is the molecular weight of each repeating unit ($\text{C}_{21}\text{H}_{40}\text{O}_2$, 324 g/mol) was tracked (**Fig. 3A**). Reaction time was used to vary the degree of polymerization and hence filtration performance such as the permeance of six organic solvents and > 98% rejection of Rose Bengal in ethanol (**Fig. 3B**). The characterization and filtration data presented in **Fig. 4** demonstrate that MOFs (HKUST-1) were successfully incorporated into a 2-(Dimethylamino)ethyl methacrylate (DMAEMA) polymer brush with promising filtration results. The FTIR spectra identified the presence of both the DMAEMA brush and HKUST-1 MOFs (**Fig. 4A**). The presence of the Br-initiator (BiBB) and the Cu in HKUST-1 were confirmed in the EDS spectrum (**Fig. 4B**). Two types of filtration results are presented in **Fig. 4C** including: (a) five organic solvents and (b) 25 ppm Rose Bengal in ethanol. The membranes include the crosslinked support polyimide (cPI, control), a DMAEMA brush membrane (cPI_DMAEMA), and DMAEMA brush membrane containing a HKUST-1 MOFs (cPI_DMAEMA_MOF). The grafting of the brush improved the rejection over the control cPI, while the addition of the MOFs improved the rejection over the control cPI and the permeability over the brush membrane by a factor of ~ 2 .

Publications Acknowledging this Grant in 2016 – present

(VII) *Exclusively funded by this grant;*

- a. Keating IV, JJ., Imbrogno, J., Belfort, G. Brushes for Membrane Separations: A Review, *ACS Appl Mater Inter*, 2016, DOI:10.1021/acscami.6b09068
- b. Keating, IV, JJ, Lee A, Belfort G. Predictive Tool for Experimental Design and Analysis of ARGET-ATRP Grafting Reactions, *Macromolecules*, 2017, DOI:10.1021/acs.macromol.7b01572
- c. Keating IV, JJ, Kocsis, I, Sorci, M, Setaro, A, Underhill, PT, Barboiu, M., Belfort, G. Atmospheric Pressure Plasma – ARGET ATRP Modification of



Poly(ether sulfone) Nanofiltration Membranes: A Combination Attack, *J Membr Sci*, 2018, DOI: 10.1016/j.memsci.2017.10.014

(VIII) *Jointly funded by this grant and other grants with leading intellectual contribution from this grant;*

- a. Imbrogno, J, Keating IV, JJ., Kilduff, J, Belfort, G. Critical aspects of RO desalination: A combination strategy, *Desalination*, 2016, DOI:10.1016/j.desal.2016.06.033.

(IX) *Jointly funded by this grant and other grants with relatively minor intellectual contribution from this grant;*

- a. Tian, Y., Zonca Jr, MR, Imbrogno, J, Unser, AM., Sfakis, L, Temple, S. Belfort, G, Xie, Y. Polarized, Cobblestone, Human Retinal Pigment Epithelial Cell Maturation on a Synthetic PEG Matrix, *ACS Biomater Sci Eng* 2017, DOI:10.1021/acsbiomaterials.6b00757. This grant supported PES modification, but not the subsequent cell attachment characterization on these membranes.
- b. Mihailescu, M., Sorci, M., Seckute, J., Silin, V. I., Hammer, J., Perrin, Jr., B. S., Hernandez, J. I., Smajic, N., Shrestha, A., Bogardus, K. A., Greenwood, A. I., Fu, R., Blazyk, J., Pastor, R. W., Nicholson, L. K., Belfort, G., and Cotton, M. Structure and Function in Antimicrobial Piscidins: Histidine Position, Directionality of Membrane Insertion, and pH-Dependent Permeabilization *JACS*, 2019, DOI: 10.1021/jacs.9b00440. This grant supported experiments using QCM-D and SPR.

(X) **Patents applications:**

- a. Belfort, G., Grimaldi, J., Imbrogno, J., Kilduff, J., Keating J.J., Synthetic membranes and methods of use thereof, International Publication # WO 2016/077827 A1, May 19th, 2016.
- b. Sally Temple, Yubing Xie, Georges Belfort, Polyethylene Glycol (PEG) Grafted Surfaces for Cell Culture, US Provisional Patent 62/423265, Nov 26, 2016.
- c. Keating JJ, Belfort G, Kocsis IZ, Sorci M, Lee AK. Combined Plasma-ARGET ATRP Method and Materials for Modifying Poly(ether sulfone) Surface. US Provisional Patent 62/531,623, July 2017.

References

- [1] K. Matyjaszewski, Atom transfer radical polymerization (ATRP): current status and future perspectives, *Macromolecules*, 45 (2012) 4015-4039.
- [2] G. Lligadas, S. Grama, V. Percec, Single-Electron Transfer Living Radical Polymerization Platform to Practice, Develop, and Invent, *Biomacromolecules*, 18 (2017) 2981-3008.
- [3] M.J. Monteiro, T. Guliashvil, V. Percec, Kinetic Simulation of Single Electron Transfer–Living Radical Polymerization of Methyl Acrylate at 25 C, *Journal of Polymer Science: Part A: Polymer Chemistry*, 45 (2007) 1835–1847.
- [4] K. Gunter, W. Xu, G. Belfort, Predictive Tool for Design and Analysis of SET-LRP Grafting Reactions., in final preparation, (2019).
- [5] W.L. Xu, P. Ramesh, M. Sorci, G. Belfort, SET-LRP modification of cross-linked polyimide membranes for organic solvent nanofiltration, in final preparation, (2019).

Exploiting Insertion Processes for Continuous Membrane-free Ion Separations

Richard M. Crooks, Jonathan R. Thompson, and Collin D. Davies

Department of Chemistry, The University of Texas at Austin

Presentation Abstract

The main goal of our DOE-sponsored research is to develop a fundamental understanding of how to use electrochemical processes to continuously redirect and separate ions. The basic research approach to this goal is to use electrochemical processes to form concentration gradients in solution. This results in a region of solution characterized by a decrease in conductivity (i.e., an ion-depletion zone, IDZ). When the solution is electrified, the IDZ forms a corresponding electric field gradient that can control the motion of ions in solution even in the absence of a membrane. In previous work, an IDZ was formed by converting ions to neutral species via electrochemical reactions at a metal electrode. In one of the most interesting applications, we proposed that electrochemical oxidation of Cl^- to Cl_2 would result in an electric field gradient useful for salt water desalination. Upon further investigation, we discovered that the proposed mechanism to form the IDZ is more complex than we initially realized. Specifically, Cl_2 is not stable in water, but rather it rapidly reacts to yield ions like H^+ and Cl^- . These ions counteract the IDZ. More recently, an alternative approach for producing an IDZ has been investigated that does not rely on Cl_2 . In this case, a fraction of the ions in a flowing stream are inserted into a battery material like Prussian blue (PB) as it is oxidized or reduced. Removal of these ions from solution yields the IDZ. In addition to eliminating byproducts like Cl_2 , this method makes it possible to control the insertion rate of electrochemically inactive ions like Na^+ , K^+ , and Ca^{2+} . In this presentation we will briefly discuss our general approach for controlling ion motion, and then discuss preliminary findings related to forming an IDZ by inserting ions into PB.

DE-FG02-06ER15758: Exploiting Insertion Processes for Continuous Membrane-free Ion Separations

RECENT PROGRESS

Using ion insertion processes for electrochemically controlled ion separations

The main goal of our DOE-sponsored research is to develop a fundamental understanding of how to use electrochemical processes to continuously redirect and separate ions. The basic research approach to this goal is to form concentration gradients in solution by electrochemical processes. This produces a region of solution characterized by a decrease in conductivity compared to the bulk solution (i.e., a local ion-depletion zone, IDZ). In the presence of an applied electric field, a disproportionate amount of the voltage is dropped within the IDZ and yields an electric field gradient. We have previously shown that the resulting electric field gradient can be used to manipulate ions in interesting ways.

In the past, we formed an IDZ by converting buffer ions to neutral species via water electrolysis. However, this approach is not suitable for generating an IDZ in solutions where the predominant ions are electrochemically inactive species like K^+ and Na^+ (e.g., biological fluids, salt water). Therefore, the goal of this project is to demonstrate that inserting these ions into an electrochemically-controlled intercalation material leads to an IDZ and corresponding electric field gradient that can be used to manipulate ion motion.

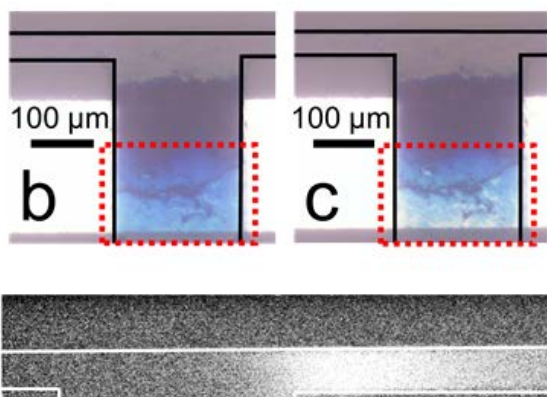
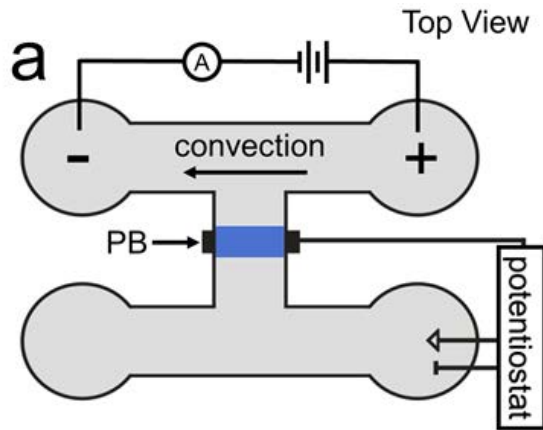


Figure 1. (a) Schematic illustration of the microfluidic device used to form an IDZ by ion insertion into PB. Optical micrographs captured (b) before and (c) during an enrichment experiment. PB color change is most apparent within the region outlined by the dashed red line in (b) and (c). (d) Fluorescence micrograph captured during application of 10.0 V across the top channel and -7.0 V (vs Ag/AgCl) to the PB-modified working electrode. Solution contained 1.0 mM KCl and

Recently, we showed that it is possible to insert K^+ into a Prussian blue (PB)-modified electrode to form an IDZ. Figure 1a is a schematic diagram of the microfluidic configuration used for separation experiments. Here, PB is electrochemically deposited atop a metal electrode (Figure 1b). Upon electrochemical reduction of PB to Prussian white, K^+ is inserted into the material and an IDZ forms in solution. Figure 1c reveals a color change upon electrochemical reduction of PB to Prussian white (notice the much lighter coloring toward the bottom of the red-boxed areas).

As mentioned above, the IDZ and corresponding electric field gradient can be used to manipulate ions in solution. During PB reduction, the resulting IDZ is sufficient to enrich a fluorescent tracer ion by electric field gradient focusing (Figure 1d). One interesting aspect of this approach to form an IDZ is that ion insertion into the PB is cation specific. In other words, if the cation in solution is too large to intercalate into the PB lattice, no IDZ should form. Preliminary results from experiments performed with cations larger than K^+ (e.g., tetrabutylammonium) suggest that IDZ formation at the PB-modified electrode is cation specific. These findings improve our fundamental understanding of ion separation by insertion processes.

Experimental and computational investigation of electrochemical Cl^- oxidation for desalination

We previously reported an approach for desalinating salt water using an electric field gradient as part of DOE-sponsored research (Figure 2a). In this approach, electrochemical oxidation of Cl^- to Cl_2 at an anode located within a microchannel decreases solution conductivity near the anode (i.e., IDZ), thereby forming an electric field gradient in solution. If convection and

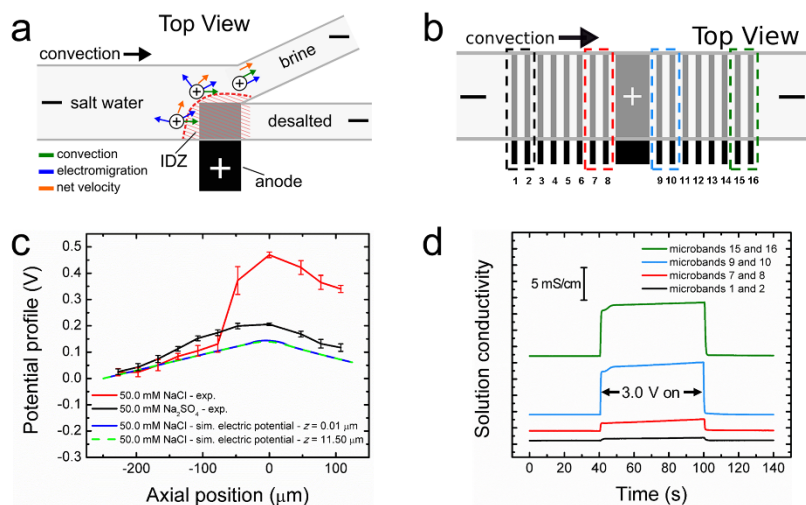


Figure 2. (a) Schematic illustration of desalination at a microchannel-embedded anode. (b) Schematic illustration of the microelectrochemical system used to characterize solution near the anode. (c) Electrochemical potential (red and black lines) measurements and simulated electric potential as a function of axial position along the channel length (blue and green lines). The anode is centered at axial position 0. Negative and positive axial positions are upstream and downstream from the anode, respectively. (d) Plot of solution conductivity at four different axial positions as a function of time. The colors of the lines in (d) correspond to the colors of the dashed lines in (b).

in mind, the goal of this project has been to better understand this process by characterizing the solution near the anode during electrochemical Cl^- oxidation (Figure 2b).

Electrochemical potential profile measurements used to approximate the electric field in solution confirm that a potential gradient forms near the anode during Cl^- oxidation (Figure 2c, red line). When the experiment is repeated with a Cl^- -free control solution (50.0 mM Na_2SO_4), water oxidation proceeds at the anode and the slope of the potential profile is nearly constant (i.e., gradient-free) upstream and downstream from the anode (Figure 2c, black line). These findings confirm that a potential gradient selectively forms close to the anode during Cl^- oxidation. We interpreted this result to indicate that an IDZ forms at the anode when Cl^- is converted to neutral Cl_2 . However, conductivity measurements reveal an increase in solution conductivity near the anode during Cl^- oxidation (Figure 2d). To understand these findings, we performed numerical simulations of the electrochemical system.

Numerical simulations confirm that electrochemical Cl^- oxidation followed by Cl_2 hydrolysis increases solution conductivity near the anode. This is because Cl_2 rapidly reacts with water to produce conductive species like H^+ and Cl^- . In addition, the slope of the simulated electric potential profile is nearly constant and gradient-free upstream and downstream from the anode (Figure 2c, blue and green lines). From these results, we conclude that electrochemical Cl^-

electromigration along the electric field gradient are similar in magnitude, then ions like Na^+ and Cl^- should be redirected away from the anode to produce brine and desalted streams. On the basis of the results of preliminary experiments and numerical simulations, we concluded that this approach leads to desalination.

More recently, we learned that the electrochemical and chemical processes described in Figure 2a are more subtle and complex than we originally realized. Specifically, Cl_2 is not stable in aqueous solutions but rapidly reacts with water to produce ions like H^+ and Cl^- . For this reason, it is now apparent that aqueous Cl_2 chemistry opposes a decrease in solution conductivity in the vicinity of the anode. With this

oxidation does not decrease solution conductivity or form an electric field gradient in solution near the anode. We now understand that the potential gradient measured during Cl⁻ oxidation arises from a shift in the *chemical* potential, rather than the *electric* potential, of solution near the anode. These findings clarify the complexities of the electrochemical and chemical processes illustrated in Figure 2a and inform future exploration of ion separations facilitated by electrochemical reactions.

Publications Acknowledging this Grant in 2016 – present

*(XI) Exclusively funded by this grant**

1. C. D. Davies; E. Yoon; R. M. Crooks "Continuous Redirection and Separation of Microbeads via Faradaic Ion Concentration Polarization" *ChemElectroChem* **2018**, 5, 877-884 (DOI: 10.1002/celec.201700450).
2. Yoon, E.; Davies, C. D.; Hooper, T. A.; Crooks, R. M. Photoelectrochemical Ion Concentration Polarization: Membraneless Ion Filtration Based on Light-Driven Electrochemical Reactions. *Lab Chip* **2017**, 17, 2491-2499 (DOI: 10.1039/C7LC00455A).
3. Hlushkou, D.; Knust, K. N.; Crooks, R. M.; Tallarek, U. Numerical Simulation of Electrochemical Desalination. *J. Phys.: Condens. Matter* **2016**, 28, Art. No. 194001 (DOI: 10.1088/0953-8984/28/19/194001).

(XII) Jointly funded by this grant and other grants with leading intellectual contribution from this grant;

n/a

(XIII) Jointly funded by this grant and other grants with relatively minor intellectual contribution from this grant

n/a

*May include attribution to a collaborator's grant or to the Robert A. Welch Fdn., which provides sustaining support for our research program in the form of an endowment.

CO₂ Separation via Guanidines Crystallization

Radu Custelcean, Neil Williams, Charles Seipp, Flavien Brethome, Kathleen Garrabrant,
Pierrick Agullo, Alexander Ivanov, Vyacheslav Bryantsev
Chemical Sciences Division, Oak Ridge National Laboratory

Presentation Abstract

In the last 4 years we have developed a new class of anion-separation agents based on iminoguanidines, self-assembled from amino- or diamino-guanidinium salts and simple (di)aldehydes or ketones. The resulting bis-iminoguanidinium (BIG) or diiminoguanidinium (DIG) structures are conformationally preorganized and complementary to oxyanions (e.g., sulfate, selenate, chromate, carbonate), and can be incorporated into crystals, lipophilic extractants, or polymeric frameworks for selective oxyanion separation by crystallization, liquid-liquid extraction, or ion exchange, respectively.

Exploring a different facet of the iminoguanidine chemistry, we developed a new approach to CO₂ separation from flue gas or air based on crystallization of highly insoluble BIG (bi)carbonate salts. Following the separation of the crystalline BIG (bi)carbonates from the aqueous sorbent by filtration, the CO₂ is released by mild heating (60-120 °C) of the crystals to regenerate the BIG ligands quantitatively and close the separation cycles. The structural, thermodynamic, and mechanistic aspects of the CO₂ capture and release will be discussed, as well as the prospects for developing energy-efficient and sustainable carbon capture technologies.

ERKCC08: Principles of Chemical Recognition and Transport in Extractive Separations

Postdoc(s): Neil Williams, Alexander Ivanov

Student(s): Charles Seipp, Flavien Brethome, Kathleen Garrabrant, Pierrick Agullo

RECENT PROGRESS

CO₂ Separation by Bis-Iminoguanidinium (BIG) (Bi)carbonate Crystallization

Drawing inspiration from the natural carbon cycle, wherein (bi)carbonate anions are involved in chemical equilibria with atmospheric CO₂, aqueous carbonic acid, and carbonate minerals (e.g., CaCO₃), we developed a new approach to CO₂ separation based on (bi)carbonate crystallization with BIGs. In the particular case of 2,6-pyridine-bis(iminoguanidine) (PyBIG), an aqueous solution of the ligand was found to react with CO₂ from the air and crystallize as a carbonate salt containing extended one-dimensional carbonate-water clusters (Seipp, 2017). The very low aqueous solubility of the PyBIG carbonate salt, on a par with CaCO₃, drives the crystallization equilibrium despite the very low concentration of CO₂ in the air (Brethome, 2018). Single-crystal neutron diffraction combined with electron density measurements from high-resolution X-ray diffraction found very strong H-bonding of the carbonate anions by the guanidinium groups and the water molecules included in the crystals, which likely contribute to the extremely low aqueous solubility of this salt (Gianopoulos, 2019). Mild heating of the carbonate crystals releases the CO₂ and regenerates the PyBIG ligand quantitatively, thereby closing the CO₂-separation cycle (Fig 1a). On the other hand, a simpler congener, glyoxal-bis(iminoguanidine) (GBIG), was found to react with CO₂ from simulated flue gas mixtures and crystallize as a bicarbonate salt containing bicarbonate-water clusters, as revealed by single-crystal X-ray diffraction (Fig 1b). The CO₂ could

be released by mild heating of the bicarbonate crystals, and GBIG could be regenerated quantitatively and recycled multiple times using 24% less energy compared to benchmark industrial sorbents. Experimental and computational investigations support a unique CO₂-release mechanism involving low-barrier surface-initiated proton transfer from the guanidinium groups to the bicarbonate anions with the formation of carbonic acid dimers, followed by concerted CO₂ and H₂O release in the rate-limiting step (Williams, 2019).

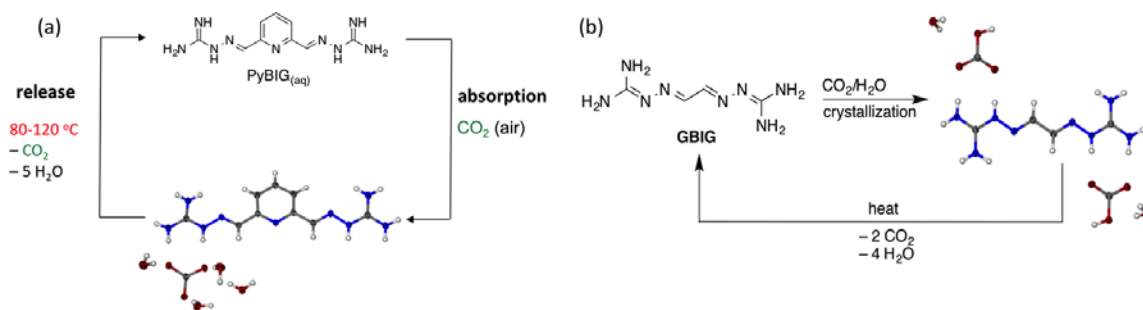


Figure 1. CO₂ capture from air or simulated flue gas by crystallization with PyBIG (a) or GBIG (b).

Publications Acknowledging this Grant in 2015 – present

(IV) Exclusively funded by this grant

13. Custelcean, R.; Williams, N. J.; Seipp, C. A. Aqueous Sulfate Separation by Crystallization. *Angew. Chem. Int. Ed.* **2015**, *54*, 10525- 10529.
14. Seipp, C. A.; Williams, N. J.; Bryantsev, V. S.; Custelcean, R.; Moyer, B. A. A Conformationally Persistent Pseudo-Bicyclic Guanidinium for Anion Coordination, as Stabilized by Dual Intramolecular Hydrogen Bonds. *RSC Advances* **2015**, *5*, 107266-107269.
15. Custelcean, R.; Williams, N. J.; Seipp, C. A.; Ivanov, A. S.; Bryantsev, V. S. Aqueous Sulfate Separation by Sequestration of $[(SO_4)_2(H_2O)_4]^{4-}$ Clusters within Highly Insoluble Imine-Linked Bis-Guanidinium Crystals. *Chem. Eur. J.* **2016**, *22*, 1997-2003.
16. Williams, N. J.; Bryantsev, V.; Custelcean, R.; Seipp, C. A.; Moyer, B. A. $\alpha, \alpha', \alpha'', \alpha'''$ Meso-Tetrahexyltetramethyl-Calix[4]Pyrrole: An Easy-to-Prepare, Isomerically Pure Anion Extractant with Enhanced Solubility in Organic Solvents. *Supramol. Chem.* **2016**, *28*, 176-187.
17. Seipp, C. A.; Williams, N. J.; Custelcean, R. Sulfate Separation by Selective Crystallization with a Bis-Iminoguanidinium Ligand. *Journal of Visualized Experiments* **2016**, *115*, e54411.
18. Seipp, C. A.; Williams, N. J.; Kidder, M. K.; Custelcean, R. CO₂ Capture from Ambient Air by Crystallization with a Guanidine Sorbent. *Angew. Chem. Int. Ed.* **2017**, *56*, 1042-1045.
19. Brethome, F. M.; Williams, N. J.; Seipp, C. A.; Kidder, M. K.; Custelcean, R. Direct Air Capture of CO₂ via Aqueous-Phase Absorption and Crystalline-Phase Release Using Concentrated Solar Power. *Nature Energy* **2018**, *3*, 553-559.
20. Williams, N. J.; Seipp, C. A.; Garrabrant, K. A.; Custelcean, R.; Holguin, E.; Keum, J. K.; Ellis, R. J.; Moyer, B. A. Surprisingly Selective Sulfate Extraction by a Simple Monofunctional Di(imino)guanidinium Micelle-Forming Anion Receptor. *Chem. Commun.* **2018**, *54*, 10048-10051.

21. Williams, N. J.; Seipp, C. A.; Brethome, F. M.; Ma, Y.-Z.; Ivanov, A. S.; Bryantsev, V. S.; Kidder, M. K.; Martin, H. J.; Holguin, E.; Garrabrant, K. A.; Custelcean, R. *CO₂ Capture via Crystalline Hydrogen-Bonded Bicarbonate Dimers*. *Chem* **2019**, *5*, 719-730.
22. Williams, N. J.; Custelcean, R. *CO₂ Capture Going BIG*. *Carbon Capture Journal* **2019**, *68*, Mar/Apr, 4-6.
23. Williams, N. J.; Roy, S.; Reynolds, C. O.; Custelcean, R. Bryantsev, V. S.; Moyer, B. A. *Enhancing Selectivity of Cation Exchange with Anion Receptors*", *Chem. Commun.* **2019**, *55*, 3590-3593.

(V) *Jointly funded by this grant and other grants with leading intellectual contribution from this grant*

5. Jia, C.; Zuo, W.; Yang, D.; Chen, Y.; Cao, L.; Custelcean, R.; Hostas, J.; Hobza, P.; Glaser, R.; Wang, Y.-Y.; Yang, X.-J.; Wu, B. *Selective Binding of Choline by a Phosphate-Coordination-Based Triple Helicate Featuring an Aromatic Box*. *Nature Commun.* **2017**, *938*.
6. Gianopoulos, C. G.; Chua, Z.; Zhurov, V. V.; Seipp, C. A.; Wang, X.; Custelcean, R.; Pinkerton, A. A. *Direct Air Capture of CO₂ – Topological Analysis of the Experimental Electron Density (QTAIM) of the Highly Insoluble Carbonate Salt of 2,6-Pyridine-bis(iminoguanidine), (PyBIGH₂)(CO₃)(H₂O)₄*. *IUCrJ* **2019**, *6*, 56-65.
7. Huang, Z.; Jia, C.; Wu, B. Jansone-Popova, S.; Seipp, C. A.; Custelcean, R. *Selective Binding of (Thio)sulfate and Phosphate in water by Quaternary Ammonium Functionalized Oligo-Ureas*. *Chem. Commun.* **2019**, *55*, 1714-1717.
8. Garrabrant, K. A.; Williams, N. J.; Holguin, E.; Brethome, F. M.; Tsouris, C.; Custelcean, R. *Energy-Efficient CO₂ Capture from Flue Gas by Absorption with Amino Acids and Crystallization with a Bis-Iminoguanidine*. *Ind. Eng. Chem. Res.* **2019**, *58*, 10510-10515.

(VI) *Jointly funded by this grant and other grants with relatively minor intellectual contribution from this grant*

6. Wang, J. C.; Aswartham, S.; Ye, F.; Terzic, J.; Zheng, H.; Haskel, D.; Chikara, S.; Choi, Y.; Schlottmann, P.; Custelcean, R.; Yuan, S. J.; Cao, G. *Decoupling of the Antiferromagnetic and Insulating States in Tb-doped Sr₂IrO₄*. *Phys. Rev. B*, **2015**, *92*, 214411.
7. Sefat, A. S.; Li, L.; Cao, H. B.; McGuire, M. A.; Sales, B.; Custelcean, R.; Parker, D. S. *Anomalous Magneto-Elastic and Charge Doping Effects in Thallium-Doped BaFe₂As₂*. *Scientific Reports* **2016**, *6*:21660.
8. Stack, A. G.; Stubbs, J. E.; Srinivasan, S. G.; Roy, S.; Bryantsev, V. S.; Eng, P. J.; Custelcean, R.; Gordon, A. D.; Hexel, C. R. *Mineral-Water Interface Structure of Xenotime (YPO₄) {100}*. *J. Phys. Chem. C* **2018**, *122*, 20232.

Interfacial Structure and Dynamics in Separations: When Molecular Simulations Meet Machine Learning

Jun Zhang, Manh-Thuong Nguyen, Eric Baxter, Venkateshkumar Prabhakaran, Grant E. Johnson, Roger Rousseau and Vassiliki-Alexandra Glezakou
Pacific Northwest National Laboratory, Physical Sciences Division, Basic and Applied
Molecular Foundations Group, Richland, WA 99352
Email: Vanda.Glezakou@pnl.gov

Abstract

Our program is tackling the selective and efficient separation of ions from liquids using novel functionalized graphene materials. We aim to connect selectivity and transport to atomic and molecular-level phenomena at these precisely-tailored interfaces that are still not adequately understood. In this first period, the theory and simulation cross-cutting task focused on developing the necessary tools to accurately model complex interfaces and the collective behavior of ions in interlayer transport channels. Large-scale *ab initio* and classical molecular simulations were used to study the effects of functionalization on the interfacial structure and dynamics of solvent molecules and solutes. Our newly developed pseudo-potentials and companion basis sets allow the efficient and accurate study of metals in realistic model systems within periodic boundary conditions. The use of machine learning (ML) approaches has enabled the development of transferable classical force fields via force matching to *ab initio* molecular simulations. Finally, ML techniques have also been implemented in the development of spectroscopic descriptors of high accuracy to connect with the characterization studies performed in the experimental tasks of the program.

FWP Number: 72353

Please classify your publications into three categories according to the source of support for the work published:

(XIV) Exclusively funded by this grant;

1. Zhang, J.; Nguyen, M.-T. ; Rousseau, R. ; Glezakou, V.-A. Adsorption, structure and dynamics of H₂O and Pb(II) at water-graphene interfaces: the role of functionalization, **2019**, *submitted to Nature Chem.*

(XV) Jointly funded by this grant and other grants with leading intellectual contribution from this grant;

1. Gao, P. ; Zhang, J. ; Glezakou, V.-A. A General Protocol for the Accurate Prediction of Molecular ¹³C/¹H NMR Chemical Shifts via Machine Learning, **2019**, *submitted to Chem. Sci.*
2. Lu, J.; Cantu, D. C.; Nguyen, M.-T.; Li, J.; Glezakou, V.-A. Rousseau, R. Norm-conserving pseudopotentials and basis sets to explore Lanthanide chemistry in complex environments *J. Chem. Theor. Comp.* **2019**, *accepted.*

Microscopy Methods for Investigating Separation Processes within Porous Particles

Joel M. Harris, Jay P. Kitt, David A. Bryce, Maryam Zare
University of Utah – Department of Chemistry
Salt Lake City, UT 84112

Presentation Abstract

In the development of new separation media, it is critical to understand how their interface composition and structure relate to their functioning for selective solute retention and separations. Confocal Raman microscopy has been adapted to examine the interior surfaces of both porous chromatographic particles and polymer films, reporting information on the structure of their interfaces and interactions with solute molecules. The spatial resolution of the confocal collection optics can selectively probe the *internal composition* of individual porous particles or thin films, yielding quantitative information on populations of molecules at interfaces within their pores. The technique is an *in situ* method, so that interfacial structure and composition can be monitored as conditions are varied. We apply this methodology to studies of assembly of hybrid-lipid bilayers onto porous C₁₈-modified surfaces; these biomimetic materials can be used for separations based on the lipid-membrane affiliation of analytes with these model interfaces. Raman spectroscopy provides insight on the conformations of grafted alkyl chains and the acyl chains of the lipid monolayer, and how these conformations change with temperature and the partitioning of analytes. Assembly of purely lipid-based supported bilayers on bare silica and cyano-derivatized silica surfaces is also being explored; the structures of these sorbent phases and their retention and selectivity for model solutes are being investigated.

DE-FG03-93ER14333: Analytical Spectroscopy Methods for Liquid/Solid Interfaces

PI: Joel M. Harris

Postdocs: Jay P. Kitt

Students: David A. Bryce, Maryam Zare, Allison Jacobsen

Visiting Faculty: Carol Korzeniewski, Texas Tech University

RECENT PROGRESS

Probing interior surface chemistry of porous particles: lipid-membrane-affinity based separations. Most practical applications of liquid/solid interfaces to chemical separations, including extraction, environmental remediation, chromatography, and membrane fractionation, are carried out in porous media. The high specific surface area of porous materials provides surface capacity but makes them challenging to investigate because most of the surface lies *within the interior*, making it inaccessible to traditional surface-selective spectroscopies. With DOE support, the Harris lab has pioneered the use of confocal-Raman microscopy [1] to probe the interior composition and interface structure of individual porous particles and thin films, providing *in-situ* vibrational spectra from regions inside of these materials with sampling volumes of 10⁻¹⁵ L or smaller.

Confocal Raman microscopy has allowed investigation of a novel approach to separations based on lipid-membrane affinity, where a model lipid bilayer is supported on the interior surfaces of porous particles. These hybrid bilayers are produced through the self-assembly of a phospholipid monolayer on n-alkane-modified silica surfaces within porous particles and used in retention studies of small molecules. Despite their applications as separation media, the structure of hybrid-bilayers in chromatographic silica was unknown. To address this question, we employed confocal-Raman microscopy (Figure 1) to observe the structure of hybrid-phospholipid bilayers in C18-modified, porous-silica [4]. The surface-density of lipids in the hybrid bilayer, the ordering of *both* C₁₈ and lipid acyl chains upon bilayer formation, and the decoupling of C₁₈ methylene C-H vibrations by deuterated-lipid acyl chains all indicate an interdigitated acyl-chain structure. We recently reported the kinetics of hybrid bilayer membrane formation, which provided insight into how structures of lipid acyl and C₁₈ chains evolve during deposition, formation, and organization into ordered structures [15].

Surfactant-based hybrid models of lipid membranes. We have made progress in forming mixed-charged surfactant-based hybrid bilayers for membrane-selective molecular separations. Our first materials for these separations (above) employed a phospholipid monolayer assembled on lower leaflet of n-alkyl chains covalently bound to C₁₈-chromatographic silica. Despite utility of these bioinspired membrane-like interfaces, the cost of phospholipids required to modify C₁₈-silica for separation applications is high. We have sought a less costly alternative for membrane-like modification of C₁₈-silica surfaces by mimicking interfacial structure of phosphatidylcholine lipids: a zwitterionic head-group and an acyl chains for each of the opposite charges. To meet this goal, we have assembled a stable monolayer of oppositely-charged long-chain surfactants on C₁₈-modified silica. The two surfactants, cetylpyridinium chloride and hexadecylphosphonic acid, have oppositely-charged head groups (quaternary amine and phosphonic acid) and 16-carbon hydrocarbon tails, comparable to 1,2-dimyristoyl-sn-glycero-3-phosphocholine (DMPC). Confocal Raman microscopy reveals formation of high-density 1:1 monolayer of mixed surfactants, which is stable for months in buffer. Acyl chains are interdigitated and exhibit a temperature-dependent ordered to disordered phase transition, comparable to a DMPC hybrid bilayer. The composition and structure of this mixed surfactant layer have been investigated along with their applications in assessing lipid-bilayer affinity of molecules based on their interactions with these surfaces.

Supported lipid bilayers in porous silica particles. A major accomplishment for the project was the successful deposition of supported-lipid bilayers on the interior surfaces of porous silica

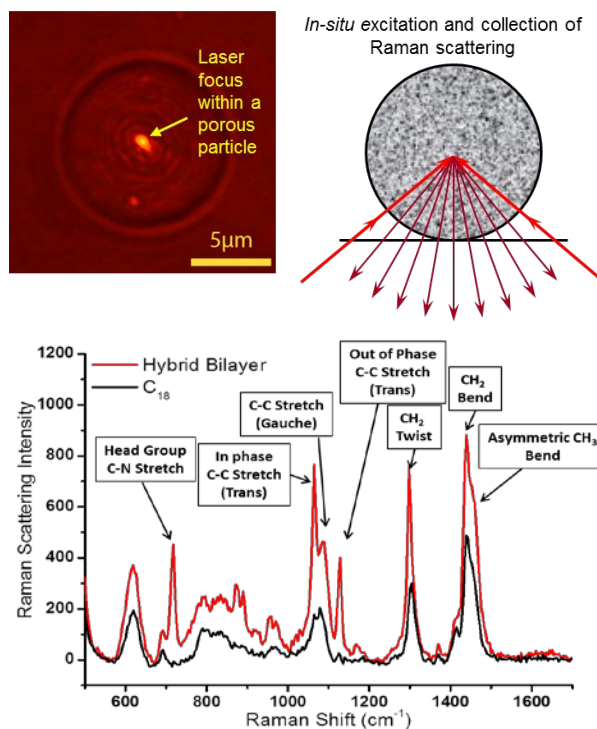


Figure 1. Raman scattering collected from within a single C₁₈ silica particle prior to (black) and following (red) surface assembly of a hybrid-lipid bilayer [4].

particles. A common approach to exploring the interactions of molecules with biological membranes is through deposition of lipid bilayers on planar supports. Investigations using these planar-membrane models are limited to high-sensitivity methods capable of detecting a small population of molecules at the interface between a planar support and aqueous solution. We discovered that supported-lipid bilayers can be deposited by vesicle fusion onto the interior surfaces throughout the pore network of *bare silica particles* without the need for C₁₈-ligands on the surface [9]. The thickness of a lipid film and head-group spacing are consistent with a bilayer deposited onto the pore surfaces. Raman spectra of porous-silica-supported DMPC bilayers are equivalent to spectra of DMPC vesicle membranes [3] both above and below their melting phase transition, suggesting comparable phospholipid organization and bilayer structure [9]. These porous-silica-supported model membranes share benefits of planar-supported lipid bilayers but with sufficient *surface area and adsorption capacity* to allow separations based on lipid-membrane affiliation [10] or membrane-bound ligand interactions [11].

Partitioning into small molecules into model phospholipid bilayers. The phospholipid-water partition coefficient is a commonly measured parameter that correlates with small-molecule toxicity and accumulation and persistence of molecules in the environment, including compounds that derive from energy production. Methods for measuring phospholipid partition coefficients are limited because vesicle membranes or planar supported bilayers are small-volume phases that challenge the sensitivity of most analytical techniques. To address this issue, we employ *in-situ* confocal Raman microscopy to probe the partitioning of membrane-active compounds into hybrid-bilayers (lipid on C₁₈-silica) and supported-phospholipid bilayers (above) deposited on the pore walls of chromatographic silica particles. Quantitative determination of lipid partitioning separations is achieved by using the phospholipid acyl-chains of the within-particle bilayer as an internal standard. This approach was tested for measurements of pH-dependent partitioning of an aromatic carboxylate (2-(4-isobutylphenyl) propionic acid) into both hybrid-lipid and supported-lipid bilayers in silica particles (Figure 2), and the results were compared with octanol-water partitioning [2]. The impact of the analyte on bilayer structure was evaluated for both within-particle model membranes and compared with the structural impacts of partitioning into vesicle lipid bilayers [10].

Probing porous polymer separation membranes.

In a very productive collaboration with Carol Korzeniewski from Texas Tech and Steve Creager from Clemson University, we have applied *in-situ* confocal-Raman microscopy in our lab to investigate the composition, structure, and ionic selectivity of porous polymer membranes that are employed as separators in fuel-cell applications. We developed quantitative confocal-Raman microscopy methods for determining ionizable group content in ion-conducting

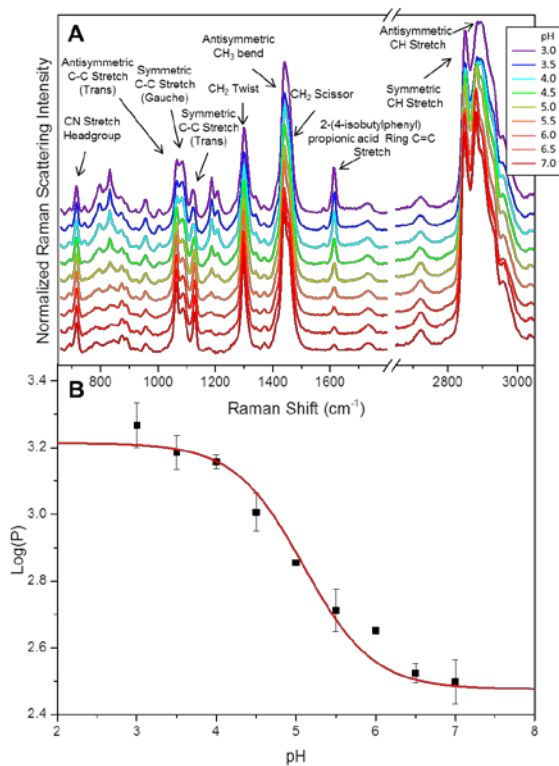


Figure 2. pH-dependent partitioning of 2-(4-isobutylphenyl) propionic acid into hybrid bilayers. A. *In-situ* Raman spectra. B. Log(P) from Raman scattering intensities.

porous polymer membranes with capability of micron-scale spatial mapping of the membrane composition and structure [7]. We also applied confocal Raman microscopy to interrogate and verify the structure of *single-layer graphene* used as a D₂-H₂ separator within a Nafion-graphene-Nafion sandwich membrane [8]. Single-layer graphene (one atomic-layer thick) was found to be an ideal thin-film material to characterize the axial spatial resolution in depth profiling by confocal Raman microscopy, useful for interpreting the depth-dependent composition of porous membranes or polymer thin films [12]. When sandwiched in proton-exchange membranes, single-layer graphene was found to confer 100-fold faster proton transmission compared to any other cations; confocal Raman microscopy played a key role both in confirming the single-layer structure of the graphene separator and in characterizing its ability to preserve cationic separation between the two halves of the membrane sandwich [13].

Publications acknowledging this grant in 2015 – present

1. Kitt, J. P.; Bryce, D. A.; Harris, J. M. Spatial Filtering of a Diode Laser Beam for Confocal Raman Microscopy. *Appl. Spectrosc.* **2015**, *69*, 513-517. (I)
2. Kitt, J. P.; Harris, J. M. Confocal Raman Microscopy for *In-Situ* Measurement of Octanol–Water Partitioning within the Pores of Individual C₁₈-Functionalized Chromatographic Particles. *Anal. Chem.* **2015**, *87*, 5340-5347. (I)
3. Kitt, J. P.; Bryce, D. A.; Harris, J. M. Calorimetry-Derived Composition Vectors to Resolve Component Raman Spectra in Phospholipid Phase Transitions. *Appl. Spectrosc.* **2016**, *70*, 1165-1175. (I)
4. Kitt, J. P.; Harris, J. M. Confocal Raman Microscopy of Hybrid-Supported Phospholipid Bilayers within Individual C₁₈-Functionalized Chromatographic Particles. *Langmuir* **2016**, *32*, 9033-9044. (I)
5. Bryce, D. A.; Kitt, J. P.; Harris, J. M. Confocal Raman Microscopy Investigation of Molecular Transport into Individual Chromatographic Silica Particles. *Anal. Chem.* **2017**, *89*, 2755-2763. (I)
6. Kitt, J. P.; Bryce, D. A.; Minter, S. D.; Harris, J. M. Raman Spectroscopy Reveals Selective Interactions of Cytochrome c with Cardiolipin That Correlate with Membrane Permeability. *J. Amer. Chem. Soc.* **2017**, *139*, 3851-3860. (I)
7. Korzeniewski, C.; Liang, Y.; Zhang, P.; Sharif, I.; Kitt, J. P.; Harris, J. M.; Hamrock, S. J.; Creager, S. E.; DesMarteau, D. D. Vibrational Spectroscopy for the Determination of Ionizable Group Content in Ionomer Materials. *Appl. Spectrosc.* **2018**, *72*, 141-150. (I)
8. Bukola, S.; Liang, Y.; Korzeniewski, C.; Harris, J. M.; Creager, S. E. Selective proton/deuteron transport through Nafion | graphene | Nafion sandwich structures at very high current density. *J. Amer. Chem. Soc.* **2018**, *140*, 1743-1752. (III)
9. Bryce, D. A.; Kitt, J. P.; Harris, J. M. Confocal-Raman Microscopy Characterization of Supported Phospholipid Bilayers Deposited on the Interior Surfaces of Chromatographic Silica. *J. Amer. Chem. Soc.* **2018**, *140*, 4071-4078. (I)
10. Kitt, J. P.; Bryce, D. A.; Minter, S. D.; Harris, J. M. Confocal Raman Microscopy for *In-Situ* Measurement of Phospholipid–Water Partitioning into Model Phospholipid Bilayers within Individual Chromatographic Particles. *Analytical Chemistry* **2018**, *90*, 7048-7055. (I)

11. Bryce, D. A.; Kitt, J. P.; Harris, J. M. Confocal Raman Microscopy for Label-Free Detection of Protein–Ligand Binding at Nanopore-Supported Phospholipid Bilayers. *Anal. Chem.* 2018, *90*, 11509–11516. (II)
12. Korzeniewski, C.; Kitt, J. P.; Bukola, S.; Creager, S.; Minter, S. D.; Harris, J. M. Single-Layer Graphene for Estimation of Axial Spatial Resolution in Confocal Raman Microscopy Depth Profiling. *Anal. Chem.* **2019**, *91*, 1049-1055. (II)
13. Bukola, S.; Beard, K.; Korzeniewski, C.; Harris, J. M.; Creager, S. E. Single-Layer Graphene Sandwiched between Proton-Exchange Membranes for Selective Proton Transmission. *ACS Appl. Nano Mater.* **2019**, *2*, 964-974. (III)
14. Liang, Y; Cai, R.; Hickey, D. P.; Kitt, J. P.; Harris, J. M.; Minter, S. D.; Korzeniewski, C. Infrared Microscopy as a Probe of Composition within a Model Biofuel Cell Electrode Prepared from *Trametes versicolor* Laccase. *Chem. Electro. Chem.* **2019**, *6*, 818–826. (III)
15. Kitt, J. P.; Bryce, D. A.; Minter, S. D.; Harris, J. M. Confocal Raman Microscopy Investigation of Self-Assembly of Hybrid Phospholipid Bilayers within Individual Porous Silica Chromatographic Particles. *Anal. Chem.* **2019**, *91*, 7790-7797. (I)

(XVI) Exclusively funded by this grant.

(XVII) Jointly funded by this grant and other grants with leading intellectual contributions from this grant.

(XVIII) Jointly funded by this grant and other grants with relatively minor intellectual contributions from this grant.

Molecular Diffusion in Self-Assembled Organic Nanotubes Studied Using Imaging Fluorescence Correlation Spectroscopy

Takashi Ito,¹ Daniel A. Higgins,¹ Hao Xu,¹ Govinda Ghimire,¹ Shinobu Nagasaka,¹ Roberto Espinoza,¹ Mikaela M. Moore,¹ Rebecca Leuschen,¹ Naohiro Kameta,² Mitsutoshi Masuda³

¹ Department of Chemistry, Kansas State University

² Nanomaterials Research Institute, AIST, Japan

³ Research Institute for Sustainable Chemistry, AIST, Japan

Presentation Abstract

An in-depth understanding of molecular diffusion and partitioning in nanoporous media is crucial to the design of better chemical separation materials. However, it is often challenging to assess molecular behavior in chemically heterogeneous systems. In this study, the diffusion behavior of fluorescent molecules (rhodamine and Nile red derivatives) within bolaamphiphile-based organic nanotubes (ONTs) was systematically investigated using imaging fluorescence correlation spectroscopy (imaging FCS). These materials had well-defined cylindrical structures with uniform inner pore diameters (10 or 20 nm) and known chemical properties: either -NH₂ or -COOH groups on their inner surfaces, glucose moieties on their outer surfaces, and hydrocarbon chains in between. Imaging FCS provided a means to measure the diffusion coefficients (D) of fluorescent molecules within individual solution-filled ONTs. The D values of fluorescent molecules within these ONTs were smaller by 3 ~ 4 orders of magnitude than those in bulk solution regardless of their charges and hydrophobicity. These results implied that the molecular diffusion was strongly influenced by interactions with the nanotube inner surfaces. Indeed, the D values of charged molecules were basically controlled by coulombic attraction/repulsion with the inner surface groups, as shown by their pH dependence. In addition, spectroscopic imaging results revealed that Nile red and its hydroxylated derivatives diffused in relatively nonpolar regions such as the solution-nanotube interface. On the other hand, the effects of ionic strength were relatively minor, suggesting the involvement of non-coulombic interactions such as hydrophobic and hydrogen bonding interactions in the molecular diffusion. Interestingly, ONTs with inner -NH₂ groups exhibited larger pH dependent changes in D than those with inner -COOH groups, suggesting their potential to design separation media that could capture and release analytes in response to changes in solution pH.

DE-SC0002362: Molecular-Level Investigations of Diffusion Behavior within Cylindrical Nanoscale Pores

PI: Takashi Ito, **Co-PI:** Daniel A. Higgins

Postdoc: Lianjie Xue

Students: Ruwandi Kumarasinghe, Govinda Ghimire, Herman Cocancigh

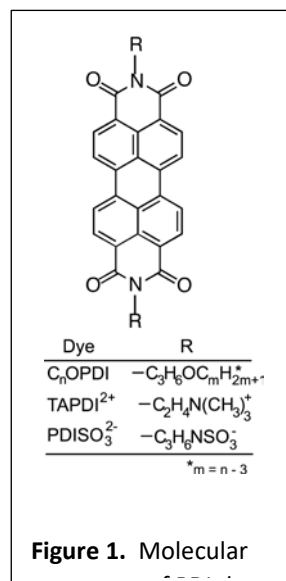
RECENT PROGRESS

Single-Molecule Translational and Orientational Motions of Charged and Uncharged Fluorescent Molecules within Surfactant-Filled Cylindrical Silica Nanopores.

Monolithic mesoporous silica capillary columns have now been employed in high performance liquid chromatography for almost two decades. These columns incorporate macropores to enhance column permeability while the mesopores afford required chemical selectivity. The functional attributes of these columns rely upon the partitioning of analytes into and out of the mesopores and their diffusion within the mesopores. In most chromatographic applications, the mesopores are filled with organic modifiers such as long alkane chains to allow their use in reversed phase separations. Monolithic silica capillary columns have unique advantages over packed, particle-based columns, affording high efficiency (*i.e.* small theoretical plate heights and large plate numbers) at relatively lower mobile phase pressures. They exhibit highest efficiencies for weakly retained analytes while particle-based columns function better for strongly retained species. The origins of these differences remain uncertain but likely result, in part, from kinetic limitations to partitioning and stationary phase mass transport in the monoliths.

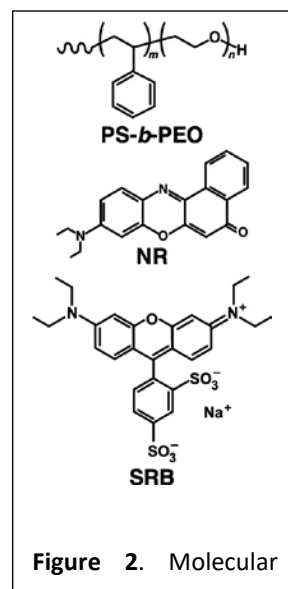
We have been employing surfactant-filled, hexagonally-arranged, locally-aligned cylindrical silica mesopores as models for these materials. We detect and track single fluorescent dye molecules moving through individual silica mesopores and use the results to identify their pathways of diffusion within the pores, to determine their diffusion coefficients, D , and to deduce their degree of confinement within the pores. Recently, we have investigated the confined translational and orientational motions of the solvatochromic Nile red (NR) dye within surfactant-filled silica mesopores.⁴ The results showed that D for NR molecules within the pores was $\sim 10^3$ -fold smaller than in bulk solution. Single molecule emission polarization (SMEP) and spectroscopic single molecule tracking (sSMT) studies showed that the dye was confined to an ~ 1 nm diameter region in the hydrophobic cores of the pore-filling micelles, suggesting a much greater level of confinement than expected from the ~ 3.7 nm diameter silica pores alone. Significant confinement of analytes within the mesopores may be important in limiting their applicability to separations of weakly retained species.

Most recently, we have been performing similar experiments with a series of uncharged and charged perylene diimide (PDI) derivatives (R. Kumarasinghe, T. Ito, D. A. Higgins, manuscript in preparation). The dyes employed (**Figure 1**) were selected to probe the influence of hydrophobic and coulombic interactions between the dyes and the pore-filling micelles, as well as intrinsic charged sites on the silica pore walls. All four dyes were found to diffuse by an apparent Fickian mechanism while occasionally exhibiting anomalous diffusion attributable to nanoscale materials heterogeneity. The cationic PDI exhibited the smallest D value in these studies, with the hydrophobic dyes displaying faster diffusion. Slower diffusion by the cationic PDI was attributed to its interactions with deprotonated silanol groups on the silica pore surfaces. Interestingly, the charged dyes exhibited relatively weaker orientational confinement, suggesting they explore a greater fraction of the pore volume, and consistent with the expectation they interact more frequently with the pore surface.



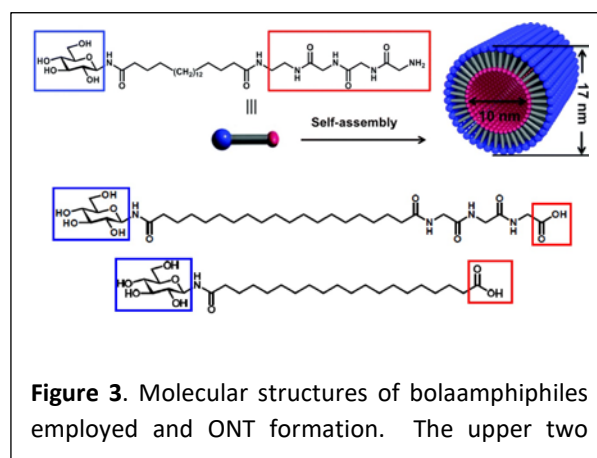
Molecular Permeability of Self-Organized Cylindrical Polymer Nanostructures upon Solvent-Induced Swelling.

Polystyrene-*block*-poly(ethylene oxide) (PS-*b*-PEO, **Figure 2**) has attracted considerable interest as a chemical separation medium and as a polymer electrolyte, because it affords PEO microdomains that provide nanoscale molecular pathways. For these applications, it is crucial to thoroughly understand how solvent-induced swelling affects the molecular permeability of the microdomains. Recently, we have investigated molecular diffusion behavior in PS-*b*-PEO films, and found that the molecular permeability of the cylindrical PEO microdomains (10 ~ 30 nm in diameter) is different from that of a PEO homopolymer (H. Coceanicigh, D. A. Higgins, T. Ito, manuscript in preparation). In this study, diffusion of Nile red (NR) and sulforhodamine B (SRB) molecules (**Figure 2**) doped in thin polymer films (20 ~ 200 nm thick) was measured using single molecule tracking (SMT) and fluorescence correlation spectroscopy (FCS). Negligible diffusion of NR molecules was observed in PS-*b*-PEO films even upon exposing the films to ethanol or water vapor. This observation reflected their preferential distribution to PS microdomains that were not swollen by the solvents, as verified by the solvatochromic emission of the dye. In contrast, the diffusion of SRB molecules in PS-*b*-PEO films was enhanced upon solvent exposure, as expected from their preferential distribution to the PEO microdomains. Interestingly, the diffusion of SRB molecules in PS-*b*-PEO films was enhanced upon their exposure to ethanol vapor, implying that PEO microdomains were swollen by ethanol. This result was unexpected, because ethanol is well-known to be a poor solvent for PEO as supported by the negligible diffusion of SRB molecules in PEO homopolymer films upon ethanol vapor exposure. The ethanol-induced swelling of the PEO microdomains is attributable to the poorer packing of PEO chains in the microdomains due to their nanoscale geometry defined by the surrounding PS microdomains.



Investigations of Molecular Diffusion within Organic Nanotubes Using Imaging FCS.

An in-depth understanding of molecular diffusion and partitioning in nanoporous media is crucial to the design of better chemical separation materials. However, it is often challenging to assess dynamic molecular behavior in chemically heterogeneous systems. We employ bolaamphiphile-based organic nanotubes (ONTs) to investigate the diffusion and partitioning of fluorescent molecules using imaging fluorescence correlation spectroscopy (imaging FCS). These ONTs have well-defined cylindrical cavity structures with uniform inner pore diameters (10 or 20 nm) and known chemical properties: either -NH₂ or -COOH groups on the inner surfaces, glucose moieties on their outer surfaces, and hydrocarbon chains in between (**Figure 3**). Previously, we investigated the diffusion and distribution of NR and its hydroxylated derivative (NR-OH) within ONTs having an inner diameter of 10 nm and inner surface -NH₂ groups (NH₂-ONT_{10nm}).⁷ We found that, as compared with NR, NR-OH was located in more polar regions, and exhibited slower diffusion, possibly due to hydrogen bonding interactions with the amine and glucose groups. We also investigated the diffusion of anionic SRB within NH₂-ONT_{10nm} in pH 6.4 ~ 8.4 solutions having different ionic

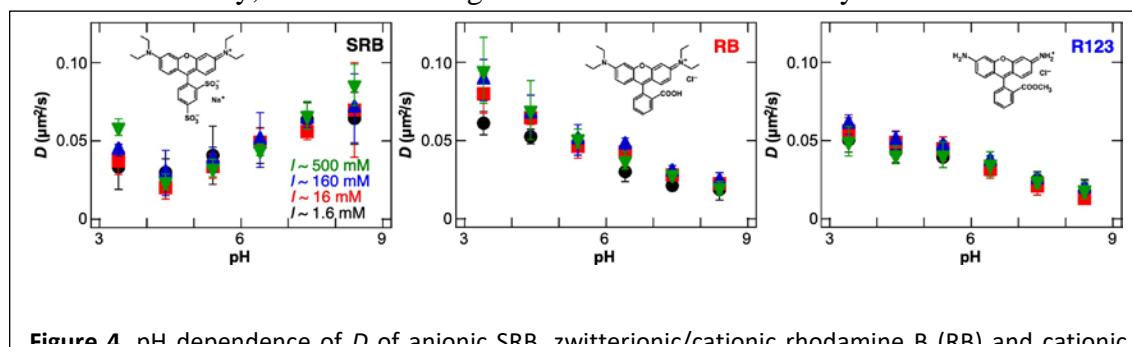


These ONTs have well-defined cylindrical cavity structures with uniform inner pore diameters (10 or 20 nm) and known chemical properties: either -NH₂ or -COOH groups on the inner surfaces, glucose moieties on their outer surfaces, and hydrocarbon chains in between (**Figure 3**). Previously, we investigated the diffusion and distribution of NR and its hydroxylated derivative (NR-OH) within ONTs having an inner diameter of 10 nm and inner surface -NH₂ groups (NH₂-ONT_{10nm}).⁷ We found that, as compared with NR, NR-OH was located in more polar regions, and exhibited slower diffusion, possibly due to hydrogen bonding interactions with the amine and glucose groups. We also investigated the diffusion of anionic SRB within NH₂-ONT_{10nm} in pH 6.4 ~ 8.4 solutions having different ionic

strengths.⁵ Larger D values were observed at pH 6.4, which was attributable to the reduction of coulombic attraction between anionic SRB and protonated $-NH_2$ groups on the inner surface of the ONT.

Recently, we undertook a more systematic investigation of the diffusion of rhodamine dyes having different charges and hydrophobicities (**Figure 4**) within NH_2 - ONT_{10nm} over a wider pH range (3.4 ~ 8.4).⁹ The pH dependence of D (**Figure 4**) indicated that the D values of the dye molecules within the ONTs were basically controlled by electrostatic attraction/repulsion with the $-NH_2$ groups on the inner surfaces. In contrast, the effects of ionic strength were relatively minor, suggesting the involvement of non-coulombic interactions such as hydrophobic and hydrogen bonding interactions in the molecular diffusion. The imaging FCS data also revealed that D was independent of ONT length, indicating that the properties of the ONTs were uniform in terms of solute loading and release.

More recently, we have investigated the diffusion of these dyes within ONTs having inner -



COOH groups and inner diameters of 10 or 20 nm (G. Ghimire, et al. manuscript in preparation). The pH dependence of D basically reflected coulombic attraction/repulsion with the inner surface $-COOH$ groups. ONTs with inner $-COOH$ groups exhibited smaller pH dependent changes in D than those with inner $-NH_2$ groups, suggesting that the latter is better suited as separation media that could capture and release analytes in response to changes in solution pH.

Importantly, the D values obtained in all the studies were in the range of $10^{-1} \sim 10^{-2} \mu m^2/s$, 3 ~ 4 orders of magnitude smaller than those in bulk solution. The slow diffusion indicates that these molecules within an ONT diffuse via a desorption-mediated diffusion mechanism controlled by coulombic and non-coulombic interactions with the inner surface groups of the ONT.

Publications Acknowledging this Grant in 2015 – present

(I) Exclusively funded by this grant:

1. Higgins, D. A.; Park, S. C.; Tran-Ba, K.-H.; Ito, T. Single-Molecule Investigations of Morphology and Mass Transport Dynamics in Nanostructured Materials. *Annu. Rev. Anal. Chem.* **2015**, *8*, 193-216.
2. Tran-Ba, K.-H.; Higgins, D. A.; Ito, T. Fluorescence Recovery After Photobleaching and Single-Molecule Tracking Measurements of Anisotropic Diffusion within Identical Regions of a Cylinder-Forming Diblock Copolymer Film. *Anal. Chem.* **2015**, *87*, 5802-5809.
3. Park, S. C.; Ito, T.; Higgins, D. A. Dimensionality of Diffusion in Flow-Aligned Surfactant-Templated Mesoporous Silica: A Single Molecule Tracking Study of Pore Wall Permeability. *J. Phys. Chem. C* **2015**, *119*, 26101-26110.
4. Kumarasinghe, R.; Higgins, E. D.; Ito, T.; Higgins, D. A. Spectroscopic and Polarization-Dependent Single-Molecule Tracking Reveal the One-Dimensional Diffusion Pathways in Surfactant-Templated Mesoporous Silica. *J. Phys. Chem. C* **2016**, *120*, 715-723.
5. Xu, H.; Nagasaka, S.; Kameta, N.; Masuda, M.; Ito, T.; Higgins, D. A. Imaging Fluorescence Correlation Spectroscopy Studies of Dye Diffusion in Self-Assembled Organic Nanotubes. *Phys. Chem. Chem. Phys.* **2016**, *18*, 16766-16774.
6. Sapkota, D. R.; Tran-Ba, K.-H.; Elwell-Cuddy, T.; Higgins, D. A.; Ito, T. Single-Molecule Tracking Study of the Permeability and Transverse Width of Individual Cylindrical Microdomains in Solvent-Swollen Polystyrene-*block*-Poly(ethylene oxide) Films. *J. Phys. Chem. B* **2016**, *120*, 12177-12183.
7. Xu, H.; Nagasaka, S.; Kameta, N.; Masuda, M.; Ito, T.; Higgins, D. A. Spectroscopic Imaging Studies of Nanoscale Polarity and Mass Transport Phenomena in Self-Assembled Organic Nanotubes. *Phys. Chem. Chem. Phys.* **2017**, *19*, 20040-20048.
8. Coceancigh, H.; Higgins, D. A.; Ito, T. Optical Microscopic Techniques for Synthetic Polymer Characterization, *Anal. Chem.* **2019**, *91*, 405-424.
9. Ghimire, G.; Espinoza, R.; Xu, H.; Nagasaka, S.; Kameta, N.; Masuda, M.; Higgins, D. A.; Ito, T. Diffusion Behavior of Differently Charged Molecules in Self-Assembled Organic Nanotubes Studied Using Imaging Fluorescence Correlation Spectroscopy, *Langmuir* **2019**, *35*, 7783-7790.

(II) Jointly funded by this grant and other grants with leading intellectual contribution from this grant:

10. Ghimire, G.; Yi, Y.; Derylo, M. A.; Baker, L. A.; Ito, T. Electron Propagation within Redox-Active Microdomains in Thin Films of Ferrocene-Containing Diblock Copolymers. *Langmuir* **2015**, *31*, 12307-12314.
11. Kisley, L.; Brunetti, R.; Tazuin, L. J.; Shuang, B.; Yo, X.; Kirkemide, A. W.; Higgins, D. A.; Weiss, S.; Landes, C. F. Characterization of Porous Materials by Fluorescence Correlation Spectroscopy Super-resolution Optical Fluctuation Imaging. *ACS Nano* **2015**, *9*, 9158-9166.
12. Sun, X.; Xie, J.; Xu, J.; Higgins, D. A.; Hohn, K. L. Single-Molecule Studies of Acidity Distributions in Mesoporous Aluminosilicate Thin Films. *Langmuir* **2015**, *31*, 5667-5675.
13. Ghimire, G.; Coceancigh, H.; Yi, Y.; Ito, T. Electrochemical Characterization and Catalytic Application of Gold-Supported Ferrocene-Containing Diblock Copolymer Thin Films in Ethanol Solution. *ACS Appl. Mater. Interfaces* **2017**, *9*, 2906-2913.

14. Coceancigh, H.; Tran-Ba, K.-H.; Siepser, N.; Baker, L. A.; Ito, T. Longitudinally Controlled Modification of Cylindrical and Conical Track-Etched Poly(ethylene terephthalate) Pores Using Electrochemically-Assisted Click Reaction. *Langmuir* **2017**, *33*, 11998-12006.
15. Ito, T.; Ghimire, G. Electrochemical Applications of Microphase-Separated Block Copolymer Thin Films, *ChemElectroChem* **2018**, *5*, 2937-2953.
16. Harandizadeh, Z.; Xie, J.; Moore, M. M.; Hohn, K. L.; Ito, T. Sensitization with Stannous Acetate in Dimethyl Sulfoxide for Silver Electroless Deposition, *J. Electrochem. Soc.* **2018**, *165*, D488-D493.

(III) Jointly funded by this grant and other grants with relatively minor intellectual contribution from this grant:

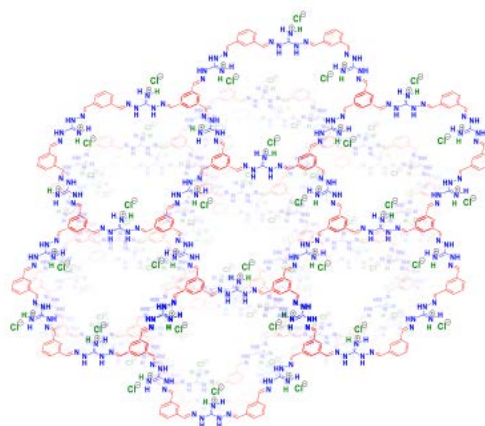
17. Collinson, M. M.; Higgins, D. A. Organosilane Chemical Gradients: Progress, Properties, and Promise. *Langmuir* **2017**, *33*, 13719-13732.
18. Li, Z.; Ashraf, K. M.; Collinson, M. M.; Higgins, D. A. Single Molecule Catch and Release: Potential-Dependent Plasmid DNA Adsorption along Chemically Graded Electrode Surfaces. *Langmuir* **2017**, *33*, 8651-8662.

Tuning Oxoanion Selectivity in Ionic COFs

Santa Jansone-Popova, Antoine Konter, Shannon M. Mahurin, Hailong Lyu
Chemical Sciences Division, Oak Ridge National Laboratory

Poster Abstract

Ionic covalent organic frameworks (iCOFs) have emerged as unique materials capable of selectively sequestering anions, including toxic pollutants, from aqueous media. Three novel COFs bearing positively charged groups were synthesized, all three show a remarkable affinity for different oxoanions. Experiments were designed to reveal the effects of the frameworks' structure induced non-covalent secondary interactions on complexation of tetrahedral oxoanions. The resulting oxoanion affinity can be finely controlled by introducing judicious changes to the structure of iCOFs (pore size, secondary interaction site, and pore surface). These fundamental insights into structure-selectivity relationships will support the development of novel oxoanion-selective materials for rapid environmental remediation.



ionic
for
to
and

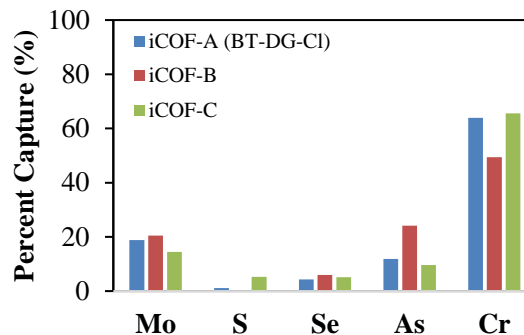
ERKCC08: Principles of Chemical Recognition and Transport in Extractive Separation

Student(s): Antoine Konter

RECENT PROGRESS

iCOFs

Three novel iCOFs built upon condensation of bis-amino guanidinium with polyaldehydes have been synthesized and their physical properties characterized. The resulting frameworks thus feature pores girded by bis-imino guanidinium groups that selectively bind oxoanions. The performance of these iCOFs was compared to that of previously developed iCOF, BT-DG_{Cl} (iCOF-A). The new iCOFs with varying structure (pore size (iCOF-B), secondary interaction site (iCOF-C), and pore surface) show a shift in affinity for different oxoanions. The iCOF with increased pore size exhibits an increased affinity for perrhenate, hydrogen arsenate, and molybdate. Interestingly, despite the increased hydrophobicity of the new



iCOFs, the increase in water uptake per ionic site also increases. The effects causing the change in oxoanion selectivity are yet to be understood and require further investigation. A collaborative effort has been established with Prof. Salehi (Univ. of Memphis), who is using the iCOF-A to design a fiber membrane that will be used for selective sequestration of aqueous pollutants.

Nanostructures with embedded crown ethers

For the first time, a planar cyclic polyether has been synthesized on a multi-gram scale, highlighting the remarkable efficiency of the developed synthesis scheme. This material has a porous cavity decorated with six oxygens and interacts with cations and, potentially, anions when oxidized. Cyclic voltammetry suggests redox-tunable separation ability of this novel compound. Using a slightly modified synthesis scheme, two extended, highly rigid spiral structures were synthesized as well. These have potential to be used as materials for highly efficient ion transport, for example, in batteries.

Publications Acknowledging this Grant in 2015 – present

(I) Exclusively funded by this grant;

1. Jansone-Popova, S.; Moinel, A.; Schott, J. A.; Mahurin, S. M.; Popovs, I.; Veith G. M.; Moyer, B. A. “Guanidinium-Based Ionic Covalent Organic Framework (iCOF) for Rapid and Selective Removal of Toxic Cr(VI) Oxoanions from Water” *Environ. Sci. Technol.*, **2018**, 53 (2), 878-883. [Journal Cover]

(II) Jointly funded by this grant and other grants with leading intellectual contribution from this grant;

2. Huang, Z.; Jia, C.; Jansone-Popova, S.; Seipp, C. A.; Custelcean, R. “Selective binding of aqueous sulfate by quaternary ammonium functionalized oligo-ureas” *Chem. Comm.*, **2019**, 55, 1714-1717.

(III) Jointly funded by this grant and other grants with relatively minor intellectual contribution from this grant;

3. Hachtel, J. A.; Huang, J.; Popovs, I.; Jansone-Popova, S.; Keum, J.; Jakowski, J.; Lovejoy, T. C.; Dellby, N.; Krivanek, O. L.; Idrobo, J. C. “Identification of Site-Specific Isotopic Labeling in Amino Acids by Vibrational Spectroscopy in the Electron” *Science*, **2019**, 363, 525-528.
4. Ivanov, A. S.; Parker, B. F.; Zhang, Z.; Aguila, B.; Ma, S.; Jansone-Popova, S.; Arnold, J.; Mayes, R. T.; Dai, S.; Bryantsev, V. S.; Rao, L.; Popovs, I. “Siderophore-inspired chelator hijacks uranium from aqueous medium” *Nat. Comm.*, **2019**, 10, 819.

Advanced Membranes for Gas Separation: Design, Simulation, and Guided Synthesis

Poster presented by: De-en Jiang, University of California, Riverside (UCR)

Part of ORNL FWP, “Fundamental Studies of Novel Separations”

PI: Sheng Dai

Co-PIs: De-en Jiang, Shannon Mahurin, Ilja Popovs, Huimin Luo, Gernot Rother

UCR team: Song Wang (graduate student), Ziqi Tian (former postdoc)

ORNL team: Wei Guo (postdoc)

Overall research goals: The overarching goal of this project is to understand chemical separation phenomena enabled by novel separation media containing ionic liquids that selectively bind and/or transport target molecular/ionic species via tailored interactions at interfaces and through the control of solvation environments and the formation of structures at multiple length scales.

Significant achievements in 2018-2019:

- Using molecular dynamics simulations, we investigated gas permeation through nanoporous **graphene membranes with the pore density varying over two orders of magnitude** (from 0.01 to 1.28 nm⁻²). For a weakly adsorbing gas such as He, we found that the gas permeation is dominated by gas-phase direct flux and hence the permeation rate per unit of membrane area increases almost linearly with the pore density. For a strongly adsorbing gas such as CO₂, we found that gas permeation is dominated by the adsorption-phase surface flux and hence the overall trend of the permeation rate with the pore density is an interplay between adsorption and surface diffusion.¹
- We proposed a novel design based on the bilayer nanoporous graphene membrane that allows **the pore size to be continuously tunable** by the offset or the relative shift between the two single layers of nanoporous graphene. Confirming the design, molecular dynamics (MD) simulations show that the effective pore size can be tuned at 0.1 Å resolution, to achieve highly selective CO₂/CH₄ and N₂/CH₄ separations, while high permeance (~10⁵ GPU) can be maintained through the bilayer membrane. The bilayer design also allows greater flexibility of the pore size in the single layer that can be as large as 25 Å for separating gas molecules.²
- Membrane air separation is challenging because of the similar kinetic diameters of N₂ and O₂. We demonstrated from MD simulations that a bilayer nanoporous graphene membrane with an effective pore size of 3.45 Å can achieve O₂/N₂ selectivity up to 26 with a permeance over 10⁵ GPU for O₂, rivalling the best available membranes. Interestingly, we found that the skinnier and shorter **O₂ molecules tumble through the elliptic-cylinder-shaped nanopore**, leading to a much **higher entropic contribution to the selectivity**. Both transition-state theory analysis and free-energy simulations confirmed the dominant contribution of entropy to the high selectivity.³
- We proposed a membrane design of an ionic liquid (IL) confined inside a charged porous framework to leverage the combined advantages of ILs and porous frameworks. MD and free energy simulations found that the porous framework increases the gas solubility in the IL, while the mobile ions enhance gas diffusivity through the charged framework. We revealed that the ion confinement impacts CO₂ and CH₄ very differently regarding their solubility and diffusivity in the composite material. By tuning the IL loading, both high CO₂ permeability and high CO₂/CH₄ selectivity can be achieved, overcoming the Robeson upper bound. This work demonstrates **the potential of confined ionic liquids in porous organic materials and the ionic-liquid/porous-material interface for superior membrane gas separation**.⁴
- Guided by the simulations, we have made important experimental progress in integrating ionic liquids (ILs) into porous membranes. We deposited the ILs on the carbon molecular sieve (CMS)

membranes to form a thin interfacial layer. The IL layer acts as a smart gate for gas entry to boost the selectivity. The hybrid membrane exhibits CO₂ permeability > 600 barrer and CO₂/N₂ selectivity > 50, surpassing the Robeson upper bound. MD simulations of the IL/CMS system confirmed the gating effect of the IL layer. This work demonstrated **our success in design- and simulation-guided synthesis** of advanced membranes that leverage the ion-pore interactions for gas separation.⁵

Science objectives for 2019-2020:

Design and simulate the interface of ionic liquids and 2D nanosystems as a mixed-matrix-membrane to interrogate how the interlayer spacing and the interface impact gas adsorption and permeation.

Simulate and understand how the interfacial interaction dictates gas separation by porous liquids made of cage compounds and nanoporous crystalline materials.

Understand how the second coordination shell impacts the separation of actinides by soft-donor ligands with charged groups in ionic liquids.

References to work supported by this project for 2018-2019:

1. Wang, S.; Tian, Z. Q.; Dai, S.; Jiang, D. E. Effect of pore density on gas permeation through nanoporous graphene membranes. *Nanoscale*, 2018, 10, 14660-14666.
2. Wang, S.; Dai, S.; Jiang, D. E. Continuously tunable pore size for gas separation via a bilayer nanoporous graphene membrane. *ACS Appl. Nano Mater.*, 2019, 2, 379–384.
3. Wang, S.; Dai, S.; Jiang, D. E. Entropic selectivity in air separation via a bilayer nanoporous graphene membrane. *Phys. Chem. Chem. Phys.*, 2019, 21, 16310-16315.
4. Tian, Z.; Dai, S.; Jiang, D. E. Confined ionic liquid in an ionic porous aromatic framework for gas separation. *ACS Appl. Polymer Mater.*, 2019, 1, 95-102.
5. Guo, W.; Mahurin, S. M.; Wang, S.; Meyer, H. M.; Luo, H.; Hu, X.; Jiang, D. E.; Dai, S. Ion-gated carbon molecular sieve membranes for enhanced gas separation that surpass the Robeson upper bond. Submitted.

Tailoring High Performance Carbon Molecular Sieve Membranes for Energy Intensive Separations

William J. Koros, Samuel Hays and Nicholas Leon
Georgia Institute of Technology, School of Chemical & Biomolecular Engineering

Presentation Abstract

This project pursues fundamental understanding of carbon molecular sieve (CMS) membranes to enable major separation cost and energy use reductions. By controlled pyrolysis of selected polyimide precursors in dense film and asymmetric hollow fibers, we have demonstrated unusually high selectivities and productivities as compared to polymeric membranes. Our work on O₂/N₂, C₂H₄/C₂H₆, C₃H₆/C₃H₈, N₂/CH₄ and CO₂/CH₄ pairs has provided fundamental insights into the basis for the superior properties of the CMS materials and approaches to improve performance. These gas pairs are not only fundamentally interesting, but also very important for large-scale applications. Recently, we have added an additional feature to expand the impact of our work. Specifically, we are now also focusing on the same fundamental materials, but seeking to show they can also be used to separate CH₄ from C₂H₆. This work is particularly important, since these two gases are key components in shale gas, and are much more valuable when separated. Currently, separation processes available for the CH₄/C₂H₆ pair are not energy efficient, and we are exploring carbon molecular sieve membranes and operational conditions tuned to address this high impact target. Insights from the work will suggest advanced CMS structures with tailored properties and preferred operating conditions for diverse challenging separations as will be discussed.

Grant Number: No. DE-FG02-04ER15510 with Supplement Funding under DE-FOA-0001664

Students: Samuel Hays and Nicholas Leon

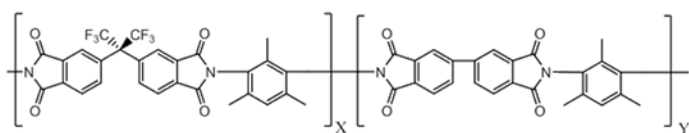
RECENT PROGRESS

1.0 Overview: Separations of important gas pairs involve discrimination of 0.1-0.5 Å, thereby making size-based separations exceedingly difficult. A “sorption-diffusion” mechanism reflected by the ratio of steady state permeabilities is even more difficult when the more strongly sorbing component in a pair is the largest of the two penetrants. This situation applies, for example, to the N₂/CH₄ pair; however, the slim nature of N₂ provides a higher diffusion coefficient than the bulky CH₄, so N₂/CH₄ permselectivity is >1. For the CO₂/CH₄ pair, the slimmer and more sorptive CO₂ has a large advantage over CH₄, so high permselectivities can be achieved. For the important CH₄/C₂H₆ pair, the slightly more compact CH₄ has a small diffusion advantage, while the high critical temperature C₂H₆ has a higher sorption coefficient, so this is even more difficult than the N₂/CH₄ case. This fact notwithstanding, we have a strategy to enable the C₂H₆ to exclude CH₄ from sorption and transport opportunities by operating at a lower temperature, and this is the basis for our supplemental support noted in the Grant Number section.

2.0 Fundamental and Experimental Advances: The size and shape selection capabilities of CMS are affected by both the precursor polymer as well as the pyrolysis and post-pyrolysis conditions. As with any glass, CMS materials undergo some physical aging, and our work has focused on clarifying how and why this physical aging occurs in CMS. Besides the earlier work we on CMS cited below, *we will be submitting a paper on this topic over the next 2-3 weeks.* The work shows

that physical aging in the CMS from the precursor we use, 6FDA:BPDA-DAM 1:1, (copolymer with equal amounts of 6FDA and BPDA in the structure) is *primarily related to diffusion coefficient changes*.

This result was not expected, but by systematically determining sorption, diffusion and permeation properties and selectivity factors, the data strongly indicate the dominance of the diffusion coefficient effects.



6FDA:BPDA-DAM (X=1, Y=1)

6FDA: 4,4'-(hexafluoroisopropylidene) diphthalic anhydride

BPDA: 3,3'-4,4'-biphenyl tetracarboxylic dianhydride

DAM: 2,4,6-trimethyl-1,3-phenylene diamine

Figure 3a: Chemical structure of semi-flexible 6FDA:BPDA-DAM (1:1) precursor.

Guided by the above fundamental insights, we have shown that by controlling the post-pyrolysis storage conditions, physical aging of the CMS can be greatly inhibited. We have an

early stage physical model to explain this exciting result, which will be discussed.

3.0 Publications—Acknowledging this Grant in 2015 → present

(I) Exclusively funded by this grant;

1. Zhang, C.; Kumar, R.; Koros, W., Ultra-Thin Skin Carbon Hollow Fiber Membranes for Sustainable Molecular Separations, *AICHE J*, **2019**, 65 (8), article no. UNSP e16611, DOI: 10.1002/aic.16611.
2. Kumar, R; Zhang, C; Itta, Arun K.; Koros, W., Highly Permeable Carbon Molecular Sieve Membranes for Efficient CO₂/N₂ Separation at Ambient and Subambient Temperatures, *J. Membr. Sci.*, **2019**, 583, 9-15.
3. Cao, Y.; Zhang, K.; Sanyal, O.; Koros, W., Carbon Molecular Sieve Membrane Preparation by Economical Coating and Pyrolysis of Porous Polymer Hollow Fibers, *Angew. Chem. Int. Ed.* **2019**, 58, 11700 –11703.
4. Kumar, R.; Koros, W., 110th Anniversary: High Performance Carbon Molecular Sieve Membrane Resistance to Aggressive Feed Stream Contaminants, *Indus. & Engr. Chem. Res.*, **2019**, 58(16) 6740-6746.
5. Adams, J. ; Itta, A.; Zhang, C. ;Wenz, G. ; Sanyal, O. ; Koros, W., New Insights into Structural Evolution in Carbon Molecular Sieve Membranes During Pyrolysis, *CARBON*, **2019**, 141, 238-246.
6. Zhang, C. Zhang, K.; Cao, Y.; Koros, W. Composite Carbon Molecular Sieve Hollow Fiber Membranes: Resisting Support Densification via Silica Particle Stabilization, *Indus. & Engr. Chem. Res.*, **2018**, 57 (47), 16051-16058.
7. Sanyal, O. ; Hicks, S.; Bhuwania, N. ; Hays, S. ; Kamath, M.; Karwa, S ;Swaidan, R.; Koros, W. Cause and Effects of Hyperskin Features on Carbon Molecular Sieve (CMS) Membranes, *J. Membr. Sci.*, **2018**, 551, 113-122.
8. Sanyal, O.; Zhang, C.; Wenz, G.; Fu, Shilu; Bhuwania, N.; Xu, Liren; Rungta, M. ; Koros, W. Next Generation Membranes-Using Tailored Carbon, *CARBON*, **2018**, 127, 688-698.

9. Koros, W.; Zhang, C. Materials for Next-Generation Molecularly Selective Synthetic Membranes, *Nature Materials*, **2017**, 16, 289-297.
 10. Qiu W.; Liu, L.; Koros, W. Effect of Block Versus Random Copolyimide Structure on Hollow Fiber Membrane Spinnability. *J. Membr. Sci.*, **2017**, 529, 150-158.
 11. Wenz, G.; Koros, W. Tuning Carbon Molecular Sieves for Natural Gas Separations: A Diamine Molecular Approach. *AICHE J*, **2017**, 63, 51-760.
 12. Adams, J.; Bighane, N.; Koros, W. Pore Morphology and Temperature Dependence of Gas Transport Properties of Silica Membranes Derived from Oxidative Thermolysis of Polydimethylsiloxane. *J. Membr. Sci.*, **2017**, 524, 585-595.
- (II) *Jointly funded by this grant and other grants with leading intellectual contribution from this grant;*
13. Joglekar, M; Itta, A.; Kumar, R.; Wenz, G.; Mayne, J.; Williams, P. ; Koros, W. Carbon Molecular Sieve Membranes for CO₂/N₂ Separations: Evaluating Subambient Temperature Performance, *J. Membr. Sci.*, **2018**, 569, 1-6.
 14. Chu, Y. H.; Yancey, D. ;Xu, L. ; Martinez, M.; Brayden, M.; Koros, W. Iron-Containing Carbon Molecular Sieve Membranes for Advanced Olefin/Paraffin Separations, *J. Membr. Sci.*, **2018**, 548, 609-620.
 15. Kamath, M. G.; Fu, Shilu; Itta, Arun K.; Qiu, W. L.; Liu, G. P.; Swaidan, R.; Koros, W. J. 6FDA-DETDA: DABE Polyimide-Derived Carbon Molecular Sieve Hollow Fiber Membranes: Circumventing Unusual Aging Phenomena. *J. Membr. Sci.*, **2018**, 546, 197-205.
 16. Fu, S.; Sanders, Edgar S.; Kulkarni, S.; Chu, Y. H; Wenz, GB; Koros, WJ. The Significance of Entropic Selectivity in Carbon Molecular Sieve Membranes Derived from 6FDA/DETDA:DABA(3:2) Polyimide. *J. Membr. Sci.*, **2017**, 329-343.
 17. Zhang, C.; Wenz, G.B.; Williams, J.P.; Mayne, J. M.; Liu, G. P.; Koros W. J. Purification of Aggressive Supercritical Natural Gas Using Carbon Molecular Sieve Hollow Fiber Membranes. *Indus. & Engr. Chem. Res.*, **2017**, 56, 10482–10490.
 18. Zhang, C.; Koros, W. J. Ultrasensitive Carbon Molecular Sieve Membranes with Tailored Synergistic Sorption Selective Properties, *Adv. Mater.* **2017**, 29, 1701631
 19. Rungta, M.; Wenz, G. B. Zhang, C.; Xu, L.; Qui, W. L.; Adams, J. S.; Koros, W. J. Carbon Molecular Sieve Structure Developments and Membrane Performance Relationships, *Carbon*, **2017**, 115, 237-248.
 20. Liu, G.P.; Li, N.; Miller S.; Kim D. ; Yi, S.; Labreche, Y.; W. Koros. Molecularly Designed Stabilized Asymmetric Hollow Fiber Membranes for Aggressive Natural Gas Separation. *Angew. Chem. Int. Ed.* **2016**, 55, 13754-13758.
 21. Fu, S.; Wenz, G.B.; Sanders, S.; Kulkarni, S.; Qiu, W.; Ma, C.H.; Koros, W. J. Effects of Pyrolysis Conditions on Gas Separation Properties of 6FDA/DETDA:DABA(3:2) Derived Carbon Molecular Sieve Membranes. *J. Membr. Sci.*, **2016**, 520, 699-711.
 22. Fu, S.; Sanders, E.; Kulkarni, S.; Wenz, G. B. Koros, W. J. Temperature Dependence of Gas Transport and Sorption in Carbon Molecular Sieve Membranes Derived from Four 6FDA Based Polyimides: Entropic Selectivity Evaluation. *CARBON*, **2015**, 95, 995-1006.

(III) *Jointly funded by this grant and other grants with relatively minor intellectual contribution from this grant*

23. Zhang, C.; Koros, W. J. Tailoring the Transport Properties of Zeolitic Imidazolate Frameworks by Post-Synthetic Thermal Modification, *ACS Appl. Mater. Interfaces.* **2015**, *7*, 23407-23411.
24. Zhang, C.; Koros, W. J. Zeolitic Imidazolate Framework - Enabled Membranes: Challenges and Opportunities, *J. Phys. Chem. Lett.*, **2015**, *6*, 3841–3849

Differences in the extent of counterion condensation of ordered block copolymer electrolytes (BCEs) versus random copolymer electrolytes (RCEs)

Qi Lei^a, Ke Li^b, Christopher G. Arges^a, and Revati Kumar^b

^aCain Department of Chemical Engineering, Louisiana State University

^bDepartment of Chemistry, Louisiana State University

Presentation Abstract

This project systematically investigates counterion condensation in microphase separated block copolymer electrolytes (BCEs) and random copolymer electrolytes (RCEs). The initial model system consists of poly(styrene-*block*-2-vinyl n-methyl pyridinium iodide/2-vinyl pyridine) and poly(styrene-*random*-vinyl n-methyl pyridinium iodide/2-vinyl pyridine). The broad goal of the research is to know the different extents of counterion condensation in microphase separated BCEs versus non-ordered, random copolymer electrolytes and to establish a relationship between the extent of counterion condensation and block copolymer period size. In the past year, three different analytical methods were developed to quantify the extent of counterion condensation in BCE and RCE thin films. These independent methods are: i.) ion-sorption and release experiments in custom built cells for thin films and using LC-MS and ion-exchange chromatography to assay changes in salt concentration, ii.) water uptake experiments of the thin films immersed in different salt solutions using a quartz crystal microbalance (QCM), and iii.) grazing-incidence small-angle x-ray scattering (GI-SAXS; for BCE samples only) that monitors changes in periodic domain size when the thin film is immersed in salt solutions. From these experiments, the Donnan equilibrium between the thin film and the salt solution is established and is used to quantify the extent of counterion condensation when knowing the thin film's ion-exchange capacity (IEC) value. The preliminary results from QCM have hint that the BCEs display less counterion condensation than the RCEs. To complement the experimental studies, all-atom molecular dynamic simulations were performed on single-chains that mimicked BCE and RCE configurations. The simulation results differ from experimental studies (i.e., the RCEs are less susceptible to counterion condensation than BCEs). However, it is important to note that the simulations are predicting a much smaller counterion condensation value because there are too many water molecules in the simulations. The team is looking to address the different findings between simulations and experimental data.

Grant or FWP Number: Understanding and manipulating counterion condensation within charged polymer electrolytes for selective and low resistant membrane separations

PI: Christopher G. Arges

Student(s): Qi Lei, Ke Li

Affiliations(s): Cain Department of Chemical Engineering and Department of Chemistry, Louisiana State University

RECENT PROGRESS

Swelling uptake experiments of BCE and RCE in different aqueous solutions of KI

A QCM with BCE or RCE was equilibrated with potassium iodide (KI) solutions. The frequency change was monitored upon introduction of the solution and was measured until a stable

frequency value was attained. The frequency shift was correlated to the mass/swelling uptake. The different swelling uptakes were plotted versus KI solution concentration to identify the Donnan equilibrium concentration (C_D). The IEC of the thin BCE and RCE film (approx. 30 nm in thickness) was determined using x-ray photoelectron spectroscopy (XPS). The fraction of condensed (f_c) counterions was determined by $1 - C_D/C_{IEC}$. The f_c for the RCE was 0.97. The BCE f_c values has not been determined yet (waiting on IEC value determination). See **Figure 1** for results.

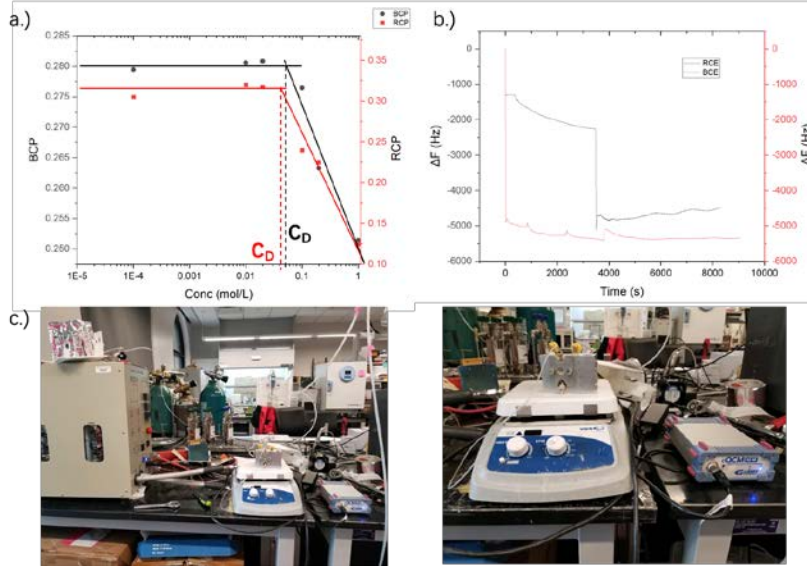


Figure 1. a.) Swelling uptake of the BCE and RCE in different KI solutions; b.) example QCM frequency changes upon introduction of KI solution with BCE and RCE thin films; c.) QCM setup in PI Arges’s lab.

Co-ion sorption experiments

BCE and RCE samples on wafer substrates were then placed in a custom-made chamber and 1mL of KI solution (a particular concentration) was injected into the chamber with a thin volume compartment above the film. Equilibrium was attained over 24h. Then, the KI solution was removed and the chamber was injected with DI water and then equilibrated for another 24h. The collected DI water was analyzed by ICP-AES for potassium content. The co-ion sorption data was compared against different simulated co-ion sorption data from the Donnan equation (equation 1). The simulated results were matched to the co-ion sorption data to get the Donnan equilibrium to determine f_c . See **Figure 2** for data.

$$c_{m+} = \frac{-c_b + \sqrt{c_b^2 + 4c^2}}{2} \quad (\text{equation 1})$$

where c is the external salt concentration, c_{m+} is the concentration of dissociated fixed positive charges in the thin film sample. C_b is constant and is simulated to be possible different Donnan equilibrium concentration values.

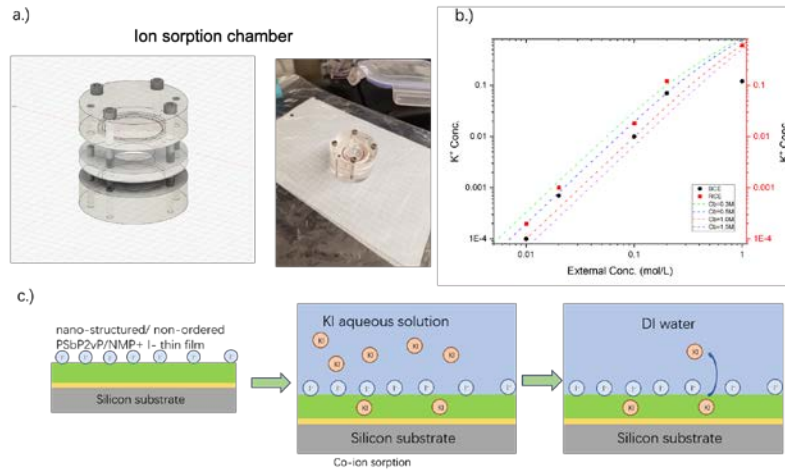


Figure 2. a.) Ion sorption chamber; b.) co-ion sorption experiments data of the BCE and RCE samples. The fitting indicates that $C_D=1M$, so 63% of counterion in the RCE were condensed; c.) A cartoon of the co-ion sorption process in thin films.

GI-SAXS experiments

GI-SAXS was performed on PSbP2VP/NMP⁺ I⁻ (40k-44k; exposed to methyl iodide vapor for 24 hr) at the 8-ID-E beamline at the Advanced Photon Source (APS). The samples were immersed in KI aqueous solution with different concentrations in the GI-SAXS environmental chamber. By monitoring the domain spacing changing with external salt concentration, the C_D and f_c were determined.

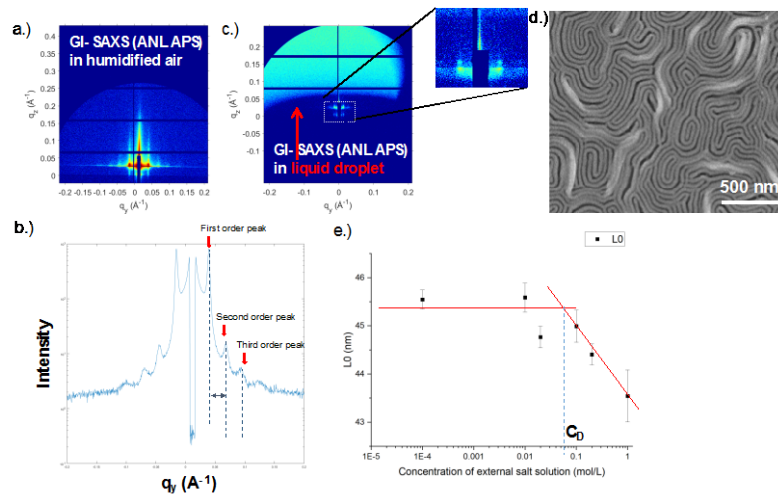


Figure 3. a.) GI-SAXS PSbP2VP/NMP⁺ I⁻ BCE (dry) and b.) line cut curve of dry BCE sample ($L_0=2\pi/\Delta q = 44$ nm). 3rd order peak indicates long range periodicity; c.) GI-SAXS PSbP2VP/NMP⁺ I⁻ BCE (wet); d.) Electron micrograph of PSbP2VP/NMP⁺ I⁻; e.) Change in L_0 for PSbP2VP/NMP⁺ I⁻ BCE exposed to different KI solution concentrations. The determined C_D showed that 95% of the counterions were condensed.

All-atom simulations

All-atom molecular simulations were performed to probe counterion condensation phenomena in model RCEs and BCEs of varying periodicity size and charge density. Classical molecular dynamics simulations were carried out using the OPLSAA all atom force-field for the polymer chains along with the TIP3P model for water. The partial charges on the polymer chains were

obtained by performing electronic structure calculations on a single unit of the polymer chain in each case. Charges from electrostatic potentials using a grid, specifically CHELPG, method was used to determine atomic charges by fitting to the ab initio electrostatic potential on a grid around the polymer brushes unit molecule. The CHELPG scheme was chosen since it is the same scheme that was used to obtain charges for the OPLSAA force field and hence was adopted here for consistency. Eight chains with different microstructure were simulated separately. Each chain was solvated with 6500 water molecules in a cubic box of length 60 Angstroms and the box was then equilibrated in the NVT ensemble for 2ns and the NPT ensemble for 2ns at a temperature of 300K and 1 atm, followed by 20ns production runs in the NVT ensemble at the same temperature. The Nose-Hoover thermostat was adopted to keep the temperature constant, and the integration time step was 1 fs. All the simulations were carried out with the LAMMPS software package under periodic boundary conditions. PPPM Ewald method were used to account for long-range electrostatics.

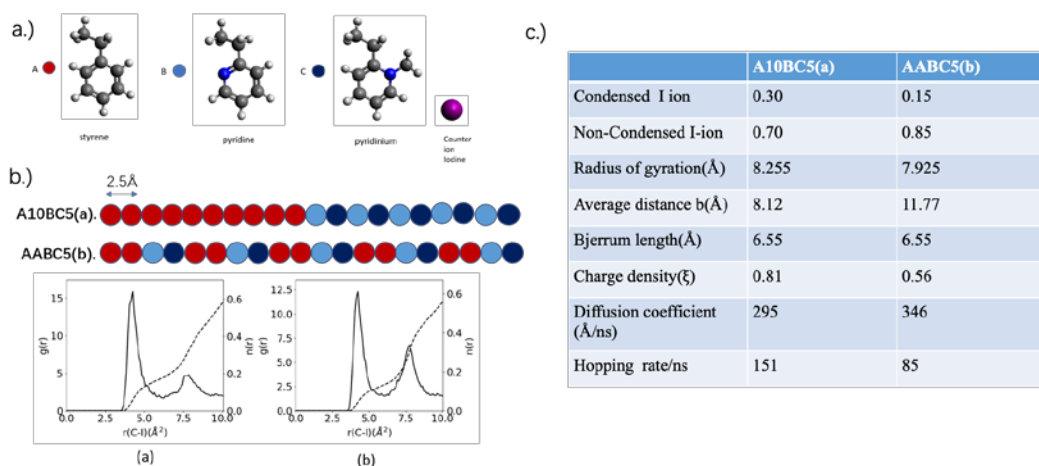


Figure 4. a.) Molecular substituents in b.) the model BCE (top) and model RCE (bottom) and their subsequent radial distribution functions; c.) results from all-atom classical MD simulations with BCE and RCE (which has less counterion condensation).

Publications Acknowledging this Grant in 2019 – present

Please classify your publications into three categories according to the source of support for the work published:

- (I) none
- (II) none
- (III) Arges, C. G.; Li, K.; Zhang, L.; Kambe, Y.; Wu, G.-p.; Lwoya, B.; Albert, J.N.L.; Nealey, P.F.; Kumar, R. *Mol. Syst. Des. Eng.*, **2019**, 4, 365-378.

Tunable, Nanoporous, Two-dimensional Covalent Organic Frameworks for Size and Charge Separations

Phuoc H. H. Duong,¹ Valerie A. Kuehl,² John O. Hoberg,² Bruce A. Parkinson,² Katie D. Li-Oakey¹

¹Department of Chemical Engineering, University of Wyoming, 1000 E. University Ave., Laramie, WY 82071

²Department of Chemistry, University of Wyoming, 1000 E. University Ave., Laramie, WY 82071

Abstract

To date, it is still the biggest challenge to the field of separation science to construct membranes via a bottom-up approach, from an atomic or molecular scale, that allow the separation of the species from solutions based on size or surface charge or both by either designing or tuning the building blocks of membrane materials. To address this challenge and probe liquid separation from the perspective of the complex microenvironments at the liquid-membrane interface, our team has synthesized and characterized an array of 2D Covalent Organic Frameworks (COFs) from simple small molecule precursors at low cost with high yields and high degrees of order due to our use of microwave synthesis. The ultrathin structure and tunability of pore size and functionality of these porous 2D COFs enable the resultant 2D COF-based membranes to achieve high flux while maintaining high selectivity towards a wide range of solutes, thanks to their highly ordered and tunable properties. Preliminary results from two types of COF-based membranes having different aromatic backbones are presented in our poster. The results show that the COF membranes exhibit ultra-fast solvent permeance for both polar and non-polar solvents, which is two orders of magnitude higher than that of the reported graphene oxide (GO) membranes. The effects of the backbone functionality of COFs on the solvent transport mechanism and solute rejection are investigated using a wide range of solvents with different physical properties and four positively charged dyes with molecular weight ranging from 351 to 1299 g mol⁻¹, demonstrating that COF composite membranes offer high separation performance and tunable separation properties, in addition to serving as an excellent platform for fundamental studies of transport mechanism.

PI ABSTRACTS SESSION IV: MEMBRANES

Fundamental Studies of Novel Separations

Sheng Dai, Principal Investigator

Co-PIs: De-en Jiang, Shannon Mahurin, Ilja Popovs, Huimin Luo, Gernot Rother

Research Team: Zhenzhen Yang (ORNL postdoc), Ziqi Tian (UCR former postdoc); Jennifer Schott (UTK graduate student), Song Wang (UCR graduate student), Nicole Onishi (UCR graduate student); Weihong Wu (UCR visiting student), Wei Xu (ORNL visiting scholar)

Overall research goals: The overarching goal of this project is to understand chemical separation phenomena enabled by novel separation media containing ionic liquids that selectively bind and/or transport target molecular/ionic species via tailored interactions at interfaces and through the control of solvation environments and the formation of structures at multiple length scales.

Significant achievements in 2017-2019:

(1) We pioneered the development of porous liquids as unique separation media. The structural characteristics and adsorption properties were investigated. We further examined these novel nanostructured liquids with intrinsic porosity for membrane gas transport.

(2) We continued our innovation in synthesis methodologies for novel mesoporous carbons, porous organic polymers, and functionalized ionic liquids. Their gas-separation performances were experimentally and computationally characterized to establish a structure-property relationship.

(3) We demonstrated that the unique solvation properties of ionic liquids can be exploited for trivalent actinide separations, in which a preorganization of the second coordination shell was discovered through task-specific ionic liquids. SANS was successfully used to characterize the extraction superstructures involved in IL-based separation.

Science objectives for 2019-2020:

The specific research topics we will investigate are:

(1) What are the design principles for Type-I porous ionic liquids to achieve tailored interactions with the separation targets?

(2) How can molecular interactions and transport be dynamically controlled via the interaction of ionic liquids with porous separation media?

(3) Can micro and meso-scale structures in ionic liquids be controlled for selective metal ion separation?

Selected references to work supported by this project 2017-2019:

1. Zhang, Z. H.; Schott, J. A.; Liu, M. M.; Chen, H.; Lu, X. Y.; Sumpster, B. G.; Fu, J.; Dai, S. Prediction of Carbon Dioxide Adsorption via Deep Learning. *Angew. Chem.-Int. Edit.* **2019**, *58*, 259-263. 10.1002/anie.201812363
2. Xu, W.; Chen, H.; Jie, K. C.; Yang, Z. Z.; Li, T. T.; Dai, S. Entropy-Driven Mechanochemical Synthesis of Polymetallic Zeolitic Imidazolate Frameworks for CO₂ Fixation. *Angew. Chem.-Int. Edit.* **2019**, *58*, 5018-5022. 10.1002/anie.201900787
3. Wang, S.; Dai, S.; Jiang, D. E. Continuously Tunable Pore Size for Gas Separation via a Bilayer Nanoporous Graphene Membrane. *ACS Appl. Nano Mater.* **2019**, *2*, 379-384. 10.1021/acsnm.8b01967
4. Teague, C. M.; Schott, J. A.; Stieber, C.; Mann, Z. E.; Zhang, P. F.; Williamson, B.; Dai, S.; Mahurin, S. M. Microporous and hollow carbon spheres derived from soft drinks: Promising CO₂ separation materials. *Microporous Mesoporous Mat.* **2019**, *286*, 199-206. 10.1016/j.micromeso.2019.04.017
5. Li, P. P.; Chen, H.; Schott, J. A.; Li, B.; Zheng, Y. P.; Mahurin, S. M.; Jiang, D. E.; Cui, G. K.; Hu, X. X.; Wang, Y. Y.; Li, L. W.; Dai, S. Porous liquid zeolites: hydrogen bonding-stabilized H-ZSM-5 in branched ionic liquids. *Nanoscale* **2019**, *11*, 1515-1519. 10.1039/c8nr07337f
6. Jiang, W.; Jia, H.; Li, H. P.; Zhu, L. H.; Tao, R. M.; Zhu, W. S.; Li, H. M.; Dai, S. Boric acid-based ternary deep eutectic solvent for extraction and oxidative desulfurization of diesel fuel. *Green Chem.* **2019**, *21*, 3074-3080. 10.1039/c9gc01004a
7. Dehaut, J.; Williams, N. J.; Luo, H. M.; Dai, S. Extraction of Rare Earths in Ionic Liquids Via Competitive Ligand Complexation between TODGA and DTPA. *Solvent Extr. Ion Exch.* **2018**, *36*, 574-582.

- 10.1080/07366299.2018.1545343
8. Zhu, X.; Hua, Y. Y.; Tian, C. C.; Abney, C. W.; Zhang, P.; Jin, T.; Liu, G. P.; Browning, K. L.; Sacci, R. L.; Veith, G. M.; Zhou, H. C.; Jin, W. Q.; Dai, S. Accelerating Membrane-based CO₂ Separation by Soluble Nanoporous Polymer Networks Produced by Mechanochemical Oxidative Coupling. *Angew. Chem.-Int. Edit.* **2018**, *57*, 2816-2821. 10.1002/anie.201710420
 9. Yang, D. Z.; Zhang, S. Z.; Jiang, D. E.; Dai, S. SO₂ absorption in EmimCl-TEG deep eutectic solvents. *Phys. Chem. Chem. Phys.* **2018**, *20*, 15168-15173. 10.1039/c8cp02250j
 10. Wang, S.; Tian, Z. Q.; Dai, S.; Jiang, D. E. Effect of Pore Density on Gas Permeation through Nanoporous Graphene Membranes. *Nanoscale* **2018**, *10*, 14660-14666. 10.1039/c8nr02625d
 11. Shan, W.; Fulvio, P. F.; Kong, L. Y.; Schott, J. A.; Do-Thanh, C. L.; Tian, T.; Hu, X. X.; Mahurin, S. M.; Xing, H. B.; Dai, S. New Class of Type III Porous Liquids: A Promising Platform for Rational Adjustment of Gas Sorption Behavior. *ACS Appl. Mater. Interfaces* **2018**, *10*, 32-36. 10.1021/acsami.7b15873
 12. Schott, J. A.; Do-Thanh, C. L.; Mahurin, S. M.; Tian, Z. Q.; Onishi, N. C.; Jiang, D. E.; Dai, S. Supported Bicyclic Amidine Ionic Liquids as a Potential CO₂/N₂ Separation Medium. *J. Membr. Sci.* **2018**, *565*, 203-212. 10.1016/j.memsci.2018.08.012
 13. Kong, L. Y.; Shan, W. D.; Han, S. L.; Zhang, T.; He, L. C.; Huang, K.; Dai, S. Interfacial Engineering of Supported Liquid Membranes by Vapor Cross-Linking for Enhanced Separation of Carbon Dioxide. *ChemSusChem* **2018**, *11*, 185-192. 10.1002/cssc.201701851
 14. Chen, D.; Zhang, P. F.; Fang, Q. R.; Wan, S.; Li, H.; Yang, S. Z.; Huang, C. L.; Dai, S. Coordination-Supported Organic Polymers: Mesoporous Inorganic-Organic Materials with Preferred Stability. *Inorg. Chem. Front.* **2018**, *5*, 2018-2022. 10.1039/c8qi00471d
 15. Zhu, X.; Tian, C. C.; Jin, T.; Browning, K. L.; Sacci, R. L.; Veith, G. M.; Dai, S. Solid-State Synthesis of Conjugated Nanoporous Polycarbazoles. *ACS Macro Lett.* **2017**, *6*, 1056-1059. 10.1021/acsmacrolett.7b00480
 16. Zhu, X.; Tian, C. C.; Do-Thanh, C. L.; Dai, S. Two-Dimensional Materials as Prospective Scaffolds for Mixed-Matrix Membrane-Based CO₂ Separation. *ChemSusChem* **2017**, *10*, 3304-3316. 10.1002/cssc.201700801
 17. Zhu, X.; Ding, S. M.; Abney, C. W.; Browning, K. L.; Sacci, R. L.; Veith, G. M.; Tian, C. C.; Dai, S. Superacid-promoted Synthesis of Highly Porous Hypercrosslinked Polycarbazoles for Efficient CO₂ Capture. *Chem. Commun.* **2017**, *53*, 7645-7648. 10.1039/c7cc03620e
 18. Zhang, P. F.; Zhang, J. S.; Dai, S. Mesoporous Carbon Materials with Functional Compositions. *Chem.-Eur. J.* **2017**, *23*, 1986-1998. 10.1002/chem.201602199
 19. Zhang, J. S.; Schott, J. A.; Li, Y. C.; Zhan, W. C.; Mahurin, S. M.; Nelson, K.; Sun, X. G.; Paranthaman, M. P.; Dai, S. Membrane-Based Gas Separation Accelerated by Hollow Nanosphere Architectures. *Adv. Mater.* **2017**, *29*. 10.1002/adma.201603797
 20. Williams, N. J.; Dehaut, J.; Bryantsev, V. S.; Luo, H. M.; Abney, C. W.; Dai, S. Selective Separation of Americium from Europium using 2,9-bis(triazine)-1,10-phenanthrolines in Ionic Liquids: A New Twist on an Old Story. *Chem. Commun.* **2017**, *53*, 2744-2747. 10.1039/c6cc09823a
 21. Wang, S.; Tian, Z. Q.; Dai, S.; Jiang, D. E. Optimal Size of a Cylindrical Pore for Post-Combustion CO₂ Capture. *J. Phys. Chem. C* **2017**, *121*, 22025-22030. 10.1021/acs.jpcc.7b05516
 22. Tian, Z. Q.; Mahurin, S. M.; Dai, S.; Jiang, D. E. Ion-Gated Gas Separation through Porous Graphene. *Nano Lett.* **2017**, *17*, 1802-1807. 10.1021/acs.nanolett.6b05121
 23. Tao, D. J.; Chen, F. F.; Tian, Z. Q.; Huang, K.; Mahurin, S. M.; Jiang, D. E.; Dai, S. Highly Efficient Carbon Monoxide Capture by Carbanion-Functionalized Ionic Liquids through C-Site Interactions. *Angew. Chem.-Int. Edit.* **2017**, *56*, 6843-6847.
 24. Li, P. P.; Schott, J. A.; Zhang, J. S.; Mahurin, S. M.; Sheng, Y. J.; Qiao, Z. A.; Hu, X. X.; Cui, G. K.; Yao, D. D.; Brown, S.; Zheng, Y. P.; Dai, S. Electrostatic-Assisted Liquefaction of Porous Carbons. *Angew. Chem.-Int. Edit.* **2017**, *56*, 14958-14962. 10.1002/anie.201708843
 25. Abney, C. W.; Do, C.; Luo, H. M.; Wright, J.; He, L. L.; Dai, S. Controlling the Intermediate Structure of an Ionic Liquid for f-Block Element Separations. *J. Phys. Chem. Lett.* **2017**, *8*, 2049-2054.

Gas Transport Properties in Poly(benzimidazoles) Physical aging and humidified permeation

Melanie M. Merrick, Joshua D. Moon, and Benny D. Freeman
The University of Texas at Austin, McKetta Department of Chemical Engineering

Presentation Abstract

Poly(benzimidazoles) (PBIs) have been of significant interest for gas separation studies at elevated temperature ($\sim 200^\circ\text{C}$) and in systems where gas permeation is occurring in the presence of humidity. Today, practical membranes for gas separations are on the order of 100 nm, and in this range, permeation properties are known to be thickness and time dependent. However, no systematic, fundamental data have been reported regarding the impact of humidity on PBI transport, and studies of gas transport properties of thin membranes at elevated temperature are not available for any material, including PBI. This presentation will focus on reporting fundamental studies of the impact of humidity on PBI transport properties and systematic studies of physical aging in thin PBI films.

Grant Number: DE-FG02-02ER15362

Grant Title: Fundamental Structure/Property Studies of New Gas Separation Membrane Polymers

RECENT PROGRESS

Humidified gas transport in PBIs

m-PBI, commercially known as Celazole[®], can uptake over 20 weight percent water, an order of magnitude more than most common commercial membrane materials. A series of studies were conducted to determine the effect of water on PBI's gas transport properties.

The presence of water can have many different effects on a polymer membrane's performance. Gas diffusivities, and therefore permeabilities, can increase if the polymer membrane becomes swollen or plasticized. Conversely, competitive sorption or antiplasticization effects can decrease the permeability of a membrane.

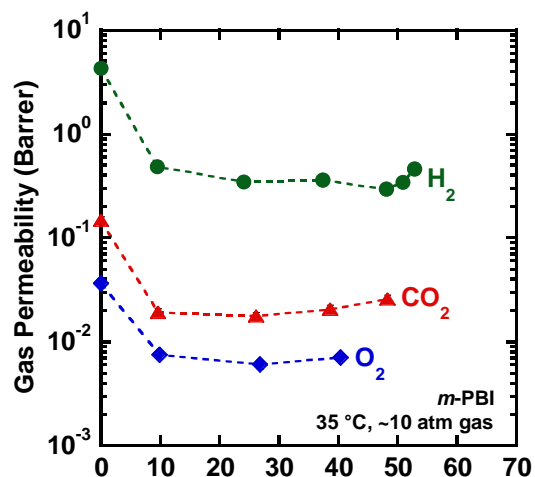


Figure 6. Gas permeabilities as a function of relative humidity for *m*-PBI.

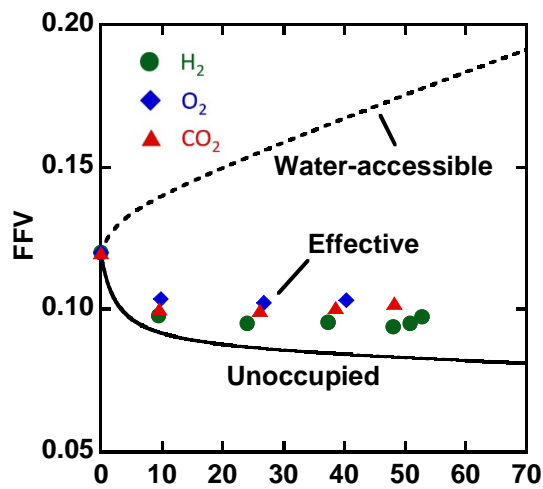


Figure 7. Fraction free volume vs. relative humidity for m-PBI.

Gravimetric sorption and vapor dilatometry of *m*-PBI were measured using a quartz spring balance apparatus. A dual-mode sorption model that accounts for the polymer's Henry Law constant and Langmuir capacity accurately describes PBI water vapor sorption and dilation at water activities up to 60 percent RH. Calculated water diffusion coefficients in PBI suggest plasticization is occurring at all humidities.

However, measurements of gas permeabilities in humid environments suggest that plasticization only dominates at higher humidities. H₂, CO₂, and O₂ gas permeabilities in a humid environment are significantly lower than dry gas permeabilities (cf.,

Figure 1). This suggests competitive sorption and anti-plasticization dominate at low humidities.

Humidified gas permeabilities correlate more closely with the unoccupied fractional free volume (FFV) than the water-accessible FFV of the membrane, although neither perfectly describes the behavior (cf., Figure 2). The effective FFVs calculated from permeability correlations with kinetic gas diameter are higher than the unoccupied FFVs which is attributed to plasticization's enhancement of polymer chain mobility.

Evidently the impacts of humidity on the gas transport properties of a hygroscopic membrane material are very complex. Direct measurement of dry and humidified gas solubilities in PBI can further elucidate the effects of humidity.

Physical aging in thin PBI films

Physical aging is known to more strongly impact the performance of thin films than bulk films. Decreases in gas permeability brought about by physical aging have been characterized for many common membrane materials near 35 °C. However, physical aging's effects on PBIs have not been measured at any temperature.

Because PBI is of interest for high temperature applications, the gas separation properties of *m*-PBI membranes were characterized at temperatures up to 190 °C. Gas permeabilities, gas selectivities, activation energies of permeation, and physical aging rates differed significantly between thin sub-micron and bulk 20-micron films.

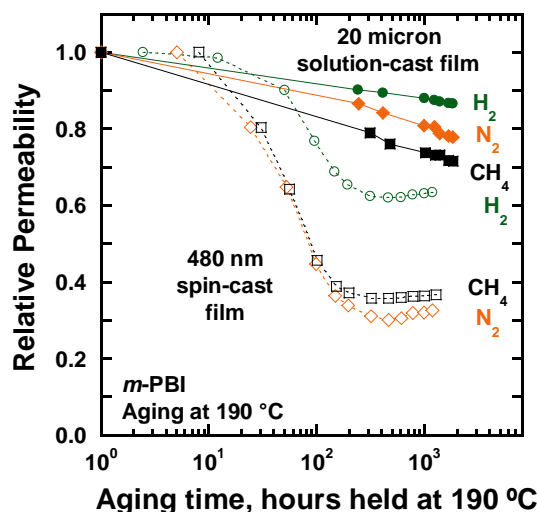


Figure 8. Relative gas permeabilities measured at 190 °C while aging over > 1000 hours at 190 °C.

Over more than 1000 hours, the gas permeabilities of a 20 μm bulk PBI film decreased by no more than 30 percent. The nitrogen and methane permeabilities of a 480 nm thin membrane

decreased rapidly in the first several hundred hours and then plateaued at about 30 to 40 percent of their starting values (cf., **Figure 3**). This plateau in gas permeability has not been observed for other membrane materials whose permeabilities generally continue to decrease even when measured over 10,000 hours at 35 °C. The cause of this plateau is being investigated using analytical methods such as spectroscopic ellipsometry and small-angle x-ray scattering.

Gas permeabilities were measured over a range of temperatures from 190 to 125 °C (cf., **Figure 4**). The thin film permeabilities were measured after the film had been aged at 190 °C for more than 1000 hours. The activation energies of permeation given in **Table 1** were calculated over this temperature range for the bulk and thin films. The activation energies of permeation were 1.5 to 4 times higher in an aged thin film than in a bulk film, suggesting a denser membrane structure and greater size-sieving ability.

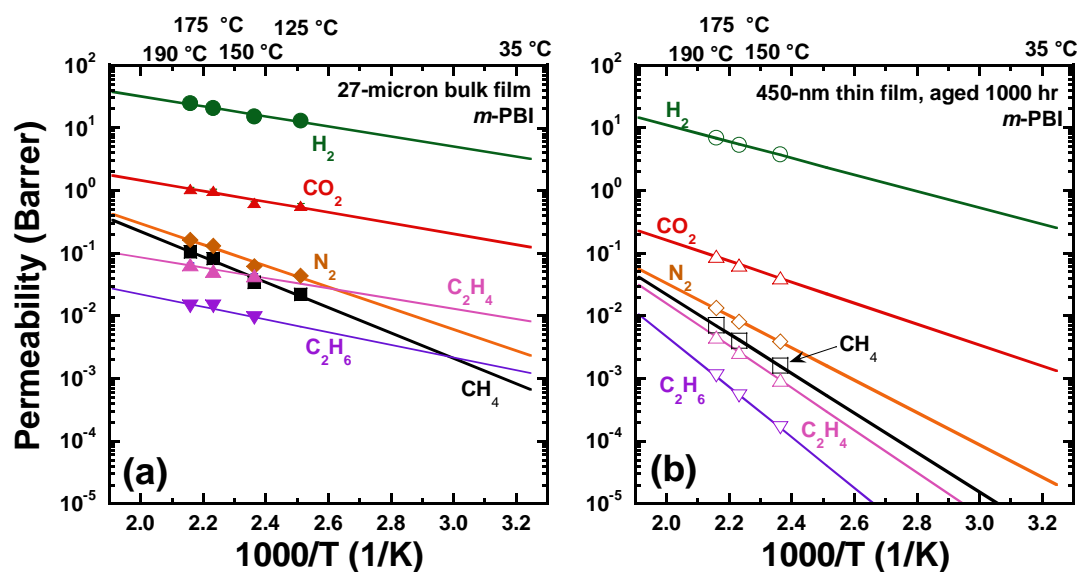


Figure 9. Permeability vs. inverse temperature for (a) bulk 20 micron film and (b) thin 450 nm thin film that had been aged 1000 hours at 190 °C.

Table 1. Activation energies of permeation (kJ/mol) for 27- μm bulk film and 450-nm aged thin film.

	E_P (kJ/mol)					
	H ₂	CO ₂	N ₂	CH ₄	C ₂ H ₄	C ₂ H ₆
Bulk film, 20 μm	15 \pm 2	16 \pm 3	32 \pm 4	39 \pm 4	16 \pm 4	19 \pm 7
Thin film, 450 nm	25 \pm 2	32 \pm 2	49 \pm 3	60 \pm 2	65 \pm 0.2	77 \pm 3

Uncertainties calculated from a linear regression of the permeability vs inverse temperature data.

The results suggest that in-depth characterization of PBI membranes at elevated temperatures is needed to better understand and predict long-term gas transport behavior. Physical aging will

also be measured at additional temperatures to better characterize PBI's gas transport behavior at elevated temperatures.

Publications Acknowledging this Grant in 2015 – present

(I) Exclusively funded by this grant

1. Stevens, K. A.; Smith, Z.P.; Gleason, K. L.; Galizia, M.; Paul, D. R.; Freeman, B.D. Influence of temperature on gas solubility in thermally rearranged (TR) polymers. *J. Membrane Sci.* **2017**, *533*, 75-83.
2. Galizia, M.; Stevens, K. A.; Smith, Z. P.; Paul, D. R.; Freeman, B. D. Nonequilibrium Lattice Fluid Modeling of Gas Solubility in HAB-6FDA Polyimide and Its Thermally Rearranged Analogues. *Macromolecules.* **2016**, *49*, 22, 8768-8779.

(II) Jointly funded by this grant and other grants with leading intellectual contribution from this grant

1. Moon, J. D.; Bridge, A. T.; D'Ambra, C.; Freeman, B. D.; Paul, D. R. Gas separation properties of polybenzimidazole/thermally-rearranged polymer blends. *Journal of Membrane Science. J. Membrane Sci.* **2019**, *582*, 182-193.
2. Joseph, R. M.; Merrick, M. M.; Liu, R.; Fraser, A. C.; Moon, J. D.; Choudhury, S. R.; Lesko, J.; Freeman, B. D.; Riffle, J. S., Synthesis and characterization of polybenzimidazole membranes for gas separation with improved gas permeability: A grafting and blending approach. *J. Membrane Sci.* **2018**, *564*, 587-597.
3. Moon, J. D.; Galizia, M.; Borjigin, H.; Liu, R.; Riffle, J. S.; Freeman, B. D.; Paul, D. R. Water vapor sorption, diffusion, and dilation in polybenzimidazoles. *Macromolecules.* **2018**, *51*, 7197-7208.
4. McGinnis, R. L.; Reimund, K.; Ren, J.; Xia, L.; Chowdhury, M. R.; Sun, X.; Abril, M.; Moon, J. D.; Merrick, M. M.; Park, J.; Stevens, K. A.; McCutcheon, J. R.; Freeman, B. D. Large scale polymeric carbon nanotube membranes with sub-1.27 nm pores. *Sci. Adv.* **2018**, *4*, e1700938.
5. Galizia, M.; Stevens, K. A.; Paul, D. R.; Freeman, B. D. Modeling gas permeability and diffusivity in HAB-6FDA polyimide and its thermally rearranged analogs. *J. Membrane Sci.* **2017**, *537*, 83-92.
6. Robeson, L. M.; Dose, M. E.; Freeman, B. D.; Paul, D. R. Analysis of the transport properties of thermally rearranged (TR) polymers and polymers of intrinsic microporosity (PIM) relative to upper bound performance. *J. Membrane Sci.* **2017**, *525*, 18-24.
7. Liu, Q.; Galizia, M.; Gleason, K. L.; Scholes, C. A.; Paul, D. R.; Freeman, B. D. Influence of toluene on CO₂ and CH₄ gas transport properties in thermally rearranged (TR) polymers based on 3,3'-dihydroxy-4,4'-diamino-biphenyl (HAB) and 2,2'-bis-(3,4-dicarboxyphenyl) hexafluoropropane dianhydride (6FDA). *J. Membrane Sci.* **2016**, *514*, 282-293.
8. Liu, Q.; Paul, D. R.; Freeman, B. D. Gas permeation and mechanical properties of thermally rearranged (TR) copolyimides. *Polymer.* **2016**, *82*, 378-391.
9. Liu, Q.; Shaver, A. T.; Chen, Y.; Miller, G.; Paul, D. R.; Riffle, J. S.; McGrath, J. E.; Freeman, B. D. Effect of UV irradiation and physical aging on O₂ and N₂ transport properties of thin glassy poly(arylene ether ketone) copolymer films based on tetramethyl bisphenol A and 4,4'-difluorobenzophenone. *Polymer.* **2016**, *87*, 202-214.

10. Liu, Q.; Borjigin, H.; Paul, D. R.; Riffle, J. S.; McGrath, J. E.; Freeman, B. D. Gas permeation properties of thermally rearranged (TR) isomers and their aromatic polyimide precursors. *J. Membrane Sci.* **2016**, *518*, 88-99.
11. Borjigin, H.; Stevens, K. A.; Liu, R.; Moon, J. D.; Shaver, A. T.; Swinnea, S.; Freeman, B. D.; Riffle, J. S.; McGrath, J. E., Synthesis and characterization of polybenzimidazoles derived from tetraaminodiphenylsulfone for high temperature gas separation membranes. *Polymer.* **2015**, *71*, 135-142.
12. Galizia, M.; Smith, Z. P.; Sarti, G. C.; Freeman, B. D.; Paul, D. R., Predictive calculation of hydrogen and helium solubility in glassy and rubbery polymers. *J. Membrane Sci.* **2015**, *475*, 110-121.
13. Smith, Z.P.; Hernández, G.; Gleason, K. L.; Anand, A.; Doherty, C. M.; Konstas, K.; Alvarez, C.; Hill, A. J.; Lozano, A. E.; Paul, D. R.; Freeman, B. D. Effect of polymer structure on gas transport properties of selected aromatic polyimides, polyamides and TR polymers. *J. Membrane Sci.* **2015**, *493*, 766-781.
14. Gleason, K. L.; Smith, Z. P.; Liu, Q.; Paul, D. R.; Freeman, B. D. Pure- and mixed-gas permeation of CO₂ and CH₄ in thermally rearranged polymers based on 3,3'-dihydroxy-4,4'-diamino-biphenyl (HAB) and 2,2'-bis-(3,4-dicarboxyphenyl) hexafluoropropane dianhydride (6FDA). *J. Membrane Sci.* **2015**, *475*, 204-214.

(III) *Jointly funded by this grant and other grants with relatively minor intellectual contribution from this grant*

1. Nebipasagil, A.; Park, J.; Lane, O. R.; Sundell, B. J.; Mecham, S. J.; Freeman, B. D.; Riffle, J. S.; McGrath, J. E. Polyurethanes containing Poly(arylene ether sulfone) and Poly(ethylene oxide) segments for gas separation membranes. *Polymer.* **2017**, *118*, 256-267.
2. Park, H. B.; Kamcev, J.; Robeson, L. M.; Elimelech, M.; Freeman, B. D. Maximizing the right stuff: The trade-off between membrane permeability and selectivity. *Science.* **2017**, *356*, 6343.

Highly Permeable and Selective Model Network Membranes for Gas Separations

Ruilan Guo

University of Notre Dame, Department of Chemical and Biomolecular Engineering

Presentation Abstract

Polymeric gas separation membranes frequently suffer from performance deterioration caused by membrane plasticization upon exposure to condensing gases (e.g., CO₂). While chemical crosslinking appears to be one of the most effective methods to improve membranes' plasticization resistance, traditional random crosslinking process inevitably leads to significantly reduced permeability with little or no gain in selectivity. Additionally, randomly crosslinked polymers have very complicated, uncontrollable structures that inevitably leads to unpredictable membrane properties, preventing fundamental structure-property relationship being elucidated for crosslinked membranes. Here we introduce a new design of crosslinked membranes based on model polymer networks prepared via end-linking of telechelic oligomers with precisely-controlled chain length and chain length distribution. This new crosslinking approach produces crosslinked polymers with well-controlled crosslink density and crosslink inhomogeneity (i.e., the uneven distribution of crosslink sites), which allows for previously unattainable tunability in the microstructure and transport properties of crosslinked membranes. Besides the observed exceptional size sieving capability, these new model network membranes show well-maintained high permeability even when heavily crosslinked, in sharp contrast to traditional randomly crosslinked polymers. This presentation will focus on the macromolecular design motifs and the fundamental relationships between exquisitely tuned crosslinked microstructures and membrane properties for these innovative crosslinked polymer membranes.

DE-SC0019024: Regulating Gas Transport in Molecularly Engineered Polymer Membranes

Students: Greg Kline (graduated in November 2018), Qinnan Zhang, Ziwei Dai

RECENT PROGRESS

Synthesis and Characterization of High Molecular Weight (MW) Linear Control

The system chosen for this project is the iptycene-based polybenzoxazoles (PBOs) that displayed extraordinary separation performance in our previous studies. This task focuses on the synthesis and characterization of high MW polymers which are used as linear controls to compare with the crosslinked counterparts. Two series of PBO linear control were developed in parallel to examine how precursor structures and thermal protocol may affect membrane properties. Specifically, the first series includes TR-PBOs prepared from a thermal rearrangement (TR) process of poly(hydroxyimide)s (PHIs) precursors as reported in our previous studies. For TR-PBO series, the synthesis of PHI precursors has been improved from previous procedures by switching the reaction solvent to *m*-cresol, which has successfully addressed the poor solubility issue of high-performing pentiptycene-based PBOs. The other series involves a major achievement in this task that produces organo-soluble PBOs (s-PBOs) via a novel one-pot, self-catalyzed thermal conversion of poly(hydroxyamide)s (PHAs) to PBOs in solution. The newly developed synthesis

approach produces iptycene-based PBOs that can be directly cast into films via solution casting method. Besides addressing the processability issues of existing TR-PBO membranes, this new synthetic method circumvents the very high temperature treatment in the TR process to obtain PBOs in solid state, thus eliminates the possibility of undesired thermal degradation in the TR conversion processes that deteriorates membranes' mechanical stability. The full PHA-to-PBO conversion is confirmed by the disappearance of $-OH$ and amide peaks of PHAs and the appearance of the characteristic peaks of benzoxazole in 1H NMR (**Figure 1**).

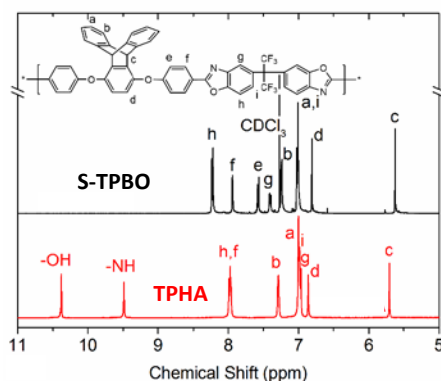


Figure 1. 1H NMR spectra of organo-soluble triptycene-PBO (s-TPBO) and corresponding TPHA precursor

Defect-free thin films (~ 40 - 50 μm thick) of all linear polymers (PHI precursors and s-PBOs) were casted from polymer-NMP solution. PHI precursor films were converted to corresponding TR-PBO films following previously reported TR process. Both TR-PBOs and s-PBOs were subjected to pure-gas permeation tests with five gases (H_2 , CH_4 , N_2 , O_2 , CO_2) with feed pressure ranging from 3 to 17 atm at 35 $^{\circ}C$. In general, TR-PBOs outperformed s-PBOs in both permeability and selectivity as expected due to more open microporous structure formed during the TR process. However, being soluble in organic solvents, s-PBOs hold great promise in facilitating membrane fabrication of crosslinked systems. Both TR-PBOs and s-PBOs will serve as linear control for comparison with their crosslinked counterparts.

Synthesis and Characterization of Telechelic Oligomers

During this reporting period, oligomers synthesis has been focused on the development of iptycene-based s-PBO series with molecular weight ranging from 3,000 to 15,000 g/mol. A facile, two-step synthesis protocol has been established that is able to produce telechelic oligomers with desired molecular weight and terminal functionality for end-linking. Specifically, the first step involves the synthesis of amine-terminated PHA oligomers, where molecular weight was controlled by adjust the molar ratio between the diamine monomer and the diacid chloride monomer. The diamine was in excess to introduce amine terminal groups to facilitate the introduction of curable phenylethynyl end groups. Following this, the amine-terminated oligomers were end-capped by a mono-anhydride monomer containing phenylethynyl group (PEPA) to introduce thermally curable phenylethynyl groups for end-linking. Upon the completion of end-capping, the PEPA-terminated oligomers were converted to PEPA-ended s-PBO oligomers in-situ via the newly developed one-pot synthesis approach.

Chemical structure of s-PBO oligomers is confirmed by ^1H NMR where the intensity of characteristic peaks of PEPA end groups increases with decreasing molecular weight suggesting molecular weight control (Figure 2). As expected, s-PBO oligomers show the same organo-solubility as their high counterparts despite of PEPA endcapping. Molecular weights of the oligomers were determined

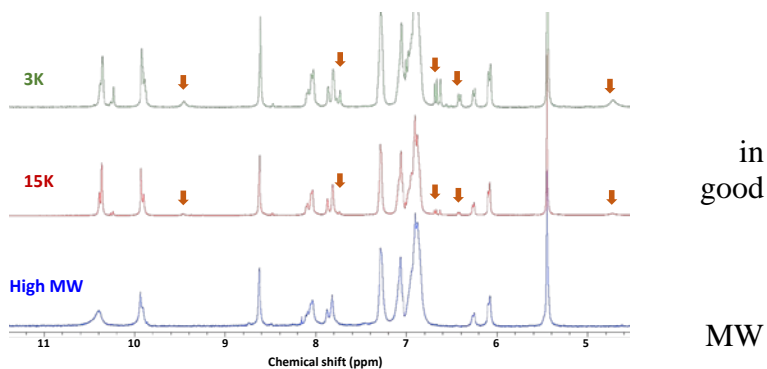


Figure 2. ^1H NMR spectra of pentiptycene-based amine-terminated s-PPBO oligomers in comparison with high MW control. (Arrows

of all by ^1H NMR spectra by comparing the integration of end-group peaks and that of main-chain peaks. Good agreement between the targeted MW and measured MW has been achieved indicating successful oligomer synthesis. For example, s-PPBO oligomers were targeted at MWs of 3000, 5000, 10000 and 15000 g/mol, and the obtained oligomers have measured MWs of 3200, 5300, 12000 and 16500 g/mol, respectively. DSC and TGA analysis showed that T_g and decomposition temperature of the oligomers increased with increasing molecular weight as expected. For example, s-PPBO-3K has a T_g of ~ 205 $^\circ\text{C}$ and s-PPBO-15K has a T_g above 300 $^\circ\text{C}$. Additionally, a broad endothermic peak appeared in the DSC profiles for all the oligomers with a starting temperature at ~ 350 $^\circ\text{C}$ and peak temperature at ~ 375 $^\circ\text{C}$ that could be ascribed to the curing reaction of PEPA end groups.

Preparation and Characterization of Crosslinked Membranes and Performance

Thermal protocol (i.e., heating rate, final curing temperature, curing time) is of critical importance in terms of obtaining defect-free crosslinked membranes balanced with good mechanical properties and complete crosslinking (i.e., high gel fraction). Different from solution casting processes involving high MW polymers, the formation of crosslinked membranes is promoted by efficient thermal crosslinking since the oligomers are not able to form continuous films without end-linking with each other due to their low MWs. According to DSC measurements, regardless of oligomer chain length, a peak thermal curing temperature of ~ 375 $^\circ\text{C}$ was observed for all oligomers. As such, a final curing temperature of 400 $^\circ\text{C}$ was chosen to ensure complete crosslinking reaction. To ensure concurrent thermal end-linking and film formation, a two-step heating protocol was adopted which involved a first stage of heating at ~ 250 - 300 $^\circ\text{C}$ (depending on the T_g of the oligomers) for 2 hours for film forming, and a final stage of heating at 400 $^\circ\text{C}$ to complete the crosslinking. The heating rate of both stages was set at 10 $^\circ\text{C}/\text{min}$ for initial study. Examination of the synergetic effect of heating rate and the first-stage heating temperature is ongoing. Following this initial thermal protocol, defect-free thin films (~ 50 - 60 μm thick) were obtained (Figure 3).



Figure 3. Pictures of heavily crosslinked s-PPBO-3K film

In year 1, efforts have been focused on preparing unimodal networks where the inter-crosslink PBO segments have the same molecular weight as that of the oligomers from which they are prepared. These unimodal network membranes were systematically varied in their crosslink density by using oligomers with various chain length, ranging from 3K to 15K. Pure gas permeabilities for these new crosslinked membranes were

measured with a feed pressure range of 30 – 230 psig at 35 °C. For all the crosslinked membranes, gas permeabilities follow an order of $P(\text{H}_2) > P(\text{CO}_2) > P(\text{O}_2) > P(\text{N}_2) > P(\text{CH}_4)$, which is consistent with the kinetic diameters of the testing gases. Additionally, permeabilities for non-polar gases showed very weak dependence on feed pressure suggesting the dominant role of size sieving in these crosslinked model network membranes. In the case of CO_2 , compared to high MW linear PBO control which showed plasticization pressure of ~180 psig, all the crosslinked membranes were much less sensitive to the feed pressure and did not show any sign of plasticization up to 230 psig feed pressure, the highest feed pressure for our current permeation testing system. Moreover, the crosslinked membranes showed minor gas permeability reduction upon crosslinking highlight the unique crosslinking mechanism of phenylethynyl group that is being further investigated.

Figure 4 shows representative upper bound comparison of s-PPBO-3k, 5K and 10K crosslinked unimodal membranes for H_2/CH_4 and O_2/N_2 separations. As shown, the crosslinked unimodal membranes have superior size sieving properties while maintaining high gas permeabilities comparable to the linear control.

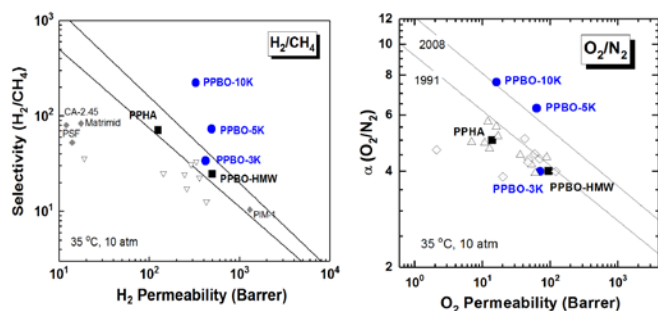


Figure 4. Upper bound plots of unimodal network membranes (s-PPBO series) with various crosslink density comparing with linear control (PPBO-HMW) for H_2/CH_4 and O_2/N_2 separations.

and 10 K). This phenomenon likely results from the combined effects of phenylethynyl crosslinking chemistry and the role of iptycene units. For membranes with long inter-crosslink chain length, the fraction of bulky phenylene groups at crosslink sites is small. As a result, regular chain densification effect upon crosslinking may dominate leading to enhanced selectivity. In addition, the presence of longer sequence of iptycene units effectively regulates the gas transport via the unique internal free volume allowing for superior size sieving properties as demonstrated in our previous reports on iptycene-based polymers. This synergetic effect may also explain the non-linear relationship between gas permeability and crosslink density where permeability first increased then decreased with decreasing crosslink density. It seems that there may be an optimal crosslink density where the two competing effects reach a balance for maximized permeability. Systematic studies on manipulation of crosslink density and crosslink inhomogeneity as well as varying thermal protocols are ongoing to explore the underlying structure-property relationships for these innovative model network membranes.

Publications Acknowledging this Grant in 2018 – present

(IV) *Exclusively funded by this grant:*

- Loianno, V.; Zhang, Q.; Luo, S.; Guo, R.; Galizia, M., Modeling Gas and Vapor Sorption and Swelling in a Triptycene-based Polybenzoxazole: Evidence for Entropy-driven Sorption Behavior, *Macromolecules*, **2019**, *52*, 4385–4395.
- Li, T.; Chen, Z. Q.; Huang, H.; Zhao, S.; Liu, J.; Guo, R.; Chen, Y., Microporous Polyimides Containing Bulky Tetra-*o*-isopropyl and Naphthalene Groups for Gas Separation Membranes, *Journal of Membrane Science*, **2019**, *585*, 282-288.

(V) *Jointly funded by this grant and other grants with leading intellectual contribution from this grant:*

- Corrado, T.; Guo, R., Macromolecular Design Strategies Toward Tailoring Polymer Free Volume for High Performance Gas Separation Membranes, (invited paper for the Special Issue of “MSDE Emerging Investigators 2020”), *Molecular Systems Design & Engineering*, **2019**, *under review*.

(VI) *Jointly funded by this grant and other grants with relatively minor intellectual contribution from this grant;*

Transport and Stability Characterization for Free-Volume-Generating Bottlebrush Polymers

Francesco Benedetti,^{1,4} Yuan He,² Sharon Lin,¹ Chao Liu,³ Yanchuan Zhao,³ Hongzhou Ye,²
Troy Van Voorhis,² Maria Grazia de Angelis,⁴ Timothy Swager,² Zachary P. Smith¹

1. Chemical Engineering, MIT, USA

2. Chemistry, MIT, USA

3. Chinese Academy of Science State Key Lab, Lanzhou, China

4. Department of Civil, Chemical, Environmental, and Materials Engineering, University of Bologna, Italy

Presentation Abstract

There are a limited number of solution processable ultramicroporous polymers that can be formed into films for membrane-based gas separations. In this presentation, a new class of ring-opening metathesis polymerization (ROMP) polymers with measurable internal surface areas have been formed into films and characterized for their transport performance, chemical stability, and physical stability. Unlike all other known polymers that have state-of-the-art separation performance for gas separations, these polymers are formed through a controlled addition polymerization mechanism and their free-volume-generating features result from their unique bottlebrush morphology, which has free-volume-generating side chains attached to a flexible polymer backbone. For CO₂ based separations, these polymers have some of the highest known permeabilities for gas separation membranes. A detailed analysis of permeability, diffusivity and solubility characteristics, as well as plasticization and physical aging behavior are considered and compared to other materials to define the current opportunities and limitations with free-volume-generating bottlebrush polymers.

Grant or FWP Number: Rational Sub-Nanometer Manipulation of Polymer Morphology for Efficient Chemical Separations

PI: Zachary P. Smith

Postdoc(s): Francesco Benedetti

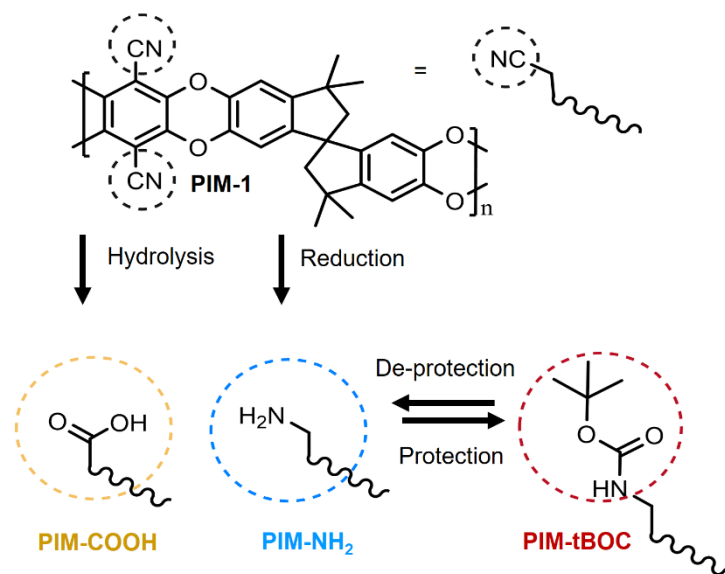
Student(s): Sharon Lin, Taigyoo Joo, Katherine Mizrahi

Affiliations(s): Massachusetts Institute of Technology

RECENT PROGRESS

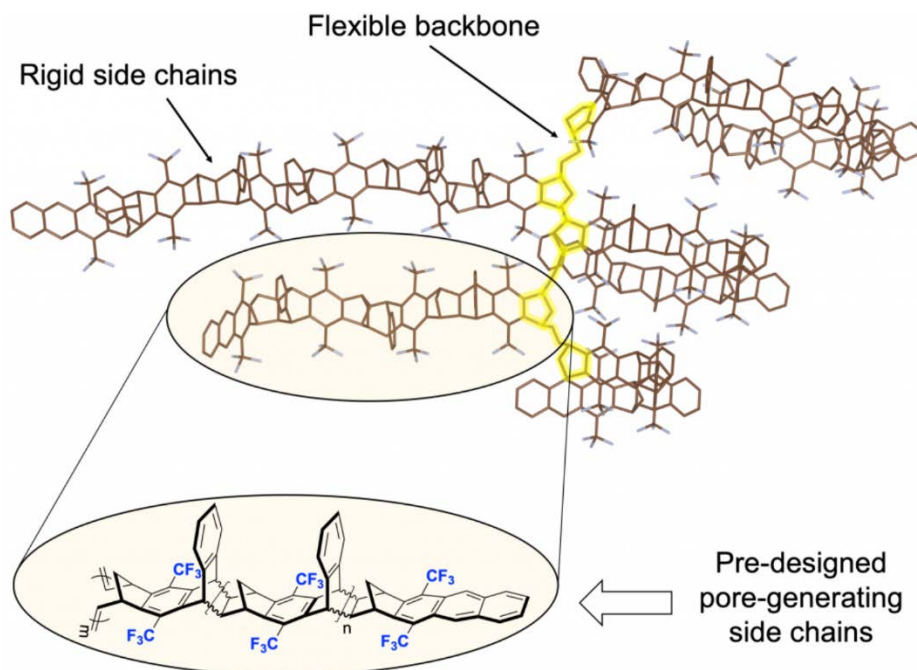
Synthesis and characterization of polymers that contain free volume modifiers

Polyimides and polymers of intrinsic microporosity (PIMs) have been synthesized that contain functional groups that can be chemically manipulated to add and detach free-volume manipulating side groups. An example of some PIMs recently synthesized for these studies is shown below:



Transport and stability characterization for a new class of free-volume-generating bottlebrush polymers

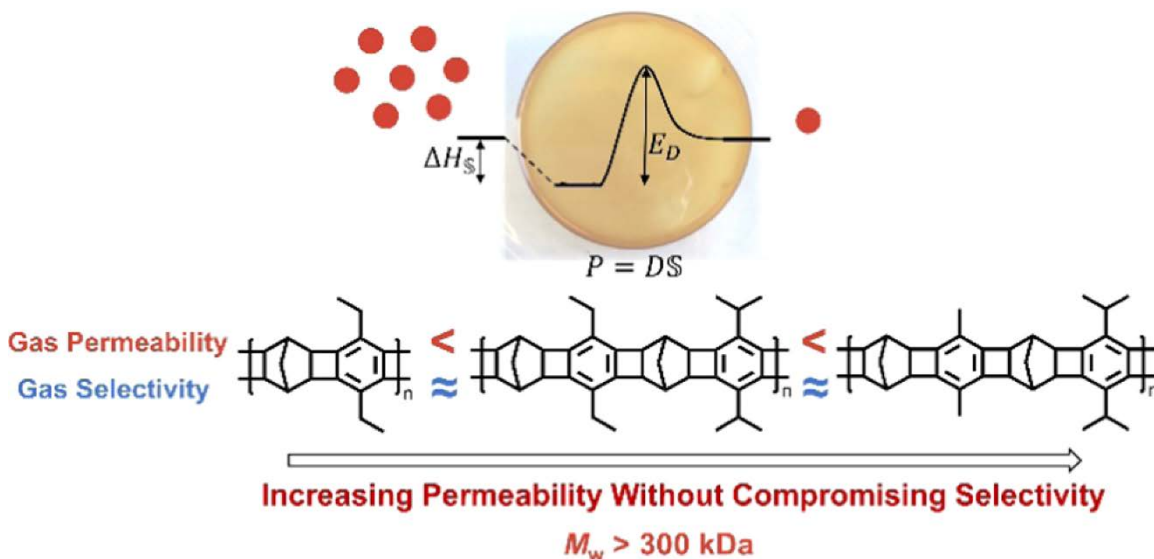
A new class of free-volume-generating polymers have been successfully formed into films. These films have been characterized for transport performance and stability. The published graphical abstract shown below contains an example structure of the materials considered:



Evaluating solution-diffusion theory in hydrocarbon-based ladder polymers

A new class of hydrocarbon-based ladder polymers have been formed into films and characterized for molecular diffusion and solubility characteristics. This analysis allows for an in-depth characterization of the applicability of a traditional transport model (the solution-

diffusion model) to non-polar, hydrocarbon-based polymers that have ultramicroporous characteristics. The published graphical abstract below shows a film of a hydrocarbon-based ladder polymer, the chemical structure of three structural analogues, and relative permeability and selectivity results.



Publications Acknowledging this Grant in 2015 – present

(IV) Exclusively funded by this grant;

(V) Jointly funded by this grant and other grants with leading intellectual contribution from this grant;

1. He, Y.; Benedetti, F. M.; Lin, S.; Liu, C.; Zhao, Y.; Ye, H. Z.; Van Voorhis, T.; De Angelis, M. G.; Swager, T. M.; Smith, Z. P., Polymers with side chain porosity for ultrapermeable and plasticization resistant materials for gas separations. *Adv. Mater.* **2019**, *31* (21), 1807871.

2. Lai, H. W. H.; Benedetti, F. M.; Jin, Z.; Teo, Y. C.; Wu, A. X.; Angelis, M. G. D.; Smith, Z. P.; Xia, Y., Tuning the molecular weights, chain packing, and gas-transport properties of CANAL ladder polymers by short alkyl substitutions (in press). *Macromolecules* **2019**, DOI: 10.1021/acs.macromol.9b01155.

(VI) Jointly funded by this grant and other grants with relatively minor intellectual contribution from this grant;

Understanding and controlling water-organic co-transport in amorphous microporous materials

Ryan P. Lively, Daniel O’Nolan, Young Hee Yoon
School of Chemical and Biomolecular Engineering
Georgia Institute of Technology

Poster Abstract

We are actively studying the fundamental sorption, diffusion, and permeation properties of water-organic mixtures in carbon molecular sieve (CMS) membranes to understand the conditions within the micropore that give rise to the various types of molecular motion and molecular selection processes possible in such complex systems. To develop this understanding, we will create a consistent set of samples that have well-defined pore sizes, with one set of samples having a “uniform” distribution (i.e., only a single pore size) and a “bimodal” distribution (i.e., possessing two different yet interconnected pores). These measurements will provide fundamental guidance in a variety of DOE-relevant challenges including wastewater remediation, transport in tight shale formations, biofuel upgrading, and other processes involving molecular transport.

Grant or FWP Number: Understanding and controlling water-organic co-transport in amorphous microporous materials

Postdoc(s): Daniel O’Nolan
Student(s): Young Hee Yoon

RECENT PROGRESS

Overview—Movement of molecules in porous spaces is an important and active area of research with major implications in industrial separations, catalysis, and geology. In practical situations, this molecular movement occurs under highly “crowded” conditions within the pore space. This becomes even more complex in cases where the pore sizes begin to approach the size of the moving molecules. Understanding of molecular diffusion at these conditions remains a significant fundamental challenge and has largely been understood by measuring molecular movement in chemically diverse materials that exhibit different pore sizes. Beyond this, creating techniques to control the mobility of organic and water mixtures in these “crowded” porous structures will open up possibilities not accessible by current materials. For instance, the steady state removal of organic pollutants from wastewater can be envisioned using a “surface selective flow” membrane with appropriate microstructure (**Figure 1**).

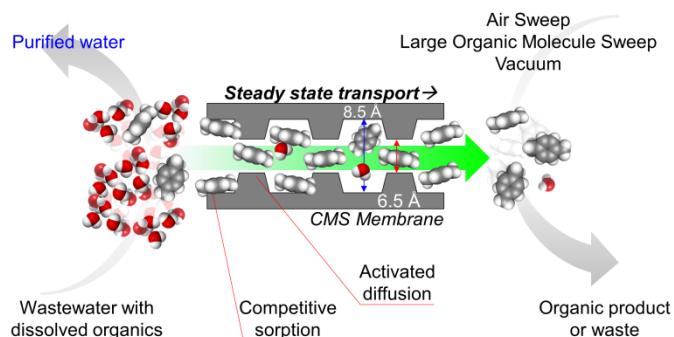


Figure 1: Illustrative example of a potential application of the proposed fundamental research. Here, a membrane continuously removes dissolved organic molecules from wastewater. Detailed co-transport insight is needed to enable concepts such as these.

Creation and characterization of CMS samples—Since the project began in the Fall of 2018, we have hired a graduate student and a post-doctoral researcher. The graduate student has taken all of her core courses and began work in the lab in earnest in January of 2019. Since she has started, we have synthesized samples with a variety of micropore architectures. Specifically, we have fabricated membranes from neat and diamine-crosslinked polyvinylidene fluoride (PVDF) and polyvinylidene chloride (PVDC), and pyrolyzed these to create carbon molecular sieve membranes with differing pore structures. We have characterized these materials using powder x-ray diffractometry, FT-IR, solid state $^1\text{H-NMR}$, and various adsorption techniques. We primarily rely on N_2 physisorption at 77K to estimate our pore size distributions. The uncrosslinked PVDF materials exhibit a uniform pore, whereas the crosslinked materials exhibit a bimodal and narrow pore size distribution (**Figure 2, left**). However, the pores from PVDC are sufficiently narrow that N_2 has difficulty accessing the entirety of the micropore structure in an experimentally reasonable amount of time. We have thus explored the use of neon vapor in the ranges of 27-32K to measure the pore size distributions of these “tighter” CMS materials. Moreover, since neon (2.75\AA) is similar in size to water ($\sim 2.6\text{-}2.9\text{\AA}$), the use of this sorbate will allow us to fully interrogate the “water accessible” structures within the CMS. Exemplar neon isotherms at 27K are shown in **Figure 2 (right)**, where we have utilized CMS from PVDF as a known quantity to validate the new experimental technique. We are in the process of updating our pore size distribution models to account for the differences in neon as a sorbate as opposed to N_2 as a sorbate.

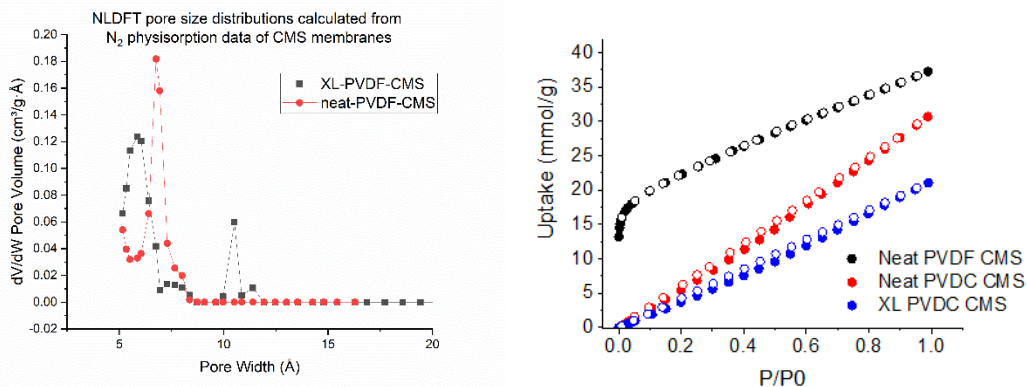


Figure 2: (left) N_2 -probed pore size distribution of CMS derived from neat PVDF and CMS derived from diamine crosslinked PVDF. (right) Neon sorption isotherms in various CMS samples at 27K. These isotherms will be utilized to calculate pore size distributions of “tight” CMS samples.

We have received beamline time at Oak Ridge National Laboratory’s NOMAD diffractometer. We will utilize the scattering data from this experiment to begin pair distribution function analysis on the CMS samples. Our aim is to relate the physical structure of the carbon materials to the microporous (i.e., void) structure of the samples.

We have also begun our collection of single component sorption and diffusion isotherms (e.g., water sorption as shown in **Fig. 3**), which are critical starting points for our multicomponent permeation model. We will utilize these as the basis for our mixture sorption estimates, which will be experimentally probed in Year 2 of the project. We will discuss the foundations of our multicomponent permeation model and how these types of measurements are crucial for developing a fundamental understanding of complex mixture permeation in microporous spaces.

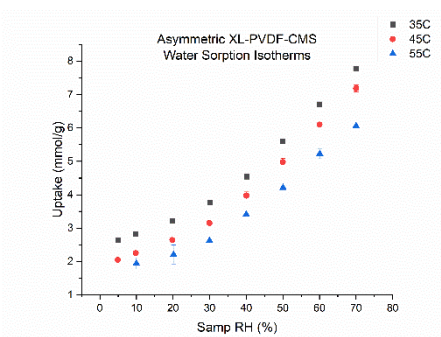


Figure 3 – Water sorption isotherms in a CMS derived from crosslinked PVDF

Publications Acknowledging this Grant in 2015 – present

Nothing to report yet.

Design and Study of Hybrid Polyimide-Ionene Architectures for Membrane Separations

Jason E. Bara, C. Heath Turner, Irshad Kammakakam, Kathryn E. O’Harra
University of Alabama, Department of Chemical & Biological Engineering

Presentation Abstract

Hybrid polyimide-ionene architectures represent a radically new way to integrate the structures of polyimide materials and ionic liquids (ILs) within the backbone of a condensation polymer. The combination of the desirable properties of each class of material within a single, covalently-bonded structure offers vast possibilities to control polymer properties such as fractional free volume (FFV) which will influence the gas permeability and gas pair selectivity of membranes formed from these polyimide-ionene hybrids. The modular approach by which hybrid polyimide-ionene materials are constructed allows for the systematic variation of multiple structural variables in the polymer backbone and is also amenable to the inclusion of elements associated with polymers of intrinsic microporosity (PIMs) and Tröger’s Base (TB) polymers. This presentation will detail the progress made in this project in the design, synthesis and study of hybrid polyimide-ionene architectures for membrane separations. Specifically, the new approaches we have taken in the design and synthesis of these polyimide-ionene hybrids from both experimental and computational approaches will be presented along with results of thermal properties, structural characterizations, processing techniques, membrane formation and transport/separation properties.

Design and Study of Hybrid Polyimide-Ionene Architectures for Membrane Separations (DE-SC001818)

PI: Jason E. Bara (PI), C. Heath Turner (co-PI)

Postdoc(s): Irshad Kammakakam

Student(s): Kathryn E. O’Harra

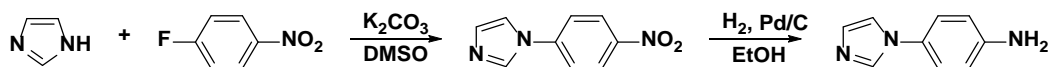
Affiliations(s): University of Alabama, Department of Chemical & Biological Engineering

RECENT PROGRESS

Synthesis of Advanced Monomers and Ionenenes and New Designs of IL Additives

Conventional ionenenes consist of ammonium cations tethered by flexible groups such as alkyl or ether chains. Typically, such ionenenes are limited in terms of their functionality, thermal stability and film forming properties. However, as we have recently demonstrated, much more robust ionenenes can be designed and synthesized by taking a step back and synthesizing better building blocks and monomers. We have emphasized the use of imidazole-aniline compounds that can be successfully synthesized at scales of up to 200 g starting from imidazole and 4-fluoronitrobenzene (4-FNB), followed by catalytic reduction according to Scheme 1:

Scheme 1: Example synthesis of imidazole-aniline derivatives.



The approach displayed in Scheme 1 has also been applied to a number of other FNB derivatives (Figure 1) which allows for control over the relative position of the amine group and the introduction of other substituents which increase steric bulk (e.g., $-\text{CH}_3$ and $-\text{CF}_3$) and may facilitate thermal rearrangement (i.e., $-\text{OCH}_3$). Furthermore, the use of other imidazole compounds (e.g., 2-methylimidazole) in Scheme 1 provides further control over material composition.

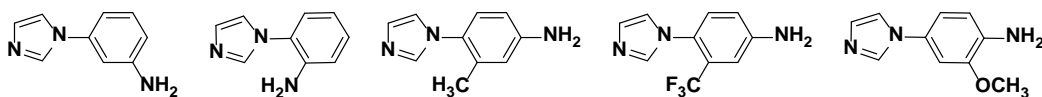


Figure 1: Other imidazole-aniline derivatives synthesized with different regiochemistry, steric bulk and thermally rearrangeable group.

One example of our unique approach to the design of advanced ionene materials is through our use of Tröger's Base. We have shown that monomers shown in Figure 1 are suitable for the formation of bis(imidazole) species linked by a Tröger's Base moiety which can then be linked to form "Im-TB-Ionenes", two examples of which are shown in Figure 2. All the Im-TB-Ionene polymers were found to have very high molecular weights (up to ~ 170 kDa) as confirmed by high resolution MALDI-TOF.

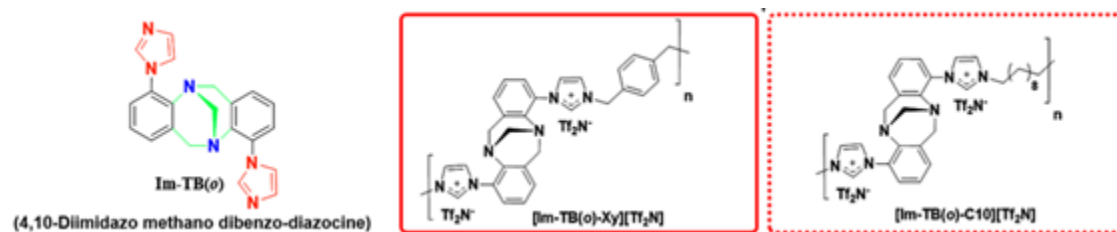


Figure 2: Example of bis(imidazole) Tröger's Base monomer (right) with corresponding ionenes linked by *p*-xylyl (center) and decyl (right) groups.

The structural and physical properties, as well as the gas separation behaviors of the copolymers of aromatic and aliphatic Im-TB-Ionenes, have been extensively investigated with respect to the regiochemistry of imidazolium groups at 'ortho' and 'para' positions of TB unit. The imidazolium-mediated TB-Ionenes showed high CO_2 solubility and hence excellent CO_2/CH_4 permselectivity of 82.5, which to our knowledge is the highest CO_2/CH_4 selectivity reported for any ionene or ionic-liquid based polymer membranes. The Im-TB-Ionenes also displayed good thermal and mechanical stabilities.

We are currently exploring further variations of these Im-TB-Ionenes with increase steric bulk about the imidazolium cation which may increase FFV and permeability, and have synthesized new Im-TB monomers (and ionenes) based on 2-phenylimidazole and benzimidazoles as shown in Figure 3.

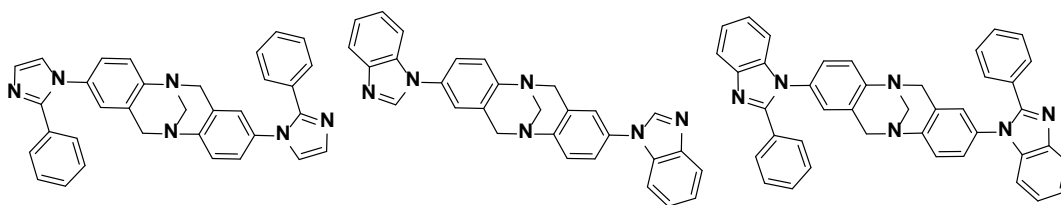


Figure 3: New Im-TB monomers synthesized by our group as starting materials for Im-TB-Ionene gas separation membranes.

We have also successfully synthesized imidazole-imide monomers and ionenes around the spirobisindane moiety found in PIMs. Figure 4 illustrates the structural units of these materials.

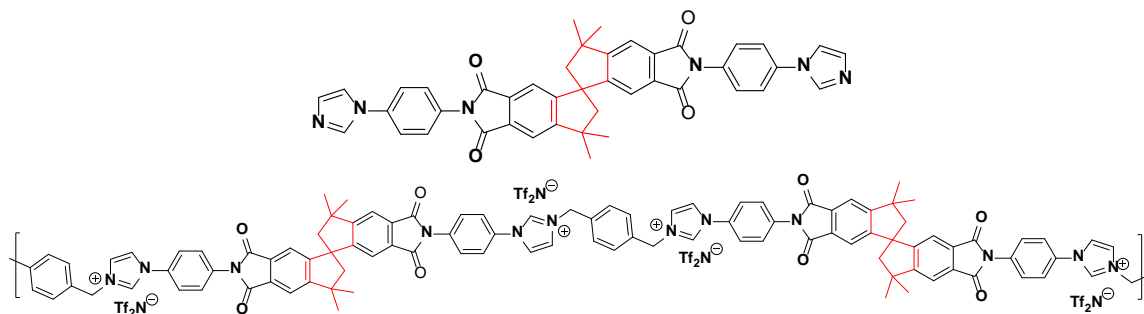


Figure 4: Example structures of spirobisindane-containing monomer (top) and ionene (bottom) synthesized by our group.

Membrane studies around these ionenes are still ongoing as we have found that the materials produced can be brittle. However, preliminary data on these samples shows good CO₂/CH₄ selectivity (~45) with CO₂ permeabilities of ~300 barrer. Thus, we are continuing to pursue ionene designs which utilize the spirobisindane moiety.

One effort to improve mechanical properties that we have employed is to synthesize new linking monomers which can enhance the mechanical properties of ionene-based membranes through interchain H-bonding. We have synthesized this reactive diamide monomer which preliminary studies have shown provides more mechanically durable materials than alkyl or xylyl linkages (Figure 5).

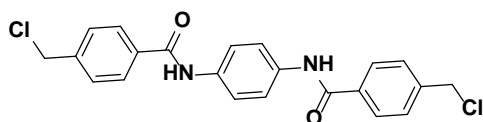


Figure 5: Structure of reactive diamide monomer for linking imidazole-based monomers.

Furthermore, we have also begun to develop new types of IL additives for our ionene polymers as means of imparting selectivity or permeability enhancements. While all polymer + IL studies to date have focused on “monovalent” ILs (i.e., +1 charge moiety paired with a -1 charge moiety), we have synthesized “multivalent” ILs wherein 2, 3 or more +1 charge moieties are paired with moieties bearing multiple -1 moieties (or vice versa). The use of ILs built around aromatic cores in combination with cationic ionenes should produce materials with higher intrinsic FFV with the potential to form highly ordered and open nanostructures. An example of this unprecedented approach to the design of ILs that can influence ionene organization is shown in Figure 6.

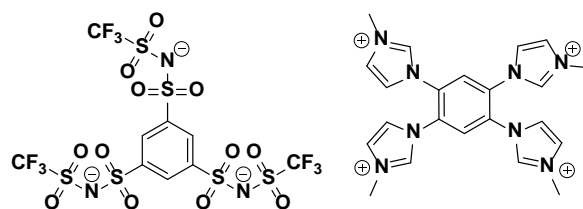


Figure 6: Example of (-3) anion bearing three individual (-1) charges (left) and (+4) cation bearing four individual (+1) charges (right).

Simulations and Computational Studies

The goal of our simulations and computational studies is to develop a multi-scale simulation approach to predict experimentally-relevant membrane performance as a function of molecular-level structure/composition, the component of which are:

- Quantum mechanical (QM): calculate partial charges on polymer backbone sites
- Molecular dynamics (MD): model the atomistic polymer structure and the short-time transport behavior of different gas molecules in the bulk polymer.
- Molecular dynamics (MD): estimate gas sorption properties at polymer interfaces.
- Kinetic Monte Carlo (KMC): simulations of a comprehensive gas/polymer/gas system to predict penetrant permeability and selectivity for the gases: CO₂/N₂, CO₂/CH₄, H₂/CO₂ and O₂/N₂.

The foundation of the modeling work is the development realistic molecular models for the molecular dynamics simulations (MD). While intramolecular parameters can be adopted from standard forcefields, the partial charge assignments need to be estimated from electronic structure methods (using Gaussian09). Different polymer fragments have been constructed, followed by energy minimization and single-point energy calculation (MP2/6-311++g(3d,3p)//B3LYP/ 6-31 g++(d,p)). Following these calculations, the partial charges are extracted using a natural bond order analysis (NBO). Currently, these calculations have been completed for the following polymer building blocks: 6-FDA, TRIPDA, and PIMDA.

We have also applied Gaussian09 to aid in the design of additional imidazole-aniline candidate compounds (cf. Scheme 1, Figure 1). The introduction of one or more methyl groups on both the imidazole and benzene rings will cause the rings to be non-coplanar, which may present further opportunities to tune void space and FFV. Computational work published to date has focused on the influence of the counter anion on material properties and the diffusion of gases through the cavities of polyimide-ionenes.

Publications Acknowledging this Grant in 2015 – present

Exclusively Funded by this Grant

Bara, J. E.; O’Harra, K. E. Recent Advances in Ionene Design – Toward Convergence with High-Performance Polymers. *Macromol. Chem. Phys.* **2019**, *220*, 1900078

Kammakakam, I.; O’Harra, K. E.; Bara, J. E.; Jackson, E. M. Design and Synthesis of Imidazolium-Mediated Tröger’s Base-Based Ionene Polymers for Advanced CO₂ Separation Membranes. *ACS Omega* **2019**, *4*, 3439-3448.

Bara, J. E.; Finotello, A.; Magee, J. W.; Qian, S.; O’Harra, K. E.; Dennis, G. P.; Noble, R. D. Properties of Imidazolium-based Ionic Liquids Bearing Both Benzylic and *n*-Alkyl Substituents. *Ind. Eng. Chem. Res.* Accepted Pending Minor Revisions

Jointly funded by this grant and other grants with leading intellectual contribution from this grant:

O’Harra, K. E.; Kammakakam, I.; DeVriese, E. M.; Noll, D. M.; Bara, J. E.; Jackson, E. M. Synthesis and Gas Separation Performances of Membranes Comprised of 6-FDA-Derived Polyimide Ionenenes and Ionic Liquids. *Membranes* **2019**, *9*, 79.

O’Harra, K. E.; Kammakakam, I.; Bara, J. E.; Jackson, E. M. Understanding the Roles of Backbone and Anions in the Structure and Thermal Stability of Imidazolium Polyimide-Ionenenes. *Polym. Int.* **2019**, *68*, 1547-1556. doi:10.1002/pi.5825

Jointly funded by this grant and other grants with relatively minor intellectual contribution from this grant:

Szala-Bilnik, J.; Abedini, A.; Crabtree, E.; **Bara, J. E.**; Turner, C. H. The Transport Behavior of CO₂ in Ionic Polyimides and Ionic Liquid Composite Membranes. *J. Phys. Chem B* In Press. doi:10.1021/acs.jpcc.9b05555

Abedini, A.; Crabtree, E.; **Bara, J. E.**; Turner, C. H. Molecular Analysis of Selective Gas Adsorption within Composites of Ionic Polyimides and Ionic Liquids as Gas Separation Membranes. *Chem. Phys.* **2019**, *516*, 71-83. doi:10.1016/j.chemphys.2018.08.039

PI ABSTRACTS SESSION V: THEORY & DATA SCIENCE

Design of OSDAs to Direct the Synthesis of Zeolites for CO₂/CH₄ Membrane Separations

Michael W. Deem

Rice University

Departments of Bioengineering and Physics & Astronomy

Houston, TX 77005

Presentation Abstract

One strategy to mitigate global warming is carbon capture and sequestration. Membrane separation is one promising approach to separation of CO₂ from feed streams. I discuss zeolites that have been predicted to be effective at separating CO₂ from methane. Using an in silico de novo design procedure, we identify organic structure directing agents (OSDAs) that are predicted to aid the synthesis of these zeolites. We design OSDAs for zeolites for which no known purely siliceous form is known, and we also design OSDAs for predicted zeolites. These OSDAs may lead to zeolites that could enable a practical separation of CO₂ from methane. I will also discuss design of OSDAs for zeolites that are capable of chiral separations.

DE-SC0019324: Gas Separations by Novel, Designed, Cost-Effective Zeolites

Research Scientist: Frits Daeyaert

Student: Fengdan Ye

RECENT PROGRESS

Machine-learning approach to the design of OSDAs for zeolite beta

Machine-learning approach to the design of OSDAs for zeolite beta

Scientific Achievement

- We here report a machine-learning strategy to aid the computational design of chemically synthesizable organic structure directing agents (OSDAs) for zeolite beta A.

Significance and Impact

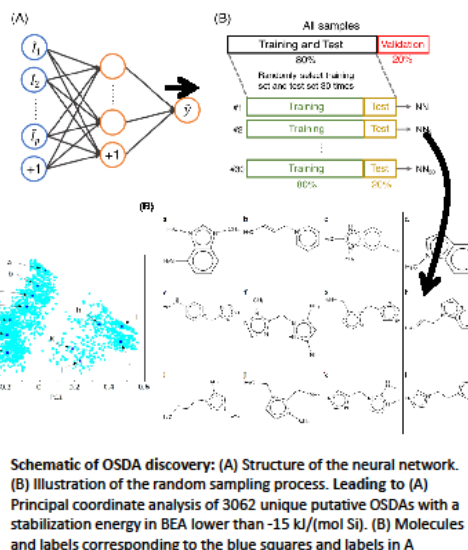
- Zeolite beta is one of the top-six zeolites of commercial interest. It is synthesized through the use of OSDAs.

Research Details

- Pure zeolite beta A has not yet been synthesized, nor has chiral zeolite beta.
- Through *de novo* materials design runs, a total of 3,062 promising OSDAs were identified
- 469 OSDAs were computed to stabilize the structure of zeolite beta A better than known compounds.
- The use of machine learning speeds up the computation by a factor of 350.
- This protocol enables an effective and computationally tractable search for novel OSDAs.

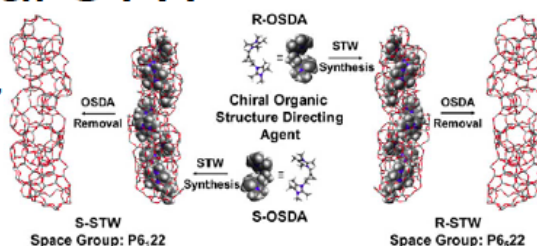
Daeyaert et al., Proc. Natl. Acad. Sci. USA (2019) doi:10.1073/pnas.18118763116.

Work was performed at Rice University



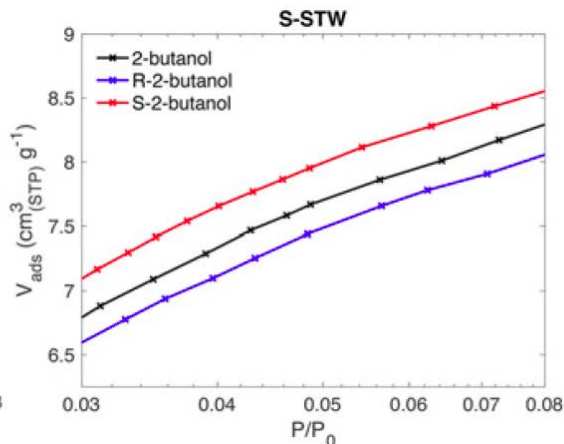
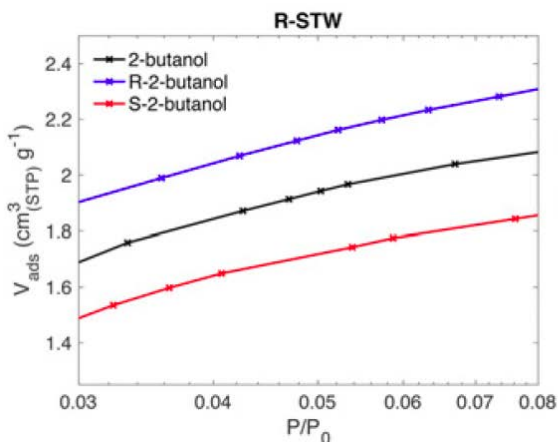
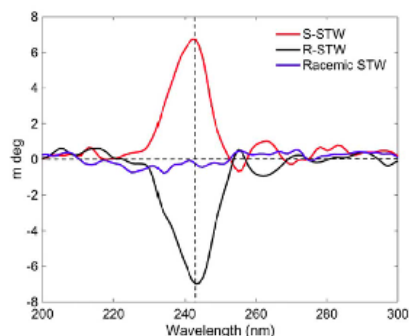
Chiral STW

S. K. Brand, J. E. Schmidt, M. W. Deem,
F. Daeyaert, Y. Mae, O. Terasaki,
M. Orazova, M. E. Davis, *Proc.
Natl. Acad. Sci. USA* 114 (2017) 5101



Proposed OSDA	$E_{\text{enantiomer 1}}$ (i.e., P6 ₂ 22)	$E_{\text{enantiomer 2}}$ (i.e., P6 ₂ 22)
	-16.32	-14.60
	-14.65	-1.37
	-15.27	-1.58

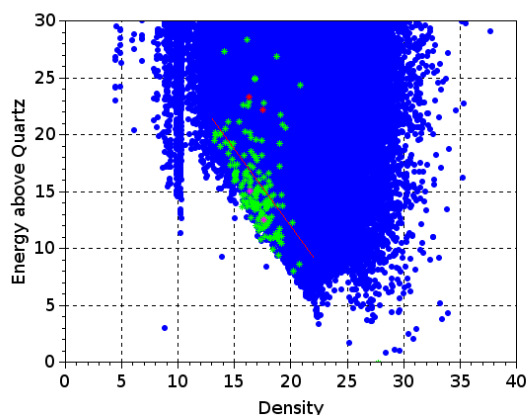
Molecule in third row: OSDA 2.



Design of OSDAs to Direct the Synthesis of Zeolites for CO₂/CH₄ Membrane Separations

In the present study, we will use our *de novo* design algorithm to design OSDAs that template the known and predicted zeolites suggested in [1] as having the best adsorption and diffusion properties for use in CO₂/CH₄ separation. To predict the suitability of a molecule to function as an OSDA for a given zeolite framework, we have developed a molecular dynamics (MD) protocol to calculate the Van der Waals interaction energy between a putative OSDA and its target zeolite.[2] Initially, replicas of the OSDAs were fitted into the zeolite using a combination of a Fourier transform method to determine the optimal translation and random rotation to determine the optimal orientation of each OSDA. The structure of the OSDA used in this procedure was the lowest energy conformation determined using a genetic algorithm for conformational analysis. Details of this algorithm can be found in.[3] The number of OSDA structures to be fitted in the zeolite unit cell depends upon the zeolite structure and was determined by trial and error (see Results section). The zeolite-OSDA structures obtained by this

fitting procedure were submitted to four rounds of molecular mechanics minimization and three MD runs at different time steps.[2] The non-bonded interaction energy between the OSDA and the zeolite is called the stabilization energy and was obtained from the average energies from the last 5 ps from the MD runs of the zeolite-OSDA complex, the individual zeolite, and the OSDAs. The energies were divided by the number of Si atoms in the zeolite. Stabilization energies are therefore reported in kJ/(mol Si). All molecular mechanics and MD runs were performed using the GULP program [4] and the Dreiding force field.[5]



Energy-density plot for the database of predicted zeolite structures (blue) and the known zeolites (green). All predicted structures have an energy within 30 kJ/(mol Si) of α -quartz. The red dots mark PCOD8186909 (rightmost) and PCOD8198030. The magenta dots mark GIS (leftmost) and ABW. The energies are in kJ/(mol Si), the densities are in Si atoms per \AA^3 .

1) Kim, J.; Abouelnasr, M.; Lin, L.-C.; Smit, B. Large-scale screening of zeolite structures for CO₂ membrane separations. *J. Am. Chem. Soc.* **2013**, *135*, 7545-7552.

2) Pophale, R.; Daeyaert, F.; Deem, M. W. Computational prediction of chemically synthesizable organic structure directing agents for zeolites. *J. Mater. Chem. A* **2013**, *1*, 6750-6760.

3) Daeyaert, F.; Deem, M. W. Design of organic structure directing agents for polymorph A zeolite beta. *J. Mater. Chem. A* **2019**, *7*, 9854-9866.

4) Gale, J. D. GULP - a computer program for the symmetry adapted simulation of solids' *J. Chem. Soc. Faraday Trans.* **1997**, *93*, 629-637.

5) Mayo, S. L.; Olafson, B. D.; Goddard, W. A. DREIDING: a generic force field for molecular simulations. *J. Phys. Chem.* **1990**, *94*, 8897-8909.

Publications Acknowledging this Grant in 2018 – present

II

Daeyaert, F.; Deem, M.W. Design of Organic Structure Directing Agents for Chiral Zeolite Beta A,. *ChemistrySelect* **2019**, *4*, 3531-3537.

Daeyaert, F.; Deem, M. W. Design of Organic Structure Directing Agents for Polymorph A Zeolite Beta. *J. Mater. Chem. A* **2019**, *7*, 9854-9866.

Daeyaert, F.; Ye, F.; Deem, M. W. A Machine Learning Approach to the Design of OSDAs for Zeolite Beta, *Proc. Natl. Acad. Sci. USA* **2019**, *116*, 3413-3418.

Daeyaert, F.; Deem, M. W. *In silico* Design of Chiral Dimers to Direct the Synthesis of a Chiral Zeolite. *Molec. Phys.* Daan Frenkel special issue, **2018**, *116*, 2836-2855.

Coordination-Chemistry-Derived Compounds Featuring Nanoscale Porosity and Selective Chemical Separation Capabilities

Joseph T. Hupp, Randall Q. Snurr, and Omar K. Farha

Northwestern University, Dept. of Chemistry and Dept. of Chemical and Biological Engineering

Presentation Abstract

- The goals of this project, and the points of focus of this presentation, center on advancing and exploiting a promising predictive, iterative, and tightly interactive cycle of computational-design/experimental-synthesis/experimental-testing for discovering and understanding porous, crystalline metal-organic-frameworks (MOF) for energy-efficient separation of mixtures of gases. The targets are separations of high interest, or potential interest, to DOE such as ethylene/ethane and ammonia/dinitrogen. The project takes advantage of and builds on: a) recent advances at Northwestern and elsewhere in MOF synthesis, b) expertise at NU in high throughput computational generation, modeling and subsequent data mining for materials discovery, and c) experience in creatively melding (a) and (b). The innovations are the application of a top-down MOF assembly algorithm and the use of enzyme-like, reversibly reactive binding of molecules to be separated. The reversible-reactive approach will be illustrated with experimental examples. The new top-down algorithm permits us to access a much wider range of MOF topologies than could be done with our bottom-up algorithm.

Grant DE-FG02-08ER15967: Coordination-Chemistry-Derived Materials Featuring Nanoscale Porosity and Selective Chemical Separation Capabilities

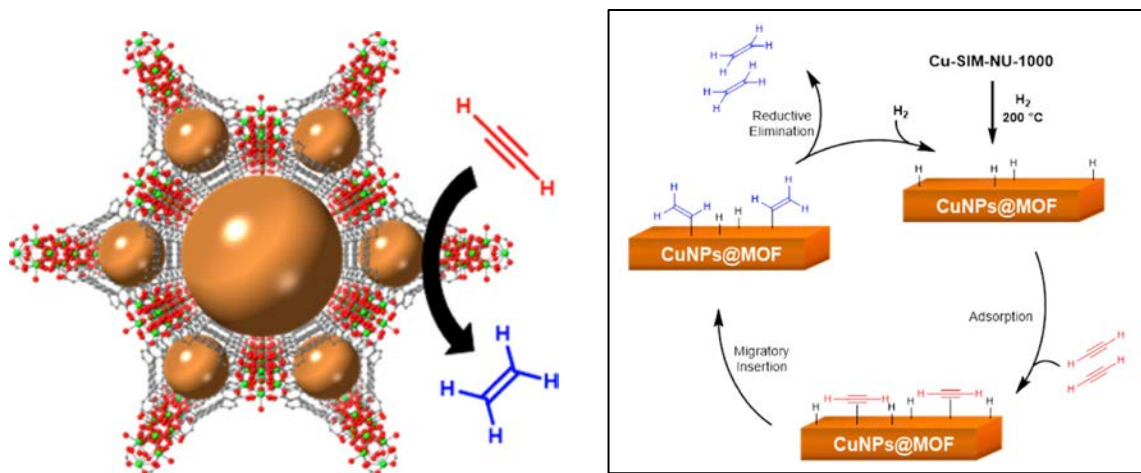
Postdoc: N. Scott Bobbitt, Jian Liu, Haoyuan Chen

Students: Yijun Liao, Rebecca Goncalves, Rodrigo Maldonado

RECENT PROGRESS

Separation via sorption and reversible chemical transformation. Mixtures of small gas molecules – especially those that lack easily recognized functional groups – can be challenging to economically separate, even by sieving approaches. Nevertheless, these mixtures are ubiquitous in gas-phase catalytic chemistry, natural gas reserves, and elsewhere. We find that appropriately functionalized MOFs are capable of reversible, catalytically facilitated, dissociative adsorption of molecular hydrogen, followed by reversible reactive insertion into the active phase of the MOF. Notably, the reactions occur at and near room temperature at modest pressures. These findings offer a stepping-stone to separation of H₂ from other small molecules. A second example involves ammonia. We find that NH₃ can reversibly react, in simple Bronsted-base fashion with suitably designed MOFs and that the reactivity can be exploited in breakthrough measurements to demonstrate separation of NH₃ from mixtures with N₂ – again at ambient temperature and modest pressures. Notably, the employed MOFs are chemically and structurally stable toward extended exposure to ammonia.

- Hydrocarbon purification via adsorption and catalytic transformation.** Acetylene is a generally undesirable in ethylene, as it can readily poison catalysts otherwise activate ethylene. An alternative to physical removal acetylene would be its elimination via conversion to ethylene (by partial hydrogenation). A challenge is to avoid concomitant conversion of ethylene to ethane (i.e. further hydrogenation). We reported the highly selective semihydrogenation of acetylene to ethylene using a Zr-based metal–organic framework (MOF; NU-1000) with Cu–oxo clusters present on the nodes as precatalysts. The active form of the catalyst is MOF-supported Cu nanoparticles generated in situ upon a brief H₂ reduction treatment at 200 °C. This composite material is stable for many catalytic cycles and effectively avoids over-reduction to ethane, a common problem for many semihydrogenation catalysts.



- MOF separation and purification.** Although macroscopic metal–organic framework (MOF) single crystals have been routinely synthesized, undesired impurity phases are sometimes obtained in MOF nanoparticle (NP) syntheses, where purification remains challenging. We reported an electrostatic adsorption strategy to separate mixed phases of MOF NPs on the basis of their metal cluster-dependent surface charge differences. As a proof of concept, two groups of mixed-phase MOF NPs were synthesized and subsequently separated on the basis of their different Coulombic attraction to negatively charged magnetic beads (MBs). Different frameworks form on the basis of the conditions used. In the first group, a combination of three possible iron–terephthalate frameworks were evaluated: MIL-53, MIL-88B, and MIL-101 (MIL = Material Institute Lavoisier). In the second group, two zirconium–terephthalate frameworks were separated: MIL-140A and UiO-66 (UiO = University of Oslo). MIL-53 and MIL-140A are not positively charged and do not adsorb onto the MBs. The extraction of adsorbed MIL-88B, MIL-101, and UiO-66 MOF NPs from the MBs was achieved by adding 4-hydroxybenzophosphonate, a surface-capping ligand that neutralizes the charge of the MOF NPs and therefore results in their desorption from the MBs. The phase purities of the isolated NPs were verified by powder X-ray diffraction as well as scanning electron microscopy.
- Computational investigation of coordinatively unsaturated, MOF-supported metal-alkoxides as sorption sites for molecular hydrogen.** The introduction of metal alkoxides has been proposed as an attractive option to enhance hydrogen binding energies in porous materials such as metal–organic frameworks (MOFs) for separation of molecular hydrogen from other gases or for room-temperature hydrogen storage. The presence of residual solvent molecules

from MOF synthesis can, however, affect the performance of these functional groups. We performed quantum chemical calculations to predict solvent binding energies onto the metal-alkoxides and the temperatures required to drive off the solvent molecules and successfully activate porous materials with these moieties. Calculations were performed for Li, Mg, Zn, Cu, and Ni alkoxides and chloroform (CHCl₃), dimethylformamide (DMF), ethanol, methanol, and water solvent molecules. We identified CHCl₃ as a promising solvent that can be removed from these alkoxides at mild temperatures, whereas DMF binds strongly to the metal alkoxides and removal would require temperatures above the present upper bound of thermal stability in MOFs. As a second objective, we calculated the binding energies of hydrogen to metal alkoxide–solvent complexes to explore the effects of solvent molecules that cannot be removed.

Publications Acknowledging this Grant in 2015 – present

Exclusively funded by this grant

1. Sikora, B. J.; Colon, Y. J.; Snurr, R. Q. Continuous fractional component Monte Carlo simulations of high-density adsorption in metal-organic frameworks, *Molec. Sim.* **2015**, *41*, 1339-1347. DOI: 10.1080/08927022.2015.1043629
2. Chung, Y. G.; Gómez-Gualdrón, D. A.; Li, P.; Leperi, K. T.; Deria, P.; Zhang, H.; Vermeulen, N. A.; Stoddart, J. F.; You, F.; Hupp, J. T.; Farha, O. K.; Snurr, R. Q. In silico discovery of metal-organic frameworks for pre-combustion CO₂ capture using a genetic algorithm, *Sci. Adv.* **2016**, *2*, e1600909. DOI: 10.1126/sciadv.1600909
3. Xu, Y.; Vermeulen, N. A.; Liu, Y.; Hupp, J. T.; Farha, O. K. SALE-ing a MOF-based “Ship of Theseus.” Sequential building-block replacement for complete reformulation of a pillared-paddlewheel metal-organic framework, *Eur. J. Inorg. Chem.* **2016**, 4345-4348. DOI: 10.1002/ejic.201600069
4. Xu, Y.; Howarth, A. J.; Islamoglu, T.; Da Silva, C. T.; Hupp, J. T.; Farha, O. K. Combining solvent-assisted linker exchange and transmetallation strategies to obtain a new non-catenated nickel (II) pillared-paddlewheel MOF, *Inorg. Chem. Comm.*, **2016**, *67*, 60-63. DOI: 10.1016/j.inoche.2016.03.002
5. Zhang, H.; Snurr, R. Q. Computational study of water adsorption in the hydrophobic metal-organic framework ZIF-8: Adsorption mechanism and acceleration of the simulations, *J. Phys. Chem. C*, **2017**, *21*, 24000-24010. DOI: 10.1021/acs.jpcc.7b06405
6. Li, P.; Vermeulen, N. A.; Malliakas, C. D.; Gómez-Gualdrón, D. A.; Howarth, A. J.; O’Keeffe, M.; Farha, O. K. Bottom-Up Construction of a Superstructure in a Porous Uranium–Organic Crystal *Science*, **2017**, *356*, 624-627. DOI: 10.1126/science.aam7851
7. Liao, Y.; Zhang, L.; Weston, M. H.; Morris, W.; Hupp, J. T.; Farha, O. K. Tuning ethylene gas adsorption via metal node modulation: Cu-MOF-74 for a high ethylene deliverable capacity, *Chem. Commun.*, **2017**, *53*, 9376-9379. DOI: 10.1039/c7cc04160h. Correction: *Chem. Commun.*, **2017**, *53*, 12244-12244. DOI: 10.1039/c7cc90418e

8. Kobielska, P. A.; Howarth, A. J.; Farha, O. K.; Nayak, S. Metal-organic frameworks for heavy metal removal from water, *Coord. Chem. Rev.*, **2018**, *358*, 92-107. **DOI:** 10.1016/j.ccr.2017.12.010
9. Zhang, H.; Bucior, B. J.; Snurr, R. Q. Molecular modeling of carbon dioxide adsorption in metal-organic frameworks, in *Modelling and Simulation in the Science of Micro- and Meso-Porous Materials*, Catlow, C. R. A.; Van Speybroeck, V.; van Santen, R. A., Ed.; Elsevier: Amsterdam, **2018**; pp 99-150.
10. Howarth, A. J.; Li, P.; Farha, O. K.; O’Keeffe, M. Bottom-Up Design and Generation of Complex Structures: A New Twist in Reticular Chemistry, *Crystal Growth & Design*, **2018**, *18*, 449–455, **DOI:** 10.1021/acs.cgd.7b01434
11. García-Holley, P.; Schweitzer, B.; Islamoglu, T.; Liu, Y.; Lin, L.; Rodriguez, S.; Weston, M.; Hupp, J. T.; Gómez-Gualdrón, D.; Yildirim, T.; Farha, O. K. Benchmark Study of Hydrogen Storage in Metal–Organic Frameworks under Tank Design Conditions Including Temperature and Pressure Swing, *ACS Energy Letters*, **2018**, *3*, 748–754. **DOI:** 10.1021/acsenergylett.8b00154
12. Bobbitt, N. S.; Snurr, R. Q. Competitive adsorption of methyl bromide and water on metal catecholates: Insights from density functional theory, *Ind. Eng. Chem. Res.*, **2018**, *57*, 17488-17495. **DOI:** 10.1021/acs.iecr.8b04377
13. Redfern, L. R.; Li, Z.; Zhang, X.; Farha, O. K., Highly Selective Acetylene Semihydrogenation Catalyzed by Cu Nanoparticles Supported in a Metal-Organic Framework, *ACS Applied Nanomaterials*, **2018**, *1*, 4413-4418. **DOI:** 10.1021/acsanm.8b01397
14. Li, Y.; Lin, L.; Tu, M.; Nian, P.; Howarth, A. J.; Farha, O. K.; Qiu, J.; Zhang, X. Growth of ZnO Self-Converted 2D Nanosheet Zeolitic Imidazolate Framework Membranes by an Ammonia-Assisted Strategy, *Nano Research*, **2018**, *11*, 1850-1860. **DOI:** 10.1007/s12274-017-1803-0
15. Bobbitt, N. S.; Snurr, R. Q. Molecular modeling and machine learning for high-throughput screening of metal-organic frameworks for hydrogen storage, *Molec. Simulation*, **2019**, in press. **DOI:** 10.1080/08927022.2019.1597271
16. Colón, Y. J.; Snurr, R. Q. The effect of co-adsorbed solvent molecules on H₂ binding to metal alkoxides, *Phys. Chem. Chem. Phys.* **2019**, *21*, 9218-9224. **DOI:** 10.1039/C9CP00754G
17. Snurr, R. Q. It’s an interesting MOF, but is it stable? *Matter* **2019**, *1*, 26-27.
18. “Metal-Organic Framework Materials with Ultrahigh Surface Areas,” U.S. patent 9,216,939. Awarded **12/22/2015**

19. “System and Method for Generating and/or Screening Metal-Organic Frameworks,” U.S. patent 9,012,368. Awarded **4/21/2015**

Jointly funded by this grant and other grants (including grants held by collaborators) with leading intellectual contribution from this grant

20. Karagiari, O.; Vermeulen, N. A.; Klet, R. C.; Wang, T. C.; Moghadam, P. Z.; Al-Juaid, S. S.; Stoddart, J. F.; Hupp, J. T.; Farha, O. K. Functionalized defects through solvent-assisted linker exchange: synthesis, characterization, and partial postsynthesis elaboration of a metal-organic framework containing free carboxylic acid moieties, *Inorg. Chem.*, **2015**, *54*, 1785-1789. DOI: 10.1021/ic502697y
21. Howarth, A. J.; Liu, Y.; Li, P.; Li, Z.; Wang, T. C.; Hupp, J. T.; Farha, O. K. Chemical, Thermal, and Mechanical Stabilities of Metal-Organic Frameworks, *Nature Reviews Materials*, **2016**, *1*, article number 15018. DOI: 10.1038/natrevmats.2015.18
22. Patel, H. A.; Islamoglu, T.; Liu, Z.; Nalluri, S. K. M.; Samanta, A.; Anamimoghadam, O.; Malliakas, C. D.; Farha, O. K.; Stoddart, J. F. “Noninvasive Substitution of K⁺ Sites in Cyclodextrin Metal-Organic Frameworks by Li⁺ Ions,” *J. Am. Chem. Soc.*, **2017**, *139*, 11020–11023. DOI: 10.1021/jacs.7b06287
23. Cui, B.; Audu, C. O.; Liao, Y.; Nguyen, S. T.; Farha, O. K.; Hupp, J. T.; Grayson, M. Thermal Conductivity of ZIF-8 Thin-Film under Ambient Gas Pressure, *ACS Appl. Mater. Interfaces*, **2017**, *9*, 28139–28143. DOI: 10.1021/acsami.7b06662
24. Hartlieb, K. J.; Peters, A. W.; Wang, T. C.; Deria, P.; Farha, O. K.; Hupp, J. T.; Stoddart, J. F. Functionalised cyclodextrin-based metal-organic frameworks, *Chem. Commun.*, **2017**, *53*, 7561-7564. DOI: 10.1039/c7cc03345a
25. Rimoldi, M.; Howarth, A. J.; DeStefano, M. R.; Lin, L.; Goswami, S.; Li, P.; Hupp, J. T.; Farha, O. K. Catalytic Zirconium/Hafnium-Based Metal-Organic Frameworks, *ACS Catal.*, **2017**, *7*, 997-1114. DOI: 10.1021/acscatal.6b02923
26. Chung, Y. G.; Bai, P.; Haranczyk, M.; Leperi, K. T.; Li, P.; Zhang, H.; Wang, T. C.; Duerinck, T.; You, F.; Hupp, J. T.; Farha, O. K.; Siepmann, J. I.; Snurr, R. Q. Computational Screening of Nanoporous Materials for Hexane and Heptane Isomer Separation, *Chem. Mater.*, **2017**, *29*, 6315-6328 DOI: 10.1021/acs.chemmater.7b01565
27. Howarth, A. J.; Peters, A. W.; Vermeulen, N. A.; Wang, T. C.; Hupp, J. T.; Farha, O. K. Best Practices for the Synthesis, Activation, and Characterization of Metal-Organic Frameworks, *Chem. Mater.*, **2017**, *29*, 26-39. DOI: 10.1021/acs.chemmater.6b02626
28. Erkartal, M.; Erkilic, U.; Tam, B.; Usta, H.; Yazaydin, O.; Hupp, J. T.; Farha, O. K.; Sen, U. From 2-methylimidazole to 1,2,3-triazole: A topological transformation of ZIF-8 and ZIF-67 by post-synthetic modification, *Chem. Commun.*, **2017**, *53*, 2028-2031. DOI: 10.1039/C6CC08746A

29. Islamoglu, T.; Goswami, S.; Li, Z.; Howarth, A. J.; Farha, O. K.; Hupp, J. T. Metal-Organic Frameworks for Targeted Applications, *Acc. Chem. Res.*, **2017**, *50*, 805–813. DOI: 10.1021/acs.accounts.6b00577. Correction: *Acc. Chem. Res.*, **2018**, *51*, 212–212. DOI: 10.1021/acs.accounts.7b00620
30. Patel, H. A.; Selberg, J.; Salah, D.; Chen, H.; Liao, Y.; Nalluri, S. K. M.; Farha, O. K.; Snurr, R. Q.; Rolandi, M.; Stoddart, J. F. Proton conduction in Tröger’s base-linked poly(crown ether)s, *ACS Appl. Mater. Interfaces*, **2018**, *10*, 25303-25310. DOI: 10.1021/acsami.8b05532
31. Majewski, N. B.; Noh, H.; Islamoglu, T.; Farha, O. K. “NanoMOFs: little crystallites for substantial applications,” *J. Mater. Chem. A*, **2018**, *6*, 7338-7350. DOI: 10.1039/c8ta02132e
32. Moghadam, P. Z.; Islamoglu, T.; Goswami, S.; Exley, J.; Fantham, M.; Kaminski, C. F.; Snurr, R. Q.; Farha, O. K.; Fairen-Jimenez, D. Computer-aided discovery of a metal-organic framework with superior oxygen uptake, *Nature Comm.*, **2018**, *9*, article number 1378. DOI: 10.1038/s41467-018-03892-8
33. Chen, Z.; Hanna, S. L.; Redfern, L. R.; Alezi, D.; Islamoglu, T.; Farha, O. K. Reticular chemistry in the rational synthesis of functional zirconium cluster-based MOFs, *Coord. Chem. Rev.*, **2019**, *386*, 32-49. DOI: 10.1016/j.ccr.2019.01.017
34. Müller, P.; Bucior, B.; Tuci, G.; Luconi, L.; Getzschmann, J.; Kaskel, S.; Snurr, R. Q.; Giambastiani, B.; Rossin, A. Computational screening, synthesis and testing of metal-organic frameworks with a bis(thiazole) linker for carbon dioxide capture and its green conversion into cyclic carbonates, *Molec. Systems. Design. Eng.*, **2019**, in press. DOI: 10.1039/C9CP00754G
35. Guo, Q. H.; Liu, Z.; Li, P.; Shen, D.; Xu, Y.; Ryder, M. R.; Chen, H.; Stern, C. L.; Malliakas, C. D.; Zhang, X.; Zhang, L.; Qiu, Y.; Shi, Y.; Snurr, R. Q.; Philp, D.; Farha, O. K.; Stoddart, J. F. A hierarchical nanoporous diamondoid superstructure, *Chem*, **2019**, in press. DOI: 10.1016/j.chempr.2019.06.011
36. Wang, S.; Liao, Y.; Farha, O. K.; Xing, H.; Mirkin, C. A. Electrostatic Purification of Mixed-Phase Metal–Organic Framework Nanoparticles, *Chem. Mater.*, **2018**, *30*, 4877-4881. DOI: 10.1021/acs.chemmater.8b01164

Jointly funded by this grant and other grants with relatively minor intellectual contribution from this grant

37. Anamimoghadam, O.; Cooper, J. A.; Nguyen, M. T.; Guo, Q. H.; Mosca, L.; Roy, I.; Sun, J.; Stern, C. L.; Redfern, L. R.; Farha, O. K.; Stoddart, J. F. Cyclotris(paraquat-p-phenylenes), *Angew. Chem.*, **2019**. DOI: 10.1002/anie.201907329

Other products

38. Chen, D. Incorporation of Metal Catecholates into a Zirconium Metal-Organic Framework for CO₂ Capture, MS thesis, **2016**.
39. Zhang, H., Computational Study of Metal-Organic Frameworks in Natural Gas Storage, Water Adsorption, and Ethane/Ethylene Separation, Ph.D. dissertation, **2017**
40. García-Holley, P., Benchmark Study of Hydrogen Storage in Metal-Organic Frameworks Under Temperature and Pressure Swing Conditions, MS thesis, **2018**
41. Audu, C., Design and Installation of Sorptive Sites on the Inorganic Node, Organic Linker and in the Pores of Metal-Organic Framework Adsorbents, Ph.D. dissertation, **2018**

A Machine Learning Approach to Understanding Chemical Separations

L. Soderholm¹, Prasanna Balaprakash², Aurora Clark³, Stefan Wild², Wei Jiang⁴, Kaitlin Lovering¹, Srikanth Nayak¹, Marek Piechowicz¹, Michael Servis³, Ilya Shkrob¹, S. Skanthakumar¹, Mark R Antonio¹, Uta Ruett⁵, Soenke Seifert⁵, Ahmet Uysal¹

¹ Chemical Sciences and Engineering Division, Argonne National Laboratory

² Mathematics and Computer Sciences Division, Argonne National Laboratory

³ Department of Chemistry, Washington State University

⁴ Computational Science Division, Argonne National Laboratory

⁵ Advanced Photon Source, Argonne National Laboratory

Abstract

As society becomes more reliant on technology, chemical separations must play a critical role in resource management by providing large quantities of high-purity, resource-limited materials in a way that addresses the growing global mandate for conservation and environmental stewardship. A “go-to” low-energy separation method is liquid-liquid extraction (LLE), which involves the initial dissolution of a chemical mixture (generally an acidic aqueous phase), that is then contacted with an immiscible low-dielectric organic phase into which the targeted species is selectively transferred. The resulting separation system has a complex, multidimensional phase diagram with a large number of tunable chemical variables. The standard approach to this problem has been to limit the sampling of the reaction space by dividing it into isolated segments despite the myriad of evidence suggesting variable interdependencies and hierarchical relationships that are not always chemically intuitive. Recognizing that the reaction phase space is incredibly large, we turn to data science approaches for guidance in isolating the underlying high-dimensional and interdependent features that define a robust LLE separation. The goal of this research program is to advance methodologies for quantifying energy drivers in chemical separations by using chemistry-aware data science approaches to provide a new perspective on how to handle multidimensional phase problems, as exemplified by LLE. We are working toward this goal by employing advanced machine learning strategies that incorporates domain-science information. The methodology developed herein will be extensible to other energy driven separations methods, including solid-liquid chromatographic, membrane, or polymer methods.

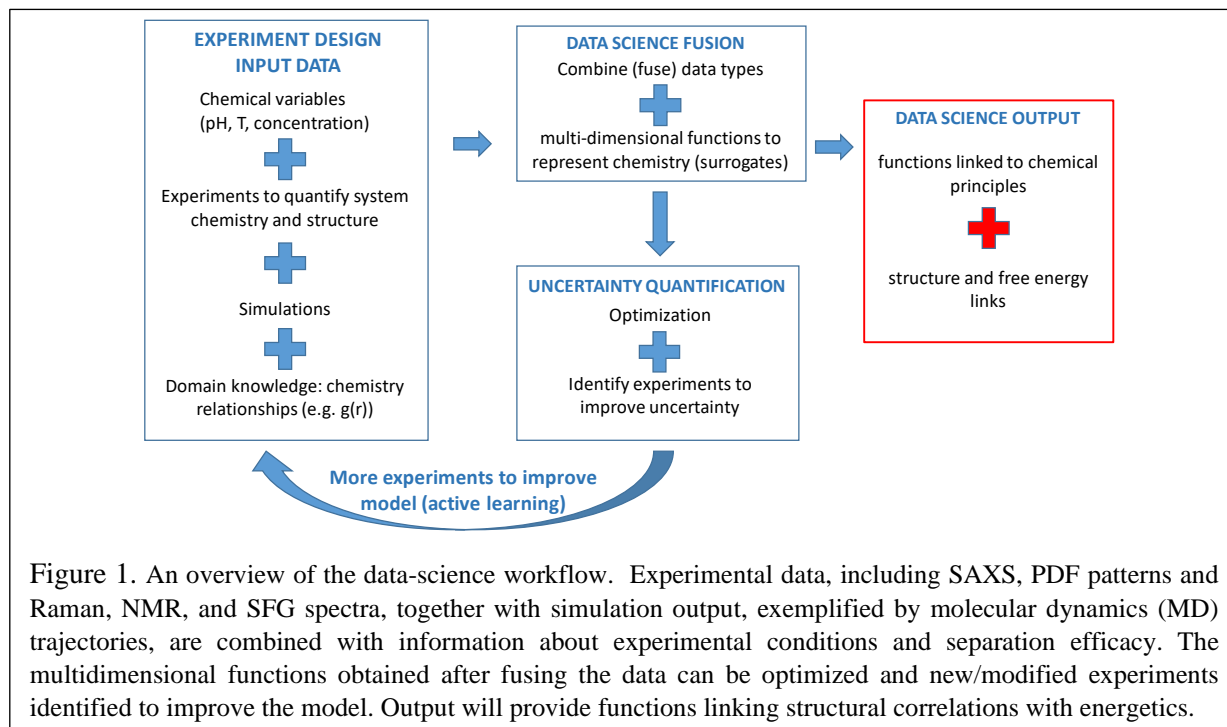
Post Docs: Kaitlin Lovering, Srikanth Nayak, Michael Servis

Students: Marek Piechowicz[#] (University of Chicago), [#]Previous SCGSR Awardee

RECENT PROGRESS

Critical to a chemical LLE is the selective transfer of targeted ions between two immiscible phases. This is a free-energy driven process with an outcome that can be strongly influenced by small variations in complexation, speciation, and structuring, sometimes extending over hierarchical lengthscales. The complexity of the multidimensional phase space involved, together with the interdependence of variables controlling the free-energy landscape, necessitates a holistic approach to understanding how go about designing a holistic system without the necessity of extensive trial-and-error experiments. We have begun our studies by defining a detailed methodology to realize our novel data-science approach to defining the energy drivers within a broadly defined

LLE system. We are working to combine emerging areas in machine learning, specifically employing deep-neural-network strategies, in combination with domain-science information. As demonstrated in Figure 1, this approach involves fusing a wide variety of data, including those obtained from experiments and simulation, with



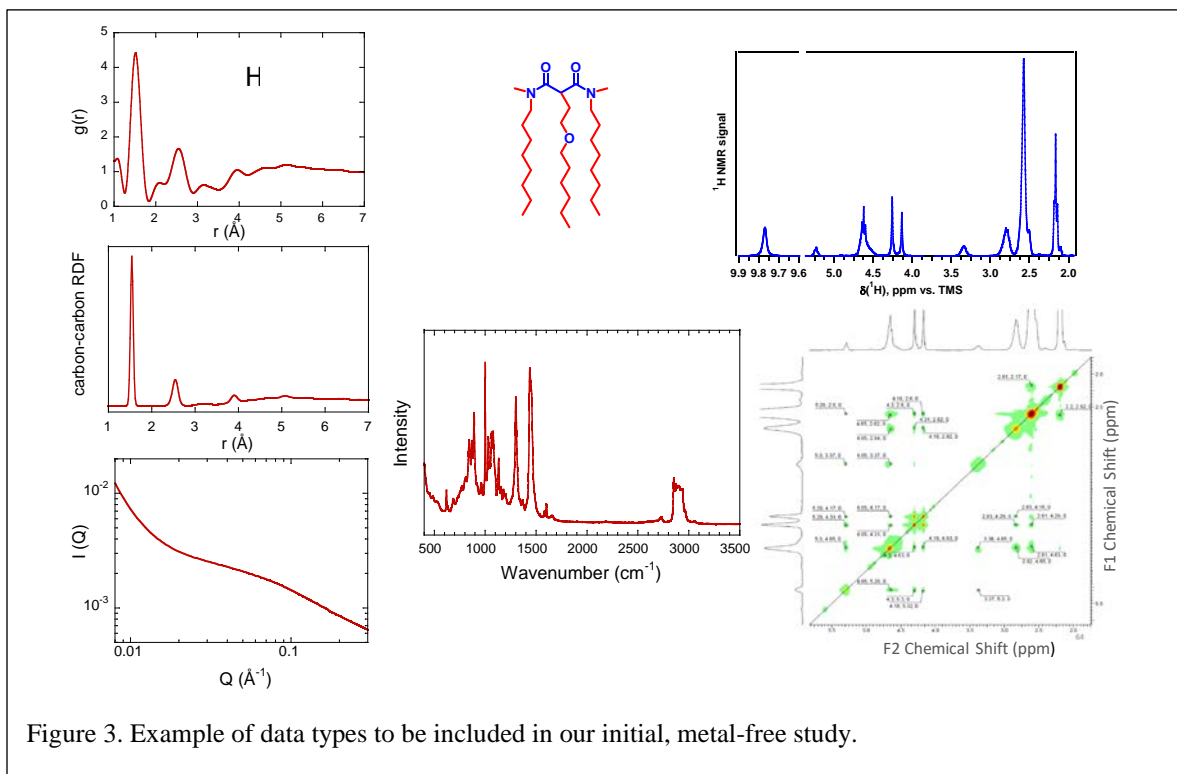
chemical variables and pre-existing chemical knowledge of the system. Large multivariable functions are used to generate surrogates to represent the data. The specific inclusion of selected, relevant, chemical knowledge directly into the machine-learning methods is significantly reducing the amount of data required to make robust predictions from the surrogate models. Improving the surrogates is done through function optimization designed to identify the optimal new experiments to be undertaken that will most improve the system model. The outcome (Figure 1) are structure-to-free-energy links that span the multidimensional phase space of a LLE system.

We began our efforts by choosing a generic, simple system for study, specifically the extraction of *f*-ions (lanthanides and actinides) from an acidic aqueous solution into an organic solution containing an extractant molecule. Within this broad context our initial series of experiments has been on metal-free solutions with nitric acid aqueous phases, dodecane as the organic diluent, and a series of malonamides as

		Measurement Temperatures									
		[HNO ₃] _{aq}	[LiNO ₃] _{aq}	[EuNO ₃] _{aq}	Contact?	Temp.	[DOHE] _{org}	Org.	Solvent	Phase	Temp.
Systems	0.0	0.0	0.0	No	23.0°	0.5	n-dodecane	dodecane	dodecane	dodecane	38°
	0.0	0.0	0.0	Yes	23.0°	0.5	n-dodecane	dodecane	dodecane	dodecane	38°
	0.0	3.0	0.0	Yes	23.0°	0.5	n-dodecane	dodecane	dodecane	dodecane	33°
	0.5	2.5	0.0	Yes	23.0°	0.5	n-dodecane	dodecane	dodecane	dodecane	33°
	1.0	2.0	0.0	Yes	23.0°	0.5	n-dodecane	dodecane	dodecane	dodecane	28°
	1.5	1.5	0.0	Yes	23.0°	0.5	n-dodecane	dodecane	dodecane	dodecane	28°
	2.0	1.0	0.0	Yes	23.0°	0.5	n-dodecane	dodecane	dodecane	dodecane	23°
	2.5	0.5	0.0	Yes	23.0°	0.5	n-dodecane	dodecane	dodecane	dodecane	23°
	3.0	0.0	0.0	Yes	23.0°	0.5	n-dodecane	dodecane	dodecane	dodecane	18°
	3.0	0.0	0.0	Yes	23.0°	0.5	n-dodecane	dodecane	dodecane	dodecane	18°

Figure 2. Example input for surrogate construction algorithms. In our first set of experiments, the EuNO₃ concentration is always zero and the extractant, (DMDOHEMA) and solvent phases (water and dodecane) do not change. Their corresponding columns are included here as “Experimental Variables” to highlight how this template is extensible to future studies.

extractants. The experimental variables (Figure 2) include nitrate concentration in the aqueous phase, which is



kept at constant ionic strength, and temperature. Examples of the data types included in this study are presented in Figure 3. Our initial surrogate model was developed using a deep neural network on high-energy X-ray scattering data from a simple subsystem. $[\text{HNO}_3]$, r , and temperature were used as inputs. The resulting size of the input and output layers were 713 and 711 respectively, which together with five hidden layers, each with 250 neurons, resulted in 671,461 trainable parameters. Despite the small number of training data and their nonlinear relationship, our results are quite promising. These results are now being expanded to include SAXS and Raman data as well as trajectories from molecular dynamics simulations.

PUBLICATIONS

This is a new project.

Computer Simulation of Complex Systems at the Extremes of pH Title Second Line

Gregory A. Voth

The University of Chicago, Department of Chemistry

Presentation Abstract

This project involves the development and application of an accurate and efficient multiscale reactive molecular dynamics approach to simulate a variety of complex heterogeneous systems at the extremes of pH (< 0 or > 14). Such systems are fundamentally important in separations science, but currently little is known about their physical properties and very limited simulation tools are available to study them. The research addresses this challenge by further developing this multiscale computational framework to accurately bridge electronic structure data with an efficient MD methodology, which is in turn is able to access the relevant large time and length scales. A fundamental understanding is being obtained for highly acidic and basic systems, including those for water-organic liquid interfaces, water-amphiphile mixtures, systems in nanoscale confinement, micelles and polymers, systems under applied voltage, and proton exchange membrane-catalyst layers. The project is also carried out in close contact with experimental characterization for certain of the key systems. In addition to providing fundamental basic knowledge, the proposed research helps to open the door to new breakthroughs in the design and control principles for novel separations processes and materials.

DE-SC0018648: Computer Simulation of Complex Systems at the Extremes of pH

Student(s): Paul Calio, Zhefu Li, Chenghan Li

RECENT PROGRESS

Our research focuses on the outstanding and important challenge of simulating highly acidic and basic systems in both homogeneous and heterogeneous environments. We are addressing this challenge by further developing our multiscale computational framework based on a multiscale reactive molecular dynamics (MS-RMD) method that recapitulates state of the art electronic structure data but with an efficiency capable of accessing the relevant time and length scales.

Hydrated excess proton in water: Addressing complexity and misconception

Previous theoretical studies have shown that the structure of the hydrated excess proton is best described as a distorted Eigen cation, $H_9O_4^+$; however, recent 2D-IR experiments have proposed that a long lived “distorted Zundel” cation best represents their spectroscopy and 2.5 ps anisotropy decay of the bending modes of flanking water bends exists within the excess proton complex. We have been working towards disentangling the discrepancies between theory and experiments by calculating anisotropy decays from equilibrium trajectories and frequency calculations from instantaneous normal mode analysis. Through anisotropy plots, we have been able to capture a reorientational timescale that agrees with the 2.5 ps from experiments, while being able to capture the “special-pair dance” dynamics characteristic of a distorted Eigen cation. Through normal mode calculations, we have been able to show vibrational frequencies that correspond to flanking water bends within a Zundel complex are additionally found in distorted

Eigen complex, which gives further verification to the solvation structure not being simply defined as a distorted Zundel complex, hence the experiments have been wrongly interpreted.

Proton transport in proton exchange membranes

Electrolyte solutions separating ultrathin electrodes are known to exhibit enhanced proton mobility (Coulomb transport) due to the potential difference that arises between the electrodes. Towards this end, we have been working to model Coulomb transport in PEM using MS-RMD to access the large timescales inaccessible to *ab initio* MD (AIMD) simulation. We can understand Coulomb transport by applying electric fields of varying strengths to bulk Nafion PEM systems. In the classical limit and first approximation, the force of the electric field on a particle is the magnitude of the electric field and the particle's charge. However, this neglects additional electric field forces in the MS-RMD method from delocalizing the excess hydrated proton charge across multiple water molecules. Therefore, we have developed the theory for applying electric fields in bulk Nafion PEM simulations using our MS-RMD method. Preliminary results of the first approximation show external electric fields indeed enhance the excess proton transport properties, but in nontrivial ways.

Ultrathin film proton exchange membranes have been shown experimentally and theoretically to vary greatly depending on the surface against which the membrane is deposited. This surface is typically a catalyst layer (CL), and the hydrophilicity of that layer can affect water uptake, PEM morphology, and proton transport. We have used MS-RMD dynamics to study the effect of catalyst layer hydrophilicity on morphology and proton transport in Nafion ultrathin film membranes. We treat the CL as a 9-3 Lennard-Jones wall, and tune the hydrophilicity by varying the relative well depth for polar and nonpolar groups. To study the effect of morphology, we compared Nafion systems having a random morphology to those with straight-chain bundles of polymer. We found that inclusion of the CL facilitates the emergence of layering, so the random morphology adopts a lamellar-like morphology. The bundle morphology undergoes a smaller transition due to its morphological integrity. We found that increasing the hydrophilicity results in a decrease in proton transport. Experimental work has shown that increased CL hydrophilicity greatly increases water uptake. Our results show that increasing the water in a system has an even more drastic effect on proton transport, but with low hydration levels still showing minimal transport.

Refining *ab initio* molecular dynamics for water and proton transport in water

The advantage of *ab initio* molecular dynamics (AIMD) is it can easily account for chemical reactions. This becomes particularly useful for simulating the hydrated excess proton which diffuses in part through the Grotthuss proton hopping mechanism. However, AIMD is commonly attributed with over-structuring and glass-like diffusive properties. One method to correct AIMD is through Experiment Directed Simulation (EDS). EDS is a method that improves molecular simulations by minimally biasing the system's Hamiltonian to reproduce certain known experimental observable values. In a previous application of EDS to AIMD simulations, we were able to correct AIMD simulations of water to reproduce its experimentally derived solvation structure. Moreover, by solely biasing the O-O pair correlation functions, we were able to improve other structural and dynamical properties that were not biased. Using recent advancements to the EDS learning algorithm, we are further improving these AIMD results by biasing the hydrogen bond to reproduce the O-H radial distribution function derived from the

highly accurate MB-pol model of water. Our preliminary work shows that instead biasing the hydrogen bond can lead to improved AIMD water properties, with structural and dynamical properties even closer to experiment than our previous EDS-AIMD model.

Deepening our understanding of proton hopping dynamics in water

In order to better understand the relative importance of concerted proton hopping events, we have also performed a series of analyses on *ab initio* molecular dynamics (AIMD) simulations of a hydrated excess proton in water. We compared both the effect of temperature and the introduction of an experimentally directed bias used to correct for the overstructuring in AIMD water. We find that in all simulations, concerted hopping events do occur, but that concerted hopping is not the dominant mechanism. The majority of hopping events are the product of the excess proton “rattling”, where the proton will rapidly exchange between two or more waters. The results are consistent with the proposed special-pair dance model of proton transfer, wherein the acceptor water molecule will quickly change, but the donating water molecule remains constant for some time until finally a decisive hop occurs. To remove the misleading effect of rattling, we applied a filter to the trajectory such that hopping events that were followed by back hops to the original water are not counted. We found a steep reduction in the number of multiple hopping events when the filter was applied, suggesting that many multiple hopping events that occur in the unfiltered trajectory are the product of rattling. Comparing the continuous correlation function of the filtered and unfiltered trajectories, we find good agreement with experimental values for the proton hopping time and Eigen-Zundel interconversion time, respectively.

Hydrated excess protons in heterogeneous environments

We further investigated the behavior of an excess proton in non-ionic reverse micelles of various sizes. We observed the hydrated excess proton has a strong affinity to the surface, and such affinity diminishes as the micelles increase in diameter. Strong affinity to the surface results in reduced proton transport due to (1) slow micellar water diffusion that leads to slow vehicular transport of proton and (2) the distorted structure of interfacial hydrated proton complex that leads to hindered proton hopping. We additionally see strong correlations between the proton dynamical properties as the micelle increases in size due to the reduced affinity to the surface. Furthermore, we observe a bi-exponential relaxation of the overall hydrogen bonds in reversed micelles, with the larger relaxation timescale comparable to that in a bulk water. A slow-relaxing component of the hydrogen bond network also contributes to the slow proton transport.

We also studied the behavior of a hydrated excess proton at a water-vapor interface. We used umbrella sampling enhanced sampling techniques to calculate the potential of mean force (PMF) for two interface definitions: (1) the Gibbs Dividing interface (GDI), which is an average interface over the entire time series, and (2) the Willard-Chandler Interface (WCI), which is an instantaneous interface calculated for each timestep. In both cases, the excess proton shows similar trends that weakly attract the hydrated proton to the interface. When the excess proton moves to the interface, the reduced water density in the interfacial region causes the coordination number of the hydrated proton (hydronium-like) structure to decrease, thus causing the dipole moment of the hydronium cation to align perpendicular to the interface. This leads to the solvation structure of the hydronium to form in a relatively higher density water region. We also discovered that the curvature of the WCI is very dependent on the location of hydrated excess

proton, which we propose is a result of the alteration of water density by the solvation shells of the hydronium cation.

We further investigated protonated water clusters dissolved in acetonitrile/water mixtures with both AIMD and MS-RMD simulation approaches. Recent 2D-IR spectroscopy experiments have proposed that water clusters in acetonitrile reveal the solvation structure of the hydrated excess proton as a Zundel cation. From our simulations, however, we discovered that the Zundel cation is not the predominant species in these water clusters. Histograms of the number of water molecules per cluster size after equilibration reveal a variety of protonated water clusters, which is contrary to what is assumed in the interpretation of the recent 2D-IR experiments. Furthermore, structural analysis of the hydrated excess proton is in much better agreement with an Eigen cation than a Zundel cation, contrary to what is proposed by the experimentalists. Additionally, the dynamical properties of the excess proton in water-acetonitrile simulations differ from that in bulk water, showing that hydrated excess protons in water-acetonitrile systems do not accurately represent a hydrated excess proton in bulk water.

Publications Acknowledging this Grant in 2015 – present

Several publications (at least five) are currently being prepared for publication from this new grant, which started approximately one year ago and has charted new research directions. All publications are exclusively funded by this grant except for one, which is jointly funded by this grant and other grants with the leading intellectual contribution from this grant. An earlier DOE grant was devoted to proton exchange membranes and had numerous publications, which are listed in the Final Report, but are not listed here.

PI ABSTRACTS SESSION VI: POSTER SESSION

Alkoxysilane-Substituted Polynorbornenes: High T_g Glassy Membranes that behave like Rubbers

Christopher R. Maroon,[†] Jacob Townsend,[†] Kevin R. Gmernicki,[†] Daniel J. Harrigan,[‡]
Benjamin J. Sundell,[‡] John A. Lawrence III,[‡] Shannon M. Mahurin,[‡] Konstantinos D.
Vogiatzis,[†] Brian K. Long^{†*}

[†]Department of Chemistry, University of Tennessee, Knoxville, Tennessee, 37996

[‡]Aramco Services Company: Aramco Research Center - Boston, Massachusetts, 02139

[‡]Chemical Sciences Division, Oak Ridge National Lab., Oak Ridge, Tennessee 37831

Presentation Abstract

Herein, we will describe how the CO₂/N₂ gas separation performance of alkoxysilyl-substituted vinyl-added polynorbornenes (VAPNBs) may be enhanced via monomer design. More specifically, we will show that by increasing the incorporation of 5-tris(2-methoxyethoxy)silyl-2-norbornene in vinyl-added polynorbornenes, a substantial increase in CO₂/N₂ selectivity is achieved with minimal changes in CO₂ permeability. This trend circumvents the traditional permeability/selectivity “tradeoff” relationship, producing an optimal membrane whose performance nears the 2008 upper bound for CO₂/N₂ separations. Though these polymers were originally designed to maximize CO₂ solubility, subsequent gas sorption studies revealed that these high T_g glassy membranes essentially lack any Langmuir sorption component. Furthermore, our investigations indicate that their improved CO₂/N₂ selectivity is due to decreased N₂ solubility within the matrix. This is supported via computational modelling that suggests that the source of this “N₂-phobicity” is likely explained via comparative analyses of polymer-polymer and polymer-gas interactions. Finally, mixed-gas permeation tests were performed to provide a more realistic look at these membrane’s real-world gas separation performance.

DE-SC0018179: Advancing Polymeric Gas Separation Membranes through Molecular Engineering

PI: Brian K. Long

Postdoc(s): none

Student(s): Christopher Maroon, Morgan Higgins, Jordan Kaiser, Alicia Doerr, C. Elizabeth O’Connell

Affiliations(s): same as above

RECENT PROGRESS

Note: The significant results described herein are organized according to information disclosed in an already, or soon to be, published manuscript.

Project 1 – The following results were published in the peer-reviewed manuscript: *Macromolecules* **2019**, 52, 1589-1600. At the conclusion of the previous reporting period, we had discovered that incorporation of ethylene glycol-like units into the siloxane-substituted polymers (Figure 1) resulted in significant enhancements in CO₂/N₂ selectivity with minimal impact on CO₂ permeability. These materials clearly did not follow the traditional permeability-selectivity trade-off (Figure 2), and the best performing polymer (**P5**) exhibited performance near the 2008 upper bound ($P_{CO_2} = 755$, $\alpha_{CO_2/N_2} = 37$).

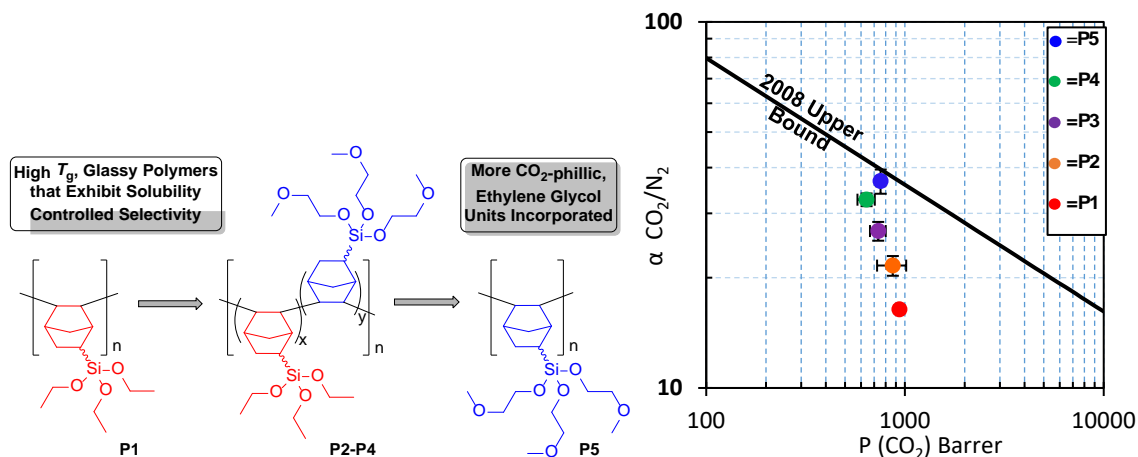


Figure 1. (left) Polymers **P1-P5** containing 5-triethoxysilyl-2-norbornene (**red**) and 5-tris(2-methoxyethoxy)-2-norbornene (**blue**) units. (right) Robeson plot of gas separation performance for polymers **P1-P5**.

To study the origins of this enhanced performance, we conducted detailed investigations into the densities, fractional free-volumes, and diffusivity and solubility coefficients of these polymers. As originally hypothesized, the observed enhancement in CO₂/N₂ selectivity results from improved solubility selectivity; however, our original hypothesis was that the incorporation of ethylene glycol-like side-groups should promote favorable polymer-CO₂ interactions. Unexpectedly, this was found to be incorrect. Careful measurement of CO₂ and N₂ sorption isotherms revealed that CO₂ sorption was essentially identical for each polymer tested, and that our materials appeared to be increasingly “N₂-phobic” as the mole % of ethylene glycol-like units were increased. Furthermore, these sorption isotherms showed that as the mole % of ethylene glycol-like units were increased, any Langmuir contributions to gas sorption were completely lost. To the best of our knowledge, this unique behavior has never been observed in another high T_g glassy material.

To better understand this behavior, detailed DFT calculations were performed. Because our materials displayed no Langmuir contribution to sorption, any sorption according to Henry’s law (dual-mode model) should be dictated exclusively by polymer-polymer and polymer-gas interactions. All calculations were performed by our collaborators blind of the experimental results. Gratifyingly, the trends observed computationally perfectly agreed with those found experimentally (Figure 2), suggesting that the observed “N₂-phobicity” could be explained by strengthened polymer-polymer interactions, enhanced polymer-CO₂ interactions, and consistently minimal polymer-N₂ interactions.

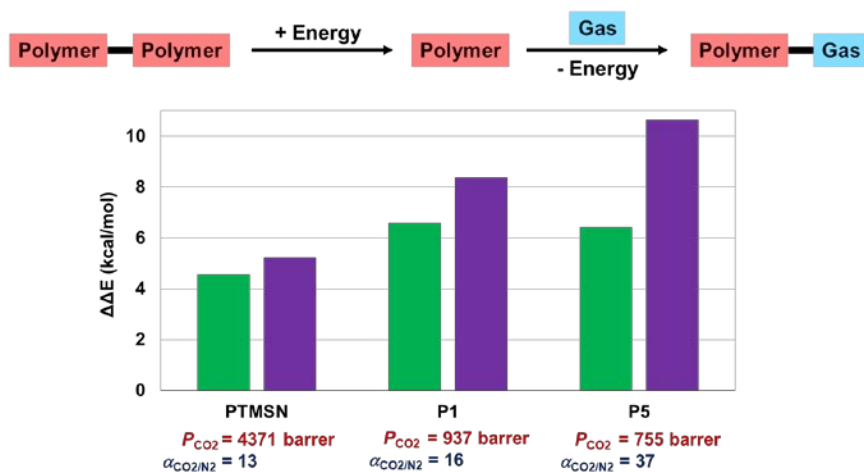


Figure 2. $\Delta\Delta E$ values for monomers comprising PTMSN (standard glassy VAPNB), **P1**, and **P5**.

Project 2 – The following results are soon to be published in a peer-reviewed journal. As highlighted in our last progress report, we identified three sets of alkoxyfunctionalized vinyl-addition polynorbornenes in an effort to develop detailed structure-property relationships for this class of polymers (Figure 3). A plot of CO_2/N_2 selectivity versus CO_2 permeability for these polymers (Figure 3) reveals clear trends within each polymer set. Specifically for polymers **P6-P7**, a traditional permeability-selectivity trade-off relationship was observed. In contrast, polymers **P7-P9** revealed that permeability and selectivity were simultaneously increased as a function of decreasing alkoxy length, with **P9** nearly reaching the 2008 upper bound. Lastly, polymers **P9-P11** showed that increasing tether lengths between the alkoxy moiety and the bicyclic norbornene unit leads to higher selectivities, but at the cost of permeability.

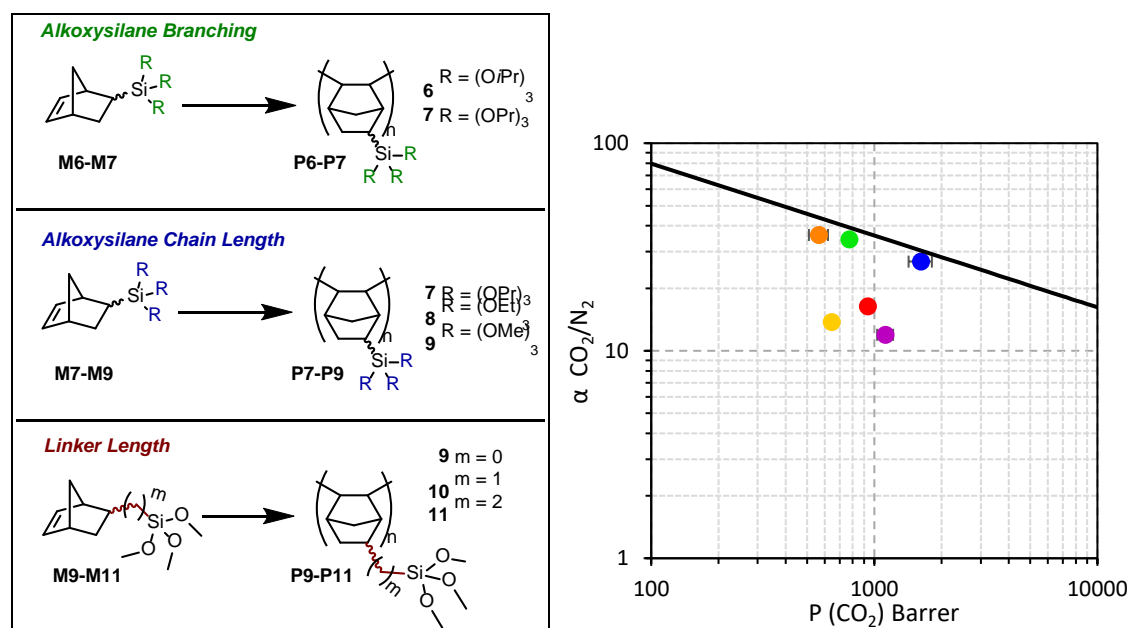


Figure 3. (left) Series of monomers and polymers designed to elucidate the structure-property relationship between alkoxy substituent identity and gas transport behavior. (right) Robeson plot for polymers **P6-P11** relative to the 2008 upper bound for CO_2/N_2 separations.

To better understand these trends, we conducted detailed investigations in the densities, fractional free-volumes, diffusivity and solubility coefficients, and sorption isotherms of these

polymers. As expected, simple changes in density and diffusivity/solubility could explain why polymer **P6-P7** and **P9-P11** displayed a permeability selectivity tradeoff behavior. However, it was less clear why polymers **P7-P9** displayed a trend completely perpendicular to the 2008 upper bound. Extraction of individual Henry's and Langmuir contributions to sorption showed that polymers bearing short alkoxy silane chains had a substantial Langmuir contribution, whereas those containing longer alkoxy silane chains displayed no observable Langmuir contribution to sorption. We surmise that this increasing Langmuir contribution as a function of decreasing alkoxy silane chain length likely accounts for the observed enhancement in gas separation performance. Lastly, these results are supported via DFT calculations.

Project 3 – The following results are soon to be published in a peer-reviewed journal. Due to the unique properties of the above mentioned alkoxy silane substituted vinyl-addition polynorbornenes, we began to brainstorm what other functional groups could be incorporated to enhance CO₂/N₂ selectivity. However, we quickly realized that though many studies have used a variety of functional groups to enhance CO₂/N₂ selectivity, a fundamental study in which those functionalities are appended to a single polymeric scaffold was missing from the literature. To address this, we used our unique ability to readily access a variety of vinyl-addition polynorbornenes bearing frequently encountered “CO₂-phillic” moieties (Figure 4).

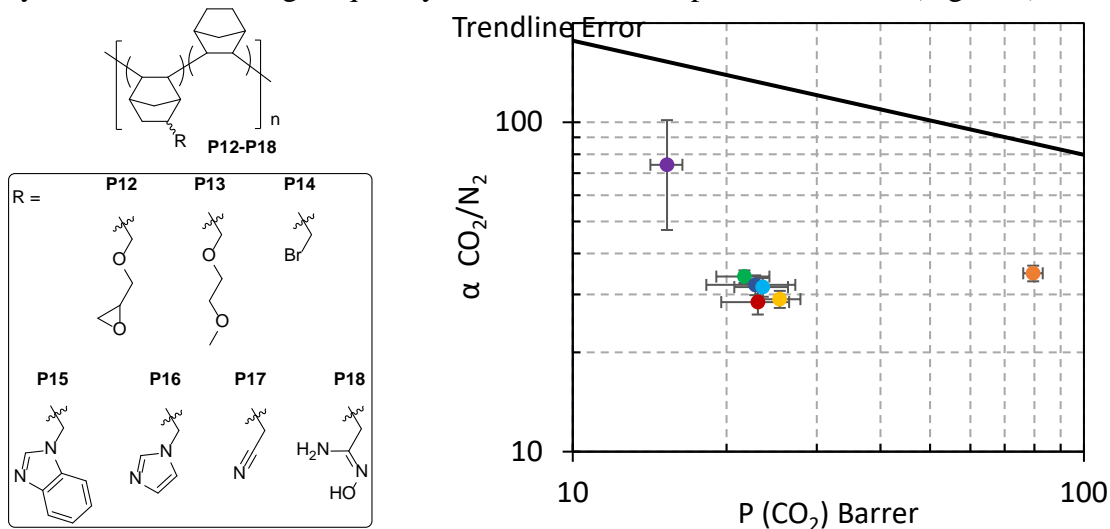


Figure 4. (left) Functionalized vinyl-addition polynorbornenes **P12-P18** to test CO₂-philicity on a consistent polymer backbone. (right) Robeson plot of functionalized polynorbornenes **P12-P18**.

Vinyl-addition polynorbornenes are a privileged polymer class as their rigid backbone prevents efficient chain packing, they readily form large area defect-free films, they are high T_g glassy polymers, and due to their tremendous oxidative, thermal, and chemical stability. Because of the incompatibility of many functional groups and commonly employed vinyl-addition polymerization catalysts, we were forced to utilize a post polymerization modification method to access the desired polymers. Shockingly, many of these functionalized polymers displayed very similar gas separation performance (Figure 4). However, those functionalized by ethylene glycol-like moieties (**P13**) and amidoximes (**P18**) displayed significantly enhanced permeability or selectivity, respectively. Our current efforts are to extract the rationale behind these observations.

Project 4 – The following results were published in the peer-reviewed manuscript: *Angew. Chem. Int. Ed.* **2019**, *58*, 5639-5642. Thanks to the work by our group and others, the interest in vinyl-addition polynorbornenes is on the rise. Though these materials are considered to be mechanically robust, it struck us that due to the presence of strained bicyclic repeat units along the

backbone that under appropriate stress, these materials may undergo mechanochemical activation. Indeed, our results showed that when commonly encountered vinyl-addition polynorbornenes were subjected to ultrasonication, the mechanical force rendered could rupture the bicyclic repeat unit (Figure 5). This ring-opening yielded units along the polymer backbone that mimic those obtained using ring-opening metathesis polymerization (ROMP), which is a completely distinct polymerization mechanism. Though this unprecedented chemistry was not directly used to modify membrane materials, we hypothesize that this information will be pivotal to any and all scientists employing this class of polymers in their work.

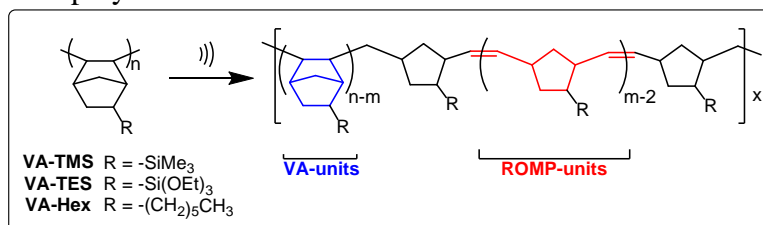


Figure 6. Schematic representation of the mechanochemical ring-opening olefination of VA-PNB to produce ROMP-PNB units.

Key Outcomes and Achievements: The key outcomes and achievements of our second reporting period are as follows:

- 1) We have established three key studies that provide fundamental insight into the design and functionalization of vinyl-addition polynorbornenes.
- 2) We have shown that though alkoxy silane-substituted polynorbornenes are high T_g glassy materials that exhibit almost exclusive solubility selectivity, and can be modified so as to eliminate any Langmuir contribution to sorption. This is incredibly unusual for such high T_g glassy polymers, and their apparent “N₂-phobicity” can be explained via enhanced polymer-polymer and polymer-CO₂ interactions as compared to polymer-N₂ interactions.
- 3) We also found that though these materials were previously thought to be mechanically robust, they may undergo ring-opening upon mechanochemical activation.
- 4) These results have yielded two published manuscripts in well-respected peer reviewed journals (*Macromolecules* and *Angewandte Chemie, Int. Ed.*).
- 5) These results have led to three invited talks at the 2019 ACS National Meeting, the 2019 North American Membrane Society meeting, and the 2019 Southeast Polymer Forum.
- 6) A graduate student working on this project, Christopher Maroon, was selected as one of four finalists for the DSM Award in Polymer Science (winner to be announced at Fall ACS National Meeting) for his work on these projects.

Publications Acknowledging this Grant in 2015 – present

Please classify your publications into three categories according to the source of support for the work published:

- (I) *Exclusively funded by this grant;*
- (II) *Jointly funded by this grant and other grants with leading intellectual contribution from this grant;*
 - a. Maroon, C. R.; Townsend, J.; Gmernicki, K. R.; Harrigan, D. J.; Sundell, B. J.; Lawrence, J. A.; Mahurin, S. M.; Vogiatzis, K. D.; Long, B. K. Elimination of CO₂/N₂ Langmuir Sorption and Promotion of “N₂-Phobicity” within High- T_g Glassy Membranes. *Macromolecules* **2019**, 52, 1589-1600.

- (III) *Jointly funded by this grant and other grants with relatively minor intellectual contribution from this grant;*
- a. Lee, D. C.; Kensy, V. K.; Maroon, C. R.; Long, B. K.; Boydston, A.J. The intrinsic mechanochemical reactivity of vinyl-addition polynorbornene. *Angew. Chem. Int. Ed.* **2019**, 58, 5639-5642.

Probing the Structure of Ionic Liquids for Separations

Poster presented by: Shannon Mahurin, Oak Ridge National Laboratory

Part of ORNL FWP, “Fundamental Studies of Novel Separations”

PI: Sheng Dai

Co-PIs: De-en Jiang, Shannon Mahurin, Ilja Popovs, Huimin Luo, Gernot Rother

UCR team: Song Wang (graduate student), Ziqi Tian (former postdoc)

ORNL team: Wei Guo (postdoc), Alex Ivanov

Overall research goals: The overarching goal of this project is to understand chemical separation phenomena enabled by novel separation media containing ionic liquids that selectively bind and/or transport target molecular/ionic species via tailored interactions at interfaces and through the control of solvation environments and the formation of structures at multiple length scales.

Abstract:

Understanding the relationship between structural properties and separations mechanisms is a key aspect of understanding and controlling gas separations processes, whether these are gas or liquid separations. For example, recent research has revealed molecular structure beyond the inner coordination sphere is essential in defining the performance of separations processes, but nevertheless remains largely unexplored. In this work, we report control over the micro- to nanoscale structure of a task-specific ionic liquid (IL) system designed for the extraction of lanthanides Ln^{3+} from spent nuclear fuel. We apply small angle neutron scattering (SANS) and X-ray absorption fine structure (XAFS) spectroscopy to investigate the structure of IL at multiple length scales. Furthermore, the molecular structure of ionic liquids can impact the adsorption and transport of gases such as CO_2 . We also explore variations in the structure of phosphonium-based ionic liquids with temperature and gas adsorption using wide-angle and small-angle x-ray scattering as well as total x-ray scattering to obtain structure factors.

Identifying the Presence of Nanoscale Spatial Heterogeneities in Deep Eutectic Solvent (DES) Films by Fluorescence Correlation Spectroscopy

Deyny L. Mendivelso-Pérez, Muhammad Q. Farooq, Kalyan Santra, Jared L. Anderson, Jacob W. Petrich, and Emily A. Smith

Iowa State University, Ames, Iowa 50011.
The Ames Laboratory, U.S. Department of Energy, and Department of Chemistry

Abstract

Deep eutectic solvents (DESs) possess interesting features, comparable to those of ionic liquids (ILs), such as low volatility, good thermal stability, and tunable polarity. DESs have some advantages over other solvents due to their facile preparation, which does not require purification steps, and to their generally lower price of preparation. These characteristics make DESs desirable substitutes to replace conventional organic solvents as well as some ILs in a variety of applications. There is, however, an urge to understand the microscopic structure (*i.e.*, nanoscale heterogeneity) and dynamics in these solvents in the interest of exploiting their potential applications in extraction and separations fields. In this study, fluorescence correlation spectroscopy (FCS) is applied to investigate the diffusional dynamics of polar and nonpolar fluorescent molecules in a series of DESs based on tetraalkylammonium chloride and tetraalkylphosphonium chloride salts with carboxylic acids in order to determine diffusional parameters and to elucidate structural heterogeneities. From the correlation functions, the diffusion coefficients of the fluorescent molecules are estimated, and it is observed that there is a decrease in the diffusion coefficient as the viscosity of the DES increases. As the fluorescent probes exhibit deviations from Brownian diffusion behavior, the results suggest the presence of nanoscale heterogeneities in the DESs studied, showing a time-dependent diffusion coefficient. The insights obtained from this study will be helpful in understanding the effect of hydrogen-bond acceptor, hydrogen-bond donor, and molecular ratio of the DESs' components in the formation of structural heterogeneities in this novel series of DESs.

Ionic Liquids and Deep Eutectic Solvents in Separation Science: An Understanding of Nanoscale Ordering

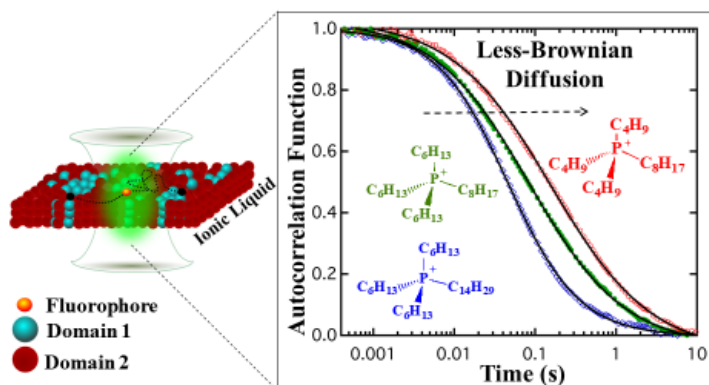
PI(s): Jared L. Anderson (PI), Emily A. Smith, Jacob W. Petrich, and Xueyu Song

Postdoc: Kalyan Santra

Student(s): Deyny L. Mendivelso-Pérez and Muhammad Q. Farooq

RECENT PROGRESS

Fluorescence correlation spectroscopy (FCS) was applied to investigate the diffusional dynamics of hydrophilic (Atto 590) and amphiphilic (DiD) fluorophores in a series of alkylphosphonium ionic liquid (IL) films ([P4448][Cl], [P6668][Cl], [P66614][Cl], and [P66614][NTf2]) in order to determine diffusional parameters and to elucidate nanoscale structural heterogeneities within the IL. From the correlation functions, the diffusion coefficients of the fluorophores were estimated, rendering values that span from 0.39 to 1.2 and 0.146 to 5.2 $\mu\text{m}^2/\text{s}$ for Atto 590 and DiD, respectively. An increase in the diffusion coefficient values is correlated to the increase in the alkyl chain length, which in turn is correlated with a decrease in viscosity. Deviations from Brownian diffusion behavior of the fluorescent probes in the ILs are observed and are attributed to the presence of nanoscale structural heterogeneities in the tetraalkylphosphonium ILs. These results experimentally confirm the presence of nanosegregation in tetraalkylphosphonium ILs, which has been previously observed in molecular dynamics studies.



As is indicated by this abstract, these studies are currently being extended to DESs.

Publications Acknowledging this Grant (*Exclusively funded by this grant*):

Mendivelso-Pérez, D. L.; Farooq, M. Q.; Anderson, J. L.; Petrich, J. W.; Smith, E. A.* Diffusional Dynamics of Tetraalkylphosphonium Ionic Liquid Films Measured by Fluorescence Correlation Spectroscopy. *J. Phys. Chem. B* **2019**, *123*, 4943–4949.

Potential-Driven Ion Separations at Solvated Electrified Interfaces

Venky Prabhakaran, Grant Johnson, and Vanda Glezakou
Pacific Northwest National Laboratory, Richland, Washington 99352

Abstract

Separation processes driven by electric fields, otherwise known as “electrochemical separations,” have been identified as sustainable and energy efficient alternatives to traditional chemical separation pathways due to potentially lower energy costs, reusability, and ease of integration with available power sources. The hydrophobicity and solvent dipole at electrochemical interfaces play a key role in the partitioning of metal ions from the bulk solution region and facilitate stable ion adsorption at interfaces which are used in electrodialysis based desalination or extraction of high-value metals. However, a critical knowledge gap remains regarding the fundamental collective motions of molecular ions (electrolyte cations, anions, separating ions), coordinating chemistries (solvated and non-solvated), polarizability (hydrophobicity, dipole), and bulk diffusion processes that underlie electric-field driven separation of ions. We hypothesized that hydrophobicity and electric fields impact the transport and separation of ions by changing the solvation environment around electrodes and ions. To test our hypothesis, we are using ion soft landing, a versatile mass spectrometry based deposition method to prepare well-defined model electrochemical interfaces by functionalizing electrodes with task-specific ionic liquid cations (*e.g.*, 1-*n*-alkyl-3-methylimidazolium cations $[C_n\text{mim}]^+$, $n = 1, 3, 5, 7, 9$) and multi-electron redox-active polyoxometalate anions to impart a different degree of hydrophobicity and Faradaic adsorption/reduction at the electrified interface, respectively. Ion soft landing enables the well-controlled deposition of mass- and charge- selected ions directly onto electrode surfaces without the counterions, solvent, and contaminants present on electrodes prepared from bulk solution. A combination of *in-situ* and *ex-situ* characterization techniques including infrared reflection-absorption (IRRAS) and Raman spectroscopy in conjunction with theoretical calculations are being employed to study the structural changes of solvation shells in hydrophobic domains and how Faradaic active sites influence the selectivity and efficacy of separation of targeted molecules under applied electric fields.

Grant or FWP Number: Interfacial Structure and Dynamics in Ion Separations, FWP 47327

PI: Grant Johnson, Vanda Glezakou, Venky Prabhakaran

Postdoc(s): Eric Baxter

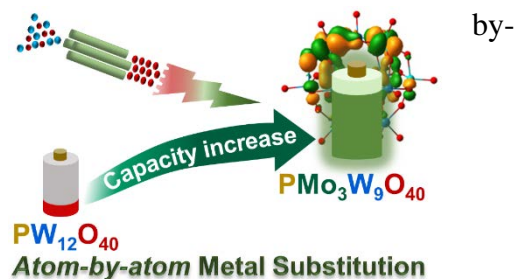
Student(s): N/A

Affiliations(s): Same as above

RECENT PROGRESS

Controlling Electrochemical Interfaces Using Atom-by-Atom Metal Substitution

Fundamental understanding of the effect of “atom-atom” metal substitution on the electrochemical properties of well-defined redox-active anions, $\text{PMo}_x\text{W}_{12-x}\text{O}_{40}^{3-}$, using ion soft landing and theoretical calculations enabled us to identify “super-active” anions, which may be used to selectively extract targeted metal cations in ion separations.



With atomically-precise control over the chemical constituents on electrodes, we have a new opportunity to study the effect of every descriptor of electrified interfaces and pave the way to rational design of efficient and stable separation systems.

Publications Acknowledging this Grant in 2018 – present

(I) *Exclusively funded by this grant;*

P. Su, **V. Prabhakaran**, G. E. Johnson, J. Laskin, In situ Infrared Spectroelectrochemistry for Understanding Structural Transformations of Precisely-Defined Ions at Electrochemical Interfaces, *Anal. Chem.* **2018**, 90, 10935.

(II) *Jointly funded by this grant and other grants with leading intellectual contribution from this grant;*

V. Prabhakaran, Z. Lang, A. Clotet, J. M. Poblet, Grant E. Johnson, and Julia Laskin, Controlling the Activity and Stability of Electrochemical Interfaces Using Atom-by-Atom Metal Substitution of Redox Species, *ACS Nano* **2019**, 13, 458.

J. Laskin, G. E. Johnson, J. Warneke, **V. Prabhakaran**, From Isolated Ions to Multilayer Functional Materials Using Ion Soft - Landing, *Angew. Chem. Int. Ed.* **2018**, 57, 16270.

G. E. Johnson, **V. Prabhakaran**, N. D. Browning, B. L. Mehdi, J. Laskin, P. A. Kottke, and A. G. Fedorov, DRILL Interface Makes Ion Soft Landing Broadly Accessible for Energy Science and Applications, *Batteries & Supercaps* **2018**, 1, 97.

(III) *Jointly funded by this grant and other grants with relatively minor intellectual contribution from this grant;*

None

Energy Transfer in Lanthanide Luminescent Complexes

Kenneth N. Raymond and Michael W. Mara
University of California, Berkeley, Chemistry Dept.

Presentation Abstract

Luminescent materials are used in a wide range of scientific and industrial applications, including lighting and display screens, lasers and fiber amplifiers, and as biomedical dyes for imaging and fluoroimmunoassays. Trivalent lanthanides have garnered particular interest in luminescence applications partly due to their sharp emission lines in the visible/near-IR and their long luminescence lifetimes, which are a product of 4f-4f transitions specific to each lanthanide. These lanthanide transitions are almost entirely metal centered due to large spin-orbit coupling and very weak interaction with the ligand field. However, since the 4f-4f transitions are highly forbidden, and consequently direct 4f excitation is very weak, bright photoluminescent lanthanide complexes instead rely on indirect photoexcitation utilizing the “antenna” effect, where a sensitizer (often an organic ligand) absorbs incident photons, leading to excitation of the lanthanide center by energy transfer. A high efficiency Tb(III) complex developed as part of our research program is now used in several commercial assays, and Eu(III) complexes based on a different ligand system also now show similar high efficiency. The overall quantum efficiency depends directly on the energy transfer efficiency, and hence determination of the energy transfer mechanism is of fundamental importance. Despite developments in the theoretical understanding of lanthanide systems, experimentally monitoring energy transfer in photoluminescent lanthanide systems remains difficult, largely due to the absence of suitable experimental methods for directly probing the non-emissive lanthanide 4f excited states, which inhibits the rational design of highly efficient lanthanide-based fluorophores. A series of highly luminescent europium(III) complexes which exhibit photoluminescence from the Eu(III) center following energy transfer from the UV absorbing organic sensitizer have been investigated using a combination of ultrafast optical transient absorption and Eu L₃ X-ray transient absorption techniques.

These provide the first direct experimental verification that Dexter electron exchange from the ligand triplet state is the dominant energy transfer mechanism in these photoluminescent systems. The optical transient absorption results imply that energy transfer for all these compounds has near unity yield, regardless of differences in the sensitization efficiencies, suggesting that the variations in the sensitization efficiencies are determined almost entirely by differences in the ligand-centered intersystem crossing rates.

DE-SC0016961: Energy Transfer in Lanthanide Luminescent Complexes

RECENT PROGRESS

Energy Transfer From Antenna Ligand to Europium(III) Followed Using Ultrafast Optical and X-ray Spectroscopy

Through a combination of optical and X-ray spectroscopic methods, our initial work has demonstrated that Dexter charge exchange from the ligand triplet state is the dominant energy transfer mechanism in our Eu(III) complexes. Remarkably, this Dexter transfer has nearly 100% efficiency, suggesting that sensitization efficiency is dictated by the singlet excited manifold. Based on these findings, we plan to extend our optical and X-ray measurements to see if this is

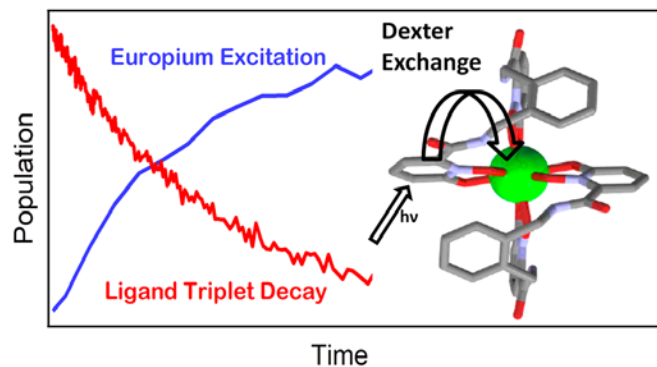


Figure 1: A schematic of the ligand light absorption and energy transfer to metal 4f center.

also the dominant energy transfer mechanism for other lanthanides and analyze the variation in sensitization efficiency with changes in the metal center. We will also use X-ray spectroscopy coupled with computational methods to understand how minor modifications in ligand structure affect spin-orbit coupling and intersystem crossing, and better develop our understanding of the ligand-centered dynamics as a whole. It is anticipated that an understanding of both the energy transfer and intersystem crossing steps will enable the rational design of highly efficient lanthanide fluorescence agents.

The organic ligands used for each complex are shown in Figure 2. Each Eu(III) complex

adopts an overall ML_2 structure, wherein each of the two tetradentate ligands bind to the metal center via each of the four bidentate 1,2-HOPO chromophores (shown in green). As shown, the ligands differ only in the backbone substituent which connects the pair of 1,2-HOPO chromophores, yet these structural modifications result in significant changes in the luminescence properties of the corresponding Eu(III) complexes. All samples were prepared according to previously published methods, and sample integrity was verified by ESI-HRMS (see publication). Since X-ray absorption measurements require larger concentrations than optical measurements, methanol was used as the solvent rather than aqueous formulations for improved sample solubility.

The relevant photophysical parameters measured in methanolic solution for these complexes are shown in Figure 2. The overall quantum yield after 350 nm excitation was determined by the optically dilute method in comparison to quinine sulfate in 0.05 M H_2SO_4 as a well-established quantum yield reference (0.508, see paper). There are two relevant efficiencies which dictate the total luminescence quantum yield: the efficiency of sensitizing the metal center and the efficiency of metal-centered radiative decay.

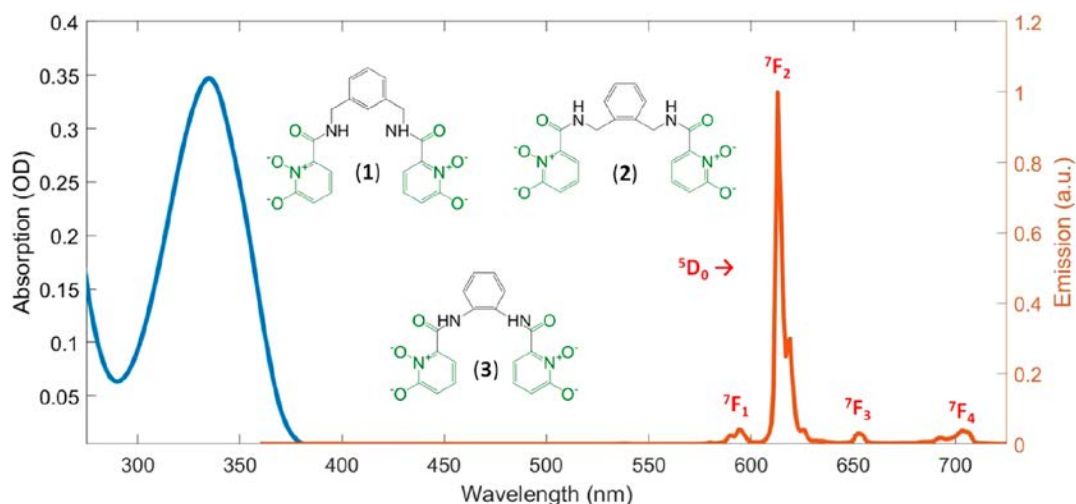


Figure 2. UV-vis absorption (blue) and emission (red) spectrum for 1. The most relevant Eu(III) emission lines are labeled. Ligand and molecular structures are shown in the middle.

We plan to use OTA measurements to probe the ligand dynamics in

luminescent lanthanide complexes with metals besides Eu(III). In particular, we aim to focus on Sm(III), Y(III), and Tb(III). Sm(III) is of interest because it utilizes the same ligands as Eu(III) and shows the same general trends in sensitization efficiency as the Eu(III) complexes, but with overall much lower energy transfer yields. This raises a question as to why energy transfer yields are so much lower in these complexes: is there a lower ISC rate than in the Eu(III) complexes, or does the >99% efficiency of triplet state energy transfer not apply here? Sm(III) is a great test case for understanding the interplay between metal centers and bound ligands, by direct comparison to the data we have gathered on the analogous Eu(III) complexes. Y(III), while not a lanthanide, is also an interesting test case; it has similar size to Eu(III) and will form ML_2 complexes with the same ligands, but we should get much smaller spin-orbit coupling from the Y(III) than the Eu(III). Because the rate of triplet production depends mostly on intersystem crossing, Y(III) will be quite useful in further interpreting our OTA spectra. Finally, Tb(III) is one of the most important luminescent lanthanides and important for commercial applications.

Publications Acknowledging this Grant in 2015 – present

(VII) Exclusively funded by this grant;

1. Mara, M. W.; Tatum, D.S.; March, D-M.; Doumy, G.; Moore, D.G.; Raymond, K.N.; Energy Transfer from Antenna Ligand to Europium(III) Followed Using Ultrafast Optical and X-ray Spectroscopy. *J. Amer. Chem. Soc.* **2019**, *141*, 11071-11081.

Layer-by-Layer Assembly of a Polymer of Intrinsic Microporosity: Targeting the CO₂/N₂ Separation Problem

Steven L. Regen and Nabendu B. Pramanik

Department of Chemistry, Lehigh University, Bethlehem, PA 18015, United States

Presentation Abstract

A polymer of intrinsic microporosity, **1**, has been successfully incorporated into a series of polyelectrolyte multilayers *via* the Layer-by-Layer (LbL) deposition method. One of these assemblies, a 6 nm multilayer derived from **1** plus poly(diallyldimethylammonium chloride) (PDDA), which was deposited onto poly[1-(trimethylsilyl)propyne] (PTMSP) film, exhibited a CO₂ permeance of 130 GPU and a CO₂/N₂ selectivity of 33. This level of performance, together with the simplicity of the LbL method and its applicability to hollow fibers, suggests that such materials could become viable alternatives to some of the most promising membrane materials that are currently being considered for the practical capture of CO₂ from flue gas.

DE-FG02-05ER15720: Hyperthin Membranes For Gas Separations

PI: Steven L. Regen

Postdoc: Nabendu B. Pramanik

RECENT PROGRESS

The onset of global warming has led to major scientific as well as major engineering challenges. One of these challenges is to design materials that can separate CO₂ from N₂ in flue gas (the major anthropogenic source of CO₂) in an economically viable manner. Although a variety of substances have been introduced that can selectively absorb CO₂, the use of absorption-desorption processes, in general, tend to be costly in terms of their energy and capital requirements. For this reason, membrane-based alternatives that are more energy-efficient and cost-effective are of particular interest.

From a basic science standpoint, the goal in creating a new membrane material for separating CO₂ from N₂ is to maximize (i) its CO₂ permeance and (ii) its CO₂/N₂ permeation selectivity. Permeance values for CO₂ and N₂ are defined by the ratios, P_{CO_2}/l and P_{N_2}/l , where P_{CO_2} and P_{N_2} are intrinsic permeability coefficients and l is the thickness of the membrane. Experimentally, permeances are determined by dividing observed flux values, J , by the pressure gradient (Δp) that is applied across the membrane (eq. 1). Typically, permeances are reported in gas permeation units (GPU) where 1 GPU = 1 × 10⁻⁶ cm³/cm²·s·cm Hg. Ideal CO₂/N₂ selectivities, α , are then given by the ratio of these permeances (eq. 2).

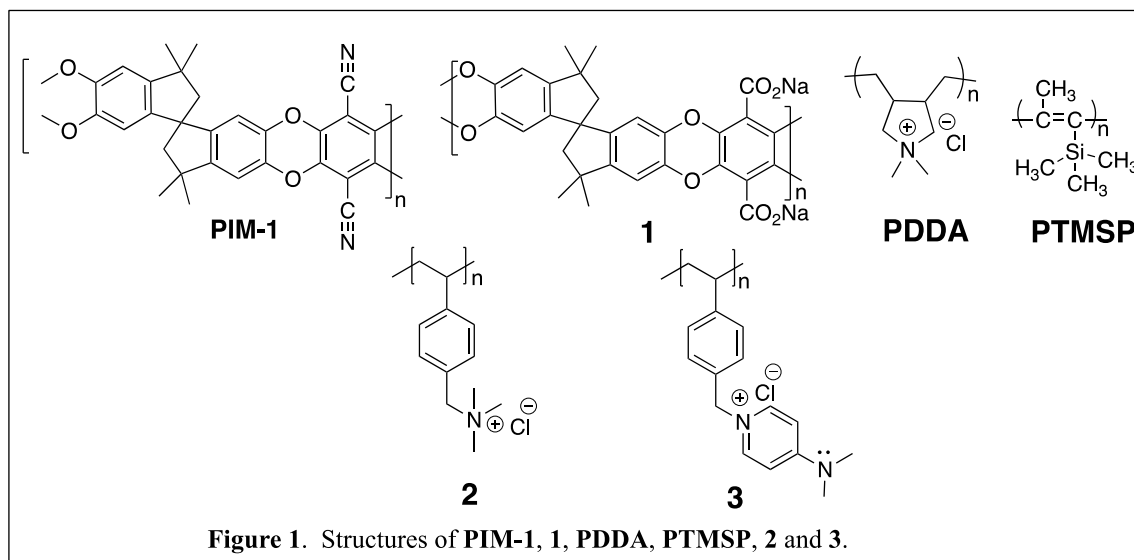
$$\frac{P}{l} = (\text{cm}^3/\text{cm}^2 \cdot \text{s} \cdot \text{cm Hg}) = \frac{J}{\Delta p} \quad (1)$$
$$\alpha = \frac{\left(\frac{P}{l}\right)_{\text{CO}_2}}{\left(\frac{P}{l}\right)_{\text{N}_2}} = \frac{P_{\text{CO}_2}}{P_{\text{N}_2}} \quad (2)$$

For a real-world membrane-based separation of CO₂ and N₂ from flue gas, cost estimates indicate that after a CO₂/N₂ selectivity of ca. 30 has been reached, further increases in membrane CO₂ permeance are more important than further increases in selectivity. Thus, *creating*

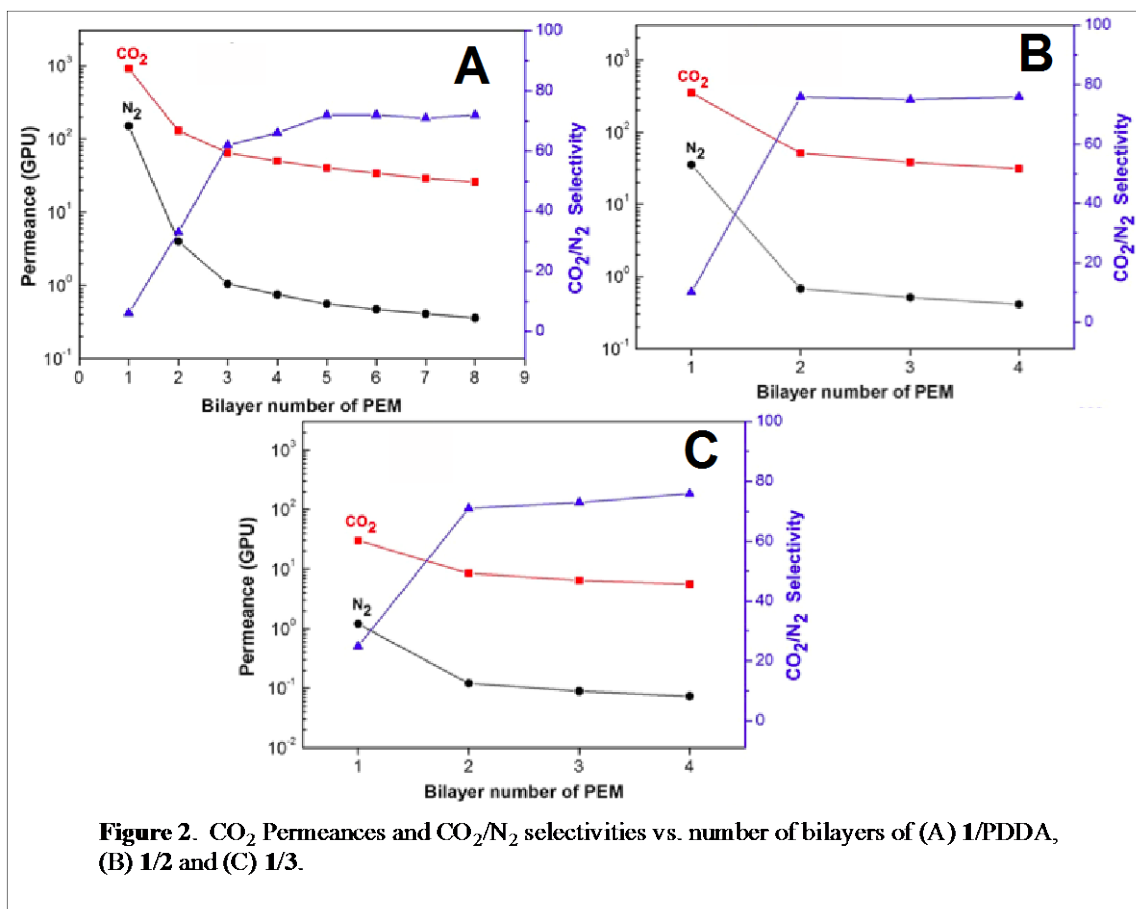
membranes having CO_2/N_2 selectivities that are ≥ 30 with CO_2 permeances as high as possible is the major scientific challenge.

Our own efforts in the gas separation area have focused, sharply, on polyelectrolyte multilayers (PEMs) as membrane materials. The fact that such assemblies can be readily fabricated in hyperthin (<100 nm) form *via* the Layer-by-Layer (LbL) method, and that the LbL method is applicable to hollow fibers, makes them especially attractive. While flue gas contains a significant amount of water vapor that can adversely affect the permeability properties of a PEM, such water can be efficiently removed using drying agents. In addition, these drying agents can be regenerated without the need of additional energy by taking advantage of the heat of combustion.

Owing to the twisted geometry of their repeat units, "polymers of intrinsic microporosity" (PIM) are capable of forming dense films having a high fractional free volume (FFV) and a high permeability. For this reason, they have been of considerable interest as membrane materials. To explore their applicability to the CO_2/N_2 separation problem, we have converted a common PIM (i.e., PIM-1) to its corresponding carboxylate form (**1**) and have fabricated polyelectrolyte multilayers with poly(diallyldimethylammonium chloride) (PDDA), **2** and **3** *via* the LbL method using poly[1-(trimethylsilyl)propyne] (PTMSP) as support material (Figure 1). The attractiveness of PTMSP derives from (i) its exceptionally high permeability, (ii) its applicability to hollow fibers, and (iii) its high stability towards oxygen, and aging (when a porous aromatic framework is included in the film).



In Figure 2 are shown the permeances observed for CO_2 and N_2 , and also the CO_2/N_2 selectivities for composite films containing varying numbers of bilayers of **1**/PDDA, **1**/**2** and **1**/**3**. Of particular significance is the fact that when only two bilayers of **1**/PDDA have been deposited on PTMSP, a CO_2 permeance of 130 GPU and a CO_2/N_2 selectivity of 33 have been reached (Figure 2A). Based on the criteria that suitable membranes should have a CO_2/N_2 selectivity ≥ 30 and CO_2 permeances as high as possible, such membranes could, arguably, be compared with some of the most promising membrane materials reported to date. For example, hollow fiber membranes (having a surface area 10 times greater per unit volume than those of spiral wound membranes), which have been coated with PTMSP and surface-modified with two bilayers of **1**/PDDA, could be considered as viable alternatives to spiral wound PolarisTM membranes having CO_2 permeances of ca. 1000-2000 GPU and CO_2/N_2 selectivities of ca. 50.



Publications Acknowledging this Grant in 2015 – present

(VIII) Exclusively funded by this grant:

- Yi, S.; Lin, C.; Regen, S. L. Splaying Hyperthin Polyelectrolyte Multilayers To Increase Their Gas Permeability. *Chem. Commun.*, **2015**, *51*, 1439-1441.
- Lin, C.; Yi, S.; Regen, S. L. Consequences of Tacticity on the Growth and Permeability of Hyperthin Polyelectrolyte Multilayers. *Langmuir*, **2016**, *32*, 375-379.
- Yi, S.; Lin, C.; Leon, W.; Vezenov, D.; Regen, S. L., Gas Permeability of Hyperthin Polyelectrolyte Multilayers Having Matched and Mismatched Repeat Units. *Langmuir*, **2016**, *32*, 12332-12337.
- Yi, S.; Leon, W.; Vezenov, D.; Regen, S. L. Tightening Polyelectrolyte Multilayers With Oligo Pendant Ions. *ACS Macro Lett.*, **2016**, *5*, 915-918.
- Lin, C.; Stedronsky, E.; Regen, S. L. pKa-Dependent Facilitated Transport of CO₂ Across Hyperthin Polyelectrolyte Multilayers. *ACS Appl. Mater. Interfaces*, **2017**, *9*, 19525-19528.

7. Lin, C.; Jordan, L R.; Stedronsky, E. R.; Wittenberg, N. J.; Regen, S. L. A Plug and Socket Approach For Tightening Polyelectrolyte Multilayers. *ChemComm*, **2018**, *54*, 9769-9772.
8. Pramanik, N. B.; Tian, C.; Stedronsky, E. R.; Regen, S. L. Layer-By-Layer Assembly Modulated By Host-Guest Binding. *ACS Appl. Polym. Mater.*, **2019**, *1*, 141-144.
9. Pramanik, N. B.; Regen, S. L. Layer-By-Layer Assembly of a Polymer of Intrinsic Microporosity: Targeting the CO₂/N₂ Separation Problem. *Chem. Commun.*, **2019**, *55*, 4347-4350.
10. Pramanik, N. B.; Regen, S. L. Hyperthin Membranes for Gas Separations via Layer-by-Layer Assembly. *Chem. Rec.*, **2019**, *19*, 1-12.

Single-molecule Dynamics in Interface-rich Separations Environments

Daniel K. Schwartz
University of Colorado Boulder

Presentation Abstract

The dynamic behavior of molecules and nanoparticles in confined environments, such as at interfaces and within porous materials, lead to complex and highly-varied phenomena, where heterogeneity may arise from spatial variation of the material/interface itself, from structural configurations (i.e. conformation, orientation, aggregation state, etc.), or temporally, through inhomogeneous dynamic behavior. In order to capture relevant information about these complex dynamics, we have developed highly multiplexed single-molecule/single-nanoparticle tracking methods that are capable of acquiring $>10^5$ trajectories in a given experiment; automated unbiased data analysis methods are used to interpret these large data sets. Recent work in our lab has extended the tracking methods to acquire fully 3D trajectories, enabling tracking of individual molecules and nanoparticles in complex environments, including porous media and thin polymer films. Results will be shown that provide new insights into the transport of nanoparticles within porous 3D environments, of polymers in confined gaps, and of small molecules within polymeric films and aqueous nanofilms.

Single-molecule Dynamics in Interface-rich Separations Environments

Postdoc(s): Dapeng Wang (2016-2017), Mark Kastantin (2015), Raphael Sarfati (2018), Daniel Kienle (2019)

Student(s): Gregory Morrin (2017-2019), Haichao Wu (2017-2018), Yu Cai (2016)

RECENT PROGRESS

3D Tracking in Confined Environments

We have developed methods to study the 3D motion of nanoparticles and molecules near surfaces, within the void space of porous materials using double-helix point-spread-function (DH-PSF) imaging. Temporal sequences of images are acquired, and trajectories linked, providing long-duration 3D trajectories for tens of thousands of particles or molecules simultaneously. Trajectories are subjected to statistical analyses, including multivariate machine-learning analytic approaches, e.g. to identify time intervals where particles are in confined/retained vs. freely diffusing “states”

DH-PSF with Variable-Angle Illumination Epifluorescence Microscopy

We demonstrated that the signal-to-noise ratio (SNR) and three-dimensional localization precision of a double helix point spread function (DH-PSF) were greatly improved by applying variable-angle illumination epifluorescence microscopy.

Three-Dimensional Tracking of Interfacial Hopping Diffusion

Theoretical predictions have suggested that molecular motion at interfaces may be dominated by “hops” through the adjacent liquid phase, where the molecule re-adsorbs after a given hop according to a probabilistic “sticking coefficient”. Here, we used 3D single molecule tracking to

explicitly visualize this process for a macromolecular probe at solid/liquid interfaces that exerted varying electrostatic interactions.

Nanoparticle diffusion within inverse opals

3D diffusion of nanoparticle probes was observed within a model porous material, an inverse opal, comprising an interconnected network of hexagonally close packed spherical cavities. Each nanoparticle trajectory was analyzed to determine its dwell time within each cavity to determine comprehensive escape-time distributions as a function of size of the channels connecting the cavities. We found that nanoparticle motion was inhibited near cavity walls and cavity escape was slower than predicted by existing theories and random-walk simulations. A combined computational-experimental analysis indicated that translocation through a nano-channel is barrier-controlled rather than diffusion-controlled.

Motion of ions in a polyelectrolyte multilayer

The diffusion of small, charged molecules incorporated in polyelectrolyte multilayers (PEMs) was tracked in three dimensions by combining conventional single-molecule fluorescence localization (to characterize lateral diffusion) with Förster resonance energy transfer (FRET) between diffusing molecules and the supporting surface (to measure diffusion in the surface-normal direction). Analysis of the surface-normal diffusion required a rigorous, model-based statistical analysis to account for the inherently noisy single-molecule FRET signal. Using this approach, we quantitatively demonstrated that the diffusion in the lateral direction was five orders of magnitude faster than diffusion in the surface-normal direction, and that both the lateral and normal displacements exhibited motion that is severely subdiffusive and temporally anticorrelated. We hypothesize that the diffusive anisotropy is due to the periodic structure of the film, which creates electrostatic barriers to motion of charged molecules across the layers.

Molecular Transport in Complex Interfacial Environments

Our studies of molecular motion at solid/liquid interfaces have described the transport in the context of a continuous time random walk (CTRW) process, in which diffusion switched between desorption-mediated “flights” (i.e. hopping) and surface-adsorbed waiting-time intervals during which the molecules were either immobilized or engaged in slow 2D diffusive motion. We recently extended this work to include interfacial transport under more complex conditions, where the surface itself exhibited some degree of fluidity and/or where molecules were increasingly crowded at the interface.

Three Distinct Regimes in Polymer Surface Crowding Dynamics

Single-molecule tracking was used to characterize the dynamics of PEG polymer on a hydrophobic surface as the concentration was systematically increased over 4 orders of magnitude from dilute surface coverage to well above monolayer coverage. We observed three characteristic regimes of dynamic behavior as a function of concentration, as evidenced by multiple statistical analyses. The Site-Blocking regime was characteristic of very dilute concentrations and exhibited faster dynamics as strong-adsorption sites were blocked. Subsequently, the Crowding regime was distinguished by increasingly sub-diffusive behavior as a function of coverage. Finally, the Brush regime occurred at higher coverage, and exhibited faster dynamics with increasing concentration.

Diffusion at Fluid Interfaces Encodes Information about Molecular Conformation

Here we employed a macromolecular probe, a cadherin ectodomain, that is known to change its flexibility as a function of solution conditions, to understand how the viscous coupling of a macromolecule to a vicinal fluid interface (a supported lipid bilayer) influences motion, and how this viscous coupling is related to molecular conformation. Rigid probe molecules exhibited a

“fast” diffusion coefficient that was identical to that of individual lipid molecules in the bilayer. Under conditions where the probe was more flexible, individual trajectories were temporally heterogeneous, exhibiting alternating periods of fast and slow diffusion. These observations suggested that more flexible molecules alternated between upright and lying-down conformations, where the latter interacted with more lipid molecules and experienced greater viscous drag

Surface Diffusion in Confined Slit-Pore Geometries

Strongly confined environments (confined dimensions between 1-100 nm) represent unique challenges and opportunities for understanding and manipulating molecular behavior due to the significant effects of electric double layers, high surface-area to volume ratios, and other phenomena at the nanoscale. Convex Lens-induced Confinement (CLiC) can be used to analyze the dynamics of individual molecules or particles confined in a planar slit geometry with continuously varying gap thickness. We developed an interferometry-based method for precise measurement of the slit pore geometry that approach permitted accurate characterization of separation distances as small as 5 nm, with 1 nm precision, without a priori knowledge or assumptions about the contact geometry. This method was used to study the diffusion of a polyelectrolyte (PLL) in a planar slit geometry slit heights below 100 nm. Independent of surface chemistry, the effective surface diffusion coefficient increased with height until saturating for slit heights <30nm. The evolution of the diffusion coefficient with slit height was faster for surfaces with which PLL exhibited stronger short-range interactions, which influenced the intermittent random walk behavior by increasing the waiting times between flights and the re-adsorption probability (a.k.a sticking coefficient) during flights.

Diffusion in Water Nanofilms

Single-molecule tracking was employed to probe the local rheology of interfacial water at silica surfaces. Fluorescent rhodamine molecules were tracked on silica surfaces as a function of ambient relative humidity, which controlled the thickness of condensed water nanofilms in the sub-nm to nm regime. At low humidity, the molecules exhibited confined diffusion in the vicinity of isolated adsorption sites characterized by a broad distribution of binding stiffness constants; subsequent chemical or physical surface passivation selectively eliminated stiffer binding sites. At increased humidity, molecularly thin water films condensed, permitting near-surface transport of rhodamine molecules. Motion was subdiffusive, with an anomalous exponent increasing with nanofilm thickness. Molecular trajectories were temporally anticorrelated, ergodic, but also featured transient binding and intermittent diffusion. Statistical modeling demonstrated that this complex motion in water nanofilms had the characteristics of fractional Brownian motion combined with a continuous time random walk. This was consistent with diffusion within viscoelastic nanofilms, suggesting persistent molecular structuring in the vicinity of the silica surface.

Single Molecule Probes of Surface Chemistry

A longstanding goal of this research program has been to develop methods that use dynamic and spectral properties of individual probe molecules to obtain local nanoscale information about the chemical properties of materials interfaces.

Nanoscale Hydrophobic Regions in a Polymer Brush

We developed a novel single-molecule fluorescent probe that identified local regions on the basis of hydrophobicity. This allowed us to characterize the structural heterogeneity of a complex polymer material, PEG brushes, which are ubiquitous due to their extraordinary non-fouling character. It has been hypothesized that there may be a trade-off between the most adsorption-

resistant brushes (at high grafting density), and less hydrophobic brushes. We correlated the effects of grafting density with local brush hydrophobicity by exploiting the solvatochromic properties of an environmentally sensitive dye (nitrobenzoxadiazole) with Mapping using Accumulated Probe Trajectories (MAPT). The results showed an increase in local nanoscale hydrophobic regions with grafting density, supporting the hypothesis that increased grafting density leads to the formation of poorly hydrated niches within the overall hydrophilic brush

Publications Acknowledging this Grant in 2015 – present

(IX) *Exclusively funded by this grant;*

J. N. Mabry and D. K. Schwartz, "Tuning the Flight Length of Molecules Diffusing on a Hydrophobic Surface", *J. Phys. Chem. Letters*, **6**, 2065-2069 (2015)

M. J. Skaug and D. K. Schwartz, "Tracking Nanoparticle Diffusion in Porous Filtration Media", *Industrial and Engineering Chemical Research*, **54**, 4414-4419 (2015).

N. Nelson and D.K. Schwartz, "Unbiased Clustering of Molecular Dynamics for Spatially-Resolved Analysis of Chemically Heterogeneous Surfaces", *Langmuir*, **31**, 6099-6106 (2015)

J.N. Mabry, M. Kastantin, and D.K. Schwartz, "Capturing Conformation-Dependent Molecule-Surface Interactions when Surface Chemistry Is Heterogeneous", *ACS Nano*, **9**, 7237-7247 (2015)

D. Wang, R. Hu, M.J. Skaug, and D.K. Schwartz, "Temporally anti-correlated motion of nanoparticles at a liquid interface", *J. Phys. Chem. Letters*, **6**, 54-59 (2015)

D. Wang, A. Agrawal, A. Williams, R. Piestun, D.K. Schwartz, "Enhanced Information Content for Three-Dimensional Localization and Tracking Using the Double-Helix Point Spread Function with Variable-Angle Epifluorescence Microscopy", *Applied Physics Letters*, **110**, 211107 (2017)

D. Wang, H. Wu, D.K. Schwartz, "Three-Dimensional Tracking of Interfacial Hopping Diffusion", *Physical Review Letters*, **119**, 268001 (2017)

Gregory T. Morrin and Daniel K. Schwartz, "Three Regimes of Polymer Surface Dynamics under Crowded Conditions", *Macromolecules*, **51**, 1207-1214 (2018).

Dapeng Wang, Lijun Liu, Haichao Wu, Jizhong Chen, and Daniel K. Schwartz, "Diffusive Escape of a Nanoparticle from a Porous Cavity", *Phys Rev Lett* (2019, in press)

(X) *Jointly funded by this grant and other grants with leading intellectual contribution from this grant;*

S. Chakraborty, N. Nelson, and D.K. Schwartz, "Anisotropic Molecular Hopping at the Solid-Nematic Interface", *Soft Matter*, **11**, 7712-7716 (2015);

D. Wang, C. He, M.P. Stoykovich, D.K. Schwartz, "Nanoscale Topography Influences Polymer Surface Diffusion", *ACS Nano*, **9**, 1656-1664 (2015).

M.J. Skaug, L. Wang, Y. Ding, and D.K. Schwartz, "Hindered Nanoparticle Diffusion and Void Accessibility in a Three-Dimensional Porous Medium", *ACS Nano*, **9**, 2148-2156 (2015)

Blake B. Langdon, Mark Kastantin, Daniel K. Schwartz, "Surface Chemistry Influences Fibrinogen Self-association", *Biomacromolecules*, **16**, 3201-3208 (2015);

D. Wang, R. Hu, J.N. Mabry, D.T. Wu, K. Koynov, and D.K. Schwartz, "Scaling of Polymer Dynamics at an Oil-Water Interface in Regimes Dominated by Viscous Drag and Desorption-Mediated Flights", *J. Am. Chem. Soc.*, **137**, 12312-12320 (2015)

D. Wang, H.-Y. Chin, C. He, M. P. Stoykovich, and D. K. Schwartz, “Polymer Surface Transport is a Combination of In-Plane Diffusion and Desorption-Mediated Flights”, *ACS Macro Letters*, **5**, 509-514 (2016); doi:10.1021/acsmacrolett.6b00183

Y. Cai, N. Shashikanth, D.E. Leckband, and D.K. Schwartz, “Cadherin Diffusion in Supported Lipid Bilayers Exhibits Dynamic Heterogeneity”, *Biophys J*, **111**, 2658–2665 (2016)

Gregory T. Morrin, Daniel F. Kienle and Daniel K. Schwartz, “Standalone Interferometry-Based Calibration of Convex Lens-Induced Confinement Microscopy with Nanoscale Accuracy”, *Analyst*, **144**, 2628-2634 (2019).

(XI) Jointly funded by this grant and other grants with relatively minor intellectual contribution from this grant;

B.B. Langdon, R. Mirhossaini, I. Sriram, J. Mabry, A. Lajmi, Y. Zhang, O.J. Rojas, D.K. Schwartz, “Single-molecule resolution of protein dynamics on polymeric membrane materials: The roles of spatial and population heterogeneity”, *ACS Applied Materials and Interfaces*, **7**, 3607-3617 (2015).

Mechanistic Understanding of Heavy Ion Adsorption, Chemistry, and Separations at Graphene Based 2D Materials Interfaces

Dr. Ahmet Uysal, Assistant Chemist
Argonne National Laboratory (ANL)
Argonne, IL 60439

Chemical separations represent a crucial component of ongoing efforts to secure our nation's increasing energy, environmental, and economic security needs, such as the cleaning of millions of tons of heavy-metal contaminated groundwater. While membrane-based separations are used in removing a variety of trace-level contaminants, the lack of a mechanistic understanding of ion selectivity and adsorption limits the ability to improve and expand these technologies. In sorbents and membrane systems selectivity and adsorption are governed by an interfacial region with a thickness that is on the order of a few nanometers. Chemical and physical properties of solute and solvent molecules can be significantly different than their bulk counterparts in this nanoscale region and in confined regions. Obtaining interface specific information that is not dominated by the overwhelmingly large bulk signal is very difficult, yet necessary to gain a predictive understanding of interfacial phenomena in these separation systems. This research project addresses these challenges by studying the fundamental surface chemistry of heavy-ion (actinide and lanthanide) adsorption on graphene based two-dimensional materials interfaces by a combination of surface specific probes, namely synchrotron x-ray scattering and sum frequency generation spectroscopy. These methods provide direct, molecular-scale, element specific, *in situ* information of ion adsorption desorption kinetics and thermodynamics from complex solutions. This research provides an understanding of the ion-specific properties related to the surface affinity, selectivity, and capacity, as well as the dependence of these properties on solution conditions and surface functionalization. In a broader scientific context, this program will be an important step towards achieving mechanistic control of interfaces and transport in complex and extreme environments in alignment with the DOE Office of Science's *Basic Research Needs for Energy and Water*.

Enhanced Cation Selectivity and Transport by Electroosmotic Flow in the Hysteresis Charge Transport through Single Conical Nanopores

Gangli Wang, Warren Brown, Ruoyu Yang, Maksim Kvetny
Georgia State University, Department of Chemistry

Presentation Abstract

New transport phenomena emerge at nanometer scale interfaces where surface effects can no longer be ignored. A single structurally defined nanopore can be viewed as a unit element in ensemble membranes used in separation applications. Selective transport of matter, ions or neutral species including solvent, can be achieved in the presence of a broken symmetry in the nanostructures and/or surface charges. This presentation builds on the series of studies on time-dependent ion transport through single nanopores in our group. The respective contributions by cation and anion to the overall hysteresis ion transport experiments are elucidated in continuum-theory based simulations. A generalizable method to diagnose and deconvolute electroosmotic flow (EOF) in the nanoscale transport processes is established by the analysis of current-potential measurements. The impacts of EOF on the time-dependent electrokinetic ion transport through asymmetric nanopores are unequivocally revealed through finite element simulation by solving Poisson, Nernst-Planck (PNP) with and without Navier-Stokes (NS) equations, and validated by conductivity and optical imaging experiments. Counterintuitively, EOF significantly improves the transference number and hysteresis charges of cations during the electrokinetic transport (current-potential measurements). The insights suggest new avenues to improve both efficient and selectivity of broadly defined separation applications when tradeoff is often inevitable in ensemble membranes or devices containing amorphous pores or channels.

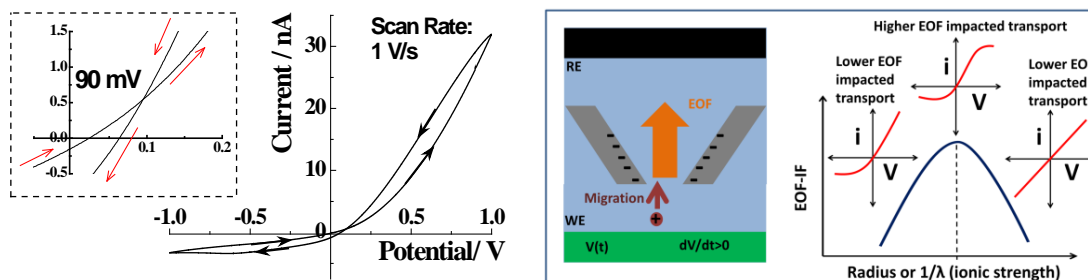
DE-SC0019043: Ion Transport Dynamics at Nanoscale Interfaces in Single Asymmetric Nanopores and Nanopore Arrays

PI: Gangli Wang

Affiliations: Department of Chemistry, Georgia State University

RECENT PROGRESS

Signatures of Electroosmotic Flow (EOF) in the Rectified Ion Transport through Single Nanopores



Left: Representative current-potential (I - V) curves demonstrating the rectified ion transport and time-dependent hysteresis in single asymmetric nanopores. Arrows indicate the potential scan directions. **Right:** Experimental and simulation setup of transport through a single nanopipette with negative surface charges in electrolyte solution. A potential is applied on the working electrode (WE/green, bottom) with respect to the reference electrode (RE /black,

top). The three red I-V sketches represent diagnostic features of non-linear shape for ion current rectification, sigmoidal for EOF presence, and more linear ohmic behaviors respectively.

Publications Acknowledging this Grant in 2015 – present

(XII) *Exclusively funded by this grant:*

1. Brown, W.; Li, Y.; Yang, R.; Wang, D.; Kvetny, M.; Zhang, H.; Wang, G.* *Deconvolution of Electroosmotic Flow in Hysteresis Ion Transport through Single Asymmetric Nanopipettes under review.*
2. Brown, W.; Kvetny, M.; Yang, R.; Wang, G.* *Lower Energy Usage and Higher Selectivity at Higher Ionic Strength in Nanopores Promoted by Electroosmotic Flow under review.*
3. Brown, W.; Kvetny, M.; Yang, R.; Wang, G.* *Enhanced Cation Selectivity and Transport by Electroosmotic Flow in the hysteresis Charge Transport through Single Conical Nanopores manuscript in prep.*

Prior publications closely relevant to this grant:

1. Wang, D.; Brown, W.; Li, Y.; Kvetny, M.; Liu, J.; Wang, G.* *Hysteresis Charges in the Dynamic Enrichment and Depletion of Ions in Single Conical Nanopores. ChemElectroChem (invited, special issue) 2018, 5 (20), 3089-3095.*
2. Wang, D.; Brown, W.; Li, Y.; Kvetny, M.; Liu, J.; Wang, G.* *Correlating Non-zero Crossing in Pinched Hysteresis Current-potential Curves with Nanogeometry and Surface Factors in Single Conical Nanopores Anal. Chem., 2017, 89 (21), 11811-11817.*
3. Li, Y.; Wang, D.; Kvetny, M.; Brown, W. Liu, J.; Wang, G.* *History-dependent Ion Transport through Conical Nanopipettes and the Implications in Energy Conversion Dynamics at Nanoscale Interfaces Chem. Sci., 2015, 6, 588-595*

Understanding the Molecular-Level Interactions Between Ionic Liquids and Molecular Species: Applications in Separations

Kevin N. West,¹ Brooks D. Rabideau,¹ James H. Davis, Jr.²

¹Department of Chemical & Biomolecular Engineering, ²Department of Chemistry
University of South Alabama

Presentation Abstract

Ionic liquids (ILs), salts which are liquids at the temperatures where they are employed, have the potential to be a platform technology for the creation of new industries and the reinvention of industrial processes and consumer products. Due to their ionic nature, they have vanishingly-low vapor pressures, reducing their potential for volatile emissions to the environment, which are a significant cause of air pollution. Additionally, their properties may be tuned by altering their chemical structures using the full palette of organic chemistry, making them highly versatile.

The program on which this work is based funds the creation of the Alabama Advanced Solvents Cluster (AASC), a multi-institutional collaboration initiated to answer fundamental questions about solute-solvent interactions in ionic/molecular mixtures. Specifically, the work will focus questions towards understanding these interactions and their influence on three topic areas relevant to developing energy efficient advanced chemical manufacturing processes: (Topic I) separation of aromatic compounds from aliphatic/aromatic mixtures, (Topic II) chemical reactions in thermally robust ILs, and (Topic III) polymerization in ILs and the development of high-performance polymers around ILs. In this presentation, we outline the vision for the newly funded project, focusing on Topic I, which emphasizes the separations aspect of the study and outlines strategies to understand the molecular-level interactions affecting separations, highlighting preliminary and foundational research.

Proposal Number: 0000246590 - DE-FOA-0002023: Understanding the Molecular-Level Interactions Between Ionic Liquids and Molecular Species to Design and Develop Novel Solvent Systems for Energy Efficient Processes

Additional PIs: Christy W. West¹, Paul A. Rugar³, Jason E. Bara,⁴ C. Heath Turner,⁴ Michael L. Curry,⁵ Amanda H. Coffman⁶

Affiliations(s):

³Department of Chemistry, University of Alabama, Tuscaloosa

⁴Department of Chemical & Biological Engineering, University of Alabama, Tuscaloosa

⁵Department of Chemistry, Tuskegee University

⁶Department of Chemistry, University of North Alabama

RECENT PROGRESS

Newly initiated award – August 2019

SEPARATIONML: A DATA-DRIVEN SEPARATION AGENT/SOLVENT DESIGN MODEL

PING YANG, STOSH A KOZIMOR, DANNY PEREZ, ENRIQUE R BATISTA, MARC J CAWKWELL,
NICHOLAS E LUBBERS, BENJAMIN STEIN

LOS ALAMOS NATIONAL LABORATORY

ABSTRACT

Advanced separation technologies are needed to recycle the residual energy content of spent nuclear fuel, minimize nuclear waste production, optimize storage conditions, and alleviate the proliferation concerns associated with reprocessing. However, rationally designing advanced separations schemes has been traditionally a slow and expensive process because of:

- 1.) limited understanding (on a molecular-level) of actinide partitioning mechanisms;
- 2.) an astronomically large chemical space;
- 3.) difficulties in appropriately modeling the relevant separation processes over realistic time scales.

Identifying methods to overcome these challenges has transformative potential in terms of augmenting predictive capabilities and developing technologies that push chemical exploration past the barriers of human intuition.

This project consists of a multidisciplinary effort that integrates modern data-centric approaches, quantum simulations, and high-throughput experimental chemical separations screening, to develop new predictive capabilities for actinide separations. We will develop an integrated design loop that leverages large-scale computer simulation and high-throughput experiments to power our predictive and interpretable *SeparationML* framework using active learning. This framework will use uncertainty quantification to search for the experiments that rapidly improve the accuracy of the model, with the end goal of producing new separation chemistry and an unprecedented understanding of reaction mechanisms. Our approach will generate novel separations, interpretable scientific knowledge that will be broadly transferable, and a powerful computational framework that can be brought to bear on a wide range of problems relevant to the DOE and to BES in particular.

PI ABSTRACTS SESSION VII: FIELDS & FILMS

Electrically Driven Ion Separations in Permeable Membranes

Merlin L. Bruening,^{a,b} Andriy Yaroshchuk,^c Chao Tang^a, Mykola Bondarenko,^d and Muhammad Ahmad^b

^aUniversity of Notre Dame, Department of Chemical and Biomolecular Engineering

^bUniversity of Notre Dame, Department of Chemistry

^cPolytechnic University of Catalonia, Department of Chemical Engineering

^dNational Academy of Sciences Ukraine, Institute of Colloid Chemistry

Presentation Abstract

During ion transport through membranes, spontaneous or applied electric fields give rise to electromigration that can lead to extraordinary selectivities, particularly when electromigration opposes convective transport. This presentation will explore electric field-induced selectivities in both ion-exchange membranes and in membranes that contain highly charged nanopores. In dialysis through an anion-exchange membrane, the $\text{Cl}^-/\text{SO}_4^{2-}$ selectivity increases from 1.3 to 13 on going from a source-phase concentration of 0.005 M to 0.1 M. Simulations suggest that this occurs because electromigration disproportionately decreases SO_4^{2-} transport due to its 2- charge and high concentration in the membrane. Coating anion-exchange membranes with poly(styrene sulfonate) (PSS)/ protonated poly(allylamine) (PAH) films leads to even higher $\text{Cl}^-/\text{SO}_4^{2-}$ selectivities that reach values of 140.

Flow through ion-exchange membranes should lead to remarkable separations even among monovalent ions. For example, during passage of ionic solutions through ion-exchange membranes streaming potentials should result in much higher flux of Li^+ than K^+ . Importantly, simulations suggest that increasing the flow rate through these membranes simultaneously enhances both selectivity and passage of the desired ion. Similarly, trace ion accumulation in a stagnant layer next to a charged nanoporous membrane occurs upon application of an electrical current that gives rise to electroosmotic flow and electromigration. The accumulation should vary with trace ion mobility to allow preconcentration of specific ions.

DE-SC0017618 and DE-FG02-98ER14907: Electrically Driven Ion Separations in Permeable Membranes

Student(s): Muhammad Ahmad, Liu Yang, and Chao Tang

RECENT PROGRESS

High $\text{Cl}^-/\text{SO}_4^{2-}$ Selectivities in Coated Anion-exchange Membranes

Anion-exchange membranes (AEMs) have high permselectivity for anions over cations, but they typically exhibit only modest selectivities among various anions. Recently, we showed that coating AEMs with poly(styrene sulfonate) (PSS)/protonated poly(allylamine) (PAH) films leads to $\text{Cl}^-/\text{SO}_4^{2-}$ selectivities as high as 140. Determination of

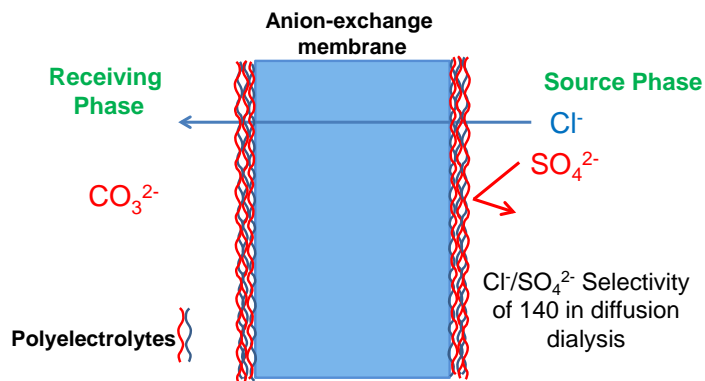


Figure 1. Schematic drawing of highly Cl^- selective dialysis through an anion-exchange membrane coated with polyelectrolyte multilayers.

steady-state selectivities requires soaking the membrane in the feed solution prior to the experiment to avoid long lag times. Figure 1 schematically shows the system, and Figure 2 presents transport data. Notably, for both bare AEMs and (PSS/PAH)₅PSS-coated membranes the selectivity increases with increasing source-phase concentration. However, at the highest concentrations the selectivity is an order of magnitude greater for the coated film. To understand the reasons behind the concentration-dependent selectivity, we simulated the

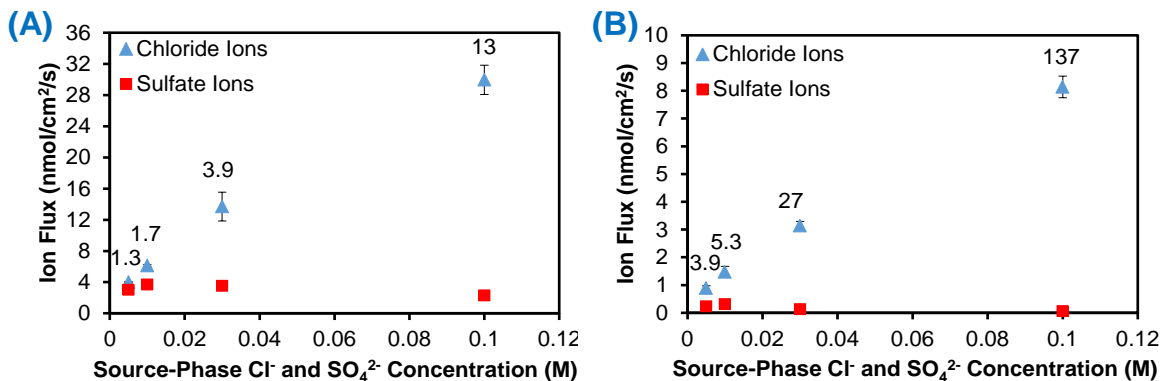


Figure 2. Plots of ion fluxes versus source-phase concentrations for diffusion dialysis through (A) bare anion-exchange membranes and (B) anion-exchange membranes coated with (PSS/PAH)₅PSS films. The source phase contained equal concentrations of Cl^- and SO_4^{2-} , and the receiving phase contained 0.01 M Na_2CO_3 . Numbers above the data points indicate the selectivity at that concentration.

fluxes using a solution-diffusion-electromigration model. Partitioning experiments and modeling suggest that the increased $\text{Cl}^-/\text{SO}_4^{2-}$ selectivities at high source-phase salt concentrations stem from enhanced Cl^- partitioning and electromigration that disproportionately decreases SO_4^{2-} flux in the AEM. Such mechanisms are effective in both bare and coated membranes, but the coating amplifies the selectivity.

Highly selective current-induced accumulation of trace ions at micro-/nano-porous interfaces

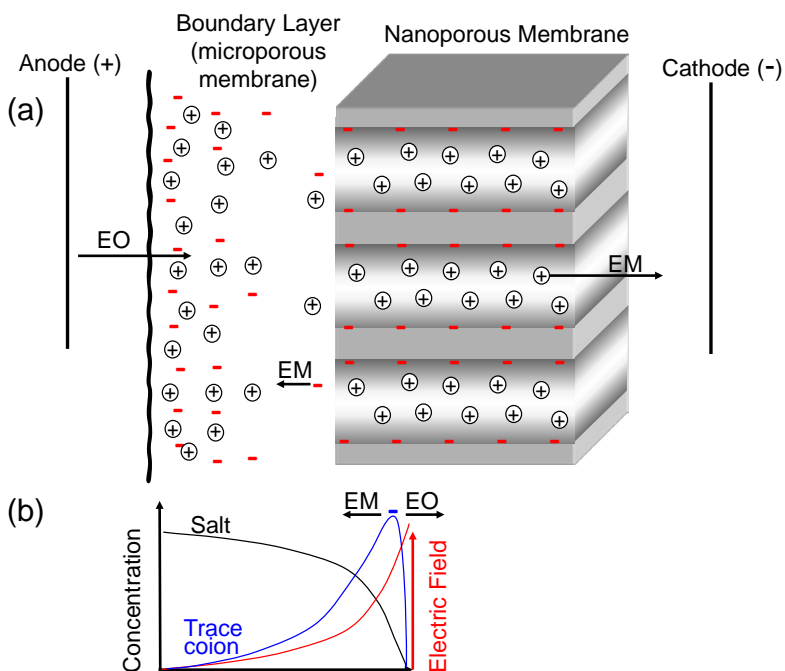


Figure 3. (a) Scheme of current-induced concentration polarization in an unstirred boundary layer in a microporous membrane adjacent to a nanoporous membrane. The cations and anions depicted in solution are those of the dominant salt. The negatively charged nanopores give rise to electroosmotic flow and exclusion of some dominant-salt anions, which leads to depletion of the dominant salt near the nanoporous membrane. (b) Qualitative plot of the dominant-salt concentration (black), the electric field (red), and the trace-coion concentration (blue) in the unstirred region (inside the microporous membrane). The high electric field gives rise to accumulation of trace ions when the absolute value of their electromigration flux component is nearly equal to their electroosmotic flux component. Abbreviations: EM- electrical migration, EO- electroosmosis-induced convection.

During application of an electrical current through a composite micro-/nano-porous membrane, trace-ion accumulation in the microporous layer should vary greatly with the ion diffusion coefficient to allow selective preconcentration of specific ions (Figure 3). We examined the theoretical enrichment factors in the microporous region as a function of current density and trace-ion diffusion coefficient to demonstrate the promise of such micro-/nano-porous interfaces for ion separations. (Schemes that take advantage of accumulation for harvesting would likely employ a simpler confined stagnant solution layer that one could collect periodically.) Trace-ion accumulation relies on charged nanopores that exclude coions (ions with the same charge as the nanopore walls) to deplete the region next to the nanopores of the dominant (high-concentration) salt. This depletion gives rise to high local electric fields. Trace ions accumulate in this region

because convection carries them toward the nanoporous interface, whereas electromigration in the opposite direction is strongest next to the interface. For ions whose diffusion coefficients are half of the corresponding value for the dominant salt, calculated preconcentration factors reach 150. In contrast depletion occurs for ions with the same diffusion coefficient as the dominant salt. Even higher enrichment factors appear for divalent ions due to their relatively low diffusion coefficients. With monovalent coions whose diffusion coefficients differ by only 2%, calculated selectivity factors reach values >1.2 (>1.8 for divalent coions), depending on the magnitudes of the diffusion coefficients. Such selectivities may prove useful in separating very similar species such as isotopes.

Electromigration-based ion-transport selectivity during flow through ion-exchange membranes

Simultaneous attainment of both high ion passage and high transport selectivity is difficult to achieve in membrane separations. Typically high selectivities occur with low passages and vice versa. Our recent simulations of transport through ion-exchange membranes suggests that high flow rates through such systems can simultaneously lead to remarkable selectivities among ions and high passages of a specific ion. The simulations employ the extended Nernst-Planck equation, which contains terms for convective, electromigration, and diffusive transport fluxes.

Figure 4 shows the mechanism of the separation. Convection moves the solution through a pore of an ion-exchange membrane, but this creates a streaming potential because the pore contains an excess of mobile cations due to the negative fixed charge in the membrane. The streaming potential causes an electromigration flux in the direction opposite to convection. Importantly, the electromigration flux in the figure is largest for the cation with the highest mobility. Hence, cations with low mobilities move through the membrane faster than those with high mobilities.

Simulations based on a uniform fixed-charge distribution in the membrane show the enticing possibility of simultaneously achieving high selectivity and passage for the desired ion. Figure 5 shows that as the water flux increases through the membrane, selectivity and passage both initially increase and eventually reach a maximum value at fluxes between 35 and 45 $\mu\text{m}/\text{sec}$. Passage, defined as the concentration in the permeate divided by the concentration in the feed, may exceed unity as long as the feed is continually refreshed with new solution. The high passage occurs due to the high

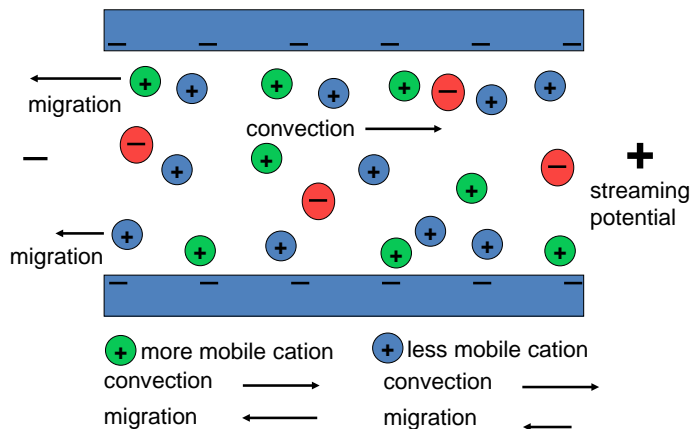


Figure 4. Scheme of flow-induced ion separation during flux through an ion-exchange membrane pore. Due to the excess positive mobile charge in the pore, flow creates a streaming potential that decreases the fluxes of both ions, but more especially the more mobile ion. Because of the high concentration of counterions in the pores, this separation mechanism can lead to both high passage of the desired ion and high selectivity.

fixed charge concentration (2 M) in the membrane, which is significantly greater than the feed salt concentrations of 0.01 M KCl and 0.01 M LiCl. Thus, the membrane contains 100 times more mobile cations than the bulk feed solution.

Selectivity reaches values >1000 when the streaming potential is high and diffusion is negligible in the membrane. This selectivity is remarkable considering that the ratio of the mobilities of the two ions in the simulation is only 2. At excessive flow rates, concentration polarization eventually acts to decrease the selectivity.

The results of the simulation in Figure 5 inspire us to pursue such separations, but there are drawbacks. First, with typical ion-exchange membranes that contain such a high charge density, attaining these high flow rates requires impractical pressure drops. Second, the simulation assumes a uniform distribution of charge, whereas typical ion-exchange membranes contain pores with charge on the walls. The dominance of flow in the center of the pores will lead to decreased selectivities and recoveries. Nevertheless, our current simulations focusing on charged pores with larger diameters also show the potential for highly selective separations, although this requires dilute solutions to exclude coions from the membrane. We are currently working on developing high-selectivity Li^+/K^+ separations using track-etched membranes with charged pores.

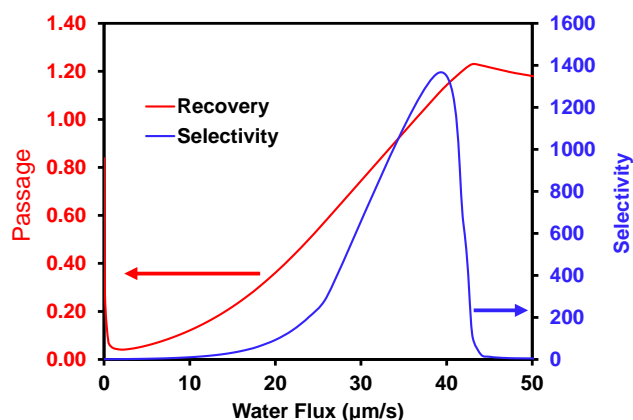


Figure 5. Plot of simulated values of ion passage (concentration in the permeate divided by concentration in the feed) and selectivity (ratio of the permeate concentrations of two cations) during cross-flow filtration of a solution containing two 0.01 M monovalent salts through an ion-exchange membrane. Both selectivity and passage show a maximum at a specific water flux. The membrane contained 2 M fixed charge, and the ion diffusion coefficients in the membrane were 4.61×10^{-10} and $2.31 \times 10^{-10} \text{ m}^2/\text{s}$ for the more and less mobile counterion, respectively. The coion diffusion coefficient in the membrane was $3.02 \times 10^{-10} \text{ m}^2/\text{s}$. In the boundary layers, the counterion

Publications Acknowledging this Grant in 2015 – present

(XIII) Exclusively funded by this grant;

1. Zhu, Y.; Ahmad, M.; Yang, L.; Misovich, M.; Yaroshchuk, A.; Bruening, M.L. Adsorption of Polyelectrolyte Multilayers Imparts High Monovalent/Divalent Cation Selectivity to Aliphatic Polyamide Cation-exchange Membranes *J. Membr. Sci.* **2017**, *537*, 177–185.
2. White, N.; Misovich, M.; Alemayehu, E.; Yaroshchuk, A.; Bruening, M.L. Highly Selective Separations of Multivalent and Monovalent Cations in Electrodialysis Through Nafion Membranes Coated with Polyelectrolyte Multilayers *Polymer* **2016**, *103*, 478-485.

(XIV) Jointly funded by this grant and other grants with leading intellectual contribution from this grant;

3. M. Ahmad, C. Tang, A. Yaroshchuk, and M.L. Bruening “Layer-by-layer Modification of Aliphatic Polyamide Anion-exchange Membranes to Increase $\text{Cl}^-/\text{SO}_4^{2-}$ Selectivity” *J. Membr. Sci.* **578**, 209-219 (2019).
4. A. Yaroshchuk, M.L. Bruening, and E. Zholkovskiy “Modelling Nanofiltration of Electrolyte Solutions” *Adv. Colloid & Interface Sci.* **268**, 39-63 (2019).
5. M.P. Bondarenko, A. Yaroshchuk, and M.L. Bruening “Highly selective current-induced accumulation of trace ions at micro-/nano-porous interfaces” *Adv. Theory & Simulations* 1900009 (2019).
6. L. Yang, C. Tang, M. Ahmad, A. Yaroshchuk, and M.L. Bruening “High Selectivities among Monovalent Cations in Dialysis through Cation-Exchange Membranes Coated with Polyelectrolyte Multilayers” *ACS Appl. Mater. Interfaces* **10**, 44134–44143 (2018).
7. Yaroshchuk, A.; Bruening, M.L. An Analytical Solution of the Solution-Diffusion-Electromigration Equations Reproduces Trends in Ion Rejections During Nanofiltration of Mixed Electrolytes *J. Membr. Sci.* **2017**, *523* 361-372.
8. Yaroshchuk, A.; Zhu, Y.; Bondarenko, M.; Bruening, M.L. Deviations from Electroneutrality in Membrane Barrier Layers: A Possible Mechanism Underlying High Salt Rejections *Langmuir* **2016**, *32*, 2644–2658.
9. White, N.; Misovich, M.; Yaroshchuk, A.; Bruening, M.L. Coating of Nafion Membranes with Polyelectrolyte Multilayers to Achieve High Monovalent/Divalent Cation Electrodialysis Selectivities *ACS Appl. Mater. & Interfaces* **2015**, *7*, 6620–6628.

Molecular Aspects of Transport in Thin Films of Controlled Architecture

Paul W. Bohn

Department of Chemical and Biomolecular Engineering
Department of Chemistry and Biochemistry
University of Notre Dame, Notre Dame, IN 46556 USA

Presentation Abstract

The scientific and technological targets of this project focus on reactions and transport in nanoscale confined volumes, because these phenomena are at the heart of a wide array of separation technologies. Studying transport on this length scale brings a core set of scientific phenomena - wetting/dewetting, hydrophobicity, stochastic fluctuations in fluid flow, electrokinetics, *etc.* - to the fore that exhibit fundamentally different behavior on the nanoscale. This occurs because scaling to nanometer dimensions changes the underlying nature of the forces that direct molecular motion, thus directly impacting molecular separations. The experiments being pursued in support of these objectives use single molecule-based electrokinetic, electrochemical and spectroelectrochemical probes of transport in nanoconfined flows under active control. As such, they are intended to develop the design rules, structural motifs, and operating principles needed to achieve control over molecular transport in nano-confined volumes.

DE FG02 07ER15851: Molecular Aspects of Transport in Thin Films of Controlled Architecture

Postdocs: Chaoxiong Ma, Seung-Ryong Kwon

Students: Erick Foster, Dane Grismer, Jin, Jia, Arielle Lopez, Christiana Oh, Wei Xu

RECENT PROGRESS

Introduction. Pore-based structures occur widely in living organisms. Ion channels embedded in cell membranes, for example, provide pathways, where electron and proton transfer are coupled to the exchange of vital molecules. Learning from mother nature, our laboratory has focused on artificial nanopore architectures to effect electrochemical control over transport and reactivity. Thus, enhanced understanding of nanofluidics has opened the way to controlling molecular transport at unprecedented levels. Beginning with the seminal work of Rice and Whitehead, who first described electrokinetic transport in nanoscale capillaries,¹ to the theory of potential driven flow developed by Levine,² to the development by Ramsey and co-workers of the first in-plane nanoporous structure for sample preconcentration,³ and our group's use of surface charge in nanocapillary array membranes to effect digital nanofluidic coupling,⁴ the great potential of nanoscale fluidic architectures to effect differential control of molecular transport has been increasingly apparent. In contrast, nanoelectrochemistry realized its beginnings from a combination of advances. Martin's group developed a robust synthesis of pore-based nanomaterials;⁵ Bard and Fan designed an elegant purely electrochemical detection of a single molecule;⁶ and Murray's group observed the charging of gold nanoparticles (quantized capacitors).⁷ Inevitably, nanopores and nanoelectrodes were combined to yield single nanopore electrodes by Zhang and White.⁸ Later, single nanopore electrodes and nanopore electrode arrays with well-defined, reproducible pore geometry and size were fabricated

lithographically.^{9, 10} The combination of nanopores, nanofluidics, and nanoelectrochemistry has been at the heart of our efforts to develop new methods to control molecular transport.

Hierarchically-Organized Biomimetic Structures for Nanoscale Transport Control.

When the size of nanochannels or nanopores approaches the thickness of the electrical double layer, unique transport phenomena, which deviate from conventional macroscopic transport theory, are observed. In order to explore this phenomenon, we have fabricated hierarchically organized structures composed of an asymmetric Nafion membrane on top of a nanopore electrode array (Nafion@NEA), *viz.* **Figure 1**. As a widely used cation-exchange membrane, Nafion efficiently transports cations but strongly excludes anions. This allows the membrane to quickly exchange charged species, while avoiding fouling that would otherwise degrade permselectivity.

The unusual properties of the Nafion@NEA system arise from the Nafion proton exchange membrane. The Nafion@NEA device, shown schematically in **Figure 1**, has a Nafion membrane

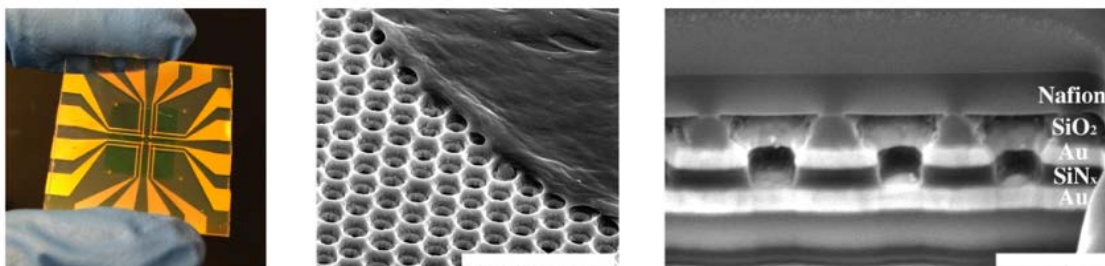


Figure 1. Schemes and SEM images of asymmetric Nafion-coated nanopore electrode arrays, Nafion@NEA. (Left) Photo of an electrochemical diode wafer consisting of 8 NEA devices and covered by a Nafion membrane (green). (Center) Tilted SEM image near the edge of the Nafion film, indicating that the Nafion conformally coats the NEA. Scale bar is 2 μm . (Right) Cross-sectional SEM image showing the stacked metal (disk)-insulator-metal (ring) (MIM) structure in the vertical direction, as well as the well-sealed Nafion at the top. Scale bar is 400 nm.

- with pores of average diameter, $d \sim 1\text{-}2$ nm, presenting negatively charged sulfonate groups - tightly bonded to the top of the NEA structure. In this design, the Nafion membrane controls access of charged redox species to the NEA. The combination of Nafion and the NEA provides double gating to control transport into the active region, a property which is illustrated by comparison of $\text{Ru}(\text{NH}_3)_6^{2/3+}$ CVs obtained within NEAs to those obtained with Nafion@NEAs, as shown in **Figure 2(Left/Center)**. We also investigated how the potential of the top electrode, E_{TE} , affects the current response in Nafion@NEAs. Each data point in **Figure 2(Right)** represents the limiting current from the bottom electrode, acquired at the sweep termination, either $E_{BE} = -0.5$ V (yellow) or $E_{BE} = +0.1$ V (blue), while the top electrode was fixed at the potential indicated on the x -axis. In both positive and negative sweeps, minimal response is observed when the potentials E_{BE} and E_{TE} are both reducing, point (B), or both oxidizing, point (E). In

contrast, maximum limiting currents are observed when E_{BE} and E_{TE} are on opposite sides of the

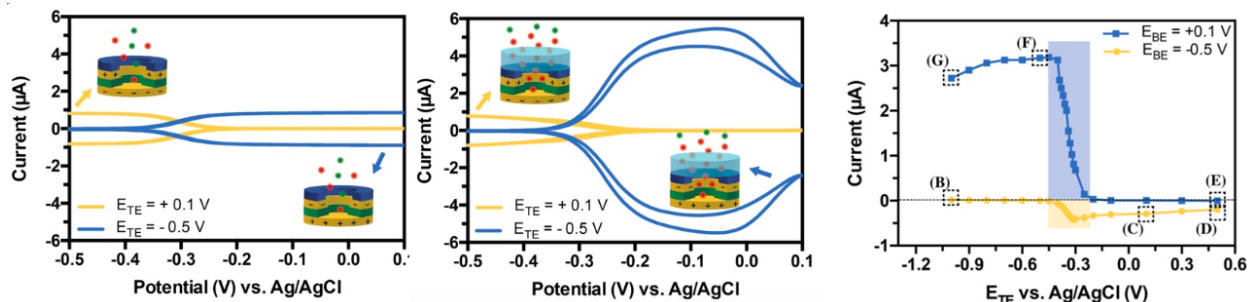


Figure 2. Asymmetric current response from Nafion@NEAs. CVs of 1 mM $\text{Ru}(\text{NH}_3)_6^{3+}$ in 1 M KCl from an uncovered NEA, (Left), and Nafion@NEA, (Center). For both panels, the currents are shown for $E_{TE} = +0.1$ V (yellow) and $E_{TE} = -0.5$ V (blue). The insets schematically illustrate the potential polarity marked by the arrows in (A) and (B). (Right) Voltage-gated ion transport in Nafion@NEAs. Limiting current magnitudes obtained from CVs of 1 mM $\text{Ru}(\text{NH}_3)_6^{3+}$ in 1 M KCl at the bottom electrode. Limiting currents were obtained at $E_{BE} = +0.1$ V (blue, positive sweeps) or -0.5 V (yellow, negative sweeps), while E_{TE} was fixed at different values, ranging from -1.0 V to $+0.5$ V. The blue and yellow rectangles denote the voltage threshold range for ion gating.

equilibrium potential. However, there is a clear asymmetry between the maximum limiting current for $E_{BE} > E_{TE}$ and $E_{BE} < E_{TE}$. These observations can be understood as a combination of voltage gating and redox cycling effects. Independent of the bottom electrode potential, CVs obtained with positive E_{TE} serve to discriminate against uptake of cations (gate closed condition). Thus, limiting currents obtained under these conditions are either small, when E_{BE} and E_{TE} are on opposite sides of E_{eq} , or zero, when E_{BE} and E_{TE} on the same side of E_{eq} . Overall, the clear current rectification represented by the behavior in **Figure 2** results from both the permselectivity of the Nafion membrane as well as the potential applied to the top (gate) electrode, E_{TE} , thus demonstrating the double gating effect.

Nanofluidically-Enabled Electrochemical Diode and Transistor Action.

Inspired by the functioning of cellular ion channels, we fabricated hierarchically-organized nanopore-based structures comprised of separate layers: a bottom nanopore electrode array and a top layer consisting of sub-5 nm nanopores, as shown in **Figure 1**. We showed that these architectures can exhibit ionotronic properties, *i.e.* manipulating the transport of ions in the same

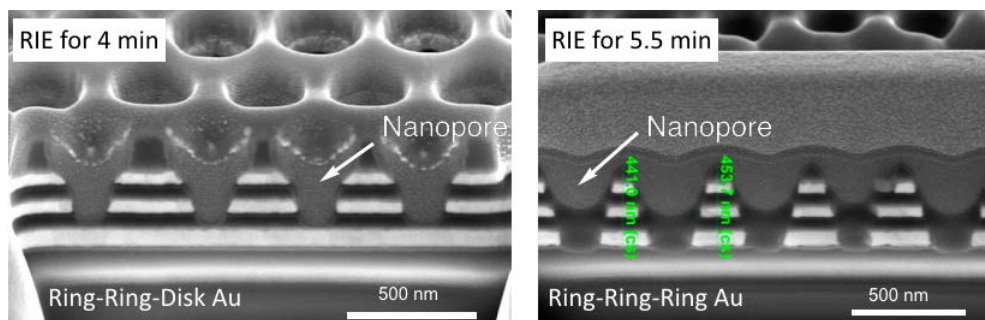


Figure 3. Cross-sectional SEM images of a small portion of 3-electrode NEA structures in the ring-ring-disk (left) and ring-ring-ring (right) configurations. Volumes exhibited by the realized using the Nafion@NEA structure discussed above. The top electrode of dual electrode

manner that diodes and transistors control electron transport, for signal processing and detection. High-performance redox cycling-based electrochemical diodes were

Nafion@NEAs can serve as a voltage-controlled switch to gate ion transport within the nanopore, allowing them to be operated as a diode. Switching voltages applied to the top and bottom electrodes of the NEA leads to a large rectification ratio and fast response time, all accomplished with simplified circuitry.

By taking advantage of closely spaced and individually addressable electrodes, redox cycling electrochemical multi-electrode structures have the potential for application to large-scale production and electrochemically-controlled circuit operations which go well beyond conventional electronic diodes or transistors. Recently, we have extended the concept to 3-electrode geometries, as shown in **Figure 3**. Remarkably, providing a SiN_x dielectric barrier to the bottom electrode, W2, produces strong rectification of the redox cycling behavior between the middle, W1, and top, C/R, electrodes, when the W2 potential exceeds a certain threshold value ($\sim \pm 1.8$ V vs. C/R), **Figure 4**. We interpret this behavior as being produced by pinhole formation in the SiN_x layer. Strong evidence for pinhole-mediated transport is provided by stochastic current fluctuations at the bottom electrode, W2, which appear above the threshold potential. These current fluctuations are similar to those observed by Xiao *et al.* in high aspect

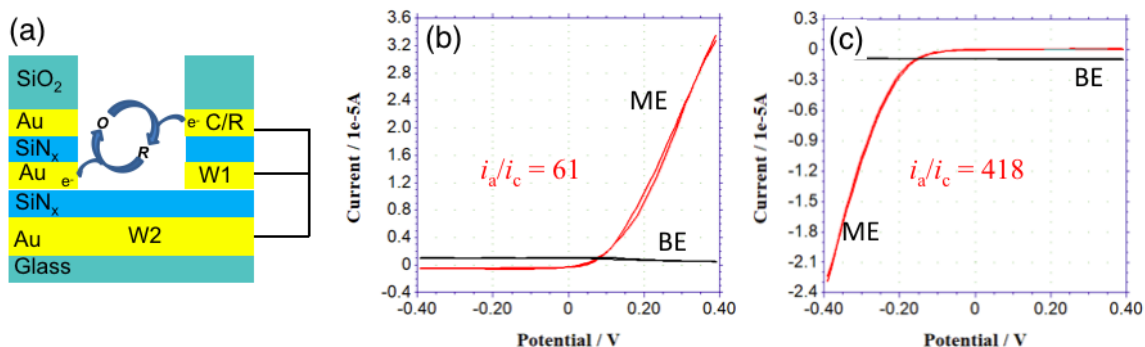


Figure 4. (a) Schematic illustration of a ring-ring-dielectric-disk modified 3-electrode structure, in which the bottom electrode, W2, acts as a gate for ion transport and controls redox cycling between the middle, W1, and top, C/R, electrodes. Redox cycling exhibits remarkable rectification behavior when the potential ratio nanopores in polymer membranes.¹¹ These fluctuations have been attributed to nanoscopic evaporation and condensation and are subject to strong perturbations by electrowetting at these scales.

- [1] Rice, C.L.; Whitehead, R. *J. Phys. Chem* **1965**, 69, 4017-4024.
- [2] Levine, S.; Marriott, J.R.; Robinson, K. *J. Chem. Soc.* **1975**, 71, 1-11.
- [3] Khandurina, J.; Jacobson, S.C., *et al. Anal. Chem.* **1999**, 71, 1815-1819.
- [4] Kuo, T.C.; Cannon, D.M., *et al. Anal. Chem.* **2003**, 75, 1861-1867.
- [5] Jirage, K.; Hulteen, J.; Martin, C.R. *Science* **1997**, 278, 655.
- [6] Fan, F.; Bard, A. *Science* **1995**, 267, 871.
- [7] Chen, S.; Ingram, R.S., *et al. Science* **1998**, 280, 2098-2101.
- [8] Zhang, B.; Zhang, Y.; White, H.S. *Anal. Chem.* **2006**, 78, 477-483.
- [9] Lemay, S.; van den Broek, D.M., *et al. Anal. Chem.* **2005**, 77, 1911-1915.
- [10] Lanyon, Y.H.; De Marzi, G., *et al. Anal. Chem.* **2007**, 79, 3048-3055.
- [11] Xiao, K.; Zhou, Y. *et al. ACS Nano* **2016**, 10, 9703-9709.

Publications Acknowledging this Grant in 2015 – present

(XV) Exclusively funded by this grant;

Contento, N.M.; Bohn, P.W. “Electric Field Effects on Current-Voltage Relationships in Microfluidic Channels Presenting Multiple Working Electrodes in the Weak-Coupling Limit,” *Microfl. Nanofl.* **2015**, 18, 131-140. [DOI 10.1007/s10404-014-1424-9]

Wichert, R.A.W.; Han, D.; Bohn, P.W. “Effects of Molecular Confinement and Crowding on Horseradish Peroxidase Kinetics Using a Nanofluidic Gradient Mixer,” *Lab Chip* **2016**, 16, 877-883. [DOI 10.1039/C5LC01413A; PMID: 26792298]

Xu, W.; Fu, K.; Bohn, P.W. “Electrochromic Sensor for Multiplex Detection of Metabolites Enabled by Closed Bipolar Electrode Coupling,” *ACS Sens.* **2017**, 2, 1010-1026. [DOI 10.1021/acssensors7b00292]

Fu, K.; Han, D.; Crouch, G.M.; Kwon, S.-R.; Bohn, P.W. “Asymmetric Nafion-Coated Nanopore Electrode Arrays as Redox Cycling-Based Electrochemical Diodes,” *ACS Nano* **2018**, 12, 9177-9185. [DOI 10.1021/acsnano.8b03751]

(XVI) Jointly funded by this grant and other grants with leading intellectual contribution from this grant;

Xu, W.; Foster, E.; Ma, C.; Bohn, P.W. “On-Demand *In Situ* Generation of Oxygen in a Nanofluidic Embedded Planar Microband Electrochemical Reactor,” *Microfl. Nanofl.* **2015**, 19, 1181-1189. [DOI 10.1007/s10404-015-1636-7]

Zaino, L.P. III; Grismer, D.A.; Han, D.; Crouch, G.M.; Bohn, P.W. “Single Molecule Spectroelectrochemistry of Freely Diffusing Flavin Mononucleotide in Zero-Dimensional Nanophotonic Structures,” *Faraday Disc.* **2015**, 184, 101-115. [DOI 10.1039/C5FD00072F; PMID: 26406924]

Xu, W.; Ma, C.; Bohn, P.W. “Coupling of Independent Electrochemical Reactions and Fluorescence at Closed Bipolar Interdigitated Electrode Arrays,” *ChemElectrochem* **2016**, 3, 422-428. [DOI 10.1002/celec.201500366]

Zaino, L.P. III; Ma, C.; Bohn, P.W. “Nanopore-Enabled Electrode Arrays and Ensembles,” *Microchim. Acta* **2016**, 183, 1019–1032. [DOI 10.1007/s00604-015-1701-7]

Zaino, L.P. III; Wichert, R.A.W.; Crouch, G.M.; Bohn, P.W. “Microchannel Voltammetry in the Presence of Large External Voltages and Electric Fields,” *Analyt. Chem.* **2016**, 88, 4200-4204. [DOI 10.1021/acs.analchem.6b00399; PMID: 27045936]

Xu, W.; Fu, K.; Ma, C.; Bohn, P.W. “Closed Bipolar Electrode-Enabled Dual-Cell Electrochromic Detectors for Chemical Sensing,” *Analyst* **2016**, 141, 6018-6024. [DOI 10.1039/C6AN01415A; PMID: 27704078]

Bohn, P.W. “Science and Technology of Electrochemistry at Nano-Interfaces,” *Faraday Disc.* **2018**, 210, 481-493. [DOI 10.1039/C8FD00128F]

Kim, J.-Y.; Han, D.; Crouch, G.M.; Kwon, S.-R.; Bohn, P.W. “Capture of Single Silver Nanoparticles in Nanopore Arrays Detected by Simultaneous Amperometry and Surface-Enhanced Raman Scattering,” *Analyt. Chem.* **2019**, 91, 4568-4576. [DOI 10.1021/acs.analchem.8b05748]

(XVII) Jointly funded by this grant and other grants with relatively minor intellectual contribution from this grant;

Ma, C.; Xu, W.; Wichert, W.R.A.; Bohn, P.W. “Ion Accumulation and Migration Effects on Redox Cycling in Nanopore Electrode Arrays at Low Ionic Strength,” *ACS Nano* **2016**, 10, 3658-3664. [DOI 10.1021/acsnano.6b00049]

King, T.L.; Jin, X.; Nandigana, V.R.; Aluru, N.; Bohn, P.W. “Electrokinetic Transport and Fluidic Manipulation in Three Dimensional Integrated Nanofluidic Networks,” in *Nanofluidics*, 2nd Edition, A. de Mello and J. Edel, Eds., Royal Society of Chemistry, Cambridge, UK, Ch. 2, pp. 37-75, **2017**.

Xu, W.; Zaino, L.P. III; Bohn, P.W. “Electrochemically Modulated Luminescence in Nanophotonic Structures,” in *Combined Luminescence and Electrochemistry: Involvements and applications in analytical chemistry, physics and biology*. F. Miomandre, P. Audebert, Eds., **2017** Springer, pp. 79-104.

Fu, K.; Xu, W.; Hu, J.; Lopez, A.; Bohn, P.W. “Microscale and Nanoscale Electrophotonic Diagnostic Devices,” in *Bioelectronic Medicine*, V.A. Pavlov and K.J. Tracey, Eds., Cold Spring Harbor Perspectives, Cold Spring Harbor Laboratory Press; **2018**. [DOI 10.1101/cshperspect.a034249]

Crouch, G.M.; Oh, C.; Fu, K.; Bohn, P.W. “Tunable Self-Organized Optical Metamaterials Enabled by Closed Bipolar Electrochemistry,” *Analyst*, **2019**, 144, submitted.

Differences in the extent of counterion condensation of ordered block copolymer electrolytes (BCEs) versus random copolymer electrolytes (RCEs)

Qi Lei^a, Ke Li^b, Christopher G. Arges^a, and Revati Kumar^b

^aCain Department of Chemical Engineering, Louisiana State University

^bDepartment of Chemistry, Louisiana State University

Presentation Abstract

This project systematically investigates counterion condensation in microphase separated block copolymer electrolytes (BCEs) and random copolymer electrolytes (RCEs). The initial model system consists of poly(styrene-*block*-2-vinyl n-methyl pyridinium iodide/2-vinyl pyridine) and poly(styrene-*random*-vinyl n-methyl pyridinium iodide/2-vinyl pyridine). The broad goal of the research is to know the different extents of counterion condensation in microphase separated BCEs versus non-ordered, random copolymer electrolytes and to establish a relationship between the extent of counterion condensation and block copolymer period size. In the past year, three different analytical methods were developed to quantify the extent of counterion condensation in BCE and RCE thin films. These independent methods are: i.) ion-sorption and release experiments in custom built cells for thin films and using LC-MS and ion-exchange chromatography to assay changes in salt concentration, ii.) water uptake experiments of the thin films immersed in different salt solutions using a quartz crystal microbalance (QCM), and iii.) grazing-incidence small-angle x-ray scattering (GI-SAXS; for BCE samples only) that monitors changes in periodic domain size when the thin film is immersed in salt solutions. From these experiments, the Donnan equilibrium between the thin film and the salt solution is established and is used to quantify the extent of counterion condensation when knowing the thin film's ion-exchange capacity (IEC) value. The preliminary results from QCM have hint that the BCEs display less counterion condensation than the RCEs. To complement the experimental studies, all-atom molecular dynamic simulations were performed on single-chains that mimicked BCE and RCE configurations. The simulation results differ from experimental studies (i.e., the RCEs are less susceptible to counterion condensation than BCEs). However, it is important to note that the simulations are predicting a much smaller counterion condensation value because there are too many water molecules in the simulations. The team is looking to address the different findings between simulations and experimental data.

Grant or FWP Number: Understanding and manipulating counterion condensation within charged polymer electrolytes for selective and low resistant membrane separations

PI: Christopher G. Arges

Student(s): Qi Lei, Ke Li

Affiliations(s): Cain Department of Chemical Engineering and Department of Chemistry, Louisiana State University

RECENT PROGRESS

Swelling uptake experiments of BCE and RCE in different aqueous solutions of KI

A QCM with BCE or RCE was equilibrated with potassium iodide (KI) solutions. The frequency change was monitored upon introduction of the solution and was measured until a stable

frequency value was attained. The frequency shift was correlated to the mass/swelling uptake. The different swelling uptakes were plotted versus KI solution concentration to identify the Donnan equilibrium concentration (C_D). The IEC of the thin BCE and RCE film (approx. 30 nm in thickness) was determined using x-ray photoelectron spectroscopy (XPS). The fraction of condensed (f_c) counterions was determined by $1 - C_D/C_{IEC}$. The f_c for the RCE was 0.97. The BCE f_c values has not been determined yet (waiting on IEC value determination). See **Figure 1** for results.

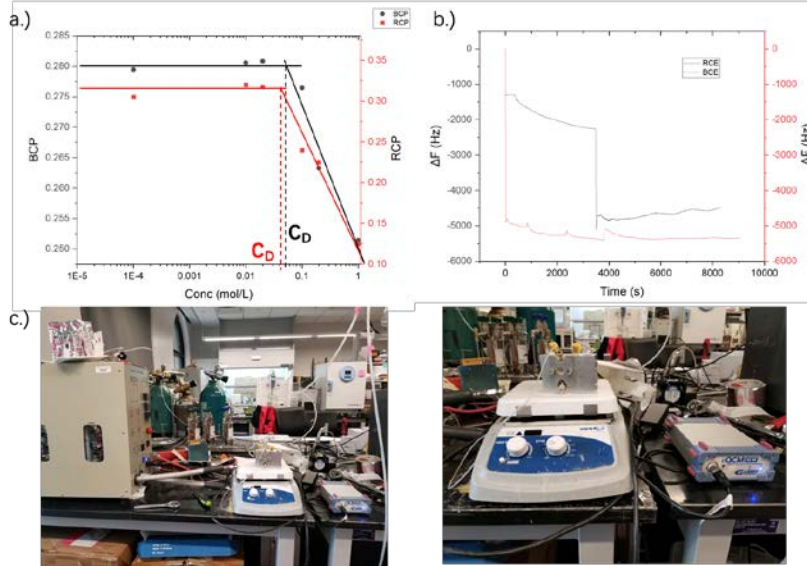


Figure 1. a.) Swelling uptake of the BCE and RCE in different KI solutions; b.) example QCM frequency changes upon introduction of KI solution with BCE and RCE thin films; c.) QCM setup in PI Arges’s lab.

Co-ion sorption experiments

BCE and RCE samples on wafer substrates were then placed in a custom-made chamber and 1mL of KI solution (a particular concentration) was injected into the chamber with a thin volume compartment above the film. Equilibrium was attained over 24h. Then, the KI solution was removed and the chamber was injected with DI water and then equilibrated for another 24h. The collected DI water was analyzed by ICP-AES for potassium content. The co-ion sorption data was compared against different simulated co-ion sorption data from the Donnan equation (equation 1). The simulated results were matched to the co-ion sorption data to get the Donnan equilibrium to determine f_c . See **Figure 2** for data.

$$c_{m+} = \frac{-c_b + \sqrt{c_b^2 + 4c^2}}{2} \quad (\text{equation 1})$$

where c is the external salt concentration, c_{m+} is the concentration of dissociated fixed positive charges in the thin film sample. C_b is constant and is simulated to be possible different Donnan equilibrium concentration values.

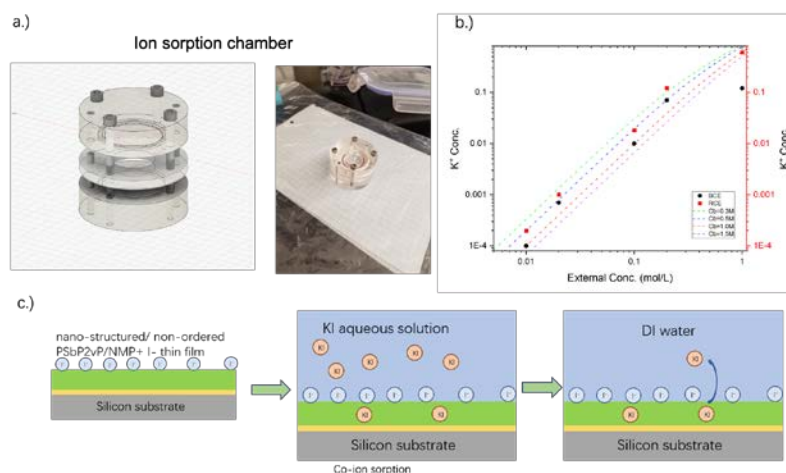


Figure 2. a.) Ion sorption chamber; b.) co-ion sorption experiments data of the BCE and RCE samples. The fitting indicates that $C_D=1M$, so 63% of counterion in the RCE were condensed; c.) A cartoon of the co-ion sorption process in thin films.

GI-SAXS experiments

GI-SAXS was performed on PSbP2VP/NMP⁺ I (40k-44k; exposed to methyl iodide vapor for 24 hr) at the 8-ID-E beamline at the Advanced Photon Source (APS). The samples were immersed in KI aqueous solution with different concentrations in the GI-SAXS environmental chamber. By monitoring the domain spacing changing with external salt concentration, the C_D and f_c were determined.

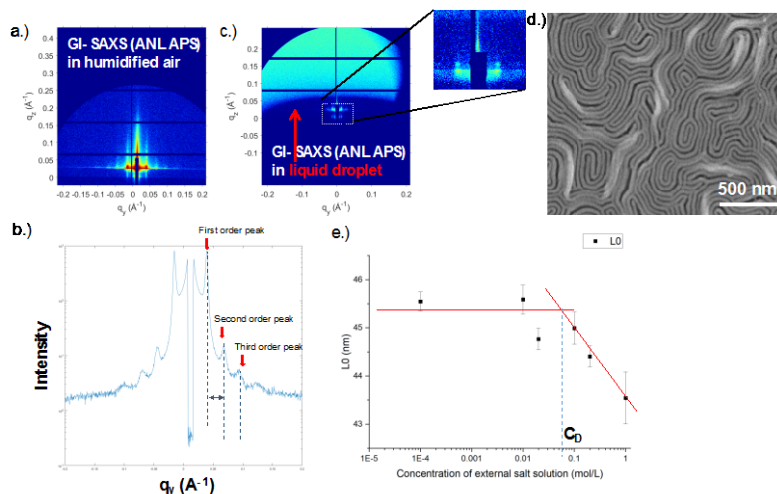


Figure 3. a.) GI-SAXS PSbP2VP/NMP⁺ I BCE (dry) and b.) line cut curve of dry BCE sample ($L_0=2\pi/\Delta q = 44$ nm). 3rd order peak indicates long range periodicity; c.) GI-SAXS PSbP2VP/NMP⁺ I BCE (wet); d.) Electron micrograph of PSbP2VP/NMP⁺ I; e.) Change in L_0 for PSbP2VP/NMP⁺ I BCE exposed to different KI solution concentrations. The determined C_D showed that 95% of the counterions were condensed.

All-atom simulations

All-atom molecular simulations were performed to probe counterion condensation phenomena in model RCEs and BCEs of varying periodicity size and charge density. Classical molecular dynamics simulations were carried out using the OPLSAA all atom force-field for the polymer chains along with the TIP3P model for water. The partial charges on the polymer chains were

obtained by performing electronic structure calculations on a single unit of the polymer chain in each case. Charges from electrostatic potentials using a grid, specifically CHELPG, method was used to determine atomic charges by fitting to the ab initio electrostatic potential on a grid around the polymer brushes unit molecule. The CHELPG scheme was chosen since it is the same scheme that was used to obtain charges for the OPLSAA force field and hence was adopted here for consistency. Eight chains with different microstructure were simulated separately. Each chain was solvated with 6500 water molecules in a cubic box of length 60 Angstroms and the box was then equilibrated in the NVT ensemble for 2ns and the NPT ensemble for 2ns at a temperature of 300K and 1 atm, followed by 20ns production runs in the NVT ensemble at the same temperature. The Nose-Hoover thermostat was adopted to keep the temperature constant, and the integration time step was 1 fs. All the simulations were carried out with the LAMMPS software package under periodic boundary conditions. PPPM Ewald method were used to account for long-range electrostatics.

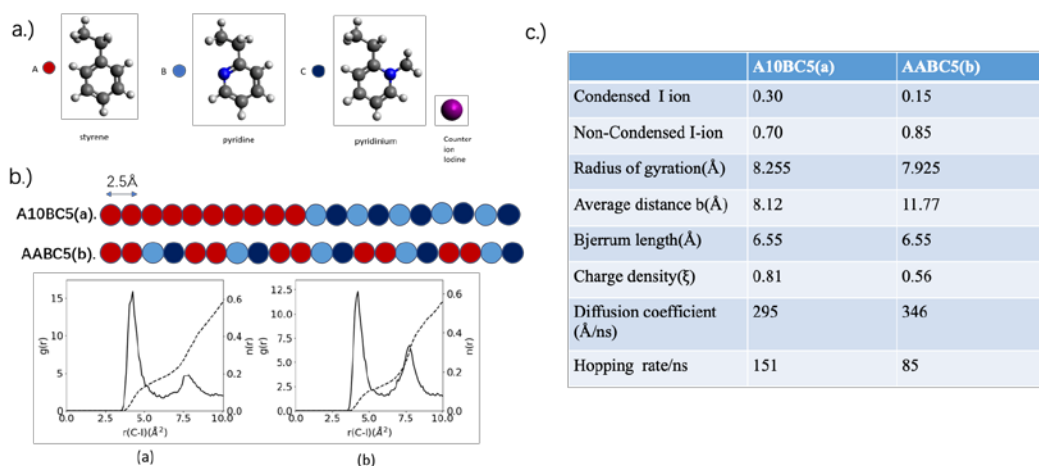


Figure 4. a.) Molecular substituents in b.) the model BCE (top) and model RCE (bottom) and their subsequent radial distribution functions; c.) results from all-atom classical MD simulations with BCE and RCE (which has less counterion condensation).

Publications Acknowledging this Grant in 2019 – present

Please classify your publications into three categories according to the source of support for the work published:

- (I) none
- (II) none
- (III) Arges, C. G.; Li, K.; Zhang, L.; Kambe, Y.; Wu, G.-p.; Lwoya, B.; Albert, J.N.L.; Nealey, P.F.; Kumar, R. *Mol. Syst. Des. Eng.*, **2019**, 4, 365-378.

PI ABSTRACTS SESSION IX: REACTIVE SEPARATION

Efforts Towards the Selective Volatilization of *f*-Element Complexes using Mechanochemistry and Chelating Borohydrides

Taylor V. Fetrow, Anastasia V. Blake, Francesca D. Eckstrom, Scott R. Daly
The University of Iowa, Department of Chemistry

Nels T. Anderson, Joseph C. Wright, Gregory S. Girolami
The University of Illinois at Urbana-Champaign, Department of Chemistry

Presentation Abstract

For the use of nuclear energy to continue, it is imperative to address the long-term storage of spent nuclear fuel. Advanced nuclear fuel cycles such as partitioning and transmutation offer possible solutions, but efficiently separating some actinides and lanthanides – especially without generating large volumes of radioactive solvent waste – remains a significant challenge. Here we describe efforts aimed at separating *f*-elements by exploiting significant differences in the volatilities of lanthanide and actinide borohydride complexes. One advantage of our approach is that the volatile complexes can be prepared with little-to-no solvent by mechanochemically grinding borohydride and *f*-metal salts together. The volatile complexes are then separated from the non-volatile complexes and reaction by-products by sublimation. The synthesis, structures, and differing volatilities of *f*-element complexes with chelating borohydrides called aminodiboranates ($\text{H}_3\text{BNR}_2\text{BH}_3^-$) and phosphinodiboranates ($\text{H}_3\text{BPR}_2\text{BH}_3^-$) will be described along with proof-of-principle *f*-element separation studies using our selective volatilization strategy.

Grant Number DE-SC0019426: Exploratory Synthesis of Metal Borohydride Complexes for *f*-Element Separations by Selective Volatilization

PIs: Scott R. Daly and Gregory S. Girolami

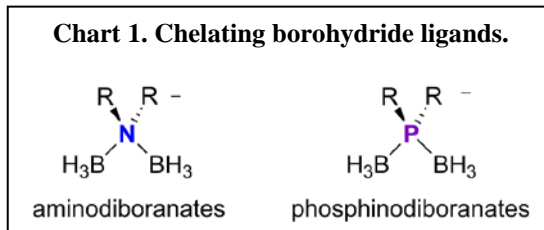
Students: Nels T. Anderson, Anastasia V. Blake, Francesca D. Eckstrom (undergraduate), and Taylor V. Fetrow

RECENT PROGRESS

Major activities conducted in the first year focused on establishing the synthesis of new borohydride ligands and *f*-element complexes for sublimation studies, demonstrating proof-of-principle separation studies with lanthanides and uranium, and developing transuranic capabilities at the University of Iowa for future synthesis and separation experiments with Np, Pu, and Am.

Activities at the University of Iowa. We have been developing a new class of chelating borohydrides called phosphinodiboranates ($\text{H}_3\text{BPR}_2\text{BH}_3^-$) to evaluate their volatility in side-by-side sublimation studies with more traditional borohydride complexes containing tetrahydroborate, alkyltrihydroborate, and aminodiboranate ligands (*Chart 1*). The objective of this work is to determine how changing the groups attached to phosphorus ($\text{R} = \text{}^i\text{Bu}$, $\text{}^i\text{Pr}$, Et, Me, and H) affects the volatility of the resulting phosphinodiboranate complexes with lanthanides and uranium.

We recently described the first *f*-element phosphinodiboranate complexes $M_2(H_3BP^tBu_2BH_3)_6$ where $M = U, Nd,$ and Er (*Chem. Commun.* **2018**, 5602). However, the problem encountered with the synthesis of these and other phosphinodiboranate complexes was their poor solution yields. Stirring $Uf_3(1,4\text{-dioxane})_{1.5}$ with three equivalents of $K(H_3BP^tBu_2BH_3)$ in Et_2O for 24 h, for example, only allowed $U_2(H_3BP^tBu_2BH_3)_6$ to be isolated in crystalline yields less than 15%. Similar results were obtained when using lanthanide iodide salts instead of $Uf_3(1,4\text{-dioxane})_{1.5}$. The poor yields sharply limited the isolation of phosphinodiboranate complexes in sufficient quantities for bulk sublimation studies.



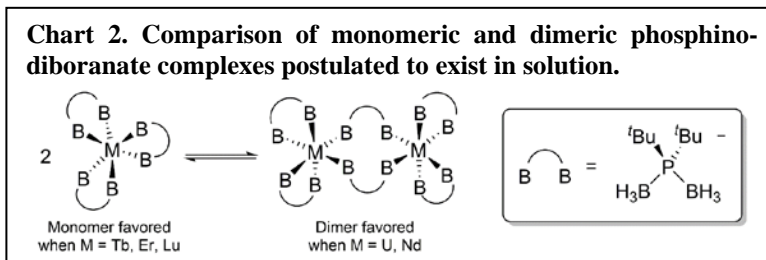
In unpublished work, we discovered that phosphinodiboranate complexes can be prepared in much higher and reproducible yields using mechanochemical reactions. In contrast to the above-mentioned solution synthesis, we discovered that mechanochemically grinding $Uf_3(1,4\text{-dioxane})_{1.5}$ with three equivalents of $K(H_3BP^tBu_2BH_3)$ for 90 min in a shaker mill with stainless steel beads allowed $U_2(H_3BP^tBu_2BH_3)_6$ to be isolated in crystalline yields consistently above 50% (our highest crystalline yield was 62%). These results will be described in an upcoming article for the Forum on “Chelating Ligands for *f*-Elements” in the journal *Inorganic Chemistry*. Several follow-up papers on the mechanochemical synthesis and properties of other *f*-element phosphinodiboranates, (including those with H, Me, ⁱPr, and Ph substituents attached to phosphorus) are in preparation. Volatility studies on the phosphinodiboranate complexes are also in progress.

A unique feature of *f*-metal phosphinodiboranates compared to other borohydride complexes is that they are excellent models for exploring thermodynamic differences in borohydride bonding between lanthanides and actinides. Phosphinodiboranates form equilibrium mixtures of monomers and dimers in solution (**Chart 2**),

and their relative abundances can be quantified by NMR spectroscopy, which has allowed thermodynamic differences in metal-ligand binding to be determined. For example, U^{3+} complex $U_2(H_3BP^tBu_2BH_3)_6$

shows a small 1.0 kcal/mol ΔH increase in the solution equilibrium compared to isostructural lanthanide complexes with Ce^{3+} , Pr^{3+} , and Nd^{3+} , which are identical. This result may be significant because subtle differences in metal-ligand bonding is thought to play an important role with respect to fundamental differences in the volatility of structurally similar actinide and lanthanide complexes.

Completing the proposed synthesis and separation studies with transuranic elements at the University of Iowa required the purchase of a dedicated inert-atmosphere TRU glovebox and upgrading our facilities to safely prepare and handle air-sensitive transuranic borohydride complexes. A VAC atmospheres glovebox was custom designed for these purposes with assistance and advice from the Kozimor and Gaunt Research Groups at Los Alamos National Laboratory. The glovebox was delivered in late March 2019 after numerous production delays due to backordered parts (namely CRL gloveports that allow the glovebox gloves to be safely changed without removing the gloves and risking exposure to the contaminated glovebox atmosphere). Facilities personnel at the University of Iowa recently completed plumbing exhaust ports into existing building ventilation with the appropriate HEPA filtration and we will be starting the



proposed synthesis and separation studies with Np, Pu, and Am this fall. All the equipment and TRU starting materials (i.e. NpO₂) have been ordered and delivered to the University of Iowa.

Activities at the University of Illinois at Urbana-Champaign. We have preliminary results that demonstrate how our proposed method of selective volatilization can be used for lanthanide/actinide and lanthanide/lanthanide separations with dimethylaminodiboranate complexes (**Chart 1**).

To demonstrate lanthanide/lanthanide separations using our method, we began by attempting to separate two trivalent lanthanide complexes prepared *in-situ* by reaction with dimethylaminodiboranate salts. In one study, one-to-one mixtures of PrCl₃ and ErCl₃ were treated with six equivalents of Na(H₃BNMe₂BH₃) and either ball-milled without solvent or allowed to stir in thf followed by removal of the solvent. The resulting solid was heated in vacuum and the Er/Pr ratio in the sublimate determined. Both methods result in reasonable separation efficiencies, the best being obtained from reactions carried out in thf. For example, removing the thf and subliming the reaction residue for 2 h at 95 °C under dynamic vacuum yielded an erbium-enriched sublimate with an 8:1 Er/Pr molar ratio. Resubliming the erbium-enriched sublimate at 70 °C for 3 h increased the Er/Pr molar ratio to 30:1. Metal recovery efficiencies depend on the sublimation times and temperatures.

In parallel with the lanthanide/lanthanide separation studies, we have also demonstrated our first lanthanide/actinide separations. In one experiment, a one-to-one mixture of UCl₄ and SmCl₃ was mixed with seven equivalents of Na(H₃BNMe₂BH₃) in thf. Removing the thf, extracting the generated U(H₃BNMe₂BH₃)₃ and Sm(H₃BNMe₂BH₃)₃ with pentane, evaporating the extract to dryness, and subliming the residue at 70 °C under dynamic vacuum overnight yielded a sublimate with 26:1 Sm:U ratio. We are continuing to optimize conditions need to increase metal recoveries, but we view the separation selectivity to be highly encouraging.

In addition to separation studies, we have been preparing new aminodiboranate and methyltrihydroborate complexes. Several new divalent aminodiboranate complexes have been prepared with Sm²⁺ and Tm²⁺, including adducts with thf, 1,2-dimethoxyethane, diglyme, and 18-crown-6. The new complexes have been characterized by NMR spectroscopy and X-ray crystallography. These new complexes will be tested in proposed divalent/trivalent lanthanide separations, as described in our proposal. Also, a number of new lanthanide methyltrihydroborate complexes with different Lewis bases have been prepared for testing in our separation schemes.

Key Outcomes. We have completed almost all the objectives proposed for year one and are already making progress on some objectives outlined for year two. Our first year has focused primarily on synthesizing many of the proposed ligands and complexes likely to be encountered in our separation studies. Synthesis and preliminary separation studies with lanthanides and uranium were explored to give us time to establish our transuranic capabilities for studies to follow in years 2 and 3. Despite the manufacturing delays for the TRU glovebox, we have now acquired all the equipment and starting materials necessary for completing the proposed transuranic studies. Finally, and perhaps most importantly, we have demonstrated the first lanthanide/lanthanide and lanthanide/actinide separations by selective volatilization of *f*-metal borohydride complexes with aminodiboranates.

Publications Acknowledging this Grant in 2018 – present

Exclusively funded by this grant;

1. Fetrow, T. V.; Bhowmick, R.; Achazi, A. J.; Blake, A. V.; Eckstrom, F. D.; Vlaisavljevich, B.; Daly, S. R. "Chelating Borohydrides for Lanthanides and Actinides: Structures, Mechanochemistry, and Case Studies with Phosphinodiboranates." *Inorg. Chem.* **2019**, accepted.
2. Anderson, N. T.; Wright, J. C.; Girolami, G. S. Synthesis and Characterization of *N,N*-Dimethylaminodiboranate Complexes of Divalent Samarium and Thulium, in preparation.

Jointly funded by this grant and other grants with leading intellectual contribution from this grant;

Jointly funded by this grant and other grants with relatively minor intellectual contribution from this grant;

Assessing Reactive Separations of CO₂

David J. Heldebrant,¹ Deepika Malhotra,¹ Jotheeswari Kothandaraman,¹ Mal-soon Lee,¹ Manh-Thuong Nguyen,⁴ Roger Rousseau,¹ Vanda Glezakou,¹ Xiao-Ying Yu,¹ Jian Zhang¹, Difan Zhang,¹ Leo Bañuelos,²

1. Pacific Northwest National Laboratory, 2. University of Texas, El Paso

Presentation Abstract

Nature has perfected reactive separation—i.e., the capture/concentration and activation/conversion of reagents in one synergistic step. With respect to power generation from fossil fuels, CO₂ capture and any subsequent conversion are performed as two distinctive energy-intensive steps. The aim of this project is to learn how to mimic nature by performing synergistic capture and conversion in the same solvent using the same chemicals. Switchable ionic liquids (SWILs) are promising solvents being studied for CO₂ capture. SWILs exhibit unique physical and thermodynamic property changes as they chemically fixate CO₂. Coincidentally, SWILs are composed of amine bases and or alcohols which have been shown to promote catalytic reduction of CO₂ to CH₃OH.

This work encompasses a joint experimental and theoretical approach that aims to (1) characterize the disparate (ionic and non-ionic) micro-domain structure in these fluids, (2) assess how this structure can be manipulated to control diffusion and chemical complexation of CO₂ in regard to capture, and (3) examine how changes in the solvent structure can be used to govern the reactivity of CO₂ captured in solution. The aim is to fully characterize the solvent structure and chemical speciation of the fluid to learn how the mesoscopic structure originates and how that dynamic structure governs the diffusion and reactivity of CO₂ in solution. In addition, this work focuses on optimizing the thermodynamics of CO₂ conversion either by matching the electrophilicity (hydride acceptor strength) of the CO₂ captured in solution to the hydride donation strength of catalysts used for subsequent catalytic conversions into fuels, or by matching the nucleophilicity of the negatively charged oxygen to strong electrophiles (e.g., epoxides) to produce value-added products.

Grant or FWP Number: FWP 67038

Postdoc(s): Jotheeswari Kothandaraman,¹ Jian Zhang,¹ Difan Zhang.¹

Affiliations(s): 1. Pacific Northwest National Laboratory

RECENT PROGRESS

Self-assembly of hierarchical liquid structures drives transport and fixation of CO₂.

We recently linked the anomalous mass transfer to the unique mesoscopic structures that arise within these liquids, only in the absence of water as a co-solvent. In that work, we demonstrated that CO₂ molecules chemically fixated in ionic regimes interact strongly with neighboring ions, which limits the rate of molecular diffusion (MD). This was exemplified by our observations that molecular CO₂ dissolved in solution dominates the macroscopic mass transfer by diffusing through the solvent via pores or channels of low-polarity (non-

ionic) regions within the fluid through which CO₂ could easily move. This phenomenon is exemplified with a molecular-level snapshot of 1-IPADM-2-BOL showing CO₂ diffusion pathways—illustrated by the green arrows moving through solvent in Figure 1. CO₂-free 1-IPADM-2-BOL (grey) is relatively low polarity and non-viscous, providing a medium where CO₂ could readily diffuse. Even at higher CO₂ loadings, CO₂ would likely diffuse through pockets or channels of CO₂-free solvent rather than the polar and viscous CO₂-bound ionic regions. Experimental data has confirmed heterogeneous structures at any CO₂ loading above 0%, suggesting that pockets or channels within the fluid always exist, providing regions wherein gases such as CO₂ could diffuse, accounting for the high degree of mass transfer.

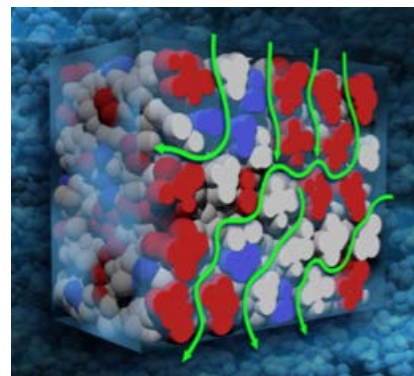


Figure 10. MD simulations of 1-IPADM-2-BOL and 1-IPADM-2-BOL-CO₂ with CO₂. Green arrows are CO₂ diffusion pathways.

Dynamic Solvation Environments Can Be Used to Solvate Catalysts, Nanoparticles and Rare Earths Via Chelation

We have recently employed X-ray absorption spectroscopy (XAS) to ascertain information on local structures, notably the primary solvation spheres of metal centers via cooperative effect of chelation and solvation. Our results show that ionic regimes within carbon capture solvents do indeed provide a handle to control the chelation or solvation. Fe^{II} or Fe^{III} species were found to

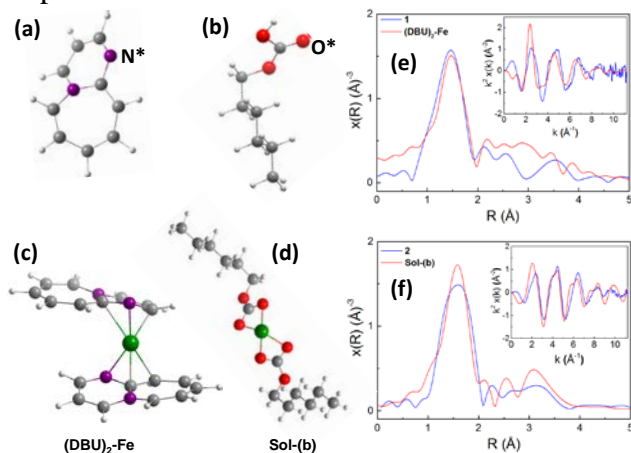


Figure 2. Structure scheme of (a) DBU molecule and (b) C₆H₁₂OC₀₂₂-; N* and O* indicate bonding sites for Fe; DFT optimized structures of (c) (DBU)₂-Fe and (d) Sol-(b), Green, purple, red, grey and white spheres represent Fe, N, O, C and H atoms, respectively. Comparison of Fe k-edge EXAFS $\chi(R)$ spectra for (e) 1 and (DBU)₂-Fe, (f) 2 and Sol-(b)

otherwise. We also learned how to control the other chemical moiety in captured CO₂: the -O- moiety, albeit as a nucleophile. We demonstrated this by coupling the -O- moiety with electrophiles (e.g., epoxides) in catalytic and noncatalytic reactions. Recent results on copolymerization of captured CO₂ with cyclohexene oxide is shown in Table 1.

remain chelated or solvated until CO₂ was removed, which resulted in Fe-Fe bond formation and subsequent precipitation of a nano-sized green rust from solution. These results suggest that the dynamic solvation environments in carbon capture solvents provide a means to control selective chelation or solvation of metal cations in solution in addition to the ability to dictate a controlled precipitation from solution.

Polymerization of Captured CO₂

We have learned how to control the reactivity of the electrophilic central carbon of carbamates and alkylcarbonates towards nucleophiles (e.g., H-) to make fuels, in turn validating our prior hypothesis that sp²-hybridized trigonal planar anionic carboxylates are more electrophilic than neutral CO₂ when conventional wisdom said

Table 1. Co-polymerization of CHO and CO₂.

Entry	T (°C)	CO ₂ (bar)	[Cr] : [CHO] : [Co-Cat]	PCHC : CHC+PEC		TON	TOF	M _w ^(b) (g/mol)	M _n ^(b) (g/mol)	PDI ^(b)
				linkages ^(a)	PCHC ^(a)					
1	84	44	1 : 3550 : -	-	-	-	-	-	-	-
2	95	44	1 : 3550 : -	81%:19%	7%	260	16	2270	3000	2.29
3	84	44	1 : 3550 : 0.5 ([DBUH ⁺]C ₆ H ₁₃ O)	93%:7%	41%	1450	91	4440	4230	1.05
4	84	44	1 : 3550 : 1 ([DBUH ⁺]C ₆ H ₁₃ O)	96%:4%	51%	1800	112	6550	6160	1.06
5	82	44	1 : 3550 : 2 ([DBUH ⁺]C ₆ H ₁₃ O)	99%:1%	82%	2900	181	11900	10500	1.14
6	82	44	1 : 3550 : 1 (DBU)	93%:7%	39%	1400	87	4930	4520	1.09
7	95	44	1 : 3550 : 2 ([DBUH ⁺]C ₆ H ₁₃ O)	98%:2%	94%	3300	206	12600	10300	1.22
8	95	44	1 : 3550 : 1 ([DBUH ⁺]C ₆ H ₁₃ O)	92%:8%	41%	1450	92	7550	6170	1.22
9	92	44	1 : 3550 : 2 (DBU)	95%:5%	41%	1450	91	12700	9310	1.36
10	92	44	1 : 3550 : 2 ([DBUH ⁺]OAc ⁻)	96%:4%	39%	1400	87	9030	6740	1.34
11	92	10	1 : 2550 : 2 ([DBUH ⁺]C ₆ H ₁₃ O)	92%:8%	63%	1600	100	7360	6470	1.14
12	92	10	1 : 2550 : 2 (DBU)	90%:10%	35%	900	56	7440	6420	1.16

CHO=Cyclohexene oxide, PCHC = polycyclohexene carbonate, CHC=cyclohexene carbonate, PEC = polyether carbonate, Cr(salen)Cl=0.02 mmol, neat CHC was used for all the experiments and the reactions were performed in an autoclave for 16h

(a) Selectivity and yield of all entries were calculated by ¹H NMR spectroscopy using 1,3,5-trimethoxybenzene as an internal standard.
 (b) Determined by GPC using polystyrene standards. Turnover number (TON)=(mol of repeating unit)/(mol of Cr). Turnover frequency (TOF)=TON/h.

Publications Acknowledging this Grant in 2015 – present

(IV) Exclusively funded by this grant; (*denotes corresponding author)

- Zheng, J.; Yu, X. Y.;* Nguyen, M. T.; Lao, D. B.; Zhu, Y.; Wang, F.; Heldebrant, D. J.* “Assessing the Impacts of Dynamic Soft-Template Innate to Switchable Ionic Liquids on Nanoparticulate Green Rust Crystalline Structure.” *ChemCom*, **2019**, *Accepted*.
- Kothandaraman, J.; Zhang, J., Glezakou, V. A.; Mock, M. T.; Heldebrant, D. J.,* “Chemical Transformations of Captured CO₂ into Cyclic and Polymeric Carbonates.” *J. CO₂ Util.*, **2019**, *32*, 196-201.
- Yu, X. Y.;* Yao, J.; Lao, D. B.; Heldebrant, D. J.,* Zhu, Z.; Malhotra, D.; Nguyen, M. T.; Glezakou, V. A.; Rousseau, R., “Mesoscopic Structure Facilitates Rapid CO₂ Transport and Reactivity in CO₂-Capture Solvents.” *J. Phys. Chem. Lett.*, **2018**, *9*, 5765-5771.
- LeClaire, J.; Heldebrant, D. J.;* “A Call to (Green) Arms: A Rallying Cry for Green Chemistry and Engineering for CO₂ Capture, Utilisation and Storage.” *Green Chem.* **2018**, *20*, 5058-5081.
- Kothandaraman, J.; Dagle, R. A.; Labarbier-Dagle, V.; Davidson, S. D.; Walter, E. D.; Burton, S. D.; Hoyt, D. W.; Heldebrant, D. J.* “Condensed-Phase Low Temperature Heterogeneous Hydrogenation of CO₂ to Methanol.” *Cat. Sci. Tech.*, **2018**, *8*, 5098-5103.
- Yao, J.; Lao, D. B.; Sui, X.; Zhou, Y.; Nune, S. K.; Ma, X.; Troy, T. P.; Ahmed, M.; Zhu, Z.; Heldebrant, D. J.;* Yu, X. Y.* “Two coexisting liquid phases in switchable ionic liquids.” *Phys. Chem. Chem. Phys.*, **2017**, *19*, 22627–22632i.
- Heldebrant, D. J.; Koech, P. K.; Glezakou, V. A.; Rousseau, R.; Malhotra, D. M.; Cantu, D. C. “Water-Lean Solvents for Post-Combustion CO₂ Capture: Fundamentals, Uncertainties, Opportunities and Outlook.” *Chem. Rev.*, **2017**, *117*, 9594–9624.
- Zhou, Y.; Yao, J.; Ding, Y.; Yu, J.; Hua, X.; Evans, J. E.; Yu, X.; Lao, D. B.; Heldebrant, D. J.; Nune, S. K.; Cao, B.; Bowden, M. E.; Yu, X. Y.; Wang, X. L.; Zhu, Z. “Improving Molecular Ion Signal Intensity for in situ Liquid SIMS Analysis,” *J. Am. Soc. Mass Spectrom.* **2016**, *27*, 2006-2013.
- Yao, J.; Zhou, Y.; Sui, X.; Lao, D. B.; Heldebrant, D. J.; Zhu, Z.; Yu, X. Y. “Switchable DBU and Hexanol Ionic Liquid Analyzed by Liquid ToF-SIMS.” *Surf. Sci. Spectra*, **2016**, *23*, 9.

10. Lao, D. B.; Galagan, B. R.; Linehan, J. C.; Heldebrant, D. J. "The steps of activating a prospective CO₂ hydrogenation catalyst with combined CO₂ capture and reduction," *Green Chem.* **2016**, *18*, 4871-4874.
 - ¹¹. Lao, D. B.; Kukkadapu, R.; Kovarik, L.; Heldebrant, D. J.;* Nune, S. K. "Switchable Ionic Liquids: A New Medium to Synthesize Green Rust." *Cur. Inorg. Chem.*, **2016**, *6*, 92-99.
- (V) *Jointly funded by this grant and other grants with leading intellectual contribution from this grant;*
1. Mehta, H. S.; Chen, Y.; Sears, J. A.; Walter, E. D.; Campos, M.; Kothandaraman, J.; Heldebrant, D. J.; Hoyt, D. W.; Mueller, K. T.; Washton, N. M. "A novel high-temperature MAS probe with optimized temperature gradient across sample rotor for in-situ monitoring of high-temperature high-pressure chemical reactions." *Solid State Nuclear Magnetic Resonance*, **2019**, *102*, 31-35.
- (VI) *Jointly funded by this grant and other grants with relatively minor intellectual contribution from this grant;*
1. Grubel, K.; Chouyyok, W.; Heldebrant, D. J.; Linehan, J. C.; Bays, J. T.* "Octane-On-Demand: Onboard Separation of Oxygenates from Gasoline." *Energy Fuels*, **2019**, *333*, 1869-1881.

PI MEETING PARTICIPANTS

**2019 Separation Science Research PI Meeting
September 9-11, 2019
Participant List**

Christopher Arges
Louisiana State University
carges@lsu.edu

Jason Bara
University of Alabama
jbara@eng.ua.edu

Bill Bates
Savannah River National Laboratory
william.bates@srnl.doe.gov

Enrique Batista
Los Alamos National Laboratory
erb@lanl.gov

Georges Belfort
Rensselaer Polytechnic Institute
belfog@rpi.edu

Paul Bohn
University of Notre Dame
pbohn@nd.edu

Kristin Bowman-James
University of Kansas
kbjames@ku.edu

Phil Britt
Oak Ridge National Laboratory
brittpf@ornl.gov

Merlin Bruening
University of Notre Dame
mbruenin@nd.edu

Aurora Clark
Washington State University
auclark@wsu.edu

Richard Crooks
University of Texas, Austin
crooks@cm.utexas.edu

Radu Custelcean
Oak Ridge National Laboratory
custelceanr@ornl.gov

Sheng Dai
Oak Ridge National Laboratory
dais@ornl.gov

Scott Daly
University of Iowa
scott-daly@uiowa.edu

Michael Deem
Rice University
mwdeem@rice.edu

Benjamin Doughty
Oak Ridge National Laboratory
doughtybl@ornl.gov

Amar Flood
Indiana University
aflood@indiana.edu

Benny Freeman
University of Texas, Austin
freeman@che.utexas.edu

Bruce Garrett
U.S. Department of Energy/BES
bruce.garrett@science.doe.gov

Gregory Girolami
University of Illinois, Urbana-Champaign
girolami@scs.illinois.edu

Vassiliki-Alexandra Glezakou
Pacific Northwest National Laboratory
vanda.glezakou@pnnl.gov

Ruilan Guo
University of Notre Dame
rguo@nd.edu

Joel Harris
University of Utah
harrisj@chem.utah.edu

David Heldebrant
Pacific Northwest National Laboratory
david.heldebrant@pnnl.gov

Daniel Higgins
Kansas State University
higgins@ksu.edu

Joseph Hupp
Northwestern University
j-hupp@northwestern.edu

Takashi Ito
Kansas State University
ito@ksu.edu

Santa Jansone-Popova
Oak Ridge National Laboratory
jansonepopos@ornl.gov

Cynthia Jenks
Argonne National Laboratory
cjenks@anl.gov

De-en Jiang
University of California, Riverside
djiang@ucr.edu

Grant Johnson
Pacific Northwest National Laboratory
grant.johnson@pnnl.gov

William Koros
Georgia Institute of Technology
wjk@chbe.gatech.edu

Stosh Kozimor
Los Alamos National Laboratory
stosh@lanl.gov

Revati Kumar
Louisiana State University
revatik@lsu.edu

Katie Li-Oakey
University of Wyoming
dli1@uwyo.edu

Ryan Lively
Georgia Institute of Technology
ryan.lively@chbe.gatech.edu

Brian Long
University of Tennessee
long@utk.edu

Shannon Mahurin
Oak Ridge National Laboratory
mahurinsm@ornl.gov

Daniel Matuszak
U.S. Department of Energy/BES
daniel.matuszak@science.doe.gov

Raul Miranda
U.S. Department of Energy/BES
raul.miranda@science.doe.gov

Jacob Petrich
Ames Laboratory
jwp@iastate.edu

Venkateshkumar Prabhakaran
Pacific Northwest National Laboratory
venky@pnnl.gov

Krishnan Raghavachari
Indiana University
kraghava@indiana.edu

Kenneth Raymond
University of California, Berkeley
knr4uc@gmail.com

Steven Regen
Lehigh University
slr0@lehigh.edu

Eric Schelter
University of Pennsylvania
schelter@sas.upenn.edu

**2019 Separation Science Research PI Meeting
September 9-11, 2019
Participant List**

Mark Schlossman
University of Illinois, Chicago
schloss@uic.edu

Daniel Schwartz
University of Colorado, Boulder
daniel.schwartz@colorado.edu

Jonathan L Sessler
University of Texas, Austin
sessler@cm.utexas.edu

Thomas Shehee
Savannah River National Laboratory
thomas.shehee@srnl.doe.gov

David Sholl
Georgia Technical Institute
david.sholl@chbe.gatech.edu

Zachary Smith
Massachusetts Institute of Technology
zpsmith@mit.edu

Lynda Soderholm
Argonne National Laboratory
ls@anl.gov

Ahmet Uysal
Argonne National Laboratory
ahmet@anl.gov

Gregory A. Voth
University of Chicago
gavoth@uchicago.edu

Gangli Wang
Georgia State University
glwang@gsu.edu

Kevin West
University of South Alabama
kevinwest@southalabama.edu

Philip Wilk
U.S. Department of Energy/BES
philip.wilk@science.doe.gov

Ping Yang
Los Alamos National Lab
pyang@lanl.gov



U.S. DEPARTMENT OF
ENERGY

Office of
Science